

1674121

M0010897T8

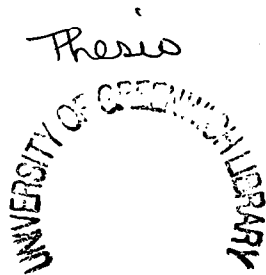
Photocalorimetry: Design, Development and Test Considerations

By

Andrew Colin Morris

Thesis submitted to the University of Greenwich in the partial fulfilment  
of the degree of Doctor of Philosophy

PhD project undertaken in Collaboration with GlaxoSmithKline, New  
Frontiers Science Park (South), Harlow, Essex



March 2004

I certify that this work has not been accepted in substance for any degree,  
and is not concurrently submitted for any other than that of Doctor of  
Philosophy (PhD) of the University of Greenwich. I also declare that this  
work is the result of my own investigations except where otherwise  
stated.

\_\_\_\_\_ Candidate

\_\_\_\_\_ Supervisors

\_\_\_\_\_

FOR MY ONE

## ACKNOWLEDGEMENTS

I would like to thank my sponsors, GlaxoSmithKline, Harlow, Essex; especially David Clapham. Without their help and assistance the PhD project would not have been possible.

I would also like to thank my supervisors, Professor Tony Beezer and Professor Joe Connor for their guidance, advice and support and for the numerous times they have rescued me from the depths of despair when the project looked to be faltering.

Thanks also to the other academic staff at Medway Sciences for their interest and support; especially Professor John Mitchell for additional support and instruction in the ways of photochemistry!

Thanks to my friends and family for their unending support and understanding over the past four years. I couldn't have done it without you.

A big thankyou to my friends - the other students at Medway Sciences. A wonderful group of people past and present; great times with great memories. Special thanks to Laura for late-night coffee, deep conversation and great friendship.

Schnarf.....

THE CONTENTS OF THIS THESIS ARE CONFIDENTIAL AND  
ALL READERS ARE BOUND BY THE CONFIDENTIALITY  
AGREEMENT SIGNED BY THE AUTHOR

## ABSTRACT

The goal of the project is to design and build a photocalorimeter capable of carrying out photostability testing in the pharmaceutical industry. A current challenge is to develop methods of testing the photostability of solid materials which are non-invasive, non-destructive and allow real time observations to be made. Calorimetry represents one such method.

Solution-phase systems are relatively straight-forward and have been applied to calorimetry for many years requiring few assumptions about the reaction system under study to be made. Previous studies have developed iterative methods to fit experimental data to established calorimetric equations. A new approach allowing the direct calculation of reaction parameters is described in *chapter two*.

For solids, the situation is more complicated than that for solutions and equations are more difficult to develop since additional parameters (such as the solid state fitting parameters  $m$  and  $n$ ) have to be accommodated. New theoretical approaches to data fitting in the solid state are also described in *chapter two*.

Having previously established that the *imidazole*-catalysed hydrolysis of *triacetin* reaction is robust and reliable, new applications, such as the effect of fill-volume on the calorimetric output and thus the reaction parameters, are described in *chapter three* in preparation for use of the system on solid state systems.

*Chapter four* describes the design and development of the photocalorimeter, together with improvements and modifications made to it as the project progressed, whilst *chapter five* describes the development of actinometric techniques. An actinometer provides a means of measuring the amount of light-energy being delivered to a target sample. Actinometric techniques are described in the literature and studies carried out on candidates for use with the photocalorimeter are outlined. Particular success was achieved with *2-nitrobenzaldehyde*,

where results within 2% error were achieved for the actinometric experiments.

The final stage of the project involves the application of the newly-developed photocalorimeter to the testing of solid samples such as *nifedipine*.

Studies were carried out both on the photodegradation caused by white light and also using monochromatic light. This allowed “causative wavelengths” of photodegradation to be investigated using the photocalorimeter – a significant area of interest in the pharmaceutical industry and the first time quantitative data has been obtained for a solid state material using non-classical techniques.

Finally, studies were carried out into establishing the photostability of an unknown solid state test material.

## CONTENTS

Abstract .....	6
Glossary .....	9
<b>CHAPTER 1</b> Introduction.....	10
<b>CHAPTER 2</b> The Principles of Calorimetry.....	17
<b>CHAPTER 3</b> Calorimetric Validation Techniques.....	50
<b>CHAPTER 4</b> Photocalorimetry: History and Development..	71
<b>CHAPTER 5</b> Actinometry.....	111
<b>CHAPTER 6</b> Applications.....	161
<b>CHAPTER 7</b> Conclusions and Further Work.....	206
References.....	210

## GLOSSARY OF TERMS

$dx/dt$	<i>Rate of reaction</i>	$G$	<i>Gibbs free energy</i>
$\mu W$	<i>Power output</i>	$A$	<i>Mass of reactable material</i>
$\Phi_0$	<i>Calorimetric signal at <math>t=0</math></i>	$H$	<i>Enthalpy of reaction</i>
$Q_T$	<i>Q at a specific temperature</i>	$S$	<i>Reaction entropy</i>
$SD$	<i>Standard Deviation</i>	$T$	<i>Temperature</i>
$F_0$	<i>Photon Flux</i>	$k$	<i>Reaction rate constant</i>
$K$	<i>Equilibrium Constant</i>	$x$	<i>Amount of reacted material</i>
$\alpha$	<i>Fraction of reacted material</i>	$n$	<i>Order of reaction</i>
$t$	<i>Time (seconds)</i>	$P$	<i>Pre-exponential term</i>
$C$	<i>Ratio of <math>t_2 / t_1</math></i>	$E_a$	<i>Activation energy</i>
$(A-x)$	<i>Quantity of unreacted material</i>	$\Delta U$	<i>Change in internal energy</i>
$dq/dt$	<i>Power (<math>\equiv \Phi</math>)</i>	$Q$	<i>Total reaction enthalpy</i>
$Y$	<i>Calorimetric Signal</i>	$V$	<i>Volume</i>
$f$	<i>Calorimetric Signal at <math>t=0</math></i>	$I_0$	<i>Irradiance</i>
$\Delta w$	<i>Change in work done</i>	$m$	<i>Fitting parameter</i>
$R$	<i>Gas constant</i>	$n$	<i>Fitting parameter</i>
$c$	<i>Speed of light</i>	$k$	<i>Reaction co-efficient</i>
$\phi$	<i>Quantum Yield</i>	$J$	<i>Joules</i>
$A$	<i>Cross-sectional area of ampoule</i>	$q$	<i>Time-dependent enthalpy</i>
$E_\lambda$	<i>Energy at a given wavelength</i>	$N_A$	<i>Avogadro's number</i>
$h$	<i>Planck's constant</i>		

# *CHAPTER 1*

## *INTRODUCTION*

## 1. Introduction and Overview of Problem

The goal of the project described herein is to design and build a photocalorimeter that can carry out photostability testing in the pharmaceutical industry.

One of the biggest problems encountered in the pharmaceutical industry is that of developing suitable test methods for the photostability testing of pharmaceutical materials in the solid state.

Consider the advancement through the various stages of testing of a new pharmaceutical entity.

A raw active ingredient molecule straight out of the discovery lab has to undergo a rapid screening process to determine whether or not it is a candidate for development, i.e. formulation. Subsequently, upon formulation, a method is required to establish the stability of the drug over long periods of time, often under “accelerated” test conditions (e.g. high temperatures and high relative humidity). Such tests necessarily include photostability studies.

Current test methods for photostability often involve the use of a “light box”, where the sample is subjected to high-intensity light for a known period of time. This method is not ideal, however, since obtaining of stability data cannot be carried out in real-time.

Consider a solid sample which has been tested in a light box for two months. In order to obtain stability data, the sample must be removed from the light box and some of it dissolved to allow solution-phase testing (e.g. using high performance liquid chromatography, HPLC). The irradiation of the sample that remains from the analysis described above then recommences but the ideal of real time testing and data collection without altering the nature of the sample has been lost.

Calorimetry presents an alternative method of photostability testing, that is non-invasive, non-destructive and allows real-time observation of the progress of a reaction.

Solution-phase systems are relatively straight-forward and easy to model and have been applied to calorimetry for years.<sup>1-8</sup> The only requirements are knowledge of the reaction rate constant,  $k$ ; the reaction enthalpy,  $H$  and the order of reaction,  $n$  which is

always an integral figure (for the individual reactions contributing to the overall mechanism)

However, when solids undergo reaction, not necessarily all of the material will react. The initial reaction is carried out at the surface but any subsequent reaction depends upon the diffusion into and out of the solid. In many solid systems, this diffusion process is so slow that the system can be described as being in equilibrium once the superficial reaction has taken place and the assumption that all the material will react given sufficient time cannot be used.

A certain degree of complexity can therefore be expected, with the fractional extent of reaction,  $\alpha$ , the reaction co-efficient  $k$  (in  $s^{-1}$ ) and the non-integral fitting parameters,  $m$  and  $n$  all needing to be dealt with. Consequently, solid state reactions are complicated to model and the equations not as straight-forward as those that describe solution-phase systems, although many have been developed in the literature.<sup>9-11</sup>

Currently, no reaction system has been adopted as a solid state test reaction. In order for the project to progress, a validation system for the calorimeter in the solid state must be developed. In the same way that the *triacetin* reaction was only adopted as solution-phase validation method once suitable equations to manipulate the data had been developed (see below), a solid-state validation reaction can only be suggested once the theory has been established.

Theoretical development is described in *chapter two* and is based on the Ng equation,<sup>10</sup> developed for dealing with reactions in the solid state.

Solution-phase equations have been applied to calorimetry for many years.<sup>1-8</sup> One such example is the application of the *imidazole* catalysed hydrolysis of *triacetin*; a reaction that has been adopted<sup>12</sup> as an internationally-recognised test reaction for calorimeters, allowing values for  $k$ ,  $H$  and  $n$  to be obtained which can then be compared with “correct” values found in the literature.<sup>13, 14</sup> Previously, an iterative method was applied to obtain the parameters but as a result of recent theoretical developments which are discussed in *chapter two*, these parameters can now be calculated directly.<sup>15, 16</sup> *Chapter three* outlines the studies carried out using the *triacetin* reaction. After establishing the reaction as a suitable method of calorimeter validation, studies are then described establishing the minimum fill volume of

*triacetin* required,<sup>17</sup> within an ampoule, to obtain reproducible results together with the optimum position for a small sample within an ampoule. In each case, the results obtained are compared with the “correct” literature values.

The results of these experiments using the *triacetin* reaction are important when it comes to photocalorimetric studies on solid state samples. For such studies, only small amounts of a solid material will be tested and small amounts of heat produced since reactions might only occur on the surface of the solid. It is therefore important to approach solid state experiments with a knowledge of the optimum test conditions for the calorimeter, as established by the *triacetin* experiments described above.

Having developed equations to analyse reactions in the solid state and having designed and built the photocalorimeter (described in *chapter four*) the next stage of the project is to investigate the methods available for measuring the amount of light delivered to a sample. Without such a method, only qualitative information about a photodegradation reaction can be obtained. There are several actinometric methods described in the literature,<sup>18</sup> the traditional method of the photoreduction of *potassium ferrioxalate* is one example.<sup>19,20</sup> Experiments with *potassium ferrioxalate* are described in *chapter five*, along with the investigation into an alternative actinometric method – the photodegradation of *2-nitrobenzaldehyde*.<sup>21, 22</sup> Additionally, a study was carried out into the use of a spectroradiometer as an alternative to the two actinometers and the results compared.

The final stage of the project is to apply the photocalorimeter, which has been validated and quantified, to “real-life” solid state systems. The example studied in the project is *nifedipine*, a photolabile solid and is described in *chapter six*. This chapter also describes the work carried out in the use of the photocalorimeter to analyse “causative wavelengths” of solid-state materials; a particular topic of interest industrially.

## 1.1 The Stability of Compounds and the Determination of Stability

All matter is in a constant state of change. Even the most long-lasting of materials is under attack from various external forces. Examples of such forces include chemical degradation (e.g. oxidation, hydrolysis and reduction), mechanical degradation (e.g. shearing, compression and stretching), acoustical and thermal degradation. All forms of degradation cause materials to have only a relatively short lifetime and it is important that degradation rates can be established so that new or modified products can be designed to resist these external forces. The measurement of degradation processes allows one to establish the rate of reaction and hence identify acceptable limits of shelf life.

There are many issues associated with current methods of stability testing for drug products and formulations. Storage testing of drugs involves rigorous long-term studies to ensure that pharmaceutical materials remain stable. For example; is a three year old tablet sitting in a medicine cabinet still exactly the same drug it was originally or have long-term instabilities lead to the formation of a toxic derivative of the original? Knowledge of a drug's stability over twenty or thirty years would require expensive and impractical testing procedures if carried out in real time. To allow production of pharmaceuticals over a shortened timescale, therefore, storage testing is accelerated wherever possible – often at higher temperatures (e.g. 50 or 60°C) over a few months and extrapolation of the data to allow estimation of the response to storage at room temperature over many years. However, these storage methods assume that instability processes at 25°C are no different from those at 50°C except for reaction rates; this may not be a true representation of long-term “real life” conditions.

These methods of testing also commonly require the stored sample to be modified in some way prior to testing. A solid-state sample that undergoes UV or HPLC testing, for example, is necessarily made into a solution and this may exhibit totally different properties from the original solid-state system.

Current methods employed for the photostability testing of pharmaceuticals have limitations. The inability to collect long-term stability data in real-time as a photoreaction proceeds is a major drawback. The current method of photostability analysis involves taking a series of “snapshots” of the substance under test via

established analytical methods such as mass spectrometry, HPLC and NMR. These snapshots are then drawn together to provide information on the photodegradation process taking place. Performing these analyses, however, often causes the natural state of the substance to be altered (as described above) and also means that the photostability test will most likely have to be restarted with a fresh sample. Such a process is costly in terms of manpower and expense and may require large amounts of a potentially very rare and expensive product under development.

Current methods also offer limited versatility in terms of changing experimental conditions during a run. Changing the humidity, temperature and the light conditions the material under test is exposed to is not easy with the majority of current test methods. Industry is increasingly showing interest in investigating individual or bands of wavelengths, that cause photodegradation within a chemical entity. This means that traditional test methods that offer only white light or a blanket wavelength range of light are increasingly found wanting.

It has been a challenge, therefore, to discover a general method of analysis that allows the determination of the cause as well as the rate of degradation (including photodegradation) for a wide range of materials both in the solid and solution phase. Identifying an instrument that could be used for the reaction analysis that can yield information on the kinetic and thermodynamic parameters and the reaction mechanism has proved difficult. It must be versatile enough to measure reaction rates for a variety of compounds, with sufficient sensitivity to allow the determination of these parameters under storage conditions in a short space of time. (This is particularly true for long slow reactions where the reaction lifetime may be 10000 years). Many analytical instruments exist capable of carrying out this type of reaction rate determination<sup>23-29</sup> although each of these instruments has been designed for one particular task and so their sensitivities vary. Mass spectrometry<sup>23</sup> for example, is used as a means of quantitative analysis, although its high sensitivity is a limitation since it can only analyse a fraction of the reaction system which may not be truly representative of a non-homogeneous sample.

Calorimetry exploits the fact that a change in enthalpy accompanies a reaction under constant pressure conditions. A calorimeter therefore records changes in heat output of a sample over time and can yield both thermodynamic and kinetic parameters. Willson *et al.*<sup>1, 4 - 8, 13, 15, 16, 30 - 35</sup> and subsequent workers have developed equations and

methods to yield such information and these are discussed in *chapter two*. The development and subsequent application of calorimetric equations, instrumentation and experience has since allowed the development of photocalorimetric studies. The development of validation techniques, equations and apparatus is described later in this thesis.

It is therefore proposed to design and build a novel photocalorimeter that can be used in conjunction with existing commercially available calorimeters that addresses the requirements outlined above.

## *CHAPTER 2*

# *SELECTED PRINCIPLES OF CALORIMETRY*

## 2. The Principles of Calorimetry

A pioneer in the field of calorimetry was Lavoisier, who in 1780 developed a calorimeter to study the metabolism of a guinea pig which was placed in an insulated box packed with ice. The guinea pig's enthalpy of metabolism melted the ice and the resulting water dripped into a small hole in the bottom of the calorimeter. The water was then collected and weighed. From knowledge of the latent heat of fusion, in *joules*, required to form that amount of water from ice, then the value of  $Q$  (the enthalpy) was determined. Knowing the body-weight of the guinea pig, the change of enthalpy for metabolism could then be found in  $J\ kg^{-1}$  and finally, if the amount of water collected was measured every hour, then the rate of metabolism could be measured as  $Jh^{-1}kg^{-1}$ .

At the end of the experiment, the guinea-pig was released from the box and scuttled away; a reminder that calorimetry is a non-invasive and non-destructive technique.

Many types of calorimeter are now commercially available. For this project, an isothermal differential heat conduction microcalorimeter was employed.

The "Thermal Activity Monitor" (TAM) (Thermometric AB, Jarfalla, Sweden) is a calorimeter which combines versatility and sensitivity<sup>36</sup>. The sensitivity allows the study of compounds at ambient temperatures but also allows the reaction environment to be precisely controlled (e.g. pH, RH (relative humidity), oxygen partial pressure, addition of reaction modifiers and temperatures etc). The sensitivity is also sufficient to allow the determination of a reaction lasting 10000 years.<sup>8</sup> The difference between reactions with first order rate constants of  $1 \times 10^{-11}$  and  $2 \times 10^{-11}\ s^{-1}$  can be established after the collection of fifty hours<sup>1</sup> of calorimetric data. No special treatment of the sample is needed before the measurement commences, nor is there any interference with the reaction by the calorimeter<sup>37</sup>.

## 2.1 The Isothermal Microcalorimeter

The isothermal calorimeter (i.e. the TAM) has four separate channels which allows four different experiments to be performed simultaneously at the same temperature. Each channel has a reference chamber (right-hand side) and a sample reaction chamber (left-hand side). The TAM works in differential mode, where a material considered to be inert is placed in the reference chamber and the sample placed in the adjacent chamber. The relative heat flow between the heat sinks of the two chambers is measured where the inert sample essentially produces no calorimetric signal. All channels in the TAM are set within a water bath whose temperature is carefully controlled using a series of thermostats and heaters.

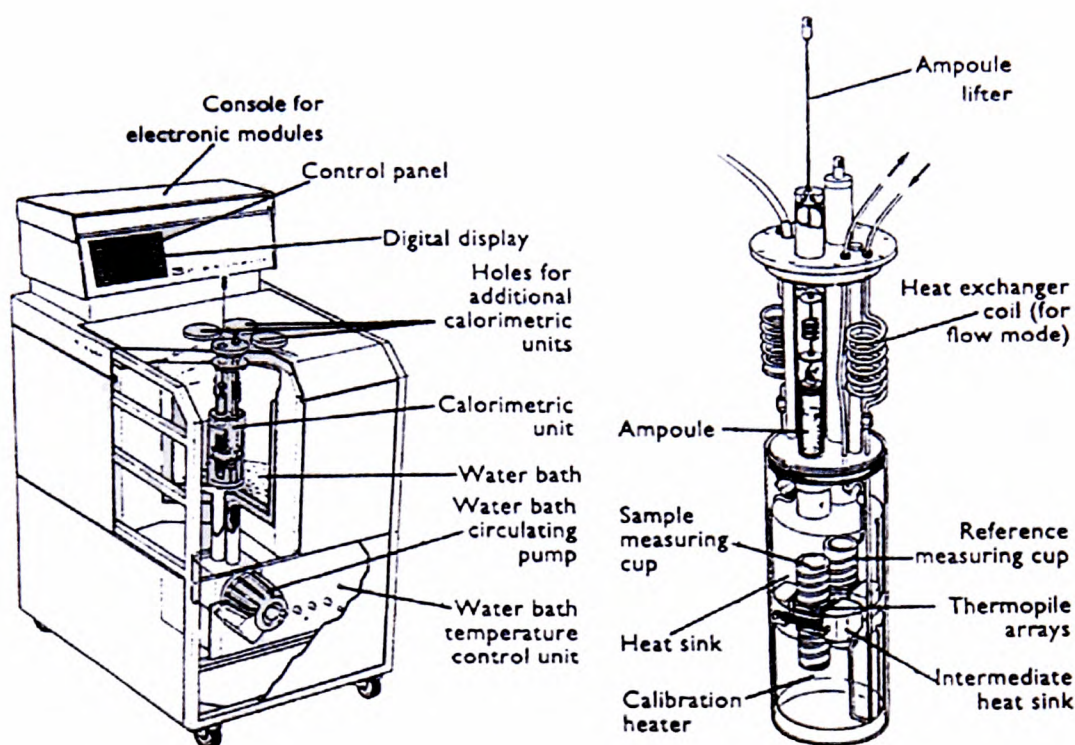


**Figure 2.1.1** The Isothermal Microcalorimeter

*Exploded view of the system... (fig 2.1.1a)*

*...and a calorimetric unit (fig 2.1.1b)*

*Figure 2.1.2* shows a cutaway of one of the four chambers inside the TAM. The sample to be analysed is lowered into the central chamber and a signal is produced as

the heat from the reaction flows from the reaction site to the heat sink or from the heat sink to the reaction site, depending on whether there is an endo or exo-thermic reaction taking place.

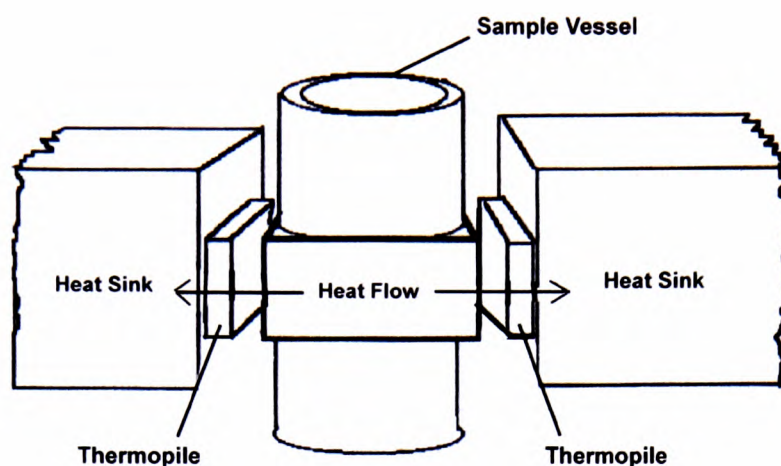


**Figure 2.1.2** The heat sink, consisting of an aluminium block and a precisely controlled water bath surrounds the sample vessel. The thermopile connects the sample vessel to the heat sink and can accurately measure the flow of heat through the system

The heat flow (thermal power,  $dq/dt \equiv \Phi$ ) for a reaction, measured in *Watts* monitored by the calorimeter is measured as a function of time (where  $q$  is the enthalpy change for the reaction at any time  $t$ ). On integration of the power-time curve, the heat output for a reaction over the observed period of measurement can be obtained. i.e. the enthalpy for the reaction. The experimental setup allows solid or solution-phase experiments to be studied and, in addition, the environmental conditions can be controlled. An alternative to using ampoules in the calorimetric chambers is specific devices commercially available to apply to the TAM such as titration units and RH perfusion units.<sup>86</sup> Information about the reactants involved in the reaction may also come from experimental design, where the removal of oxygen, for example, may identify an oxidative reaction. Experiment design, therefore, is very important so that the maximum amount of information about the reaction may be gained.

Two types of data are obtained from the calorimeter. Heat flow (kinetic term) and a reaction time dependent enthalpy change (thermodynamic term). The calorimeter

records enthalpy change, in joules. For solution-phase systems, if the **whole** reaction can be observed within the calorimetric observation period, i.e. until the reaction has gone to *completion* the change in enthalpy for the reaction (in *kJ*) can be calculated simply as;

$$Q = A \cdot H \qquad \text{Eqn 2.1.1}$$

where  $A$  is the amount of reactable material placed in the TAM (*mol*)

and  $H$  is the enthalpy of reaction (*kJmol<sup>-1</sup>*)

However, where  $A$  or  $Q$  is unknown, the determination of enthalpy change becomes more difficult using the calorimeter. ( $Q$  can, in principle, be detected by the integration of the entire output – although  $A$  may not be known).

For any reaction  $A \rightarrow B$ , the progression from its initial to subsequent state can only proceed if there is a reaction pathway available, i.e. a least one defined route from A to B. This pathway is often complex and there are three requirements of a reaction to be able to proceed;

Firstly, the molecule or substance reacting must have the ability to interact (i.e. has the correct chemical bonds etc in the correct orientation to allow an interaction).

Secondly, the reaction must be thermodynamically feasible. The value of the Gibbs Function (the most important thermodynamic parameter in the reaction) is determined by two terms; the reaction entropy and the reaction enthalpy. All changes in the reaction going from A to B must be accompanied by a change of enthalpy and a change in entropy. A reaction route going from A to B depends on the changes in entropy ( $\Delta S$ ) and enthalpy ( $\Delta H$ ) and is defined as the Gibbs Function ( $\Delta G$ , which must  $< 0$ ), *Equation 2.1.2*:

$$\Delta G = \Delta H - T\Delta S \qquad \text{Eqn 2.1.2}$$

*From now onwards, these symbols will be written G, H and S for clarity.*

In enthalpy terms, an exothermic reaction,  $-H$ , is favoured when going from reactant to product; whilst in entropy terms, the reaction favours an increase in disorder  $+S$  in going from reactant to product. It is obvious that the most favourable case is for an exothermic reaction with increased entropy. However, a reaction with a large enough  $+S$  can outweigh the contribution to the reaction of a positive enthalpy (endothermic) term and *vice versa*. A negative value of  $G$  indicates a feasible reaction thermodynamically, whilst a positive value of  $G$  indicates the reaction will not occur under the defined conditions.

No information on the rate of reaction term or the mechanism can be obtained from equilibrium thermodynamics. Between very fast and very slow reactions, there is an observable reaction rate, which can, in principle, be measured.

Thirdly, the reaction requires some kinetic parameter. The reaction rate is governed by three main parameters. The quantity of reactants available for the reaction, the fraction of the quantity available for the reaction with sufficient energy to overcome the energy of activation barrier, and the reaction order,  $n$ , Equation 2.1.3:

$$\frac{dx}{dt} = k.(A-x)^n \quad \text{Eqn 2.1.3}$$

The term  $(A-x)$  is the quantity of material available for reaction at time  $t$ .  $k$ , the rate constant, is described by the Arrhenius Equation (Equation 2.1.4) and is proportional to the quantity of reactants  $(A-x)$  that possess sufficient energy to overcome the activation energy barrier.

$$k = A.e^{\frac{-E_a}{RT}} \quad \text{Eqn 2.1.4}$$

where  $A$  is the pre-exponential factor

$-E_a$  is the activation energy

$R$  is the gas constant

and  $T$  is the temperature (K)

Note that the quantity term,  $A$ , can be converted to a concentration term by multiplying by the volume of solution under test ( $V$ ). This term has been omitted for clarity.

Note also that the rate of reaction (*Equation 2.1.4*) has a dependency on temperature, which is provided solely from the rate constant. Finally the order of reaction ( $n$ ) is a power function and is related to the contribution that the reactant has to the reaction rate. e.g. if the order of reaction is one then the rate of reaction is proportional to the quantity of reactant available; *Rate*  $\propto (A-x)$ . However, if the order of reaction is two, then the rate of reaction is proportional to the quantity of material available for the reaction squared. *Rate*  $\propto (A-x)^2$  The overall reaction order is the sum of the order with respect to the individual reaction components. The order of reaction is not the molecularity of the reaction.

Hence a reaction going from A to B must possess a reaction mechanism and be thermodynamically and kinetically observable. Once these three criteria have been met, the reaction will proceed.

In 1995, Willson *et al.*<sup>30</sup> improved the versatility of the interpretation of the calorimetric data to obtain reaction kinetics through a process of iteration (described later in this chapter). Previously it had been a requirement that the data was forced to conform to a simple kinetic equation<sup>38–40</sup> such as *Equation 2.1.5*;

$$Y = f \cdot \exp^{-k \cdot t} \qquad \text{Eqn 2.1.5}$$

where

$Y$  is the calorimetric signal

$f$  is the calorimetric signal at time  $t = 0$

$k$  is the first order rate constant

and

$t$  is the time

Plotting  $\ln$  *power* as a function of time yields a graph of slope  $-k$  (the first order rate constant)

These methods of analysis, which were used up until 1995, have severe limitations in that they are not sufficiently general, nor do they yield information which allows complete characterisation of the reaction. Willson *et al.* therefore sought a new method of analysis that was more general and could yield kinetic, thermodynamic and other required parameters. The method should also require no previous knowledge about the reaction mechanism, assumptions about the reaction kinetic scheme or the complexity of a reaction.

Resulting from their work, Willson *et al.* presented, in 1995, a new method for the interpretation of calorimetric data that, when applied in the correct way, revealed more information from the data. The approach adopted for data manipulation and the method of interpretation are perfectly general and can be applied to solution and solid phase reactions. (See later in this chapter) From this new method, the reaction parameters that can be determined are; the rate of reaction, the reaction rate constant, the change in enthalpy, the reaction order and the heat change for the reaction medium studied ( $Q$ ).

## 2.2 The Significance of the defined Calorimeter Parameters

Each of the parameters determined from the calorimeter has a contribution to make to the determination of the rate and mechanism of the reaction. The reaction mechanism can be deduced, in part, from the reaction order, the activation energy, the change in enthalpy and entropy, the quantity of material reacted and the experimental design (to a lesser degree).

The reaction order will determine the dependency that the rate of reaction has on the reaction components. The determination of the reaction order with respect to the individual reactants will yield the dependency of the reaction rate on the individual reactants. An estimation of the change in enthalpy could be made from bond energy tables and compared with the experimental change in enthalpy. (It is recognised that bond energies relate to gas phase species and not to solution or solid phase species). Similar comparisons could be made from charts of entropy changes and activation energies; these tables are not available for a wide range of reaction types.

A direct comparison for the rate of all reactions, regardless of their reaction order, can be made in terms of the percentage of reaction over a specified time period. Knowledge of  $Q$ , that can now be calculated from the method to be outlined later in this chapter can lead to a determination of the percentage degradation of a substance;

$$\frac{Q}{Q_T} \times 100 = \% \text{ degradation} \quad \text{Eqn 2.2.1}$$

And using this measurement, *Table 2.2* shows the percentage degradation over different time periods that can be used for the classification of reaction rates. This Table can be simplified arbitrarily further into fast, medium and slow reactions.

Table 2.2

First order rate constant ( $s^{-1}$ )	Half Life	Reaction Rate	
$1 \times 10^{-2}$	69 sec	$> 1\% s^{-1}$	Fast
$1 \times 10^{-3}$	693 sec	$1\% s^{-1}$	
$1 \times 10^{-4}$	1.9 hours	$30\% \text{ hour}^{-1}$	
$1 \times 10^{-5}$	19.25 hours	$3.5\% \text{ hour}^{-1}$	Medium
$1 \times 10^{-6}$	8 days	$8\% \text{ day}^{-1}$	
$1 \times 10^{-7}$	11.5 weeks	$5.8\% \text{ week}^{-1}$	
$1 \times 10^{-8}$	2.2 years	$2.4\% \text{ month}^{-1}$	
$1 \times 10^{-9}$	22 years	$3\% \text{ year}^{-1}$	Slow
$1 \times 10^{-10}$	222 years	$0.3\% \text{ year}^{-1}$	
$1 \times 10^{-11}$	2207 years	$0.03\% \text{ year}^{-1}$	

Rate constants for reactions with different orders can be compared by the percentage of reaction at a particular time. These can be further classified as fast, medium and slow reactions.

## 2.3 The analysis of Calorimetric Data

To address the issues described in the previous chapter, many approaches of data analysis can be taken: A new method of calculating reaction parameters *directly* will follow later in this chapter, whilst Willson *et al.* in 1995 developed an iterative method for calorimetric data that would allow the calculation of reaction parameters necessary for the characterisation of a reaction.

The method consists of various approaches for the manipulation of data. The rate of reaction largely determines which method of analysis should be used. A reaction can be deemed as being fast, medium or slow (*Table 2.2*). For a reaction where a proper characterisation is required in terms of kinetic and thermodynamic parameters, the method of analysis had, up until recently, involved solely iteration. This method depends on the assumption that all of the material placed in the calorimeter will react given sufficient time.

If a reaction is long and slow and it is assumed that  $A$ , the amount of material placed in the material that can react is known, then the rate constant  $k$ , the enthalpy of reaction  $H$  and the order of reaction  $n$  can be established through the iterative process. However, for faster reactions where a plot of the power output of the calorimeter,  $\Phi$  versus time  $t$  shows significant curvature then  $n$  may possibly be derived directly from the data without the need for iteration. The newly-found value of  $n$  can then be inserted back into the iterative fitting procedure and used to reduce the burden of iteration on the remaining parameters  $k$  and  $H$ .

The iterative theory is discussed in this chapter. However, it is important to note that knowledge of  $n$  does not enable the *direct* calculation of  $k$  and  $H$ .

To verify the correctness of the iterative fit, various tests are available and have been applied which involve plotting, for example,  $\Phi$  versus  $(Q-q)$  which yields a slope equal to  $k.H^{1-n}$ . Such tests are also described in this chapter.

The iterative analysis is derived from a differential form of a kinetic equation describing a reaction scheme. This equation describes the rate of reaction in terms of the quantity of material available for the reaction at time  $t$ . Integration of the reaction describes the quantity of material remaining as a function of time.

Consider a simple reaction scheme where the differential kinetic equation can be discussed:



Hence

$$\frac{dx}{dt} = \frac{d(A - x)}{dt} \quad \text{Eqn 2.3.2}$$

And it is this type of equation that can be transformed into one in calorimetric form.

If we consider, for example, a mono-molecular kinetic equation such as that in *Equation 2.3.3*;

$$\frac{dx}{dt} = k \cdot (A - x)^n \quad \text{Eqn 2.3.3}$$

then from basic thermodynamics, ( $q$ ) the time dependent enthalpy change for the reaction is the quantity of material reacted to time  $t$ , multiplied by the change in enthalpy for the reaction;

$$q = x \cdot H \quad \text{Eqn 2.3.4}$$

and  $x$ , the amount of product formed, can be substituted for by  $q / H$  to give;

$$\frac{dq}{dt} \cdot \frac{1}{H} = k \cdot \left( A \cdot V - \frac{q}{H} \right)^n \quad \text{Eqn 2.3.5}$$

This equation can be rearranged to form the **basic calorimetric equation**;

$$\Phi = k \cdot H \cdot \left( A - \frac{q}{H} \right)^n \quad \text{Eqn 2.3.6}$$

where, for clarity, the volume term,  $V$  is dropped and  $A$  becomes the quantity of reactable material as opposed to the concentration, as was the case in *Equation 2.3.5* above.  $\Phi$  is the power (in *Watts*) and  $q$  is the time-dependent enthalpy (*Joules*) for the reaction.

The calorimetric data, which comes directly from the TAM is in the form of  $\Phi$  (power) as a function of time. Integration of the  $\Phi$  vs. time curve gives the time-dependent enthalpy for the reaction ( $q$ ). Hence both the power ( $\Phi$ ) and the time-dependent enthalpy change ( $q$ ) terms found in *Equation 2.3.6* can be derived directly from the calorimeter.

### Slow Reactions - Calorimetric Data Fitting

If a reaction is slow,  $n$  can be determined through iteration.

In the general equation;

$$\Phi = k \cdot H \cdot \left( A - \frac{q}{H} \right)^n \quad \text{Eqn 2.3.6}$$

it can be seen that the two variables,  $\Phi$  and  $q$ , are both obtained directly from the calorimeter. Since  $k$ ,  $H$ ,  $A$  and  $n$  are constant they will remain the same for the lifetime of the reaction (assuming the mechanism is constant throughout the lifetime of the reaction) and analysis involves fitting the plot of  $\Phi$  against  $q$  using Origin™.

The data is imported as an ASCII file from which a graph is plotted of  $\Phi$  vs.  $q$  to find appropriate values for  $n$ ,  $k$  and  $H$  ( $A$  is assumed known and is set equal to the load placed in the calorimeter). An appropriate reaction formula is selected (e.g. Equation 2.3.6) and the iteration procedure started. Through iteration  $k$ ,  $H$ , and  $n$  can be determined, with constraints on their values to ensure a good fit. The first constraint is that  $Q = A \cdot H$ . The second constraint is that plotting  $dq/dt$  against  $(Q-q)^n$  will yield a straight line with slope  $k \cdot H^{1-n}$ . The third constraint is that the calculated half life is consistent with that obtained from extrapolation of the calorimetric data.

Initially, the iterative procedure can be assisted by adding approximate values for the fixed parameters in the fitting process to reduce the burden of iteration. The computer then uses these values to plot a line through the calorimetric data points and the theoretical curve determined from the values of the constants of the equation. The programme continues to fit until the value of the constants satisfy the required values to construct a simulated output through the calorimetric data points.

### Fast to Medium Reactions - Calorimetric Data Fitting

In faster reactions than those described above, there may be significant enough curvature of the plot of  $\Phi$  versus  $t$  to determine  $n$  from the calorimetric data without the need to iterate.

#### Calculation of $n$

Consider the equation below:

$$\Phi = k \cdot H^{1-n} \cdot (Q - q)^n \quad \text{Eqn 2.3.7}$$

If *Equation 2.3.7*, a general form, is considered and integrated under the conditions when  $t = 0$ ,  $q = 0$ , *Equation 2.3.8* is produced, the time-dependent enthalpy for the reaction as a function of time:

$$Q - q = \left[ k \cdot t \cdot H^{1-n} \cdot (n - 1) + Q^{1-n} \right]^{\frac{1}{1-n}} \quad \text{Eqn 2.3.8}$$

where  $t$  can be expressed as:

$$t = \frac{(Q - q)^{1-n} \cdot Q^{1-n}}{(n - 1) \cdot k \cdot H^{1-n}} \quad \text{Eqn 2.3.9}$$

And by substituting  $dq/dt$  ( $\Phi$ ) for  $k \cdot H^{1-n} \cdot (Q - q)^n$ , we obtain;

$$t = \frac{\left( \frac{\phi}{k \cdot H^{1-n}} \right)^{\frac{1-n}{n}} - Q^{1-n}}{k \cdot H^{1-n} \cdot (n - 1)} \quad \text{Eqn 2.3.10}$$

and, if two time points,  $t_1$  and  $t_2$  are chosen for *Equation 2.3.9* with corresponding values of  $\Phi_1$  and  $\Phi_2$ , then two equations result and dividing one by the other gives;

$$\frac{t_2}{t_1} = \frac{\phi_2^{\frac{1-n}{n}}}{\phi_1^{\frac{1-n}{n}}} \quad \text{Eqn 2.3.11}$$

From the calorimetric power-time curve, two values of  $\Phi$  are selected (i.e.  $\Phi_1$  and  $\Phi_2$ ) that are a known percentage of the original calorimetric signal at  $t=0$  ( $\Phi_0$ ). From these two values (e.g. 99% and 50% of the original signal), the ratio of the two associated time values,  $t_2$  and  $t_1$  at  $\Phi_1$  and  $\Phi_2$  can be determined. This ratio is a constant value and is independent of the rate constant, the reaction enthalpy or the initial value of the signal at time  $t = 0$ .

i.e.

$$\frac{t_2}{t_1} \propto n \quad \text{Eqn 2.3.12}$$

where

$$n \equiv C$$

Using *Equation 2.3.12* and a computer spreadsheet such as Mathcad™, a table can be constructed showing the value of the  $t_2/t_1$  constant ( $C$ ) as a function of the reaction order for the given percentages of  $\Phi_1$  and  $\Phi_2$  (see *Table 2.3*).

**Table 2.3**

Reaction Order ( $n$ )	$t_2 / t_1$ ratio 99-80	$t_2 / t_1$ Ratio 99-50	$t_2 / t_1$ Ratio 99-20	$t_2 / t_1$ Ratio 99-5
0.1	10.01	11.54	11.56	11.56
0.3	17.51	34.58	42.13	43.10
0.5	20.00	50.00	80.00	95.00
0.7	21.22	59.79	115.93	168.22
0.9	21.94	66.41	146.71	253.68
1.1	22.41	71.15	172.36	342.46
1.3	22.75	74.70	193.70	429.09
1.5	23.01	77.45	211.57	510.89
1.7	23.20	79.65	226.68	586.78
1.9	23.36	81.44	239.59	656.55
2.1	23.49	82.93	250.72	720.44
2.3	23.59	84.19	260.41	778.87
2.5	23.68	85.26	268.91	832.31
2.7	23.76	86.19	276.43	881.25
2.9	23.82	87.00	283.12	926.16
3.1	23.88	87.72	289.11	967.46

*The values of the constant,  $C (t_2/t_1)$  corresponding to a given reaction order. There is an increase in discrimination of the constant  $t_2/t_1$  as the differences in the percentages of the chosen values odd  $dq/dt$  increase*

Use of this method requires there to be a significant difference between the two time points, and hence between  $\Phi_1$  and  $\Phi_2$  in order to determine accurately the reaction order. However, there must be sufficient time to allow the reaction to progress far enough to realise the selected lower fraction  $\Phi_2$ .

### Determination of $Q$

If it is possible to know  $n$  then it is possible to determine  $Q$  directly from calorimetric data. To determine  $Q$ , two points from the calorimetric power-time curve are selected, along with the associated integrated values of  $q$ . From *Equation 2.3.13*;

$$\Phi_1 = k \cdot H^{1-n} \cdot (Q - q_1)^n \quad \text{Eqn 2.3.13}$$

and

$$\Phi_2 = k \cdot H^{1-n} \cdot (Q - q_2)^n$$

and on dividing the equations;

$$\Phi_1/\Phi_2 = \frac{(Q - q_1)^n}{(Q - q_2)^n} \quad \text{Eqn 2.3.14}$$

Setting

$$R = \left( \frac{\Phi_1}{\Phi_2} \right)^{\frac{1}{n}}$$

then

$$R = \frac{(Q - q_1)}{(Q - q_2)} \quad \text{Eqn 2.3.15}$$

so that

$$Q \cdot (1 - R) = q_1 - Rq_2 \quad \text{Eqn 2.3.16}$$

or

$$Q = \frac{q_1 - Rq_2}{1 - R} \quad \text{Eqn 2.3.17}$$

A required assumption in the theory described above is that all the sample placed in the calorimeter would react given sufficient time. As a result of the new theory described below, it is now possible to determine *directly* the actual quantity of sample placed in the calorimeter that *will* react. Thus it becomes possible to determine additionally the equilibrium constant,  $K$ , for the reaction studied; together with the associated values of the Gibbs function and energy changes,  $G$  and  $S$ . Moreover, as the reaction is to be studied over a temperature range, the activation energy,  $E_a$  is also accessible.

## 2.4 The *Direct* Calculation of Reaction Parameters

It has previously been proposed that isothermal heat conduction microcalorimetry be used to determine thermodynamic and kinetic parameters for chemical reacting systems.<sup>14-19</sup> These conclusions have been subsequently been reached by Selzer *et al.*<sup>41</sup>. The disadvantage is that an iterative procedure is required to determine the desired quantities ( $n$ , the order of reaction,  $k$ , the rate constant,  $H$  the reaction enthalpy). The explicit assumption in applying the method is that all the sample placed in the calorimeter *would* react. This assumption is a severe constraint in the flexibility and application of the method (see earlier).

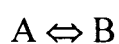
It would be useful, over a wide range of applications, to be able to determine the extent of reaction for a sample placed into the calorimeter. There is a requirement, therefore, to determine the equilibrium constant for a reacting system. The developed procedures should, for maximum utility, enable *calculation* of the required parameters (i.e. no requirement for iterative procedures). The calculations should result in values of the parameters listed above and, if it is possible to calculate the equilibrium constant,  $K$ , then since  $H$  is known, the Gibbs Function change  $G$ , and the entropy change,  $S$  should be calculable. The developed methods require that the reacting system be studied over a range of temperatures and, as a result, the availability of  $k$  as a  $f(T)$  allows, in addition, access to the activation energy,  $E_a$ .

The basic methods for constructing the calorimetrically based equations from the classical kinetic expressions have been well documented for  $n^{\text{th}}$  order reactions and for both sequential and parallel reaction systems.<sup>14-19</sup> It should be noted that, as is often true, first order kinetic reactions form a special case and hence both general solutions and solutions specific to the first order case will be presented.

The equations, which are developed below, have been tested against simulated calorimetric data and have been shown to be successful in allowing the determination of the parameters listed above.

### 2.4.1 The Equations for *Direct* Calculation of Solution Systems

The development of these equations will be explored through a simple reaction system;



where A and B refer to reactant and product *amounts* (it is simple to convert these equations into those described by concentrations – however, in the final equations it must be quantities that are used since  $H$  is a ‘per mole’ parameter which is essentially independent of concentration). A commentary on the simple extension of the equations to more complex reaction systems is given below.

Selzer *et al.*<sup>41</sup> note that, following identical earlier treatment of Willson *et al.*,<sup>30</sup> it is possible to write that the calorimetric output at time  $t = 0$  is given, for the general case, by

$$\Phi_0 = kHA^n_T$$

and for the first order case by

$$\Phi_0 = kHA_T$$

where  $A_T$  is the load placed in the calorimeter. Here, as subsequent development will show, this can be the total sample quantity. Thus a plot of  $\ln \Phi_0$  vs.  $\ln A_T$  will be linear with slope equal to the order of reaction  $n$  (this is also true for  $n = 1$ ). There is, however, a simple and direct test for a first order process that consists of simply plotting  $\ln \Phi_0$  vs.  $t$ . A linear plot results only from a first order reaction and the slope of this plot is  $-k$ , the first order rate constant. It is appropriate to identify  $A_T$  as the sample quantity loaded into the calorimeter since, if there is incomplete reaction (i.e.

an equilibrium exists between reactants and products), then the same fraction of any quantity loaded into the calorimeter will react at the given isothermal conditions. This has the consequence that the slope of the  $\ln\Phi_0$  vs.  $\ln A_T$  plot will always remain equal to  $n$  but the intercept value could vary. However the intercept value is not required in the subsequent development.

In general, the value of  $\Phi_0$  is not measured directly since the experimental procedures for the operation of isothermal heat conduction calorimeters require an initial equilibration period which can last, from the preparation of sample through the equilibration period. In order to obtain the appropriate value of  $\Phi_0$  it is necessary to develop a method that uses the experimental data recorded over the experimental observation period. We have concluded that the application of successively higher order polynomial fits to, say, the first 20 hours of experimental data allows successful extrapolation of the data for each experiment back to time  $t = 0$ . *Table 2.4* (from data simulated using Mathcad™) shows that for a range of values of  $k$  (over 10 orders of magnitude) and  $H$  (ranging from -10 to -100  $\text{kJ mol}^{-1}$ ) the correct value of  $\Phi_0$  is found as the limiting value of the first term in the polynomial fit equations.

Thus  $n$  is easily found.

## 2.4.2 Temperature Studies

### Theory

In the most general case, the total area under the  $\Phi$  vs.  $t$  curve from  $t = 0$  to  $t = \infty$  (here designated  $Q$  and associated with  $A$ , that fraction of the load that can react) can be calculated from the observation period of 50 hours or so. This value,  $Q$ , clearly represents the number of joules involved in the complete reaction of all the reactable material. This is expressed in this way to make clear the distinction between that amount that *will* react  $A$ , (associated with the number of joules  $Q_T$ , which would be observed if all the sample,  $A_T$ , had reacted.)  $Q$  can be calculated as follows (as outlined earlier)

$\Phi_1 = kH(A-x)^n$ ; here  $x$  is the number of moles of product formed at time  $t_1$ .

Recognising that  $A = Q/H$  and that  $x = q_1/H$  where  $q_1$  is the area under the curve from  $t = 0$  to  $t = t_1$ . Then the equation becomes:

$$\Phi_1 = kH^{1-n}(Q-q_1)^n.$$

Writing this equation again for  $t = t_2$  and dividing one equation into the other produces:

$$[\Phi_1/\Phi_2]^{1/n} = (Q-q_1)/(Q-q_2)$$

If  $[\Phi_1/\Phi_2]^{1/n}$  is set equal to  $R$  then  $Q$  can be calculated from:

$$Q = (q_1 - Rq_2)/(1-R)$$

For the first order case from  $\Phi = kH(A-x) = k(Q-q)$  and since  $k$ ,  $\Phi$  and  $q$  are known as a  $f(t)$  then  $Q$  can be determined.

### 2.4.3 Calculation of the Equilibrium Constant

For the reaction  $A \rightleftharpoons B$ , the equilibrium constant can be written as:

$K = B/A$  and, as here B is equivalent to the  $x$  used in the above kinetic equations then it is clear that  $B = Q/H$  and that  $A = (A_T - B) = (Q_T/H - Q/H)$ . Thus

$$K = (Q)/(Q_T - Q)$$

This expression can be written for studies at different temperatures ( $T_m = 1, 2$  and 3 say) and  $Q_T$  will have the same value if equal  $A_T$  is loaded into the calorimeter at each of the study temperatures or  $Q_T$  is normalised to a per gram or per mole basis. For a two state reaction the *van't Hoff isochore*<sup>42</sup> relates  $K$  and  $T$  through  $H/R$ . Thus it is possible to write;

$\ln(K_1/K_2) = -H/R (1/T_1 - 1/T_2)$ . This expression can be written again for temperatures 2 and 3.

Now provided the following equality holds

$T_1 T_2 / (T_2 - T_1) = T_2 T_3 / (T_3 - T_2)$  then it is easy to demonstrate that  $K_1/K_2 = K_2/K_3$ . From the expression for  $K$  given above this latter relationship can be expressed in terms of  $Q_m$  (for temperatures  $m = 1, 2, 3$ ) and  $Q_T$  and subsequently solved for  $Q_T$  as:

$$Q_T = (Q_2^2 Q_1 + Q_2^2 Q_3 - 2Q_3 Q_2 Q_1) / (Q_2^2 - Q_3 Q_1)$$

Since both  $Q_T$  and  $A_T$  are known then  $H$  is calculated from  $H = Q_T/A_T$ . Now  $H$  is known then it is easy to calculate  $A$  from  $A = Q/H$ .  $K$  is now clearly accessible and thus values of  $G$  and  $S$  follow from standard equations *viz.*  $G = -RT \ln K$  and  $G = H - TS$ .

For more complex equilibria such as  $A + 2B \rightleftharpoons C + D$  then provided that the quantities of A and B are known it will be possible to calculate the required  $K_s$ . The quantities of C and D formed can always be expressed through  $Q$  and  $Q_T$  with  $H$  being determined on, say, a 'per mole of A' basis.

Even if the quantities of A and B are not known it will be possible to evaluate the required parameters provided B is present at an essentially constant amount since in this circumstance one can formulate  $K'$  in the manner similar to that described above recognising now that  $K'$  is equivalent to  $K [B]$  (or as necessary, some form such as

$KH[B]$ ). Therefore a plot of  $\ln K'$  vs.  $1/T$  will again (always) yield the value of  $H$  from the slope.

To check the soundness of these equations, calorimetric data ( $\Phi$  vs.  $t$ ) were simulated via Mathcad™ software and for values of  $K$  from 0.5 to 50 and for  $H$  values from 10 to 100  $\text{kJmol}^{-1}$  the required values of  $Q_T$  were recovered. Hence all the target parameters were calculated.

It is of interest to note that in the case where  $A_T$  (say for a complex, unspecified sample) is not known but the reaction has a determinable order then the equations outlined above can still be employed.  $Q_m$  values are determinable for standardised loads placed into the calorimeter and studied over a suitable temperature range and a value of  $Q_T$  derived. That is models for an equilibrium reaction can be explored i.e. models could be fitted and an appropriate model which allowed calculation of a constant  $Q_T$  found. By appropriate is meant one which yields a linear plot of  $\ln K$  vs.  $1/T$  (here  $K$  is formed in an appropriate way in terms of  $Q$  and  $Q_T$ ; the necessary assumption is that the reaction under study conforms to the requirements of the *van't Hoff* isochore). The consequence of this approach is that from the *van't Hoff* relationship it will be possible to calculate the value of  $H$ . Possession of the value of  $H$  will permit calculation of the number of moles of potentially reactable material present in the sample from  $A_T = Q_T/H$  and the number of moles actually reacted,  $A$  from  $A = Q/H$ . As always such information does not contain any evidence relating to the *identity* of the reacting material.

A suitable test for a reaction system where there is either a dependence of  $\Delta_R C_P$  on temperature or a mechanism change (i.e. multiple reactions occurring simultaneously) over the temperature range is: calculate  $Q_T$  for temperatures  $m = 1,2,3$  and compare with the value calculated for temperatures  $m = 2,3,4$ . If there is conformity with the *van't Hoff* requirements then the values of  $Q_T$  must be independent of  $T$ . In principle, it may be expected that changing the temperature range significantly could emphasise one reaction over another thus reducing curvature in the *van't Hoff* plot, whereas the effect may be not so pronounced if the curvature was the result of the temperature dependence of  $\Delta_R C_P$ .

**Mathcad™ Worksheet – Calculating  $Q_T$** 

$$C := 0.004 \quad R := 8.314 \quad H := 60 \cdot 10^3 \quad T := 298$$

and from the *van't Hoff isochore* (where  $T$  is at first 298 K);

$$\ln(L) := \left( \frac{-H}{R} \right) \cdot \left[ \left( \frac{1}{T} \right) - \left( \frac{1}{298} \right) \right] + \ln(3)$$

(where 3 comes from  $k = 0.003 / (0.004 - 0.003) = 3$ )

$$\text{Hence } K := e^{\ln(L)} \quad \text{and } K = 3$$

From the equation  $K = X / (C - X)$ ,  $X = KC / (1 + K)$

$$\text{Therefore } X := \frac{(K \cdot C)}{(1 + K)} \quad X = 3 \times 10^{-3} \quad \text{at 298K}$$

$$\text{and } Q_1 := X \cdot H \quad \text{Hence } Q_1 = 180 \quad \text{at 298K}$$

Then simulate values for  $H$ ,  $C$ ,  $X$  and  $T$  where  $T$  is 303 K:

$$H := 60 \cdot 10^3 \quad C := 0.004 \quad T := 303 \quad R := 8.314 \quad \text{where } X \text{ is } 0.003$$

$$\text{Hence } \ln(L) := \left( \frac{-H}{R} \right) \cdot \left[ \left( \frac{1}{T} \right) - \left( \frac{1}{298} \right) \right] + \ln(3)$$

Where 3 comes from  $k = 0.003 / (0.004 - 0.003) = 3$ )

$$\text{Hence } K := e^{\ln(L)} \quad \text{and } K = 4.474$$

From the equation  $K = X / (C - X)$ ,  $X = KC / (1 + K)$

$$\text{and so } X := \frac{(K \cdot C)}{(1 + K)} \quad X = 3.269 \times 10^{-3} \quad \text{at 298 K}$$

$$\text{and } Q_2 := X \cdot H \quad Q_2 = 196.155 \quad \text{at 303 K}$$

Finally, simulate values for  $H$ ,  $C$ ,  $X$  and  $T$ , when  $T$  is 308.2 K;

$$H := 60 \cdot 10^3 \quad C := 0.004 \quad T := 308.2 \quad R := 8.314$$

And putting these three values together allows us to calculate  $Q_T$ ;

Hence

$$\ln(L) := \left( \frac{-H}{R} \right) \cdot \left[ \left( \frac{1}{T} \right) - \left( \frac{1}{298} \right) \right] + \ln(3)$$

(where 3 comes from  $k = 0.003 / (0.004 - 0.003) = 3$ )

$$\text{Hence } K := e^{\ln(L)} \quad \text{and} \quad K = 6.687$$

From the equation  $K = X / (C - X)$ ,  $X = KC / (1 + K)$  )

$$\text{Therefore } X := \frac{(K \cdot C)}{(1 + K)} \quad X = 3.48 \times 10^{-3} \quad \text{at } 298 \text{ K}$$

$$\text{and } Q_3 := X \cdot H \quad \text{Hence } Q_3 = 208.776 \quad \text{at } 298 \text{ K}$$

$$Q_1 := 180 \quad Q_2 := 196.155 \quad Q_3 := 208.776$$

$$Q_T := \frac{\left[ (Q_2^2 \cdot Q_1) + (Q_2^2 \cdot Q_3) - (2 \cdot Q_3 \cdot Q_2 \cdot Q_1) \right]}{(Q_2^2) - (Q_3 \cdot Q_1)} \quad Q_T = 240.737$$

And the percentage agreement between this calculated and chosen values of  $Q$  equals

$$\left( \frac{Q_T}{0.004 \cdot 60 \cdot 10^3} \right) \cdot 100 = 100.307$$

where  $Q_T$  (chosen) is calculated from multiplying the chosen value of  $C$

- the quantity placed in the calorimeter that can react multiplied by  $H$  (where  $Q_T = A \cdot H$ )

From this 100% agreement, we can confidently conclude that the theoretical different temperature method works.

ie. as long as the experiment is carried out at 298, 303 and 308.2 K, it is possible to calculate the amount of material that actually reacts in the calorimeter, with a knowledge only of the mass of material that can react.

Two assumptions:

- a) That the same amount of material reacts at each different temperatures
- b) That  $H$  is unchanged at different temperatures

This theory can now be tested for practical application

## 2.5 The *Direct* Calculation of *Solid State* Reaction Parameters

Until the development of the solution-phase direct method of parameter calculation described in *section 2.4*, all data were analysed via the iterative procedure described at the beginning of this chapter. For integral order solution-phase reactions, this was a satisfactory procedure. However, for reactions in the solid-state which are not normally of integral order, a new approach to data analysis must be sought.

The fitting parameters expressed in the (modified) Ng equation<sup>10</sup>  $m$  and  $n$  (*Equation 2.5.1* below) are not usually integral and the equations are complicated. The Ng equation can be described as a common equation that defines most solid-state reactions.

$$\frac{d\alpha}{dt} = k(1-\alpha)^n(\alpha)^m \quad \text{Eqn 2.5.1}$$

where  $\alpha$  is the fractional extent of reaction at time  $t$

and  $k$  has the units of  $s^{-1}$  and is a rate coefficient and not a rate constant

The majority of solid-state calorimetric studies consider reactions that can be measured over relatively short times to significant fractional extents ( $\alpha$ ) of completion. It is regarded as essential to obtain values for the activation energy and pre-exponential factor. From these data, it is hoped that accurate explanations of kinetic behaviour can be made. Galwey and Brown<sup>43,44</sup> have discussed, at a theoretical level, isothermal kinetic analysis of solid-state reactions using plots of rate vs. derivative function of the rate equation.

The work detailed below seeks to extend the application of isothermal heat conduction microcalorimetry into the area of longer, slower solid-state reactions. As for solution-phase reactions, only a small extent of reaction can be observed and the data used for analysis. 50 hours is normally sufficient to allow the determination of  $k$ ,  $n$  and  $H$  for a reaction that has a first order rate constant, for example, of  $10^{-11} s^{-1}$ . It will be necessary, therefore, in addition to developing the equations, to have to use simulated

data to test the derived equations. Also, it is important to determine the minimum data set required to allow proper specification of the simulated solid-state reaction system. The model only used to achieve this will be the Ng equation.

### 2.5.1 Theoretical Development

Calorimetric forms of the Ng equation have been previously written <sup>7</sup> and analysed <sup>9</sup> through an iterative procedure i.e. values of  $n$  and  $m$  were sought in addition to those for  $H$  and  $k$ . (For solid-state reactions,  $k$  is the rate co-efficient). In *Equation 2.5.2*,  $Q$  is the total number of joules involved in the reaction to time  $t = \infty$  and  $q$  is the number of joules involved up to any time  $t$ . Thus  $\alpha$  can be set equal to  $q/Q$  and *Equation 2.5.1* becomes:

$$\Phi = kQ \left[ 1 - \left( \frac{q}{Q} \right) \right]^n \left( \frac{q}{Q} \right)^m \quad \text{Eqn 2.5.2}$$

The need to determine  $n$  and  $m$  in addition to  $k$  and  $H$  increases the demand on the iterative procedure.

Following the capacity to directly determine reaction parameters in the solution-phase <sup>15, 16</sup> attention was turned to directly calculating parameters for solid-state reactions. The equations developed and their applications to simulated data are outlined below. The use of simulated data allowed the examination of the utility of the outlined procedures and hence to specify the accessible range.

As for the direct calculation of the parameters in solution-phase reactions <sup>15, 16</sup> the first problem in the analysis of microcalorimetric data is the determination of the order (or in the case of the Ng equation) the fitting parameters of  $m$  and  $n$ . A recently-described procedure <sup>34</sup> now permits these values to be determined from a method which relies only on the knowledge of the values of  $\Phi$  and  $q$  for paired time points

throughout the power-time curve ( $\Phi$ - $t$ ) recorded during the observation period. Note that the observation period is not set to  $t = \infty$ , i.e.  $Q$  is not measured experimentally.

Given that  $m$  and  $n$  can be calculated from paired ( $\Phi$ - $t$ ) values, then from inspection of *equation 2.5.2*, the issue is to determine (not measure) the value of  $Q$ . This again can be achieved through the use of paired data points. Writing *Equation 2.5.2* for two data points and forming the ratio between them yields *Equation 2.5.3*:

$$\frac{\phi_1}{\phi_2} = \frac{\left(1 - \frac{q_1}{Q}\right)^n \left(\frac{q_1}{Q}\right)^m}{\left(1 - \frac{q_2}{Q}\right)^n \left(\frac{q_2}{Q}\right)^m} \quad \text{Eqn 2.5.3}$$

If now the values of  $q_1$  and  $q_2$  are selected such that  $q_2$  is a known factor of  $q_1$  (e.g. that  $q_2$  is equal to  $cq_1$  and hence  $q_2/q_1 = c$  and setting  $R$  as:

$$R = \left[ \frac{\phi_1}{\phi_2} (c)^m \right]^{\frac{1}{n}} = \frac{\left(1 - \frac{q_1}{Q}\right)}{\left(1 - \frac{cq_1}{Q}\right)} \quad \text{Eqn 2.5.4}$$

Then *equation 2.5.4* is solvable for  $Q$ :

$$Q = \frac{q_1(cR - 1)}{(R - 1)} \quad \text{Eqn 2.5.5}$$

Possession of  $m$ ,  $n$  and  $Q$  allows calculation of  $k$  for each value of  $\Phi$ . Thus the arithmetic appears straight-forward and the remaining issue is the range of application of the equations.

Firstly all ranges of values for  $m$  and  $n$  (they each range between 0 and 1, and the particular combination of values describes<sup>10</sup> the mechanism of the process under

study) are determined<sup>34</sup> from the proposed method. The issue is how much data is required in order to fully determine  $Q$  and hence  $\alpha$  (equal to  $(q/Q)$ ) at any time  $t$  then to determine  $k$ , the rate coefficient and hence the reaction lifetime. Clearly, determination of both  $\alpha$  and of  $k$  allows calculation of an appropriate shelf life for, for example, a pharmaceutical product.

### 2.5.2 Data simulation and manipulation

As noted in the introduction, simulated data has been used to establish the minimum value for  $\alpha$  (i.e.  $(q/Q)$ ) for given values of  $m$  and  $n$  that allows characterisation of the model system. As previously carried out for solution-phase systems<sup>15</sup>, programmes were written in Mathcad<sup>TM</sup> to allow data simulation. However, in this instance, these data were exported to Microsoft Excel<sup>®</sup> for calculation of values of  $Q$  and  $k$ . Comparison of the set values with the calculated values allows the minimum range of  $\alpha$  to be specified.

For the simulation of data for the values of  $m$ ,  $n$ ,  $Q$  and  $k$ , data were simulated using MathCad<sup>TM</sup> for solid state reactions where  $Q$  ranged from 10-10000  $J$ ; the rate coefficient,  $k$ , ranged from  $10^{-4} - 10^{-8} s^{-1}$  and values for  $m$  and  $n$  between 0 and 1. Data were produced in the form of  $\Phi$  vs.  $q$  for a range of values of  $\alpha$  up to a maximum of  $\alpha = 1$ . The data were then analysed using an algorithm written in Microsoft Excel<sup>®</sup> and values of  $Q$  calculated for varying ratios of  $\Phi_2 / \Phi_1$  (where  $\Phi_2$  was fixed as the value of  $\Phi$  when  $\alpha$  is at a maximum). It can be shown that from an  $\alpha$  value as small as around 0.01 (when  $Q$  is assigned a value of 100  $J$ ) it is possible to recover the correct values for the target parameters. It should be noted that for successful analysis, the ratio of  $\Phi_2 / \Phi_1$  should be as large as possible. As the value of  $\Phi_1$  approaches  $\Phi_2$  (i.e.  $\Phi_2 / \Phi_1$  approaches 1) the analysis becomes more difficult. The separation required between  $\Phi_1$  and  $\Phi_2$  depends on the values of  $Q$  and  $\alpha$ . If  $Q$  is small then  $\alpha$  must be large enough to allow sufficient separation between  $\Phi_1$  and  $\Phi_2$ .

The maximum required value of  $\alpha$  depends on the value of  $Q$ ; the maximum value of  $\alpha$  required for satisfactory analysis is 0.1 for solid state reactions with values of  $Q$  as low as 2  $J$ . That is, long, slow reactions of solids are amenable to study. Without

specifying the time base, data sets of 17000 points were used in these analyses. It would therefore appear that from these simulated data, it should be possible to identify the appropriate values for  $m$ ,  $n$ ,  $Q$  and  $k$  for real reaction systems. Furthermore, the necessary extent of reaction to permit this analysis is very small. This is in contrast to the more classical procedures where, for example,  $\alpha$  values are required<sup>45</sup> to range up to 1 (i.e. the reaction should approach completion). Note this analysis does not rely upon the exploration of particular models of the reaction process (except that the defining equation is the Ng equation<sup>10</sup>). The data analysis returns values for the target parameters which may conform to a model. This approach could therefore be regarded as relatively model-free.

### 2.5.3 Conclusions on the approach

The data presented above demonstrates from a theoretical development and simulation trial, that it is

1. Possible to make *direct* calculation of values for the target parameters  $m, n, k$  and  $Q$
2. Apparent that simulated data for fractional extents of reaction as low as  $\alpha = 0.01$  will allow such calculations

These outcomes give confidence to pursue the practical exploitation of this new approach.

## *CHAPTER 3*

# *CALORIMETRIC VALIDATION TECHNIQUES*

### 3. Calorimetric Validation Techniques

As previously stated in my MSc Thesis,<sup>46</sup> any calorimetric analysis of reactions must be preceded by a process of validation of the calorimeter.

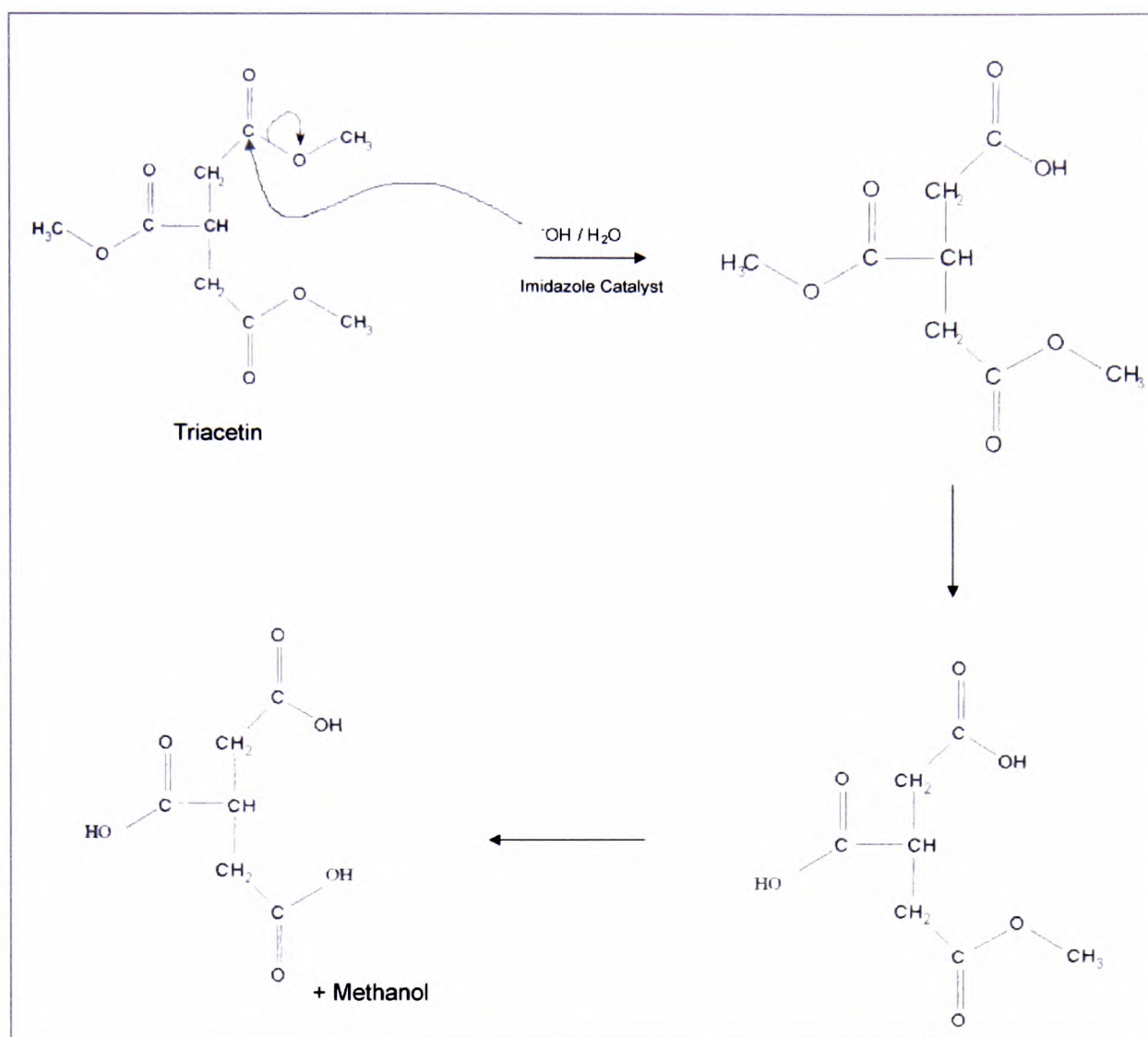
The *imidazole*-catalysed hydrolysis of *triacetin* has been previously suggested<sup>13-14</sup> as a suitable test reaction for a solution-phase system. The use of this system as a test reaction will be discussed here. Additional studies into the application of the *triacetin* reaction will also be reported; including the effect of fill-volume on derived reaction parameters of rate constant and enthalpy and the effect on sample position within an ampoule.

For the validation of the photocalorimeter, a number of test reactions have been discussed in the literature<sup>18-22, 47-52</sup> with the photoreduction of *potassium ferrioxalate* officially adopted,<sup>19, 20</sup> although this system is not without its limitations

Another potential solution-phase test reaction for the photocalorimeter is the photodegradation of *2-nitrobenzaldehyde* to form *2-nitrobenzoic acid*.<sup>21, 22</sup> These will both be discussed at length in *chapter five*.

#### 3.1 The *Imidazole*-Catalysed Hydrolysis of *Triacetin*

There have been several proposals for a suitable test reaction for the isothermal microcalorimeter. However, no quantitative data could be obtained using such reactions, limiting their application. The *imidazole*-catalysed hydrolysis of *triacetin*, proposed by Wadso<sup>14, 36, 53</sup> is a medium-term solution-phase reaction with an apparently simple and constant mechanism for the reaction half-life. This reaction has been proposed as an international test reaction since its kinetic and thermodynamic parameters are well-known and robust when obtained from a standard testing protocol. The hydrolysis of *triacetin* involves three reaction sites where the hydrolysis of a methyl ester group occurs;



**Scheme 3.1** The imidazole-catalysed hydrolysis of triacetin

Laboratories worldwide have compared results for this reaction, following a standard protocol<sup>33</sup> to produce values of the thermodynamic and kinetic parameters which have been published in the literature<sup>14, 53</sup>

The reliability of the reaction in terms of the obtaining the correct reaction parameters is useful in the following applications:

- training – new operators have a “correct” set of values to aim for
- trouble-shooting – experienced operators of a calorimeter can use the reaction to test for successful solving of an operational problem
- new instrument validation

NB A recent paper has dealt extensively with sources of error and their correction in the analysis of this reaction. <sup>54</sup>

### 3.1.1 Standard 3ml Test Reaction

#### Experimental Method – 3ml test

TAM Temperature: 298K

Buffer Solution: 1.6g acetic acid, 2.72g imidazole  
Make up to 10ml with deionised water

Reaction Solution: weigh 0.267g triacetin  
make up to 5ml with buffer solution  
mix thoroughly – triacetin is not readily soluble  
note time of addition of buffer to triacetin (this is time  $t = 0$ )

- 3ml of reaction mixture and 3ml of buffer were pipetted into the sample and reference ampoules respectively
- The ampoules were lowered into the “load” position in the TAM
- After 30 minutes, the ampoules were lowered into the measuring position
- The data recording was started immediately and the time elapsed since the addition of buffer was noted
- The data was exported into Origin™ (Microcal, Amherst, MA, USA) a graphics fitting program

The resultant data for the 2<sup>nd</sup> order reaction was fitted to the following equation:

$$\Phi = -HVk \left[ \frac{(A_0)}{1 + (A_0)kt} \right]^2 \quad \text{Eqn 3.1.1}$$

where  $\Phi$  is the thermal power  
 $k$  is the reaction rate constant  
 $H$  is the reaction enthalpy change  
 $(A_0)$  is the initial concentration of *triacetin*  
 and  $V$  is the volume of solution placed in the calorimeter

In the fitting procedure,  $V$  and  $(A_0)$  are fixed (i.e. the values are known), whilst  $k$  and  $H$  are allowed to vary. This procedure has been described previously in *chapter two*. The plot of  $\Phi$  vs. time, along with the iterative fit line can then be produced.

## Results

Figures 3.1.1, 3.1.2 and 3.1.3 below are typical plots for the *triacetin* run procedure described above. In each case, the red line indicates the region of the plot analysed by Origin™;

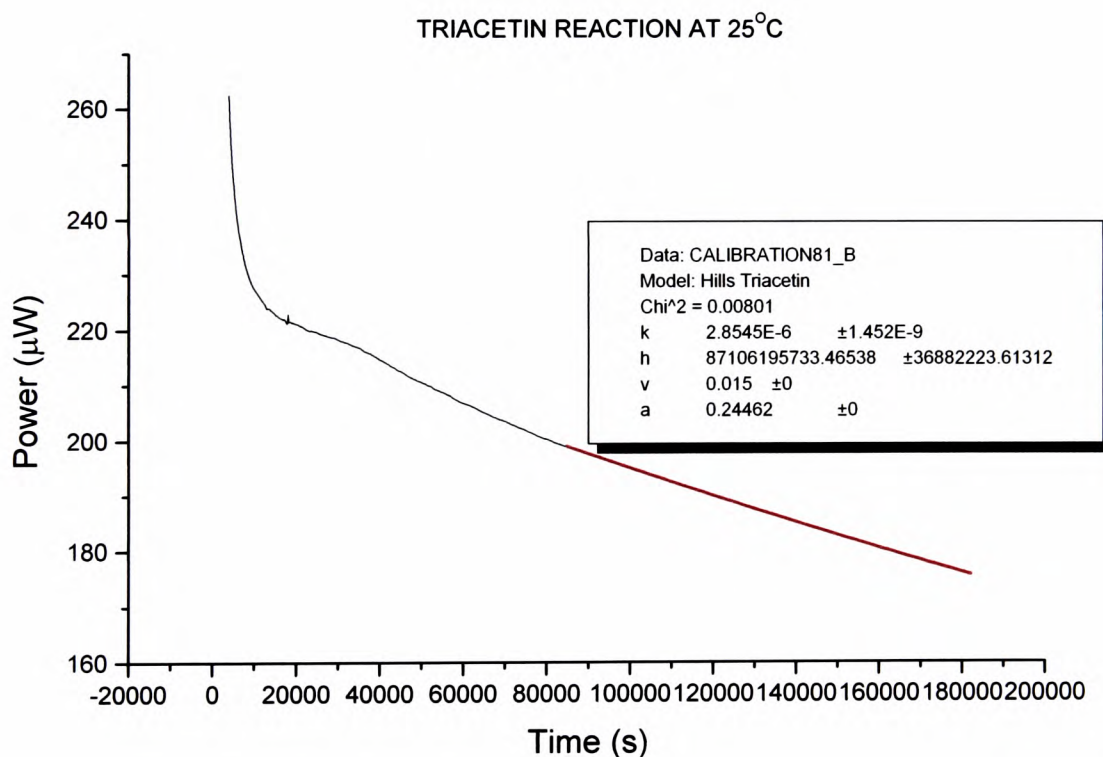


**Figure 3.1.1** A plot showing the iterative fit of triacetin data showing the iterated values of  $k = 2.9 \times 10^{-6}$  and  $H = -87.1 \text{ kJmol}^{-1}$

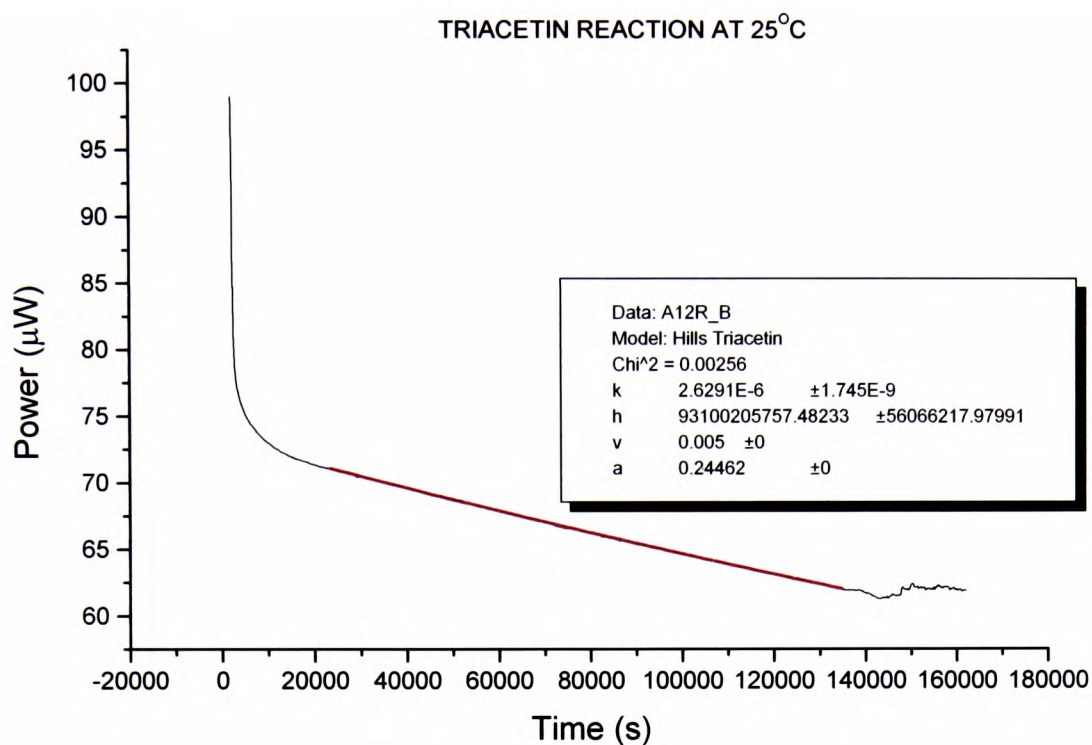


**Figure 3.1.2** A plot showing the iterative fit of triacetin data showing the iterated values of  $k = 2.6 \times 10^{-6}$  and  $H = -93.1 \text{ kJmol}^{-1}$

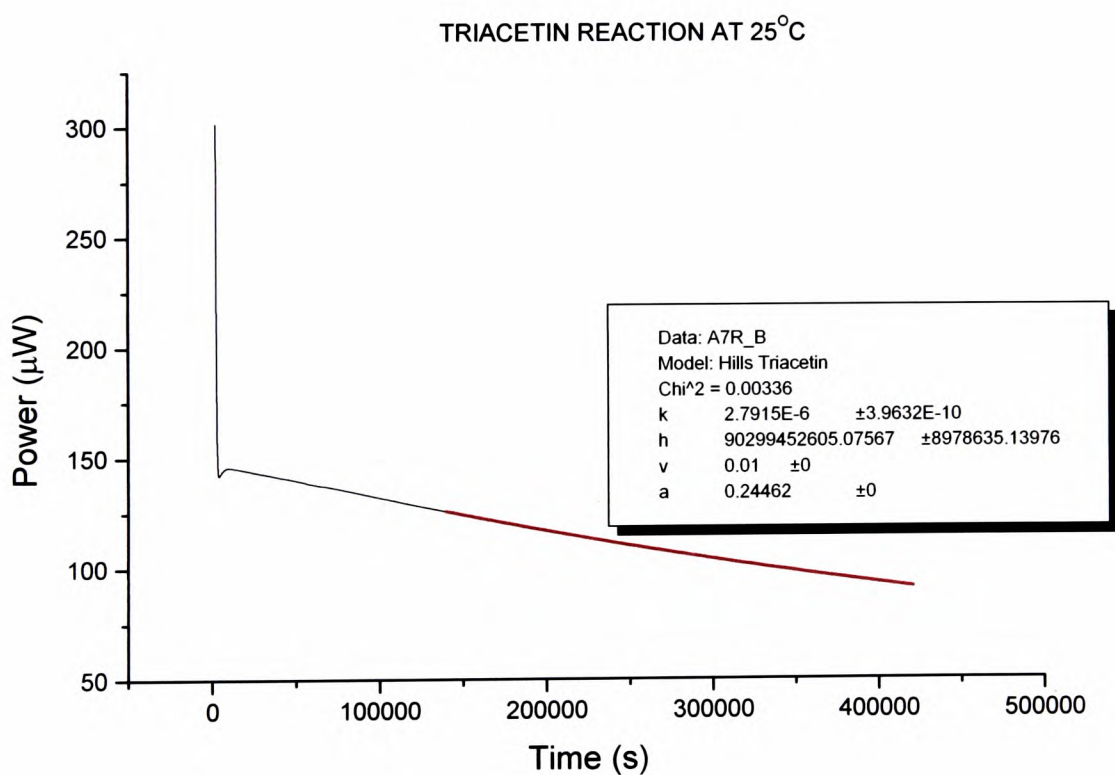


**Figure 3.1.3** A plot showing the iterative fit of triacetin data showing the iterated values of  $k = 2.8 \times 10^{-6}$  and  $H = -90.3 \text{ kJmol}^{-1}$

Only the later hours of the recorded reaction need to be analysed for the *triacetin* reaction. In the examples above, the iterative process was carried out once the initial “thermal shock” that the calorimeter exhibits early on, caused by the loading and lowering of the ampoules into the chamber had been fully negated. The time taken for this “calming” process was previously established by loading and lowering empty ampoules into the calorimeter.

### 3.1.2 International Testing of the Reaction

*Figure 3.1.4* shows the values of  $k$  and  $H$ , obtained as a result of the iterative process. These values can be compared with those obtained by various institutions around the world. The published figures are reproduced in *Table 3.1 (abridged)* and incorporate the experiments plotted in *Figures 3.1.1, 3.1.2* and *3.1.3* above:

**Table 3.1 International Triacetin Results**

Experiment Number <sup>33</sup>	Originator	$[A_0]$ ( $\text{mol dm}^{-3}$ )	$V$ ( $\text{dm}^3$ )	$H$ ( $\text{kJ mol}^{-1}$ )	$k$ ( $\text{dm}^3 \text{mol}^{-1} \text{s}^{-1}$ )
1	Hills	0.245	0.003	-89.39	$2.98 \times 10^{-6}$
2	Hills	0.245	0.003	-96.20	$2.61 \times 10^{-6}$
3	Hills	0.245	0.003	-91.40	$2.83 \times 10^{-6}$
4	Lane <i>et al.</i>	0.245	0.003	-95.76	$2.73 \times 10^{-6}$
5	Lane <i>et al.</i>	0.245	0.003	-87.74	$2.96 \times 10^{-6}$
6	Lane <i>et al.</i>	0.245	0.003	-92.18	$2.85 \times 10^{-6}$
7	Wolf <i>et al.</i>	0.245	0.009	-89.60	$2.81 \times 10^{-6}$
8	Wolf <i>et al.</i>	0.245	0.009	-90.90	$2.84 \times 10^{-6}$
9	Wolf <i>et al.</i>	0.245	0.009	-97.30	$2.62 \times 10^{-6}$
10	DSC	0.245	0.005	-93.70	$2.76 \times 10^{-6}$
11	DAK	0.245	0.005	-91.80	$2.89 \times 10^{-6}$
12	Kierstan	0.245	0.003	-90.03	$2.80 \times 10^{-6}$
13	Kierstan	0.245	0.003	-92.41	$2.78 \times 10^{-6}$
14	Kierstan	0.245	0.003	-95.53	$2.69 \times 10^{-6}$
15	O'Neill	0.245	0.003	-91.11	$2.79 \times 10^{-6}$
16	O'Neill	0.245	0.003	-94.03	$2.75 \times 10^{-6}$
17	O'Neill	0.245	0.003	-85.87	$2.82 \times 10^{-6}$
18	Morris	0.245	0.003	-93.10	$2.60 \times 10^{-6}$
19	Morris	0.245	0.003	-90.30	$2.80 \times 10^{-6}$

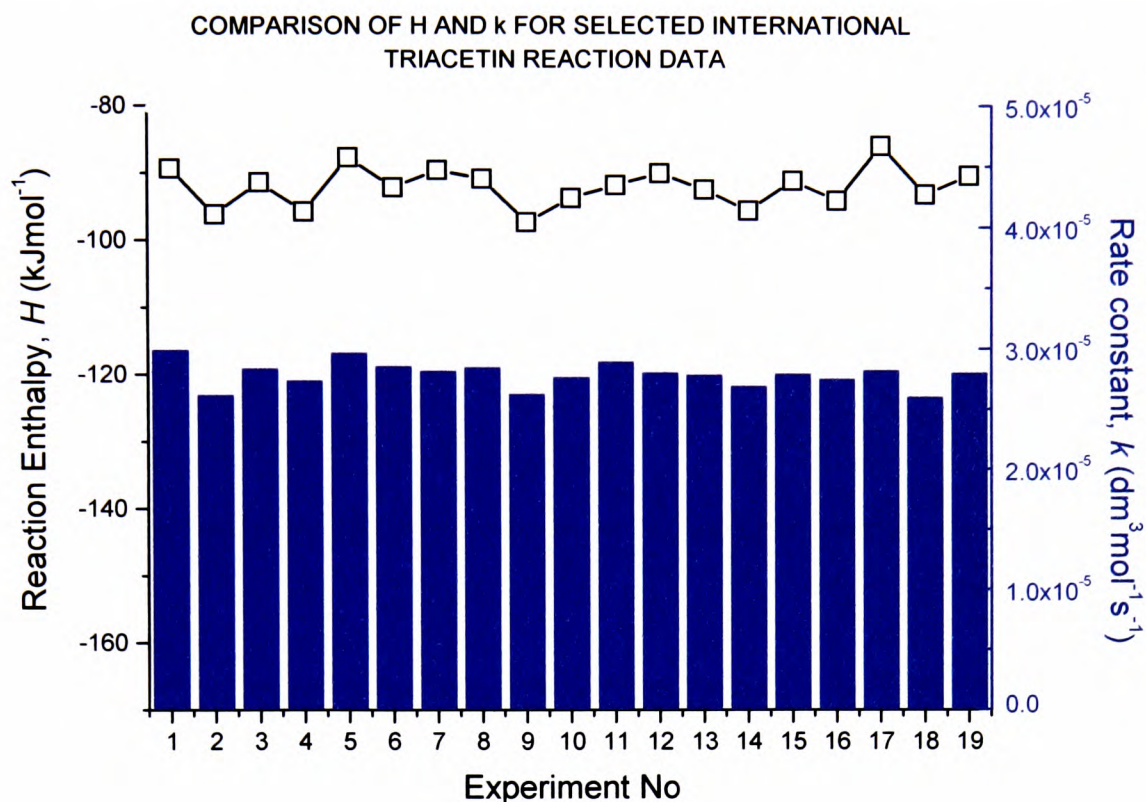


**Figure 3.1.4** Chart showing comparative values of the iterative fit for triacetin

### 3.1.3 Conclusion

The values for  $k$  and  $H$  obtained for the three examples reported in *section 3.1.1* happily fit within the data set of the international test results described in *section 3.1.2*. Indeed, it is clear from *figure 3.1.4* that as long as the Hills protocol is followed consistently, the *imidazole*-catalysed hydrolysis of *triacetin*, is a reaction that meets the criteria required of an international test reaction for validation of the microcalorimeter. Indeed it has also been demonstrated here that other calorimeters beside the TAM, such as the DSC can also be tested using this reaction.

The accepted error for the parameters produced for the reaction is  $\pm 3\%$  and consideration of the values for  $H$  and  $k$  entered in *Table 3.1*;

**Reaction enthalpy,  $H$ :**

Mean = -92.01

SD = -2.96

% error = 3.22

**Rate constant,  $k$ :**Mean =  $2.78 \times 10^{-5}$ SD =  $1.05 \times 10^{-6}$ 

% error = 3.76

It is clear that the errors produced stand up pretty well considering results were gained worldwide from a variety of scientists using a variety of different supplier's chemicals on more than one type of instrument.

The results also demonstrate that any discrepancy in the numbers produced when carrying out the test are probably the result of either operator error or instrument malfunction. It is unlikely to be errors originating in the chemical reaction.

The iterative process described above produces reliable evaluation of the parameters  $k$  and  $H$  which can be used in future *triacetin* reaction studies described later in this chapter. It should be noted however that, as described in *chapter two*, an alternative method of calculating the parameters *directly* without the need of the iterative process has since been developed. *Triacetin* studies in the future will be better carried out using this new method of analysis.

NB A full list of experimental data relating to this collaborative study can be found in A K Hills' thesis, 2000. <sup>33</sup>

### 3.1.4 Test Reaction – Considerations of other Test conditions

Having established the reliability and robust nature of the *triacetin* reaction described above, attention is now turned on taking advantage of these qualities to investigate how varying the test conditions of this experiment may affect the result.

As outlined in the introduction to this thesis, the ultimate aim is to develop a photocalorimeter that can analyse solid-state reactions. Consider a solid material packed in a column which is then exposed to the atmosphere. It is unlikely that oxygen and water vapour etc will be able to penetrate much below the surface of the solid meaning that all reactions that take place will be superficial. The same situation exists in the case of irradiance where photoreaction will only take place on or just below the surface of the solid. A monolayer of solid will only undergo reaction, therefore and tests must be carried out to simulate this before photocalorimetry can be carried out.

This is achieved in the solution-phase by testing the effect of fill-volume of *triacetin* within an ampoule on the kinetic and thermodynamic parameters obtained calorimetrically.

#### 3.1.4.1 Variable Fill Volume and Sample Position

No previous studies have been carried out into the effect of changing the volume of *triacetin* placed in an ampoule when carrying out a test. The effect of the position of a sample within an ampoule (i.e. the top, middle or bottom of the vessel) has also not been investigated.

It must be established whether an ampoule that is partially filled with reaction solution (e.g. 25%) gives the same results for the reaction parameters as an ampoule that is 50% or 100% filled. If there are discrepancies between results at different values, then it must be established whether there is a minimum fill volume (or fill fraction) that is required to produce an acceptable set of results for the *triacetin* reaction. Further, if a minimum volume sample is established, what is the importance of adjusting its position within the ampoule? For example, does the sample placed at the bottom of the ampoule give the same parameters as a sample placed in the middle or the top?

### Variable Fill Volume Study – 20ml Ampoules

Using 20ml reusable stainless steel ampoules, the fill-volume study was carried out at 298K using exactly the same triacetin test conditions and protocol described above with solution fill volumes ranging from 2.5ml to 20.0ml. The sample solution was placed in the left hand side of the TAM, with the reference of buffer placed in the right. Each volume was tested in duplicate and the iterative procedure, described previously, used to produce values for the rate constant,  $k$  and reaction enthalpy  $H$ . The results were then compared graphically with each other and also with the “correct” value given in the literature. These are shown below;

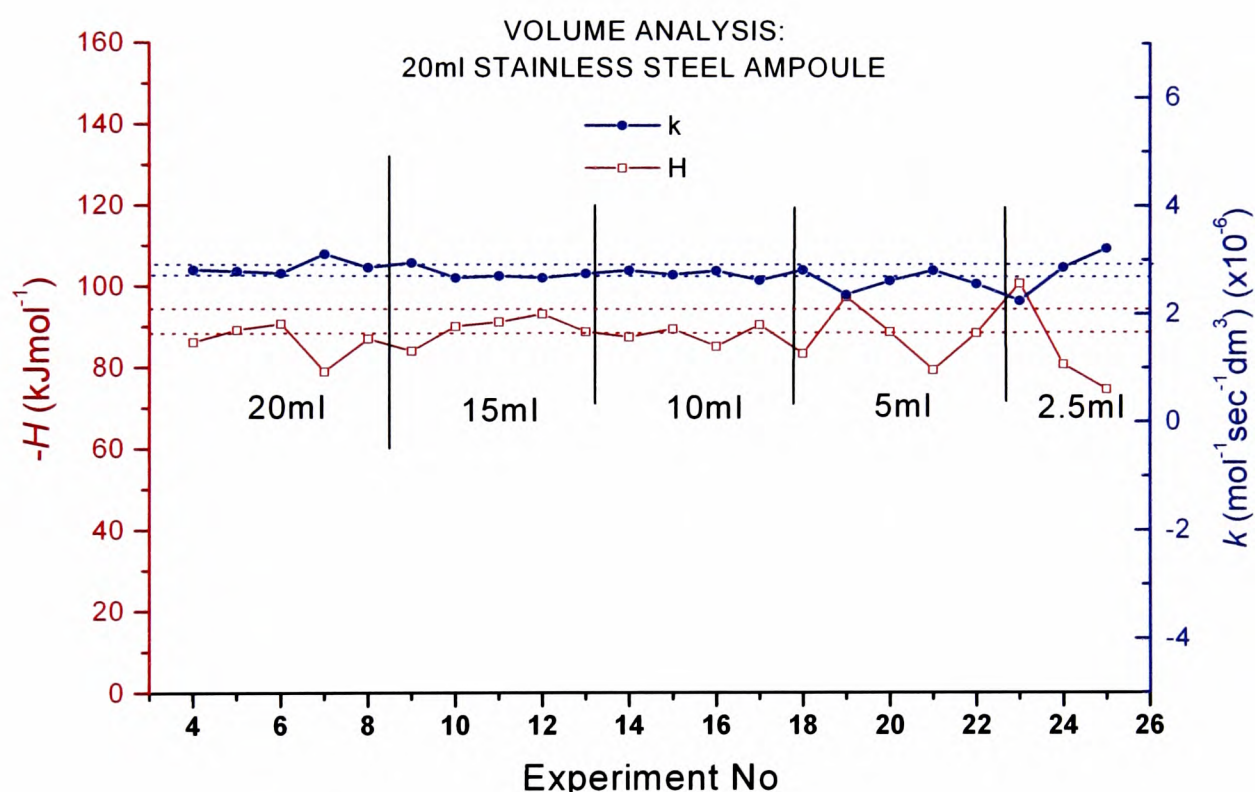


**Figure 3.1.5** Variance of enthalpy and rate constant with decreasing fill volume

It can be seen that decreasing fill volumes lead to increasingly poor values of both the rate constant and reaction enthalpy. It is reasonable to say that between 10ml to 20ml (50% fill volume) the results are repeatable and accurate. However, at 5ml the results are more variable; whilst below 5ml fill, it could be considered unrealistic to derive

accurate values for  $k$  and  $H$ . This may have a detrimental effect on solid state work where a fill volume of below  $5\text{ml}$  may be quite a common scenario to face.

### 3.1.4.2 Variable Fill Volume Study – $3\text{ml}$ Ampoules

Following the  $20\text{ml}$  tests reported above, a similar study was carried out using disposable glass  $3\text{ml}$  ampoules<sup>17</sup>. Under the same test conditions as before, the range of fill volumes went from  $0.5\text{ml}$  to  $3.0\text{ml}$ . Again, the results are compared graphically below;

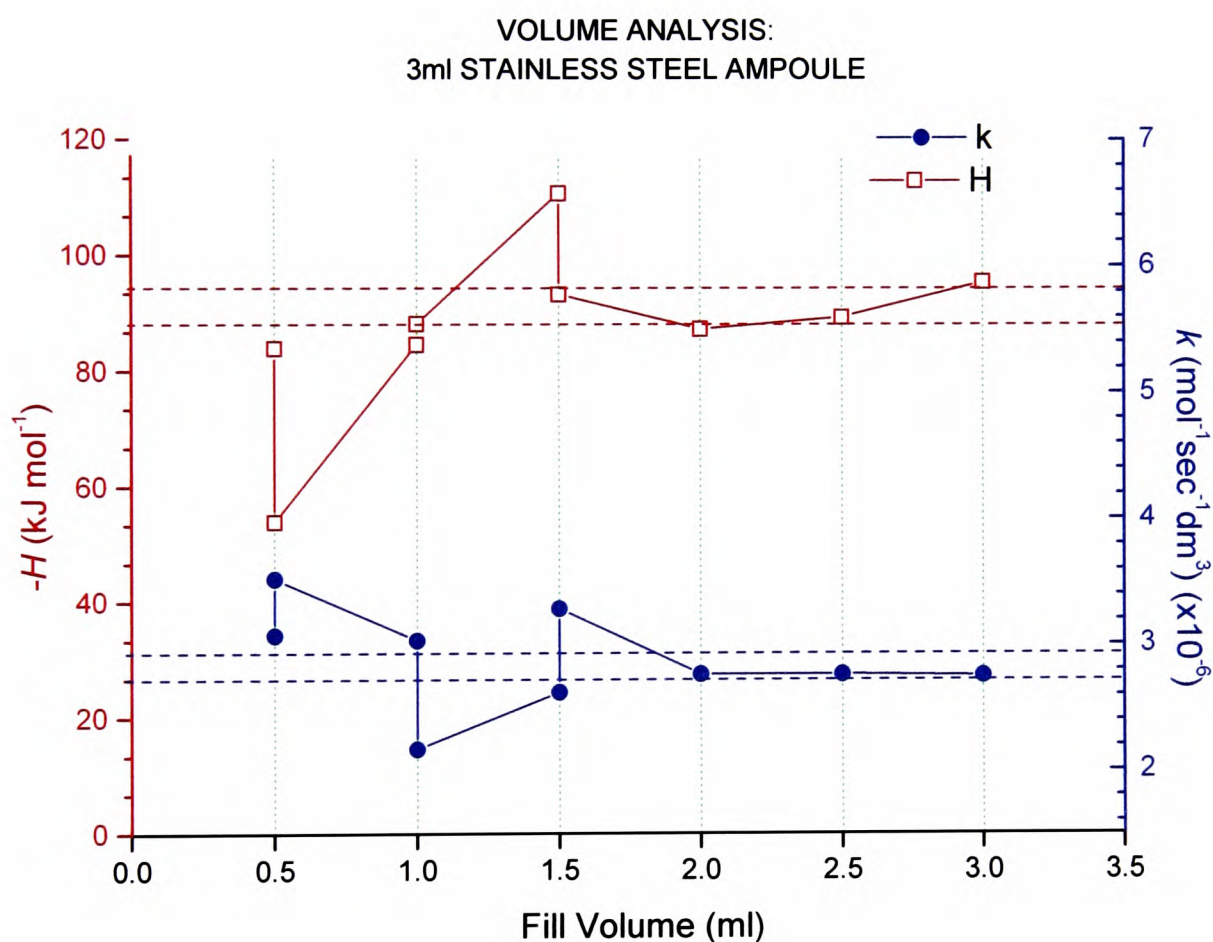


*Figure 3.1.6* Variance of enthalpy and rate constant with increasing fill volume

Clearly, similar trends exist for the  $3\text{ml}$  system as for the  $20\text{ml}$  system.

For both systems, the results suggest the test conditions are best from the point of 50% volume fill and upwards; but slightly diminished, surprisingly, at 100% fill volumes in both cases.

From this observation, there are two factors that need to be considered as possible explanations;

- Signal / noise ratio changes
- Sample position within chamber

### **Signal / Noise Ratio**

A consequence of reducing the volume of solution present in the ampoule is that the ratio of signal to noise is reduced, leading to detection problems for the TAM.

A useful experiment in the future in this area will be to increase the concentration of triacetin, leaving the solution volume unchanged.

### **Sample Position**

A lot of the explanation of why sample position is important comes from the design of the 20ml calorimetric chamber where an array of sensitive thermopiles runs the entire vertical length of the ampoule when in the measuring position (*Figure 3.1.7*). “End effects” must be considered as a cause of the erratic nature of the results observed for the low fill and high fill volume ends of the experimental range described above for the 20ml system.

The 3ml system is of a different design where the ampoules do not cover the entire vertical length of the system. However, the same reasons for the change of signal with sample position can be applied here.

The system used for the photocalorimeter features the 20ml design upon which attention will be focussed.

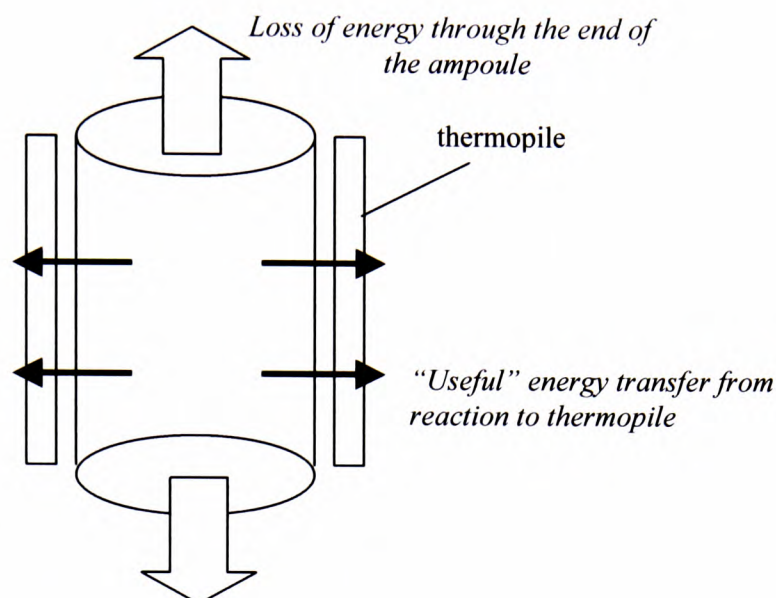


**Figure 3.1.7** Illustration of how “end effects” may affect the repeatability of the results

It is known that the column of liquid under test in the ampoule is subject to losses because of heat conduction through the top and bottom ends of the ampoules (i.e. the bottom and the lid). In these positions, thermal conduction is maximised possibly leading to errors. At minimum fill volume conditions, the “end effect” is at its greatest since the surface area of a greater proportion of the total system than it would be at higher fill volumes. At maximum fill, as the top of the ampoule is approached by the test solution, the second “end effect” comes into play. From these observations and thoughts, it is probable that best results are achieved somewhere just below 100% fill, and it may therefore be of significant benefit to try experiments raising the sample away from the bottom of the ampoule into somewhere towards the middle.

Using the *triacetin* reaction and its expected output parameters, a series of experiments was carried out using a custom-built pair of inserts, to establish the effect of sample position on calorimetric output.

The inserts are shown below.

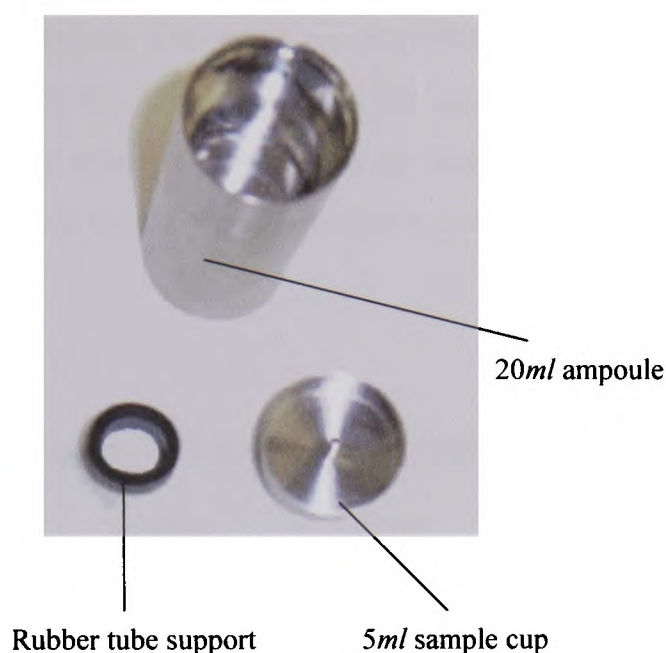


**Figure 3.1.8** 20ml Stainless Steel calorimetric ampoule together with custom-made inserts

The 5ml volume cups are of a slightly smaller diameter than the ampoule to allow insertion and removal and feature a small air-hole in the centre which is raised above the bottom of the cup to prevent leakage of the test-solution. To allow the cup to sit at the desired position of testing within the ampoule, a duplicate series of small rubber tubes were cut to various lengths. These were then placed on the ampoule floor and the cup sat on the top. This setup is illustrated in *figure 3.1.8* above.

NB Care was taken to ensure that the inserts were made to be identical as possible for both sides of the differential system. For a sensitive instrument, such as the TAM, small differences in the contents of the left-hand and right-hand sides of the system could introduce significant imbalances to the thermal contact of each side of the instrument. These may adversely affect the results obtained for the thermodynamic and kinetic parameters.

Following the standard triacetin test protocol previously described in *section 3.1.1*, 3ml of solution was placed in the left hand ampoule and 3ml of buffer placed in the right hand side. A number of experiments was carried out at each of the pre-selected heights above the ampoule floor; 0.0cm, 1.0cm, 1.5cm and 2.0cm. If the “end effects” theory is correct, then the best results will occur at some point away from the top and bottom of the ampoule.

The results are shown below. The solid red and blue horizontal lines represent the “correct” literature values for  $H$  and  $k$ , whilst the dotted lines above and below both lines mark the  $\pm 3\%$  error margins regarded as acceptable for the *triacetin* reaction. A subsequent paper has dealt with the correction of sources of error in microcalorimetric data.<sup>54</sup>

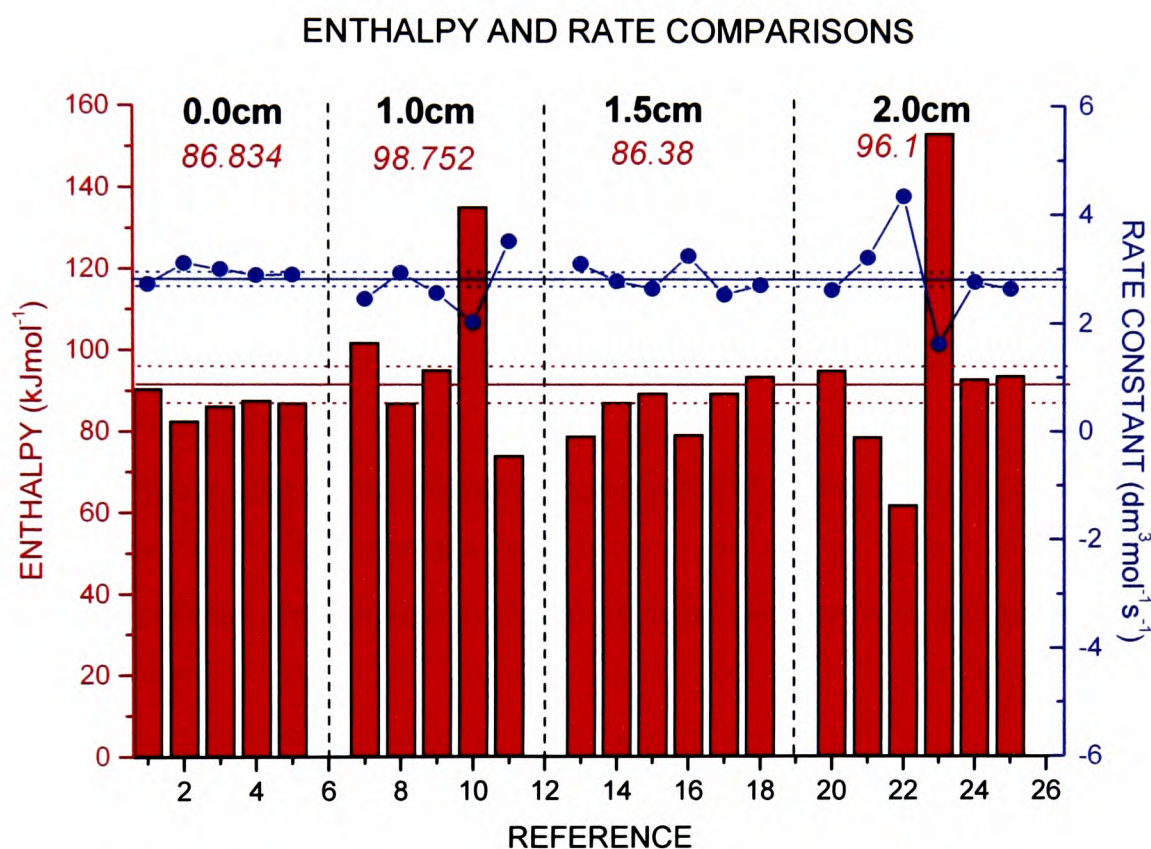


**Figure 3.1.9** Graphical results comparison for the one-piece 20ml ampoules

The results show that a change in sample position within the ampoule leads to a change in the iterated values of  $k$  and  $H$  for the *triacetin* reaction. The mean values of the enthalpy at each sample position are shown on the figure in red. It can also be seen that the results become increasingly poor the greater the height of the sample above floor level.

Most significantly, it is apparent that the best position for a sample to be in is at 0.0cm where no inserts have been used and the sample is simply left to sit on the bottom of the ampoule. It is possible that this is because the addition of additional items into the ampoule adds extra heat capacity to the system and corresponding errors.

As a result of these findings, all future project work, whether on *triacetin* or photocalorimetry, will involve no addition of inserts into the ampoules, with all samples placed on the floor (i.e. at 0.0cm).

NB It is of interest to note that, for the results seen above, a sample position of 1.5cm above the floor would yield the most repeatable results if somehow the sample could be kept in position without the need of any error-causing insert.

Before leaving the reaction behind, a study was carried out on the analysis of the same data to compare the results obtained through iteration with those obtained through a new *direct* method of parameter calculation described in the previous chapter. The development of this method has allowed the writing of a Mathcad™ protocol that calculates values of  $k$  and  $H$  after the input, by the user, of directly-obtained calorimetric data. The standard 3ml *triacetin* reaction in 3ml disposable glass ampoules was utilised for this test.

For each of the results already compared graphically in *section 3.1.2.1* the Mathcad™ protocol was used to calculate the parameters  $k$  and  $H$ . The values required for the protocol to perform the calculation are all obtained directly from the calorimeter and are three values of the TAM output in micro-Watts ( $\mu W$ ) ( $\Phi$ ) along with their corresponding values of  $q_1$  and  $q_2$  the time-dependent enthalpies.

A typical Mathcad™ protocol worksheet is shown below, with the directly-calculated values of  $k$  and  $H$  produced at the bottom. The theory is modified for ease of use from that described in *chapter two*.

## The *Direct* Determination of $k$ and $H$

**Step 1** Enter directly-obtained values of  $\phi_1$ ,  $\phi_2$  and  $\phi_3$  (in Watts)- assigned in Mathcad as  $W, X$  and  $Y$

$$W := 6.9 \cdot 10^{-5} \quad X := 5.828 \cdot 10^{-5} \quad Y := 5.151 \cdot 10^{-5}$$

**Step 2** Enter directly-obtained values of  $q_1$  and  $q_2$  in Watts- assigned in Mathcad as  $q$  and  $r$

$$q := 9.05 \quad r := 14.65$$

**Step 3** Enter the number of moles of triacetin placed in the ampoule (in mol) - assigned in Mathcad as  $A$

$$A := 1.2236 \cdot 10^{-3}$$

**Step 4** Using the equation below, Mathcad will calculate the value for  $Z$  which represents the product  $k.H$

$$Z := \exp[ [\ln(W) - 2 \cdot (\ln(A)) ] ] \quad \text{Hence } Z = 46.086$$

**Step 5** Mathcad will calculate the value for  $(\phi_1 / \phi_2)$  which is assigned  $R$  and also the value of  $Q$  - the total number of joules that would be recorded if the reaction went to completion

$$R := \left( \frac{X}{Y} \right)^{\frac{1}{2}} \quad Q := \left[ q - \frac{(R \cdot r)}{(1 - R)} \right] \quad Q = 253.73$$

**Step 6** Mathcad will calculate the values for  $k$  and  $H$  using the equations below

$$H := \frac{\left[ \sqrt{\frac{Z \cdot (Q - q)^2}{X}} \right]}{1000} \quad k := \frac{\left( \frac{Z}{H \cdot 1000} \right)}{200}$$

$$H = 217.582 \text{ kJ / mol} \quad k = 1.059 \times 10^{-6} \text{ mol}^{-1} \text{ dm}^3 \text{ s}^{-1}$$

The calculated values can then be compared with the iterated values obtained previously by fitting data by Origin™. The comparison is shown below;

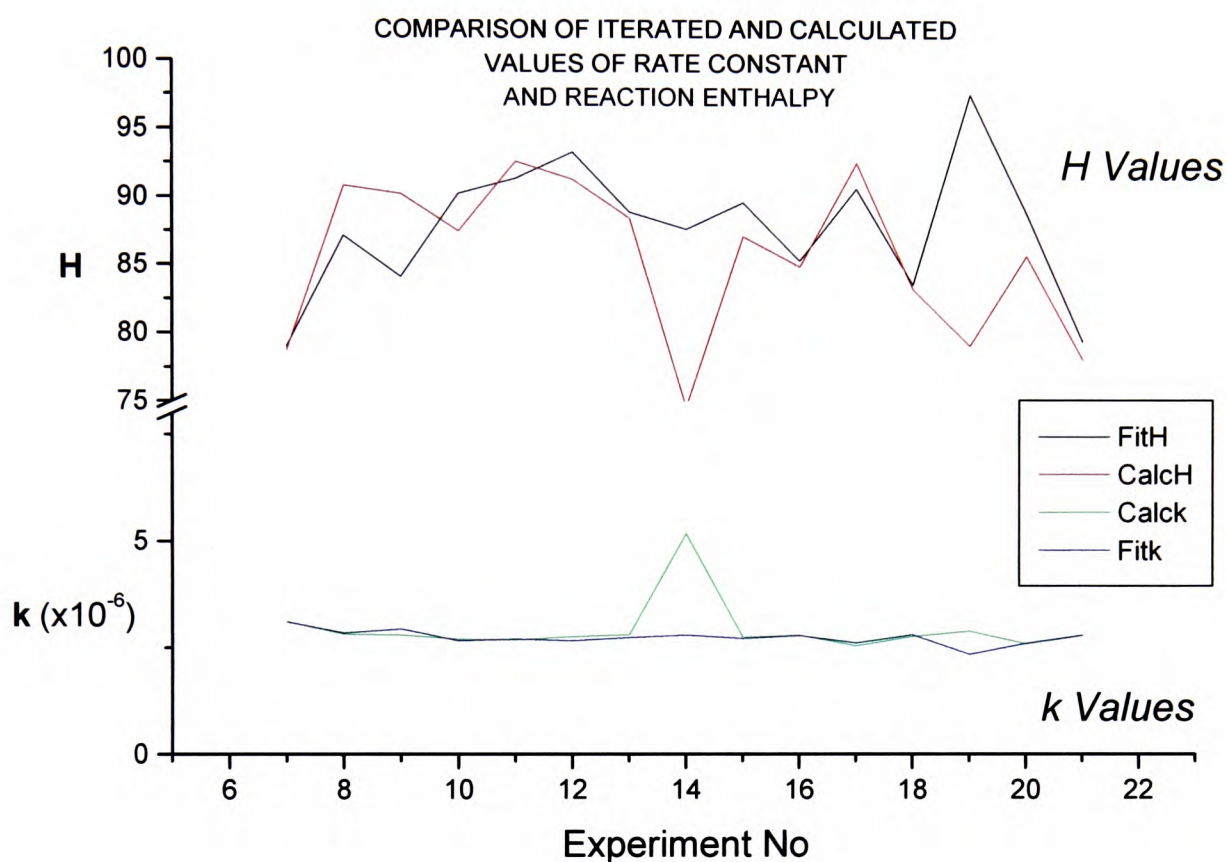


**Figure 3.1.10** Graphical comparison of iterated and calculated values for  $k$  and  $H$

The results show that the calculated parameters fall within experimental error for the range of experiments tested. It is feasible therefore, that direct calculation may be utilised as the preferred method in all future work since global fits for the data can be carried out as opposed to the iterative method which only provides local fits.

### 3.1.4.3 Conclusion

The study on fill volume and position has shown that in an ideal world, a sample might be best positioned about 1cm from the base of an ampoule to achieve the best results for the *triacetin* reaction parameters. Because of the increased variability in results, however, caused by the addition of the inserts to the system, the best results in practice are achieved by letting the reaction mixture sit on the ampoule floor.

This study has also highlighted the difficulties involved in adding any additional inserts into the calorimetric ampoules caused by the increase in thermal conductivity to different extents to both left and right hand side ampoules.

An alternative approach of investigating the conditions of ampoule fill on the results would be to try increasing the concentration of *triacetin* in the reaction. This may improve the signal to noise ratio and hence the reliability of results even at small volumes of *triacetin*.

The comparison of the direct calculation method of results and the iterative technique has shown that there some discrepancies in their evaluation of the values of the rate constant,  $k$  and the reaction enthalpy,  $H$ . Further study is needed but it is clear that the calculation method described in *chapter two* is a better way of calculating the reaction parameters and should be used from here on in.

*CHAPTER 4*

*PHOTOCALORIMETRY: HISTORY  
AND DEVELOPMENT*

## 4. Photocalorimetry: History and Instrument Development

Having developed *triacetin* as a test-reaction for the calorimeter, the next step is to turn attention to the development of the photocalorimeter itself.

Thermodynamical examination of materials sensitive to light has been carried out for many years using calorimetric techniques.<sup>55</sup> However, to observe slow and low-energetic reactions, hardly any instruments have been developed. For such an instrument, sensitivity and stability would be of great importance.

The first attempt at building a system commercially-available to tackle this problem was based on the work by Teixeira *et al*<sup>55, 68</sup> who developed an irradiation cell made as an accessory to the commercially-available TAM. Teixeira *et al* tested the suitability of the system for use in the determination of kinetic and thermodynamic parameters using the photoreduction of *potassium ferrioxalate* – this reaction is described in *chapter five*.

It is the design of this system developed by Teixeira *et al*. which forms the basis of the design of the novel apparatus described in this thesis.

Lehto *et al*.<sup>65</sup> later used a similar system to investigate the photostability of *nifedipine* at different wavelengths, although no quantitative data was obtained.

*Chapter six* will describe the first tests carried out on the completed photocalorimeter, using *nifedipine* as a model solid test material which represents the first time quantitative data has been obtained for a solid material using photocalorimetry.

The development of the photocalorimeter is described in this chapter, along with the modifications and improvements made to the system as the project progressed.

This chapter also introduces the reasons why the development of such a novel instrument is important; describes the history of photocalorimeter development and reports on the stages of the development and modifications made to the photocalorimeter as the project progressed.

It is well known that light can change the properties of different materials and products. Evidence of this includes the bleaching of coloured compounds such as paint and textiles or as a discolouration of coloured products. For many years, photostability has been a concern in many areas of the chemical industry including textiles, paints, food, cosmetics and agriculture. In the field of pharmacy, the study of photostability has played an important role in past years, whilst the number of drugs produced found to be photochemically unstable has increased steadily. The European Pharmacopoeia prescribes light protection for about 250 medical drugs and adjuvants with new compounds added to the list all the time.<sup>56</sup>

Current photostability testing carried out in the pharmaceutical industry is commonly conducted in accordance with the ICH (International Conference on Harmonisation) guidelines,<sup>57</sup> developed as a result of the need to harmonise photodegradation study practices worldwide.<sup>58-60</sup> These guidelines have been developed over many years<sup>61-64</sup> and provide a simple pass/fail type decision, giving no information about the kinetics of the process nor about the factors influencing photostability. With high intensity solar simulation light sources it is possible to run the experiment, including associated analyses in a day. However when such light sources are not available or are considered inappropriate the experiment can take several weeks.

With current equipment, if it is desired to obtain an understanding of the causative wavelengths responsible for the degradation process it is necessary to run a series of studies on individual samples using filters to select wavelength bands. These filters inevitably reduce the irradiation of the sample leading to prolonged experimental times. A similar argument applies for studies designed to understand the kinetics of the process. A number of photo-induced reactions require either oxygen or water vapour to proceed. Again studies designed to fully understand the effect of these environmental factors can be complicated and time consuming. For example, it is known that the hydrolysis of the blue-coloured *Indigo Carmine* to colourless species is accelerated in the presence of moisture. Tablet film coatings containing this dye are quite stable to light in the absence of moisture. Unfortunately the environment within many photostability test chambers tends to be dry as a result of the elevated temperatures found within them. When humidified air is supplied to such a chamber the colour fade is significantly more rapid. Conversely reactions which are oxidative

in nature can be slowed when the sample is blanketed with dinitrogen. Again these sorts of study are time-consuming.

A final issue is that current photostability testing procedures are specific to the spectral power distribution of the light source used. Sunlight simulation sources have a spectral power distribution that is reasonably flat in the visible region and has significant UVA and UVB components. Many environments where pharmaceutical formulations are stored are illuminated with fluorescent lights. The spectral power distribution of these sources is far from uniform with distinct spikes at various wavelengths. If a sample's degradation is mediated by wavelengths which are relatively abundant in a fluorescent source then the degradation may be worse under such an illuminant than in a sunlight simulation source for the same overall illuminance. It is, therefore, not possible currently to extrapolate reliably from one light source to another.

All the methods described above still require the sample to be analysed in the solution-phase. This is the problem that will be addressed by the building of the photocalorimeter.

## 4.1 Principles and History of Photocalorimetry

External factors, such as heat, moisture, oxygen and the acidity of the surrounding atmosphere, together with light, may dramatically affect the unstable behaviour of materials individually or in cooperation. These factors can cause physical and chemical changes in the material. Many pharmaceutical drug molecules are known to be sensitive to light and degrade under light.

Previous studies into photosensitivity have been carried out by chromatography, spectrophotometry and colorimetry.<sup>65</sup> There are, however, a number of limitations to these techniques with kinetic studies demanding long observation times to get reliable results for slow reactions. Furthermore, it would be advantageous to detect the effects of light in the sample material in real time.

The basic principle of a differential photocalorimeter involves shining light into the reference and sample sides of the calorimeter. If a photoreaction occurs, the signal in the sample side of the system will be out of balance with that in the reference side and thermal output results which is observed by the calorimeter.

In general, a photo-induced reaction requires the determination of two quantities; the change in heat energy of the sample brought about by the isothermal photochemical transformation, and the amount of material, in moles, transformed in the reaction.<sup>66</sup>

The basic components required for a photocalorimeter<sup>67</sup> are the light delivery system (lamp source and power supply, filters or monochromators and appropriate optics for beam steering), the calorimeter, which contains the sample and provides the actual measurement and the recording device (normally a PC). This setup can be illustrated schematically in *Figure 4.1.1*:

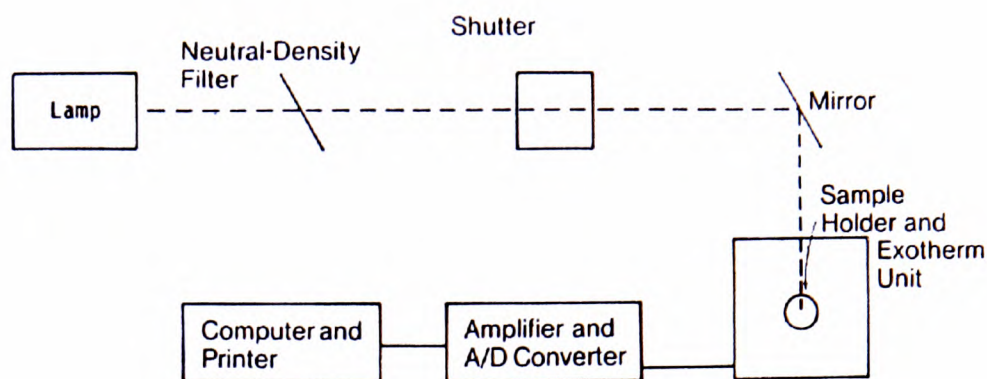


**Figure 4.1.1** Basic photocalorimeter schematic

The first use of a photocalorimeter was reported by Magee *et al.* in 1939<sup>69</sup>, who developed a technique for the thermal determination of the quantum efficiency of photosynthesis by the organism *Chlorella*.

The calorimeter consisted of a small, thin-walled quartz cell mounted in an aluminium container, with a multijunction thermocouple to measure the difference between the cell and the container. Calibration was carried out at different light intensities using a solution of india ink or other chemically-inert, opaque liquid.

*Figure 4.1.2* below shows a schematic of this early photocalorimeter:

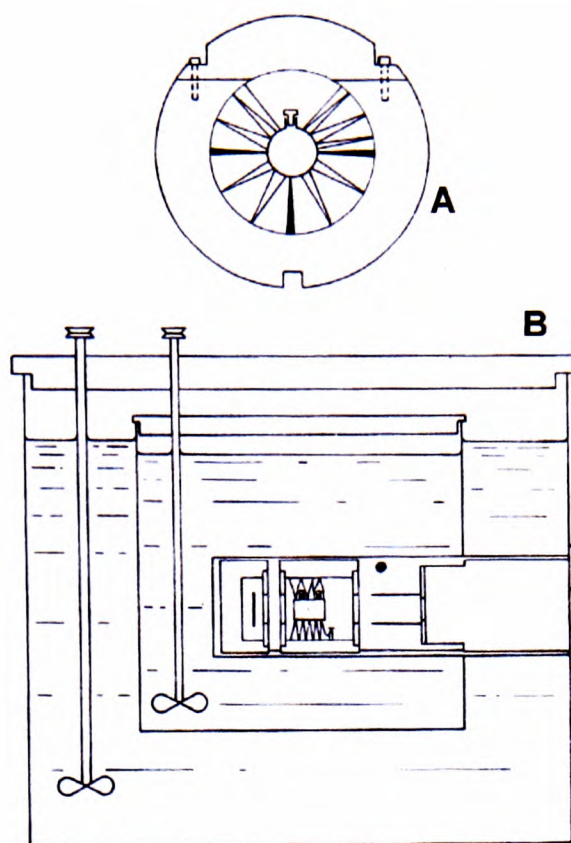


**Figure 4.1.2** The first photocalorimeter. A: end view. B: side view in thermostat <sup>69</sup>

For the measurements of the thermal efficiency of photosynthesising algae (*Chlorella pyrenoidosa* and *Chlorella vulgaris*), a 500W projection lamp was used and the samples irradiated at one week at high light intensity and one week at low intensity. In order to calculate the efficiency, the rate of heat absorption by respiration, as well as photosynthesis, had to be known. The net amount of radiation being dissipated as heat by the algae per unit time was calculated by measuring the difference between the deflections caused by the photosynthesis and the respiration.

Schaarschmidt and Lamprecht <sup>70</sup> described two different calorimetric vessels with light guides in 1973, designed for studies of living yeast cells. One vessel, with quartz light guides 10mm in diameter was used to investigate the yeast cells' sensitivity to UV radiation; whilst the other vessel, with two thin light guides of 1mm diameter, was used to determine simultaneously the heat production and optical density.

In 1976, Cooper and Converse <sup>47</sup> fitted an LKB batch microcalorimeter with optical fibre bundles for their study of the photochemistry of *rhodopsin*. The schematic of their assembly is shown below:

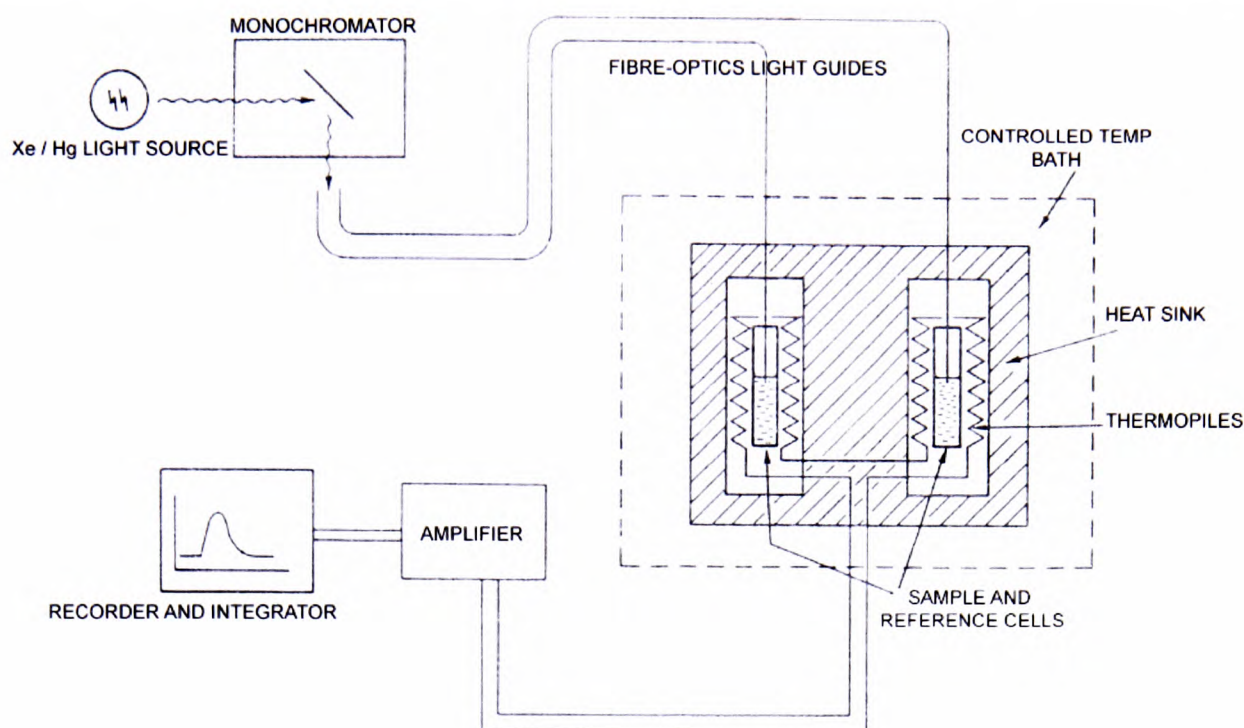


**Figure 4.1.3** Photocalorimeter schematic.<sup>47</sup> Not shown are the shutter and the movable fibre optics mount at the exit slit of the monochromator, which allow either cell to be illuminated independently

McIlvaine and Langerman in 1977<sup>71</sup> used a semi-adiabatic titration calorimeter fitted with a 7mm quartz fibre bundle in their calorimetric measurements of luminescent bacteria.

In 1978, Adamson *et al.*<sup>72</sup> described a photocalorimeter for the determination of enthalpies of photolysis of *trans*-azobenzene, ferrioxalate and cobaltioxalate ions, hexacarbonylchromium and decarbonyldihonium, where the procedure determines the light-induced enthalpy change of a reaction (see figure 4.1.4)

If the light of flux  $F^0$  is absorbed by a solution, yet no photochemical reaction occurs, the energy appears as heat,  $F^0 t$  (where  $t$  is the time of irradiation). However, if a photo-induced reaction occurs, the observed rate of heat production will be some different value,  $F$ , and the quantity  $(F^0 - F) t$  gives the enthalpy change associated with the amount of reaction that has occurred.<sup>72</sup>

NB The terms of  $F^0 - F$  are proportional and not direct measurements of heat ( $J$ )

This particular application of photocalorimetry suffered in precision because it depended upon the difference in heat ( $F^0 - F$ ) and if  $\phi$  (the quantum yield for the photoreaction) is small, this technique could also be insensitive.

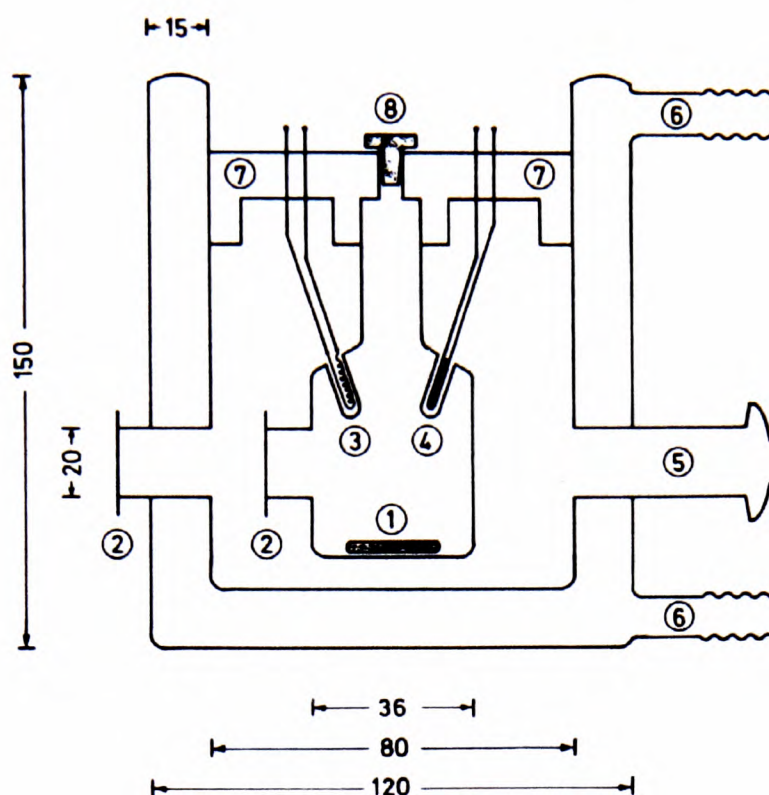


**Figure 4.1.4** Schematic of the photocalorimeter cell (dimensions in mm); (1) coated magnetic stir bar, (2) quartz windows, (3) heating coil, (4) thermister, (5) to vacuum pump, (6) to thermostat, (7) metal cover, (8) cap to inner cell

In 1990,<sup>73</sup> Teixeira and Wadsö described a photocalorimetric system using twin calorimeters, where six optical cables of single fibres of 1mm diameter take light from the monochromator to the two vessels of the two calorimeters. For each of the two calorimeters, the differential signal was recorded. This experimental setup is the first example of a modern differential photocalorimeter upon which the design of the photocalorimeter is based. It is shown schematically below:

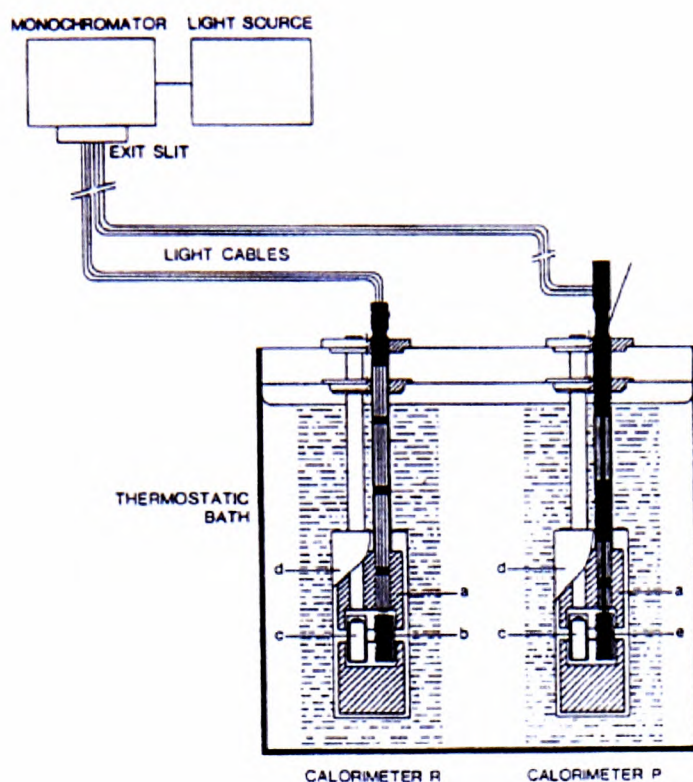


**Figure 4.1.5** Simplified schematic of a photocalorimetric system

### Application to Solution Photocalorimetry and Photopolymerisation

In 1994, Teixeira and Wadsö made use of **solution photocalorimetry** as a means of analysis of pharmaceutical photochemical reactions using techniques that had been developed during recent years and had become increasingly used in solution thermochemistry and in biology.<sup>74</sup> These techniques were essential for work with expensive, hazardous or slightly soluble substances.

The first use of photocalorimetry in **photopolymerisation** was reported by Fouassier, *et al.*<sup>75-81</sup>, Theweleit *et al.*<sup>82</sup> and Fischer *et al.*<sup>83</sup>

More recently in 1992, a photocalorimeter was successfully used by Hoyle<sup>67</sup> to follow free-radical and cationic initiated photopolymerisation. For free-radical polymerisation, a photon of light ( $h\nu$ ) is absorbed by the photoinitiator ( $P$ ) to yield  $P^*$ , an excited species, which readily decomposes to give free-radicals ( $R$ ). These free radicals then initiate polymerisation by reacting with monomer ( $M$ ) (the initiation step); followed by successive addition of monomer units ( $M$ ) to the growing polymer chain ( $RM_n$ ) (propagation step). It is the repetition of this step that evolves the large amounts of heat detected by the photocalorimeter. Two polymer radicals interacting together then leads to termination.

The data obtained from the photocalorimeter (i.e. the actual heat generated) was then compared with the known heat of polymerisation for full monomer conversion, to calculate the percent conversion.

### **Instruments Applicable to the TAM**

In 1999, Lehto *et al.*<sup>65</sup> first addressed the task of constructing an irradiation cell made as an accessory to the conventional isothermal calorimeter to be used to observe slow and low-energetic photosensitive reactions in both the solid and solution phase.

Lehto *et al.* designed an irradiation cell for use with the TAM 2277 microcalorimeter (Thermometric AB, Sweden) that would fit into the commercial 4ml ampoule microcalorimetric unit. The design of the cell, which has been adapted in the design of the photocalorimeter is shown below:

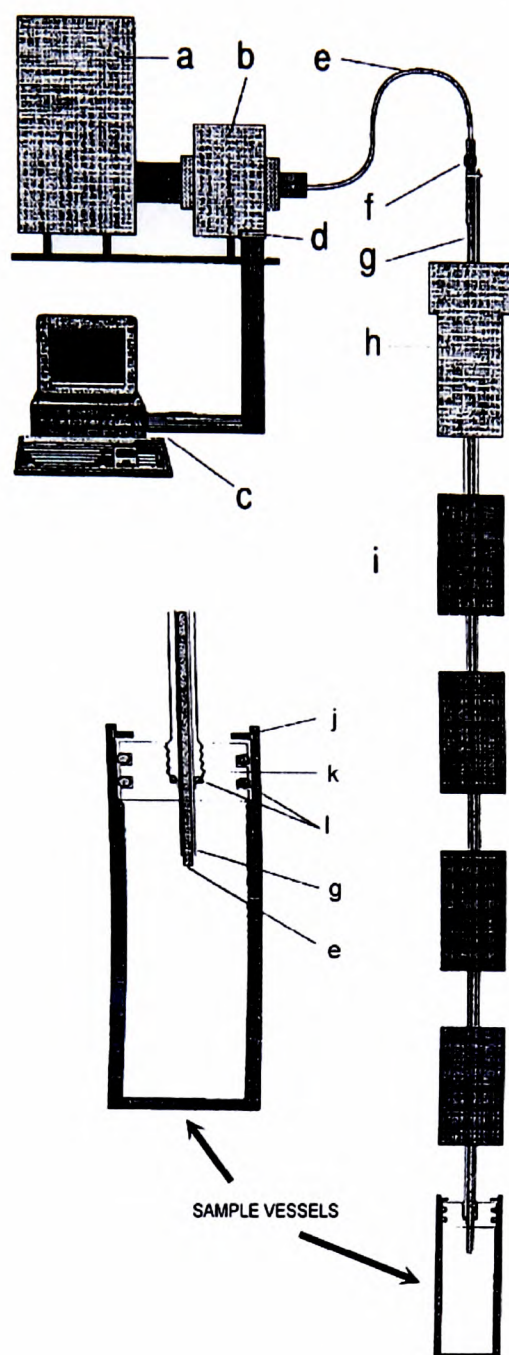


**Figure 4.1.6** The design of Lehto et al's irradiation cell. The beam from the monochromator is split into two parts and conducted into identical irradiation cells <sup>65</sup>

a) lamp house b) monochromator c) PC d) step motor e) light cable f) SMA connector g) insertion tube for light cable h) plastic holder i) heat exchanger j) locking ring k) teflon lid l) O-ring

The light was produced using a 75W xenon arc lamp, passed through a grating monochromator via focussing mirrors and a shutter, before entering two identical 1mm optical cables. The wavelength of the light was controlled with a PC-driven stepper motor. During the measurement, two separate yet technically identical irradiation cells were positioned in the sample sides of the two twin calorimetric units.

Of particular interest to the project is the development of a method for validating photoreactions (see *chapter five*). The photodegradation of *nifedipine* is proposed as such a reaction in the solid state (see *chapter six, section 6.3.1*) and it is of interest that Lehto *et al.*<sup>65</sup> considered this reaction when evaluating their system, incorporating the effect of the variation of wavelength on the degradation of the material.

## 4.2 Considerations of Instrument Design

Before building a new type of photocalorimeter, there are many individual aspects of design that need to be considered and a lot of experimental work to be carried out.

### 4.2.1 General Design Considerations

Based on the work of Lehto and Laine,<sup>65</sup> the following design was drawn up as a model;

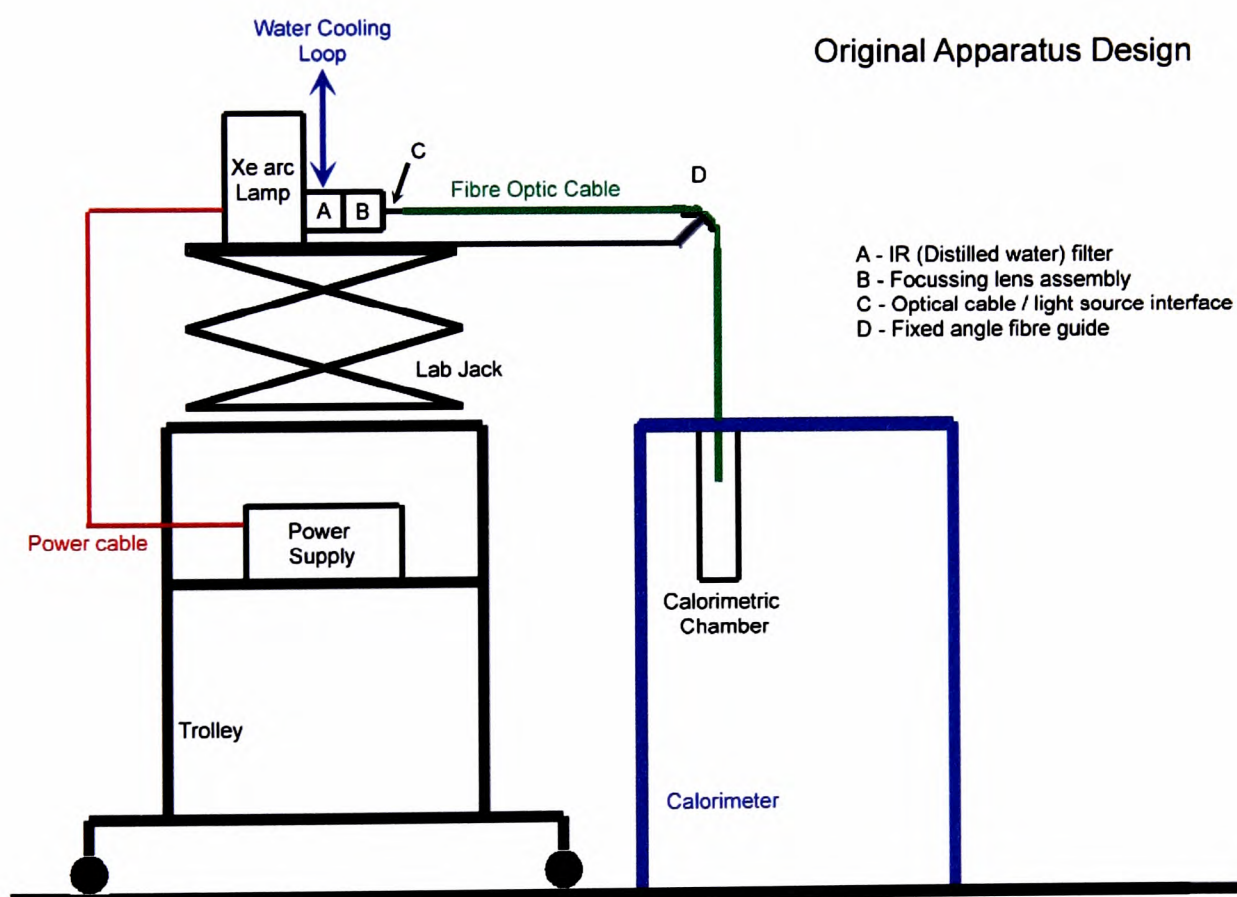


Figure 4.2.1 Basic design of novel photocalorimeter

Since the TAM is already commercially-available and has been previously used in the research group for many years, it is logical to seek a design of photocalorimeter that can be easily adapted for use with existing apparatus.

The system must supply equal amounts of light to two individual calorimetric ampoules as well as a third supply to a spectroradiometer - enabling quantitative analysis of the amount of light being delivered to a drug sample in real time. The development of actinometric techniques is discussed in *chapter five*.

The apparatus also needs to be able to incorporate a monochromator so that different wavelengths of light that cause photodegradation could be looked at selectively. The wavelength range needs to cover approximately 200nm to 1000nm.

Requirements of specific areas of the apparatus were considered and reviewed as follows:

#### **4.2.2 Trolley**

Designed to match the vertical height of the TAM, the trolley is of mass approximately 100kg and designed to be strong enough to support the considerable weight of the light source and monochromator as well as the power source which is stored on a shelf below. The trolley is mounted on wheels which allow ease-of-movement and can be locked once the kit is in position. Dimensions are approximately 1000mm (h) x 700mm (w) x 700mm (l)

#### **4.2.3 Lab Jacks**

Two identical mechanical hand-wound lab jacks, (of mass approximately 10kg each) mounted one on another allow the whole kit to be raised and lowered vertically. Their dimensions are approximately 400mm square. After raising the ampoules to a suitable height above the top of the TAM to be loaded and unloaded, the jacks need to be able to lower the ampoules down through a distance of around 400mm to reach the measuring position within the TAM.



**Figure 4.2.2** The jacks allowed movement through a range of 400mm

### 4.2.3 Light Source

Since it was initially unclear how powerful a lamp was going to be required to cause sufficient photodegradation without overloading the sensitive range of detection of the TAM, a mid-range 300W light source was chosen. The xenon arc lamp is *ozone-free* and comes with its own lamp housing (170mm (*w*) x 170mm (*l*) x 400mm (*h*)) and power source (500mm (*w*) x 500mm (*l*) x 100mm (*h*)) which is exceptionally heavy (~40kg). The expected lifetime of a bulb is approximately 1000 hours. Upon assembly of the apparatus, the bulb was installed, tested and focussed according to the LOT Oriel manual.<sup>84</sup> The power-supply allows the lamp to be run at  $\pm 20\%$  of its rating (ie between 240W and 360W) which can be pre-selected before the lamp is ignited. The lamp housing allows adjustment of the focus of the bulb and also provides a time-elapsd indicator for the shining of the lamp to give an idea of remaining life in the bulb.

*Figures 4.2.3, 4.2.4, and 4.2.5* below show the component parts of the light source;



**Figure 4.2.3** The lamp housing showing focussing adjustment levers on the left-hand side. Also shown are the IR filter and the focussing lens assembly (described later)



**Figure 4.2.4** The power supply allowing  $\pm 20\%$  adjustment of the lamp power



**Figure 4.2.5** The xenon arc lamp. Each bulb has an expected lifetime of  $\sim 1000$  hours

#### 4.2.4 IR Filter, Cooler and Focussing Lens (A and B on design)

The infra-red filter utilises distilled water to remove any emissions of infra-red light from the light source are approximately 150mm long when connected together. On the outside of the filter is a water-cooling jacket, allowing cold water to be pumped around the filter-casing, removing the substantial heat generated by the Xe arc lamp. The cooling system is shown in *Figure 4.2.7* below.

The focussing lens assembly converts a collimated light source into a fibre optic source and is shown in *Figure 4.2.8*<sup>85</sup> The assembly also has a shutter to allow the light to be removed from a sample without the need to extinguish the light source first. This is of particular use when allowing the lamp to “warm up” and produce a stable light output before illuminating a sample.



*Figure 4.2.7* The IR filter, water cooling system and focussing lens assembly. The silver shutter control can also be seen

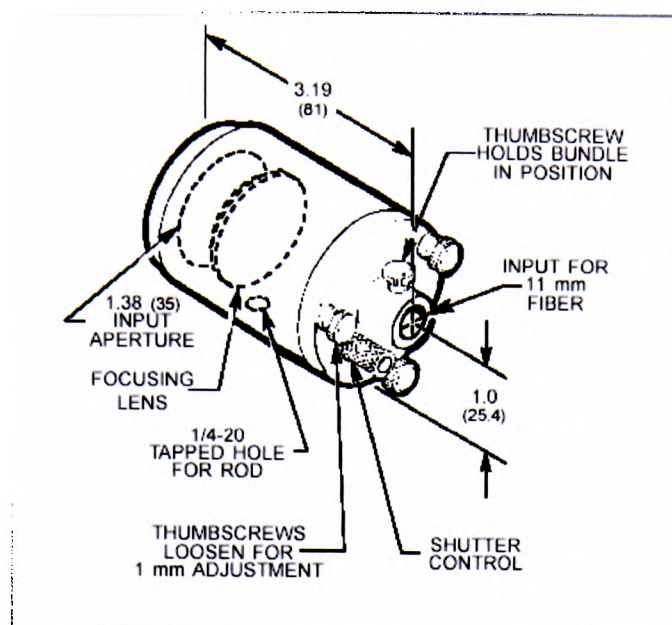


**Figure 4.2.8** Schematic of the focussing lens assembly<sup>85</sup>

#### 4.2.5 Optical Cable / Light source Interface (C on design)

At the point at which the light source is focussed down to a point by the focussing lens described above, the interface allows the three-bundle end of the light cable to be fixed securely in place and the light to pass into and along the fibre optic cable. The light source could be removed from the cable at any time by drawing the one away from the other with a small amount of force.

#### 4.2.6 Stainless Steel Fibre-Optic Cable Guide

Since the whole system moves up and down through some 400mm, a method of ensuring that the fibre-optic cables are kept in the same orientation at all times is necessary. Without such a system, the 90 degree angle in the cables as they change from the horizontal to vertical orientation will become obtuse as the system is raised and acute as it is lowered. It is also important that the cables are fixed in position relative to each other, remaining a fixed distance apart to allow an easy and consistent entry into the calorimeter on lowering.

The guide is shown in *Figure 4.2.9* below showing (in yellow) the path of the fibre optics cables;

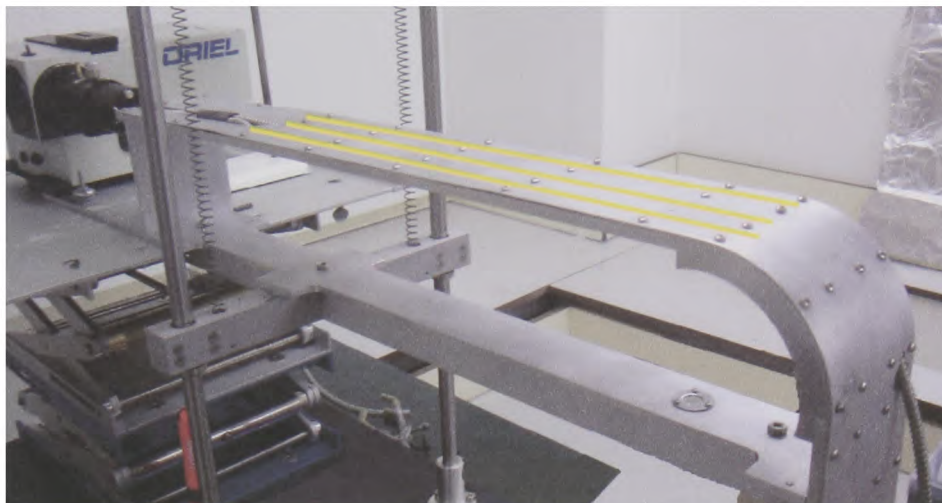


*Figure 4.2.9* Light cables contained within cable guide

#### **4.2.7 Fibre-Optic Cable**

The 1000mm long fibre-optic cables are trifurcated with the split point 150mm after the light source end. The common end diameter is 5.5mm and the diameter of the three branch ends are each 3.2mm. Quartz was chosen as the best transmitter of UV light.

At the ampoule-end of the cables, specially-made plastic lids (manufactured at GSK) were screwed onto the cable sheathing which allowed an air-tight interface between the cable and the ampoule. When ‘loaded’ into the lids, the ampoules are held in place with metal circlips. The ampoules therefore hang freely from the fibre-optic cables themselves. The fibre optic cables and the lids are both illustrated below;

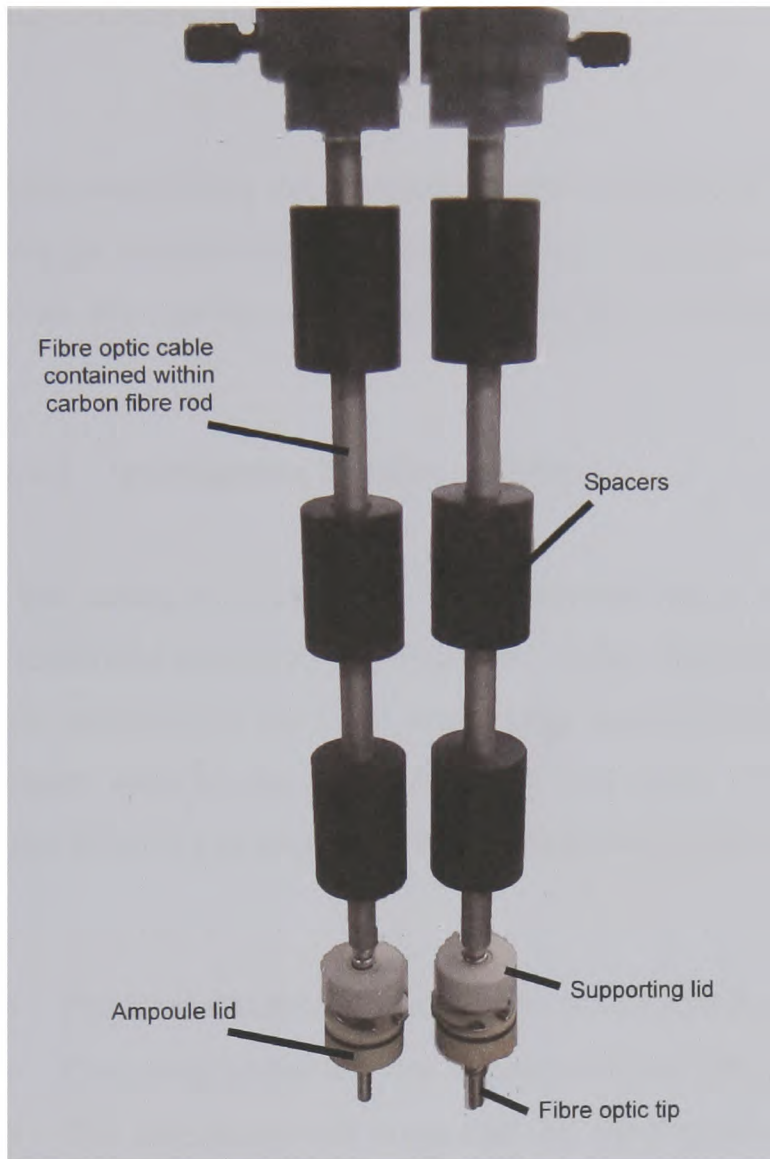


**Figure 4.2.10** Fibre optic cables, spacers and lids

### 4.3 Modifications and Additions

After establishing the photocalorimeter according to the design shown in *Figure 4.2.1* and the considerations described above, modifications and improvements were made to the basic design over a period of 2 years as the project progressed.

#### 4.3.1 Investigating baseline stability

First attempts to obtain a stable baseline upon lowering the ampoules into the calorimeter proved to be problematic. A big challenge with the system was combining the sensitivity of the TAM with a large mass of stainless steel light source equipment blown upon by the air-conditioning vent in the 21°C temperature-controlled room. The following investigation was carried out into the reproducibility of the baseline.

- The 20ml stainless steel ampoules were washed in *ethanol*
- The empty ampoules were clipped onto the fibre optic cables
- The ampoules were suspended by fibre optic cables and positioned above the calorimetric channels in the TAM
- The ampoules were lowered into the TAM using a modified lowering process: The ampoules were lowered halfway into the chamber. After 30 minutes, the ampoules were lowered into the measuring position. before lowering down to the bottom of the chamber (see also *section 4.3* below)
- The recording of the TAM signal was then commenced and baseline data collected
- The data was analysed using Origin™

Five experiments were run using the above procedure. These are plotted and compared directly below:

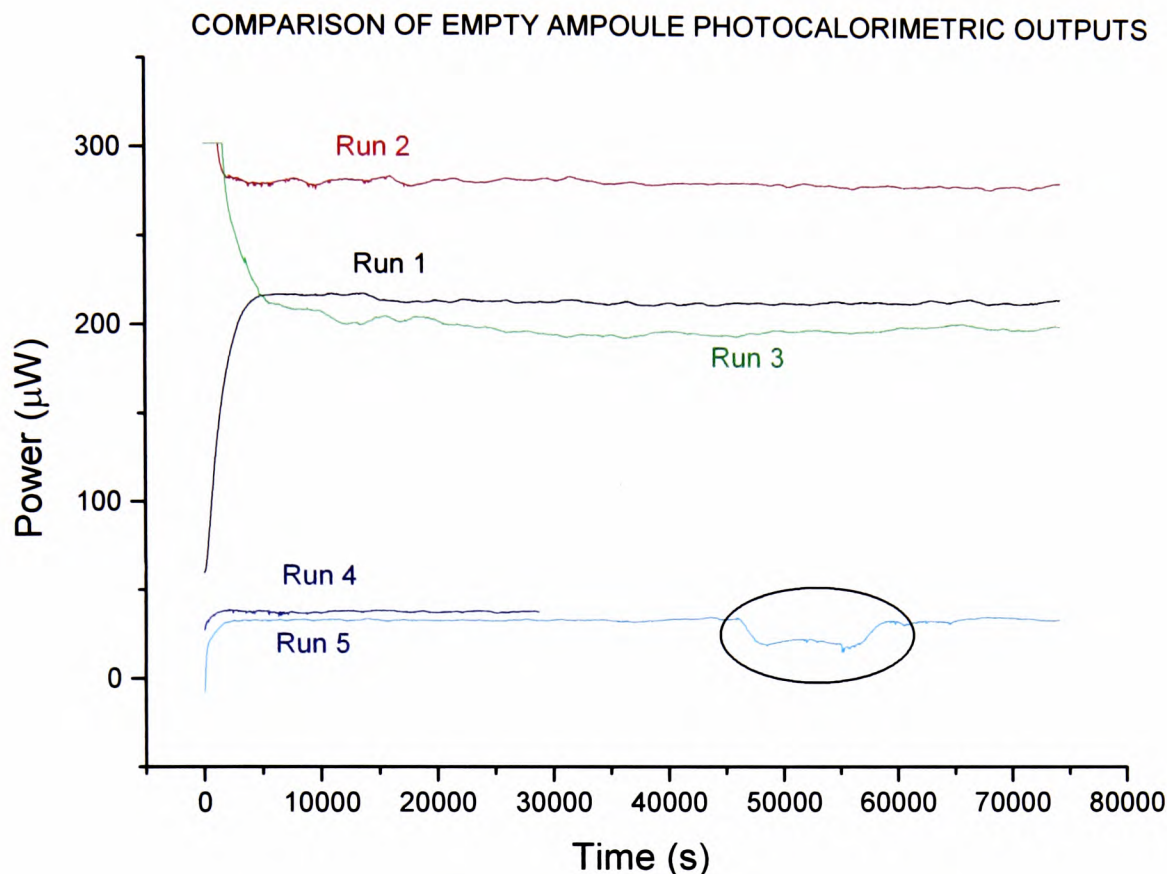


**Figure 4.3.1** The 5 runs carried out with empty 20ml steel ampoules

The outputs clearly indicate there is a problem achieving a repeatable baseline. The values vary from around  $40\mu\text{W}$  to  $200\mu\text{W}$  and  $300\mu\text{W}$  and not  $0\mu\text{W}$  as expected.

It was decided during *experiment 5* of the experiment to look into why the baseline settled at  $40\mu\text{W}$  and not  $0\mu\text{W}$ . It was thought that external influences in the constant temperature room, such as the air conditioning fan blowing directly onto the steel apparatus could be having some effect. An experiment was therefore carried out to investigate any effect of shielding the kit by placing sheets of foam between the apparatus and the air-conditioning fan. The ringed section on the above figure represents the point at which this experiment took place *experiment 5*. The output is shown in more detail below:

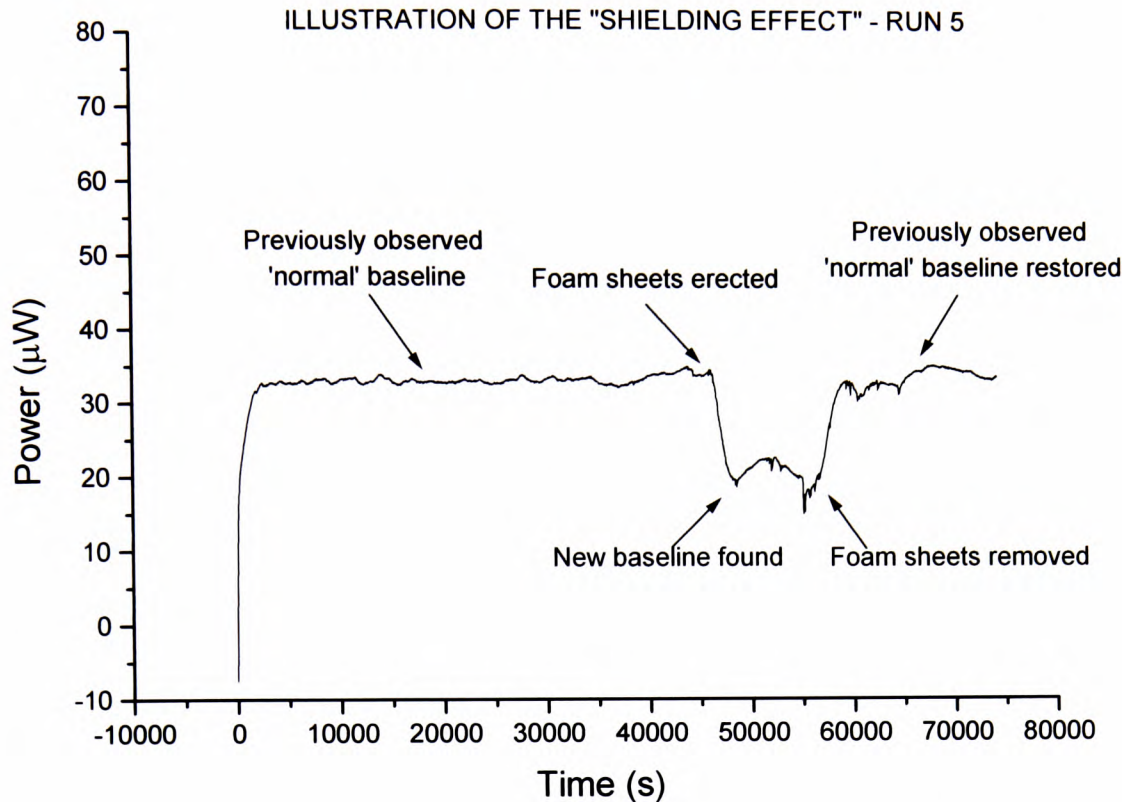


**Figure 4.3.2** Experiment 5 – showing the effect of equipment shielding

The output shows a reduction in the baseline signal of ~33% and suggests that with sufficient protection of the photocalorimetric kit, it should be possible to reduce the baseline output right down to a value much nearer to  $0\mu W$ . This is unlikely to ever be  $0\mu W$  since the paired fibre-optic cables are never going to be an exact match. The two sides of the differential system will therefore always be non-identical, producing a non  $0\mu W$  baseline.

A *plastic shroud* was designed to encase the metal cable guide completely thus shielding the apparatus from the air-conditioning. The shroud could be removed to allow access to the cable guide underneath. The shroud covering the cable guide is shown in *Figure 4.3.3* below and has the dimensions of mass ~1kg; and length ~900mm:



**Figure 4.3.3** The green shroud covers the length of the fibre-optic cables

In addition to the shielding of the equipment from the air-conditioning, a second issue was identified; that of air conduction within the calorimetric chamber between the top of the ampoule in the measuring position and the top of the column.

To minimise this effect, *plastic “spacers”* of almost identical external diameter as the internal diameter of the calorimetric chambers were constructed based on the design of commercially available perfusion shafts sold by Thermometric AB, Jarfalla, Sweden.<sup>86</sup> The spacers were placed at regular intervals down the length of the vertical section of the fibre-optic cables. This arrangement is illustrated in *Figure 4.2.10* above and improved the baseline stability and repeatability of the system considerably.

Combining the effect of the addition of the spacers and the shield meant that the next stage of development could begin; the addition of light to the system.

### 4.3.2 The effect of light

Having established the baseline stability of the instrument when loaded with empty ampoules, the next stage was to test the response of the TAM when light was applied to the system.

The 300W Xe arc lamp (discussed earlier in this chapter) was tested at 240W, 200W and 150W power outputs and the light shone into the empty ampoules already tested for the baseline stability work.

It was hoped that in a differential system, no net signal would be recorded by the TAM since the light-outputs from the pair of fibre-optic cables were expected to be equally matched. A TAM signal would indicate an imbalance in the amount of light being delivered by the optical cables.

The experiment began by repeating the procedure described in *section 4.3.1*. Once a stable baseline had been achieved, the lamp was ignited, allowed to “warm up” for an hour, (as instructed by the LOT Oriel manual <sup>84</sup>) before the shutter was opened and the light allowed to irradiate into the ampoules. The resultant data was recorded using the TAM and then plotted and compared as below:

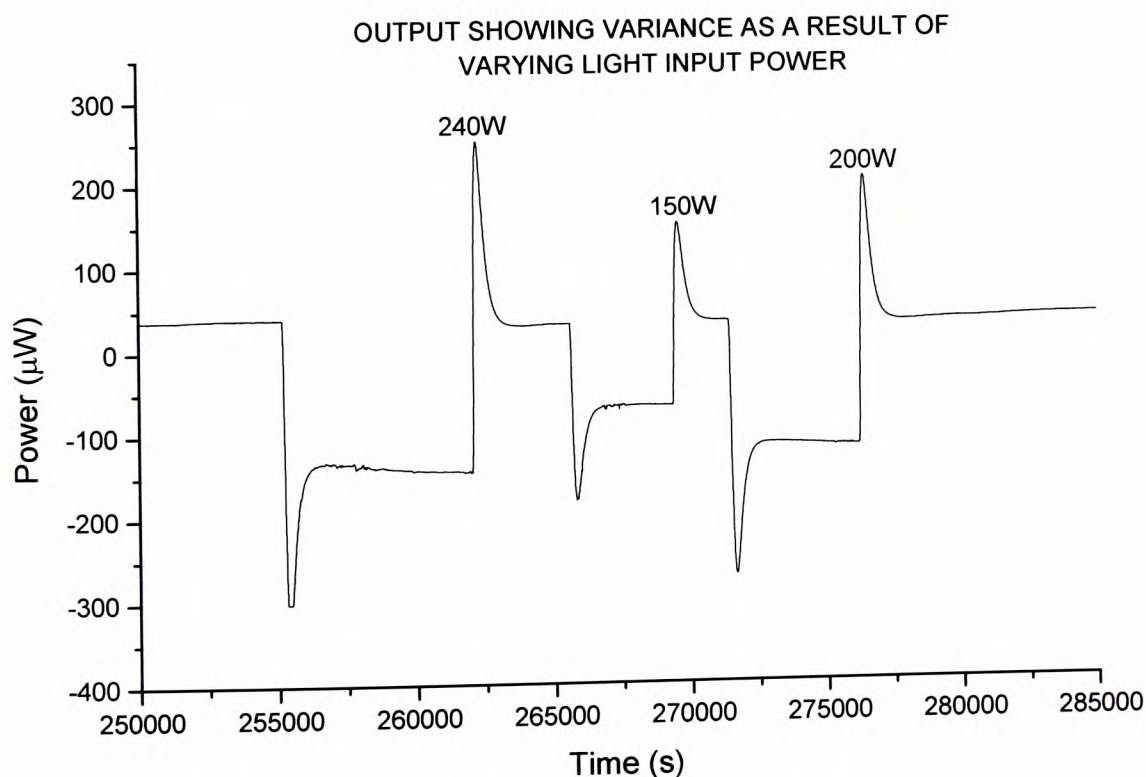


**Figure 4.3.4** TAM output when the light is added and removed from the system

The light shining into the ampoules has a dramatic effect on the TAM output and suggests an imbalance in the light delivery in each cable. Consider the power output at  $240W$  as an illustrative example:

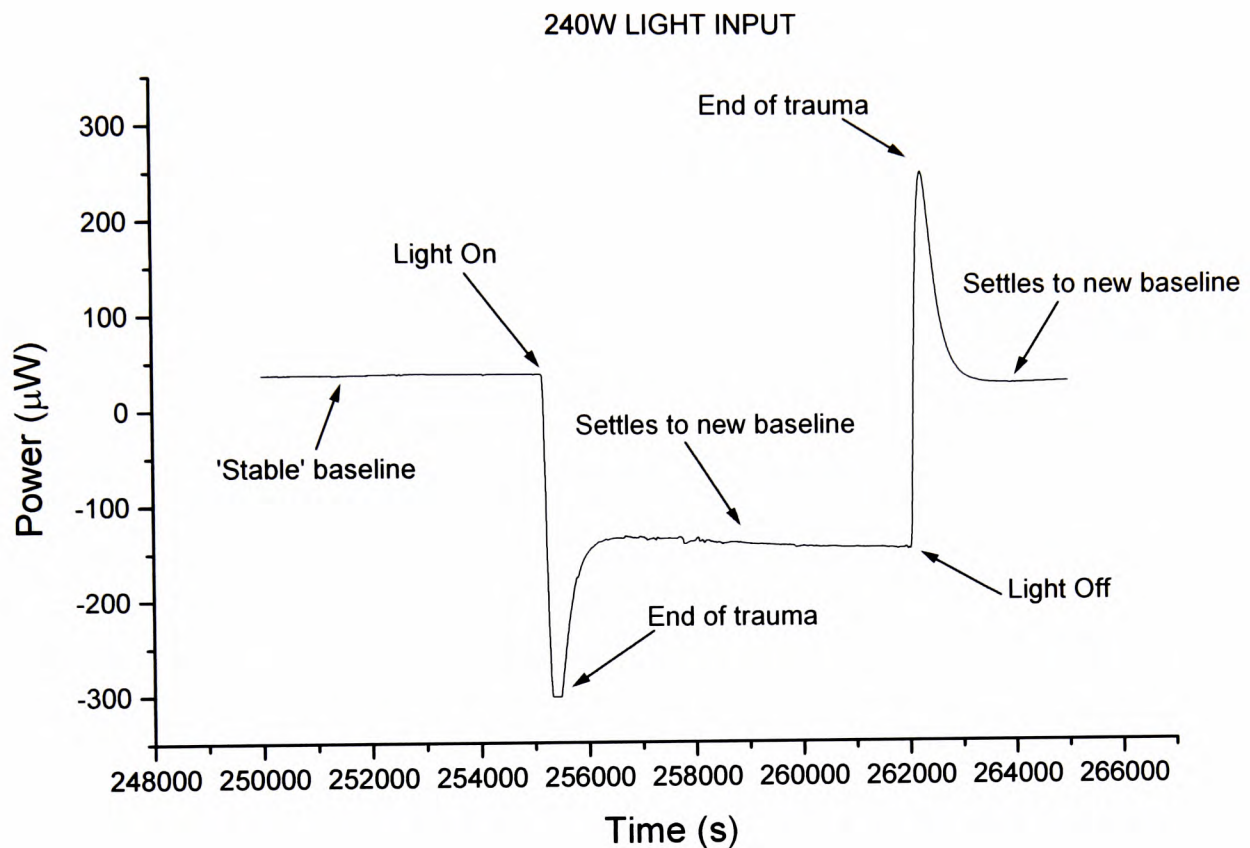


**Figure 4.3.5** TAM output when the light is added and removed from the system at  $240W$  input

The experiment began with the observed baseline at  $\sim 40\mu W$  for the pair of empty stainless steel  $20ml$  ampoules. At the point at which the light is turned on, the system experienced an 'overthrow' reaching a deep minimum before recovering to settle at a new baseline (when the light was on) of around  $-150\mu W$ . This plateau was achieved after approximately 2000 seconds and represents the offset equilibrium reached as a result of the out of balance signal of the two fibre-optic cables. The light was then switched off and positive thermal shock was observed, with the calorimetric signal increasing to  $\sim 250\mu W$  before settling down back to the original baseline at  $\sim 40\mu W$ .

#### 4.3.3.1 Measuring the throughput of each cable

If the fibre-optic cables were better balanced, then the baseline value with the light on should occur at a value much closer to zero than those observed previously ( $\sim 180\mu W$ ) and the slope of the line at the ‘light on’ baseline should be flat.

Using the spectroradiometer (see *chapter five*), the imbalance in the fibre optic cables was addressed by obtaining direct numerical comparisons of each of the light output capacities of the three cables. In each case, the light meter was connected to a branch of the fibre optic cable and the *daylight entering the trifurcated cable* recorded using the designated software.<sup>87</sup>

NB Measuring the light transmitted through each cable from the Xe Arc Lamp was not possible due to the lamp producing light of far too high an intensity for the light meter to cope with.

It was hoped that out of this experiment would come data indicating which two of the three cables were the better matched and therefore best used as the right hand and left hand side inputs into the TAM.

Typical output spectra for the three cables are shown below in *Figure 4.3.6* :

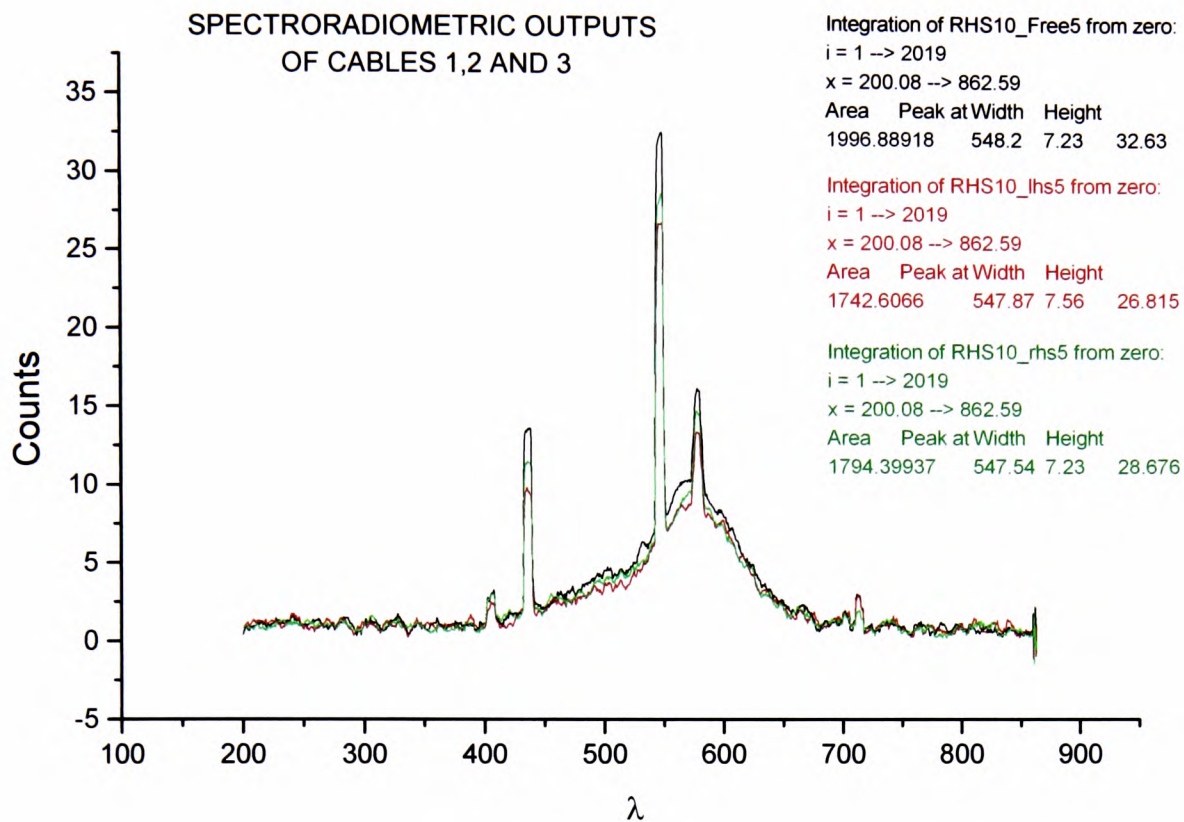


**Figure 4.3.6** TAM output when the light is added and removed from the system at 240W input

The figures quoted in the figure above are the result of integrating the area under each spectrum. They are repeated here for clarity and are typical of the trends shown across all 10 experiments carried out:

Reference (free) Cable:	1996.88918
Left Hand Side:	1742.6066
Right Hand Side:	1794.39937

Clearly, from these results (and all ten sets of results recorded), the best-matched pair of ampoules are those which happily are already in use in the left and right-hand sides of the TAM. The effect of imbalance in light output from the fibre optic cables is therefore already minimised.

### 4.3.3.2 The effect of light with the addition of the shroud

To test the effectiveness of the plastic shroud, the “light on – light off” experiments described above were repeated but this time comparing the baseline gaps when adding and removing the shroud from the apparatus.

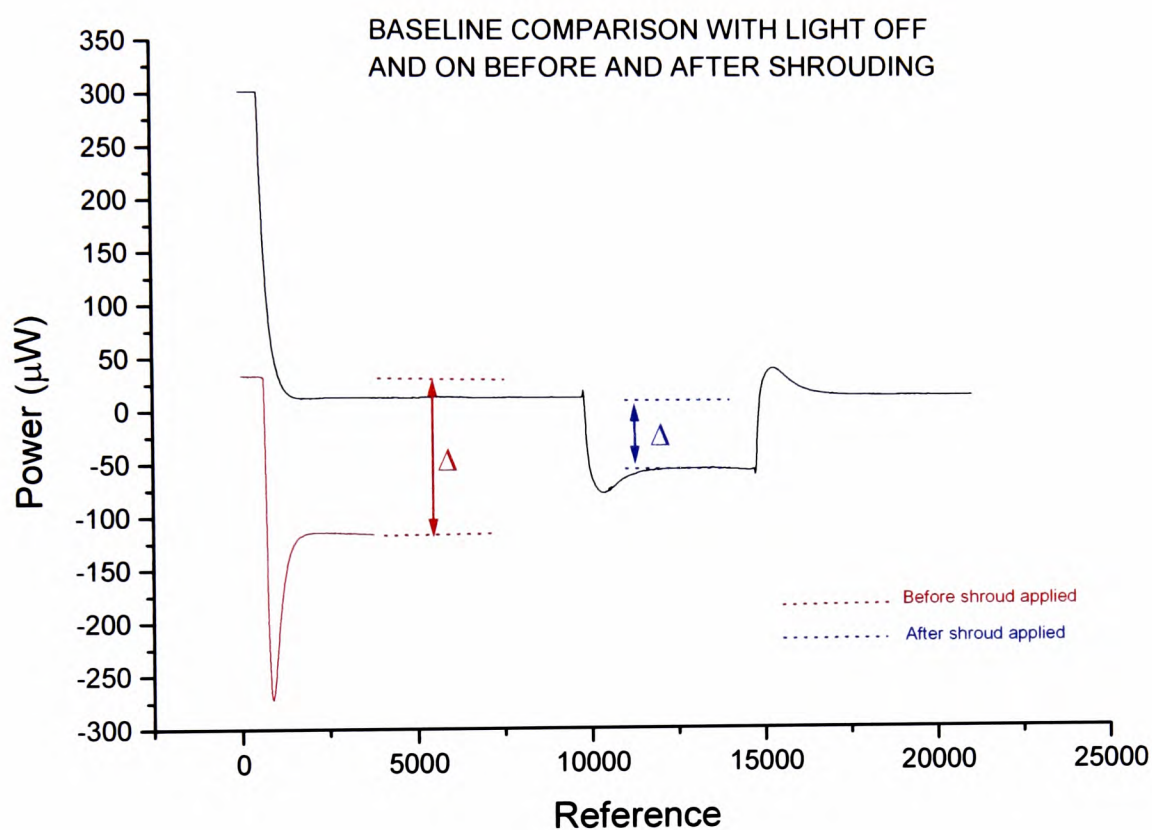


**Figure 4.3.7** TAM output when the light is added and removed from the system at 240W input- the effect of shrouding

The figures compare as follows:

Signal difference without shroud =  $\sim 150\mu\text{W}$

Signal difference with shroud =  $\sim 42\mu\text{W}$

Clearly, application of the shroud has a significant effect on the baselines observed during the experiments. The shroud allows baselines to be much nearer the ideal

situation of no difference in baseline between light on and light off readings; both occurring at  $\sim 0\mu W$ .

#### 4.3.3.3 The correlation of baseline signal difference and light power input

It was noted that increasing differences in the scale of the thermal shock and the gap between the two baselines (light on and light off) were observed with increasing lamp power. To establish whether the widening gap with increasing lamp power was linear, a plot was made of gap distance ( $\Delta$ ) vs. lamp power – as illustrated below for the 240W section of the plot:

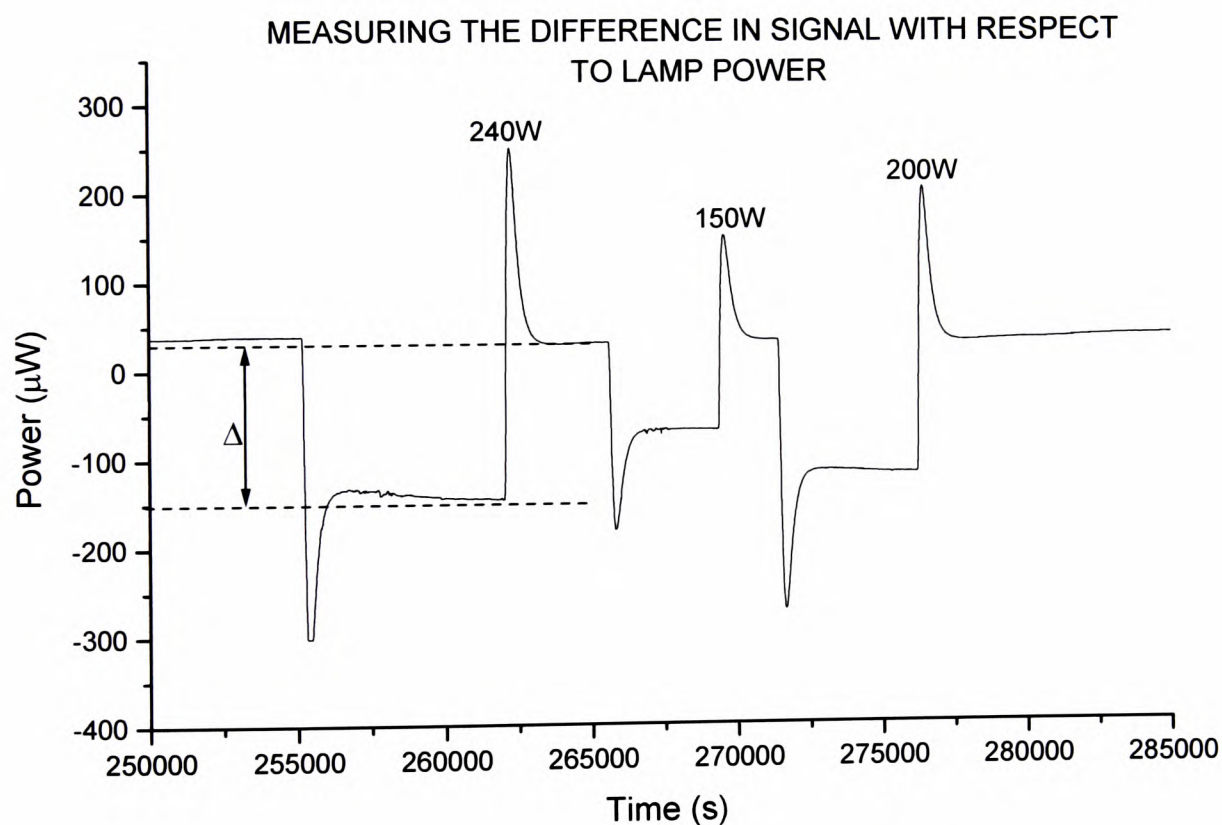


*Figure 4.3.8* Measuring the signal difference at each lamp power output

This plot of the difference in baseline values with lamp power is shown below and the fitting regression value of 0.997 confirms a linear relationship.

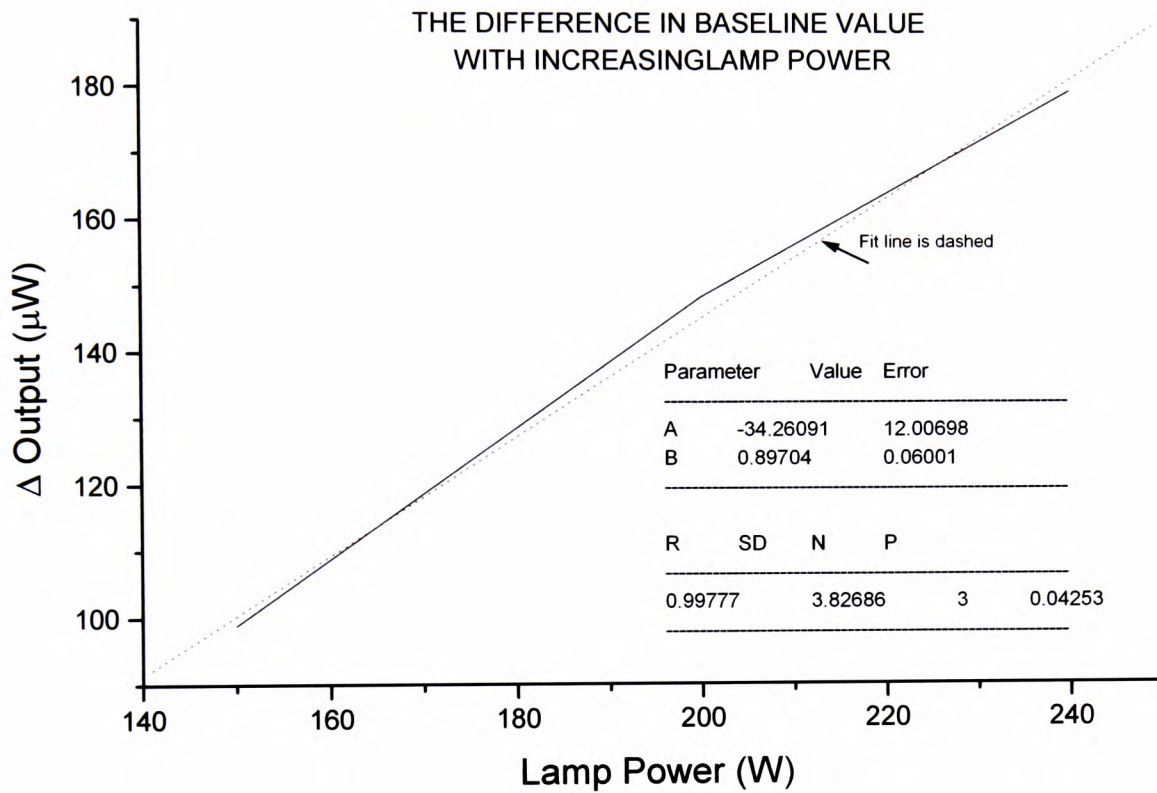
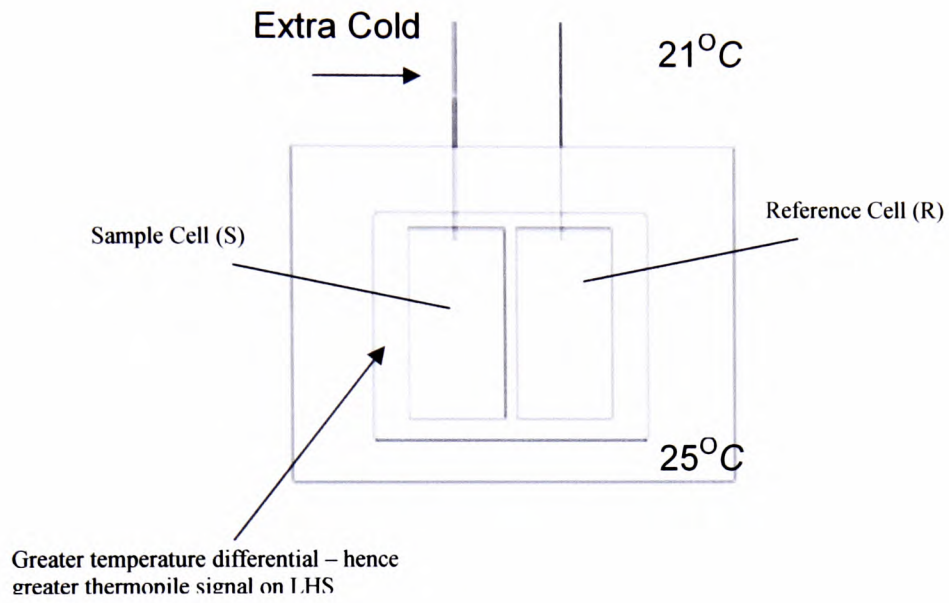


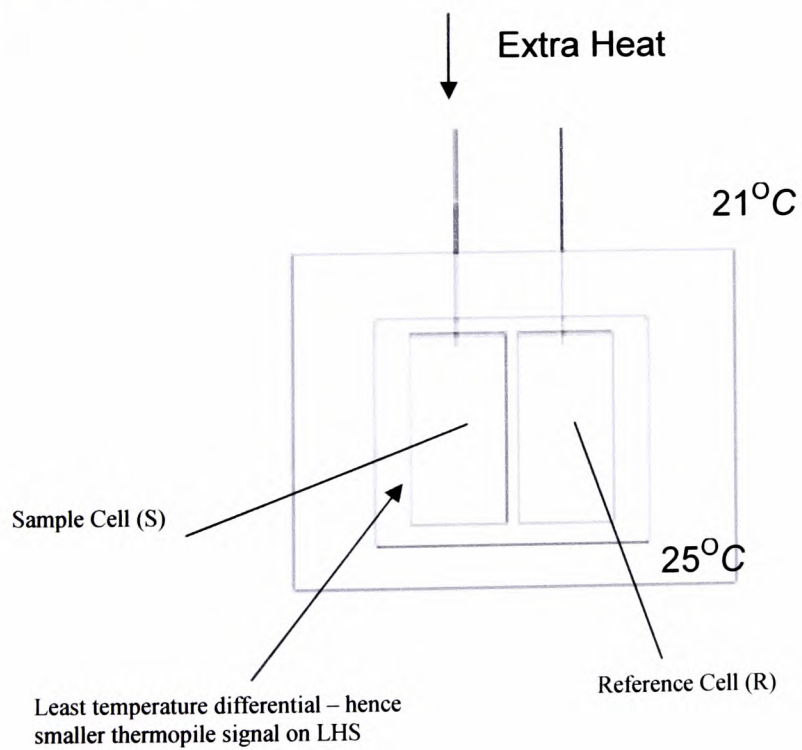
**Figure 4.3.9** The baseline value difference with increasing lamp power

A theory as to why the baseline values are not settling at  $0\mu W$ , why a positive signal is observed when the system is at rest and why a negative signal that falls away is observed when the light is on is outlined below:

**Case A – Light off**



**Case B – Light on**



Consider and compare cases A and B:

### **Case A – Light off**

In the first case, the TAM is at  $25^{\circ}\text{C}$  and the constant temperature room is at  $21^{\circ}\text{C}$ . However, the LHS of the kit is being cooled by air from the air-conditioning unit and so the temperature differential on this side between the TAM and the room will be increased. There will therefore be a greater differential signal from the thermopiles in the LHS of the system, which leads to a positive TAM output. [We see  $\sim 40\mu\text{W}$ ].

### **Case B – Light on**

Here, the TAM is still at  $25^{\circ}\text{C}$  and the room is still at  $21^{\circ}\text{C}$ . However, the two fibre-optic cables are not delivering the same amount of light into their respective ampoules (see actinometric work later in this report). The cable on the LHS has a greater photon flux (*einstein/s*) than that on the RHS and so more energy, and hence heat, is being delivered to the LHS. The temperature differential between the room and the TAM is therefore minimised on the LHS and so the RHS thermopile signal will be the greater. This leads to a negative TAM signal. [We see  $\sim -180\mu\text{W}$ ]. The continually decreasing negative signal is due to the fact that the longer the light is on, the warmer the LHS becomes and the greater the differential signal on the RHS thermopiles. The slope of the line observed when the ‘light on’ baseline is reached is an indication of the rate of heating of the ampoule. This in turn is related to the output power of the lamp.

According to this model, therefore, the effect of shrouding the kit from the effect of the air-conditioning unit will be as follows:

### **Case A – Light off**

Now the effect of the air-conditioning unit is minimised, the temperature differential on the left and right hand sides of the system should be approximately the same and the baseline reading should be closer to zero than the  $\sim 40\mu W$  observed previously.

### **Case B – Light on**

If the imbalance of the two fibre-optic cables is not addressed then it is expected that the shrouding will have an adverse effect on the calorimetric output. The imbalance will mean that the LHS is heated more than the right but with the shroud in place there will be no cooling effect from the air-conditioning to redress the balance. The temperature differential for the LHS will be minimised relative to the RHS and so the signal from the RHS will be large – leading to a large negative signal on the TAM. The signal is still expected to become more negative. This time with a steeper slope, as a result of the increased heating effect described above.

This model works well as the expectations outlined here in the theory are observed experimentally.

## 4.4 The final Design

The final design of the photocalorimeter is shown below in *Figure 4.4.1*:



*Figure 4.4.1* Final photocalorimer design

In arriving at this final experimental setup, many other experiments and background studies were carried out. These considerations are described elsewhere in this thesis but can be summarised as follows;

- Evaluation of Irradiance of the light source

It is essential to have quantitative information on the amount of light a sample has been exposed to over a given period of time. Several methods of achieving this have been proposed in the literature. This area is discussed extensively in *chapter five*.

- Volume of Sample and its Position within an Ampoule

The effect of the position of a sample and / or the volume to which an ampoule is filled on the thermodynamic and kinetic parameters obtained for a reaction is a crucial consideration when developing a new instrument. Considerations have been discussed in *chapter three*.

- Choice of Suitable Test Reactions

As well as the considerations made in *chapter three* (see above), test and validation reactions have been discussed as part of the development of actinometers (*chapter five*). The choice of a model solid-state material will be discussed in *chapter six*.

## 4.5 Consideration of Experimental Method

In recent years' work with the isothermal microcalorimeter, a standard method of ampoule loading and lowering into the measuring position of the TAM has always been followed. However, the new apparatus and experimental conditions that the development of the photocalorimeter has brought have allowed the opportunity to investigate the best method of lowering 20ml ampoules into the TAM; the method that most quickly allows measurement of thermal activity to begin once the signal has settled down from "thermal shock" (*see section 3.1.1*).

The traditional method of lowering is as follows:

- Load ampoules into equilibrium position in the TAM
- Wait 30 minutes to obtain thermal equilibrium
- Lower ampoules slowly into measuring position and immediately begin recording

It has been noted, however, that starting the data recording immediately after the lowering down into the measuring position often leads to some thermal shock being recorded by the TAM in the first few minutes of the experiment. Indeed, investigations into this effect and apparatus to counteract it are currently under development.<sup>88</sup>

Experiments have been carried out to investigate what difference various lowering methods make to the initial calorimetric data in an experiment.

The two 20ml glass ampoules were both filled with 15ml distilled water under "normal" calorimetric test conditions (i.e. Relative humidity, 25°C, 24 hour test).

The following four "lowering methods" were evaluated:

**Method 1** – Load samples and immediately lower to measuring position. Start recording immediately.

**Method 2** – Load samples and immediately lower to measuring position. Wait 30 minutes then start.

**Method 3** – Load samples and lower to equilibrium position. Wait 30 minutes then lower to measuring position. Wait 30 minutes and then start recording.

**Method 4** - Load samples and lower to equilibrium position. Wait 30 minutes then lower to measuring position then start recording immediately.

The combined outputs from the TAM were then compared graphically as shown in *Figure 4.5.1* below:

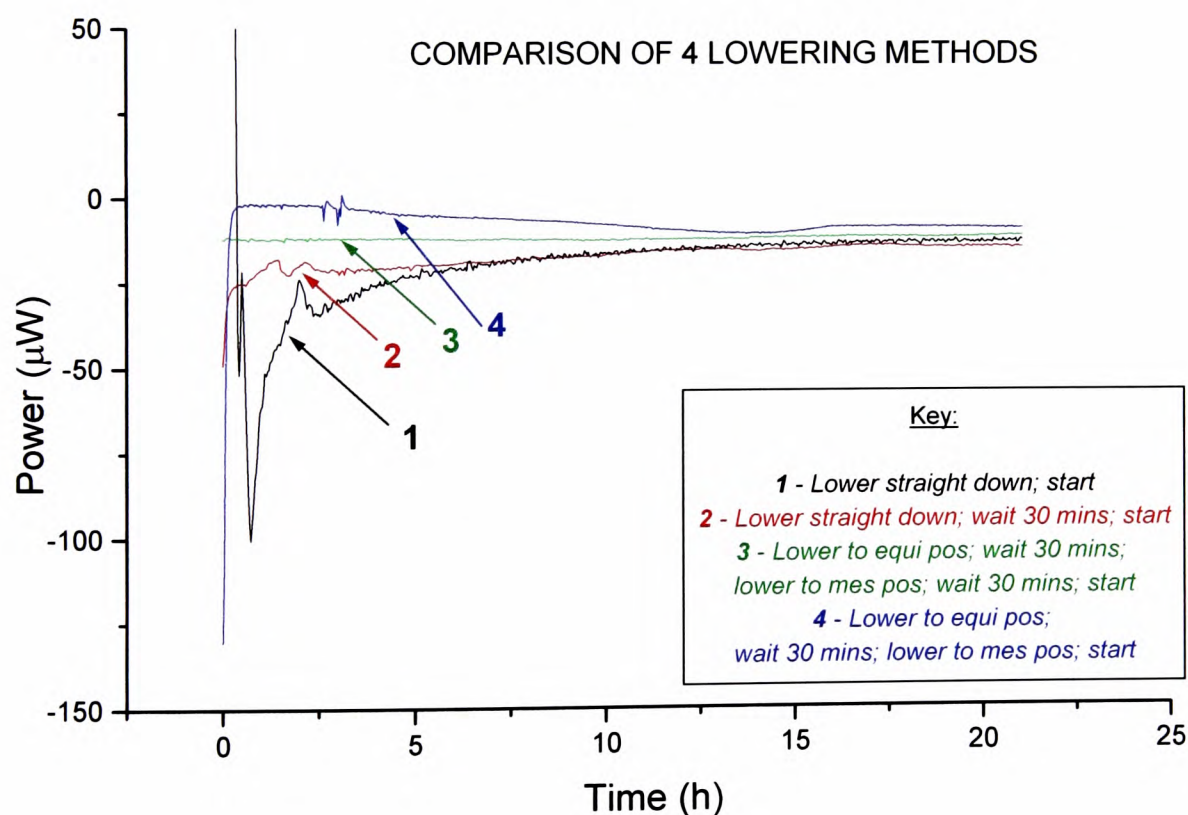


*Figure 4.5.1* Graphical comparison of four different methods of ampoule lowering

As can be clearly seen from the figure, the different lowering methods do have an effect on the calorimetric output. As expected, lowering the ampoules straight down from loading without spending any time at the equilibrium position caused significant thermal effects. However, the experiments where the ampoules were at first held at the equilibrium position before recording of the experiment began, exhibited much more stable outputs. *Method 3* showed particular stability over the 24 hour test period.

It can be concluded from this work that *methods 3 or 4* (i.e. held at the equilibrium position first) are the only procedures for lowering ampoules that should be used to avoid thermal effects at the beginning of an experiment. Out of these two, the preference should be *method 3*, which exhibited the most stable output of all

This lowering method will be used in all experimental work from now on in the project, unless stated otherwise.

It is not until all these issues were resolved that the final stage of the project could be commenced; that of using the photocalorimeter to establish the wavelengths of light that cause photodegradation in drug products and formulations.

*Chapter five* describes the use of the novel photocalorimeter, developed as described above, to establish methods of validation and quantification of the delivery of light to a sample placed in the calorimetric ampoule.

*CHAPTER 5*

*ACTINOMETRY*

## 5. Actinometry

Following the development of the photocalorimeter, described in *chapter four*, and having validated the calorimeter using the *triacetin* reaction, described in *chapter three*, the next step is to develop a suitable method of actinometry.

Actinometric methods allow the measurement of the light energy to which a sample is exposed when undergoing reaction. This measurement is the photon flux, with units of *watts per square metre* ( $Wm^{-2}$ ), which allows quantitative measurement of the photon flux to which a sample under test is exposed.

The two main actinometric methods under consideration for use with the photocalorimeter are chemical actinometry and spectroradiometry.

Although the aim of the project is to develop an instrument that can analyse solid and solution-phase systems, the development of an actinometric method for use with the photocalorimeter, which is described below, will be for use with solutions only. Limited numbers of actinometric methods have been recommended in the literature<sup>18-22</sup> for use with solid-state materials; and the possibility of using the photodegradation reaction of *nifedipine* as a solid state test material is described in *chapter six*.

### 5.1 Chemical Actinometry

The use of chemical actinometry to measure light dose during drug photostability testing is an absolute method in that it allows the absolute number of photons impinging on a sample to be measured. Data obtained is then converted to standard photon flux units of  $Wm^{-2}$ .

Typically, a chemical actinometer is a solution containing a chemical compound that undergoes a specific chemical reaction as a result of photon absorption. The rate at which this reaction takes place is related to the rate at which photons are absorbed by the actinometer. In the case of drug stability studies, the actinometer solution is transferred to an appropriate container and illuminated under the same conditions as the drug samples. The actinometer reaction is followed as a function of illumination

time and the data used to compute the photon flux to which the drug samples are exposed in the ampoule.

Many methods of chemical actinometry<sup>18-22, 89, 90, 94</sup> and its general principles have been discussed for years in the literature.

The currently approved method of chemical actinometry using quinine solutions (as outlined by the ICH monograph)<sup>91</sup> is simple but has been demonstrated to have some disadvantages<sup>92, 93</sup> which limits its usefulness.

Two principal candidates for use as chemical actinometers are the photodegradation of *2-nitrobenzaldehyde* and the photoreduction of *potassium ferrioxalate*.

Both have useful properties that set them apart from many other actinometers. *Potassium ferrioxalate* is of particular interest since it is the recommended IUPAC actinometric method, whilst *2-nitrobenzaldehyde* is an interesting alternative, as described in the literature. Both systems are explained in the following sections.

### 5.1.1 The Photodegradation of 2-nitrobenzaldehyde under white light

The photochemistry of 2-nitrobenzaldehyde has been studied on numerous occasions, <sup>95, 96, 97, 98</sup> particularly for reactions involving UV light.

The use of this material in actinometry has some unique advantages. Firstly, the actinometer has the potential to be used in solid, solution or colloidal dispersion systems. Secondly, the quantum yield for the photodegradation reaction is not wavelength-dependent and therefore the use of a monochromator to select “causative wavelengths” for photosensitive materials (as described in *chapter six*) would not affect the actinometer in any way. Thirdly, performing experiments on 2-nitrobenzaldehyde is relatively straight-forward and finally, the photoreaction is zero order <sup>22</sup> (i.e. linear loss of 2-nitrobenzaldehyde as a function of irradiation time).

The photoreaction of 2-nitrobenzaldehyde, shown in *Figure 5.1.1* below, <sup>22</sup> proceeds via an intramolecular rearrangement involving transfer of an –NO<sub>2</sub> oxygen atom to the aldehyde functionality yielding the nitrosobenzoic acid product.

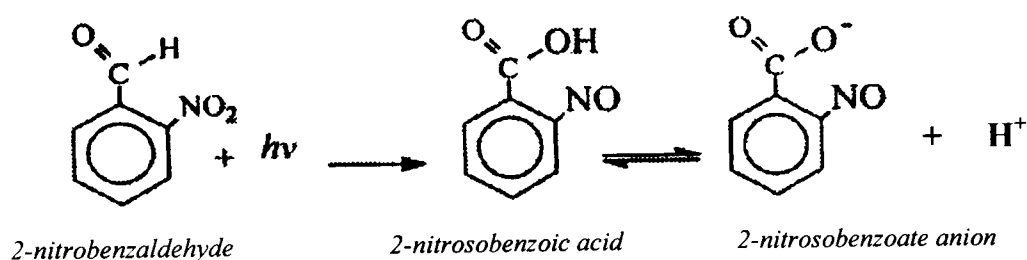


*Figure 5.1.1* The photodegradation of 2-nitrobenzaldehyde

The photochemistry of 2-nitrobenzaldehyde (from now onwards 2-NB) was first described in 1900 by Ciamician and Silber. <sup>95</sup> Since then, Bowen *et al.*, <sup>96</sup> Lucy and Leighton <sup>97</sup> and Pitts <sup>98</sup> have established the quantum yield for the photolysis of 2-NB.

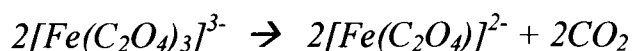
In the range of 300 - 410nm the quantum yield is known <sup>22</sup> to be 0.5. The quantum yield can be defined as the number of moles of the compound which reacted divided

by the number of *einsteins* absorbed by the compound. For a quantum yield of 0.5, 1 *einstein* (1 mole of photons) will cause 0.5 moles of 2-NB to undergo conversion to product. This conversion is independent of wavelength and temperature.

### 5.1.2 The Photodegradation of *Potassium Ferrioxalate*

*Potassium ferrioxalate* has been employed as a chemical actinometer for many years.<sup>19, 20, 99-107</sup> First developed by Hatchard and Parker,<sup>108</sup> it is capable of accurately measuring small doses of ultra-violet light across a wide wavelength range accurately.

On exposure to light of wavelength less than 490nm, solutions of the *ferrioxalate* ion undergo decomposition according to the equation (which is not balanced);



The *potassium ferrioxalate* actinometer has the four following advantages:

#### **Sensitivity**

The minimum detectable amount of energy is of the order  $5 \times 10^{-10}$  quanta.<sup>108</sup>

#### **Wavelength Coverage**

The quantum efficiency increases gradually from about 0.9 in the region of 480nm to about 1.2 at ~253nm.<sup>108</sup>

#### **Photolyte stability and Photolysis Products**

In the absence of light the actinometer solution can be kept for long periods without decomposition. The 'blank' value is low.<sup>108</sup>

#### **Simple to Operate**

A large number of determinations can be made in a short time. Large or small amounts of decomposition can be measured with equal accuracy.<sup>108</sup>

### 5.1.3 Actinometric Theory

Knowledge of quantum yield and reaction order, presents the opportunity to use photodegradation reactions as chemical actinometers to calculate the light flux.

A paper by Willett *et al.*<sup>109</sup> outlines the procedure for calculating the irradiance,  $I_0$  (in *einstein dm<sup>-3</sup>s<sup>-1</sup>*) and subsequently the light flux,  $F_0$  (in *Wm<sup>-2</sup>*) for a light source provided either the rate constant,  $k$  or the enthalpy of reaction,  $H$  can be determined.

The basic calorimetric equation for zero-order reactions relates rate constant, enthalpy and calorimetric output as follows<sup>46</sup>;

$$\Phi = k.H.V \qquad \text{Eqn 5.1.1.1}$$

where

- $\Phi$  is the calorimetric output (*W*)
- $k$  is the rate constant (*mol dm<sup>-3</sup> s<sup>-1</sup>*)
- $H$  is the reaction enthalpy (*Jmol<sup>-1</sup>*)
- $V$  is the volume of reaction solution (*dm<sup>3</sup>*)

However, the product  $k.H$  requires a value of  $k$  or  $H$  to be known to allow separation of the variables. A value of  $k$  is known for the *potassium ferrioxalate* reaction but not for *2-NB*.

For *2-NB*, the value of  $k$  could be found theoretically from bond-enthalpy calculations. However, literature values are quoted for gas-phase systems and for accurate calculations these are unacceptable.

An alternative means of obtaining an initial value for  $k$  or  $H$  must therefore be sought for *2-NB* which can then be applied to the calorimetric equation above for future calculations. This method is described in *section 5.1.5.1* below.

The final stage of the process is to apply established values of  $k$  to find the irradiance and photon flux of the Xe arc lamp.

The stages of the calculation are outlined below. Reference should be made to the Mathcad™ worksheets printed below:

### Calculation of Irradiance

The irradiance can be calculated using the following equation:

$$I_o = k_o / \phi \quad \text{Eqn 5.1.1.2}$$

where  $k_o$  is the rate constant for the photodegradation ( $\text{mol dm}^{-3} \text{s}^{-1}$ )  
 $\phi$  is the quantum yield

### Calculation of Photon Flux

The photon flux,  $F_o$  (in  $\text{W m}^{-2}$ ), can be calculated from the following:

$$F_o = I_o \cdot V \cdot N_A \cdot E_\lambda / A \quad \text{Eqn 5.1.1.3}$$

where  $I_o$  is the irradiance ( $\text{einstein dm}^{-3} \text{s}^{-1}$ ) (and 1 *einstein*  $\equiv$  1 *mol* of photons)  
 $V$  is the volume of solution ( $\text{dm}^3$ )  
 $A$  is the cross-sectional area of exposed actinometric solution ( $\text{m}^2$ )  
 $N_A$  is Avogadro's number ( $\text{mol}^{-1}$ )  
 $E_\lambda$  is the energy of a photon of wavelength  $\lambda$  (in  $\text{J photon}^{-1}$ )

The cross-sectional area of exposed solution,  $A$ , is found from

$$A = \pi r^2 \quad \text{Eqn 5.1.1.4}$$

where  $r$  is the radius of the ampoule ( $\text{m}$ )

hence  $A = \pi \times 0.0125 \times 0.0125 = 4.911 \times 10^{-4} \text{ m}^2$  for the ampoules used here

Finally, the energy of a photon can be calculated from *Planck's Law*:

$$E_{\lambda} = h\nu = hc/\lambda \qquad \text{Eqn 5.1.1.5}$$

where  $h$  is Planck's constant ( $6.63 \times 10^{-34} \text{ Js photon}^{-1}$ )

$c$  is the speed of light ( $2.99 \times 10^8 \text{ ms}^{-1}$ )

$\lambda$  is the average wavelength over which the actinometer is used ( $m$ )

NB the average wavelength is calculated by multiplying the wavelength and irradiance together over the range of interest (typically 290-400nm) and dividing by the irradiance over each bandwidth summed over the range of interest. This value is known as the weighted-average wavelength and is supplied by the manufacturers of the lamp.

It should be noted that the irradiance value is therefore imbedded in future calculations for evaluating the photon flux,  $F_0$  and may be a source of error (see *section 5.1.3*).

Mathcad™ then produces values for the irradiance and photon flux for all actinometric experiments carried out with the Xe arc lamp at 240W output. These values are shown in *sections 5.1.5.2* for 2-NB and *5.1.6.2* for *potassium ferrioxalate* which include the mean values of  $I_0$  and  $F_0$ ; the standard deviations and the corrected values.

The corrected value of the photon flux is evaluated by multiplying by 3/2 since only two of the three fibre optic cables were used in the experiments; hence two-thirds of the light and therefore two-thirds of the real photon flux will have been recorded.

NB This correction factor assumes precise division of the fibre bundles meaning some degree of error will be introduced into the evaluation.

### 5.1.4 Experimental procedure

The first task is to run a pair of identical photodegradation experiments in the TAM to obtain a value of  $\Phi$  for both a sample of the actinometer and a blank run obtained by the irradiation of a pair of empty ampoules.

NB The blank experiment is necessary to compensate for the variable nature of the *power axis* displacement of the TAM signal when the light was switched on. Assuming the setup of the apparatus is unchanged for both runs, subtraction of the blank signal from the sample signal ensures the difference in the displacement is only as a result of the photodegradation of the actinometer solution.

The experimental method applied is outlined below:

#### *Reference Experiment*

- The Xe arc lamp (240W) was switched on one hour in advance of ampoule loading
- Two empty 20ml stainless steel ampoules were lowered into the TAM using the standard photocalorimeter lowering method (see *chapter four*). The temperature of the TAM was set at 298K
- Once a stable baseline had been achieved with the ampoules in the measuring position, the data recording process began
- After approximately 2 hours, the shutter was opened and the ampoules irradiated
- The “light on” output was recorded until a stable signal had been achieved – this took approximately 2 hours before the light source shutter was closed
- The TAM continued to record a signal until the baseline had returned to its original value

*Sample Experiment*

- As above with one difference. The ampoules were filled with actinometer solution and distilled water in the sample and reference sides respectively

For zero-order processes, including the photodegradation of 2-NB and the photoreduction of *potassium ferrioxalate* a plot of power output ( $\Phi$ ) vs. time will yield a line with no slope (i.e. a horizontal line) since the reaction is only dependent on time and not on the concentration of the reactant. Thus the required value of  $\Phi$  is obtained by subtracting the reference output from the sample output once both outputs have reached equilibrium and produce horizontal lines.

### 5.1.5 Application of theory to 2-NB

#### 5.1.5.1 Alternative method for finding the rate constant, $k$ for 2-NB

The alternative method of finding  $k$  referred to in *section 5.1.3* is to measure the formation of the photoproduct with time using titration analysis. The photoreaction converts *2-nitrobenzaldehyde* into *2-nitrobenzoic acid* and if the solution is exposed to UV light for a known period of time, titration of the resulting acidic solution with sodium hydroxide solution enables the calculation of the number of moles of acid formed during the reaction. Consequently, a value for the zero-order rate constant in  $\text{mol dm}^{-3}\text{s}^{-1}$  can be obtained by dividing the number of moles formed by the irradiation time. This value can then be applied in *section 5.1.3* to *Equation 5.1.1.2* to find the irradiance and to *Equation 5.1.1.3* to find the photon flux.

#### Experimental Method – Preparation and Analysis of 2-nitrobenzoic acid

- 1.5112g of *2-nitrobenzaldehyde* was crushed to aid dissolution using a mortar and pestle
- The solid was dissolved in a mixture of 100ml ethanol and 100ml distilled water and stirred
- 3.5ml of 2-NB solution was pipetted into the 20ml stainless steel ampoule and exposed to the pre-ignited UV lamp, set at 240W for a known period of time
- The exposed solution was transferred to a glass vessel and titrated with 0.03M NaOH until the pH of the solution (measured with a pH meter) became neutral
- The volume of NaOH allowed the calculation of the number of moles of acid formed
- The number of moles formed was divided by the irradiation time to obtain a zero-order rate constant for the reaction

NB A titration of fresh-unirradiated 2-NB was carried out to establish a reference.

**Evaluation of  $k$** 

The table below shows the results for the 240W light experiments, together with the corresponding plot of moles formed against time. The average rate constant was then taken as the slope of the plot and applied to the calculation worksheet in Mathcad™ to calculate values for the irradiance,  $I_0$  and the light flux,  $F_0$ .

**Table 5.1 240W Xe arc Lamp Output**

Irradiation Time (s)	Product formed ( $\text{mol dm}^{-3}$ )
3600	$4.44 \times 10^{-5}$
3600	$8.57 \times 10^{-5}$
5400	$1.43 \times 10^{-4}$
5400	$1.43 \times 10^{-4}$
6300	$4.14 \times 10^{-4}$
7200	$6.57 \times 10^{-4}$
8100	$6.29 \times 10^{-4}$

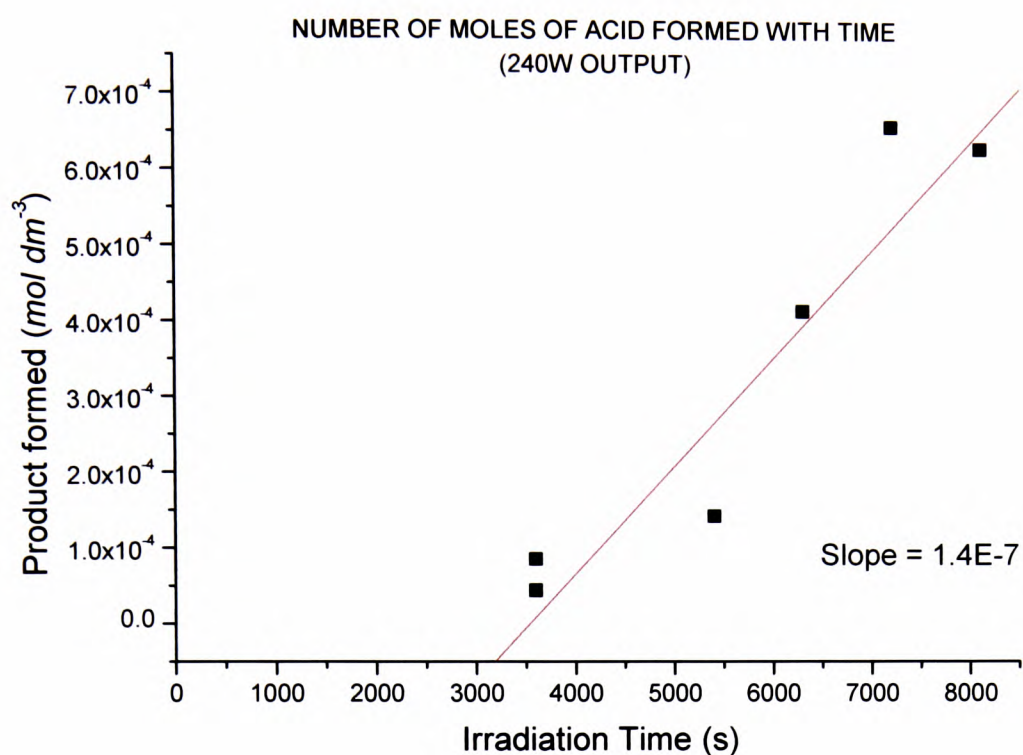


**Figure 5.1.5.1** Product formed with time at 240W

The rate constant obtained from the slope of the plot is:

$$k = 1.4 \times 10^{-7} \pm 2.6 \times 10^{-8} \text{ mol dm}^{-3} \text{ s}^{-1}$$

This value of  $k$  for 2-NB will be applied to calculate the irradiance and photon flux as described in *section 5.1.3*

### 5.1.5.2 Photodegradation experiments: 2-NB

Note: In all the calculations that follow, the raw data values displayed on the graphs are approximated to one significant figure.

As explained in *section 5.1.4* above and in *chapter four, section 4.3.2*, a zero order reaction results in a calorimetric output of a horizontal line achieved after the TAM has recovered from the “thermal shock” of the shining of light into the system. The offset observed below in *Figure 5.1.5.2* of  $\sim 66\mu W$  is the result of the imbalance in the capacity of the fibre optic cables.

The calibration photodegradation TAM output is shown below in *Figure 5.1.5.2*, together with the difference in the two outputs, assigned  $\Delta$ . Note the outputs confirm that the photoreaction of 2-NB is zero-order:

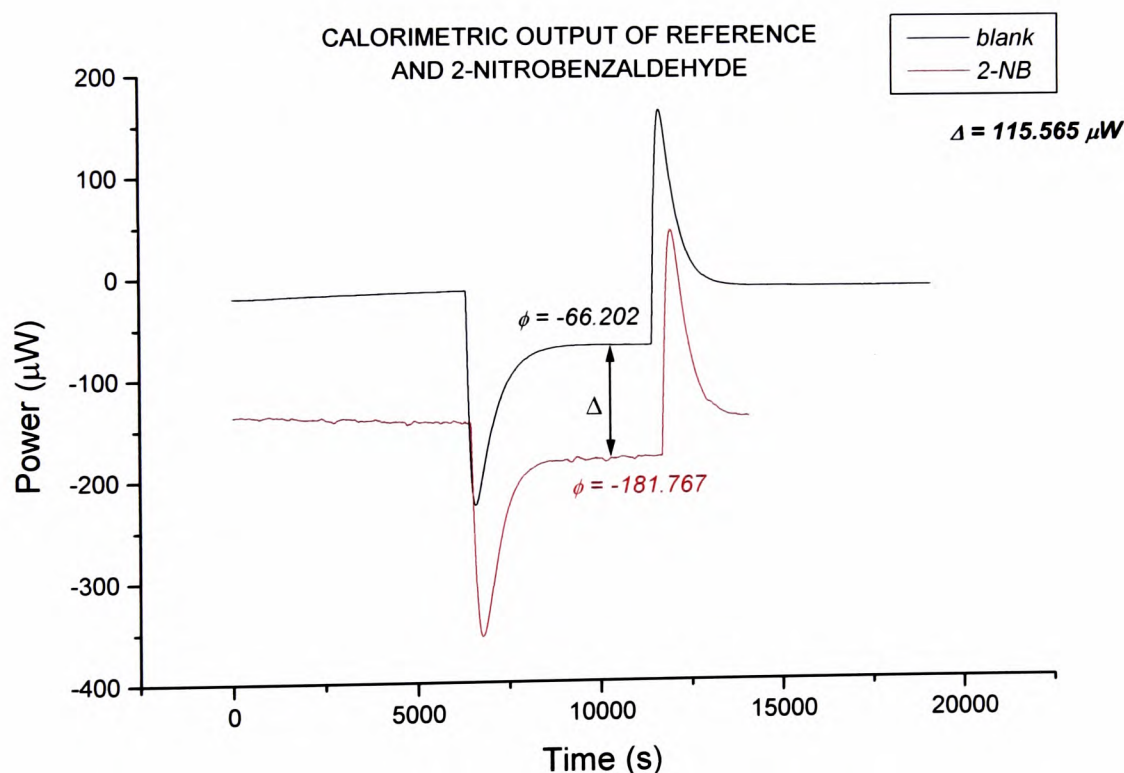


**Figure 5.1.5.2** The photodegradation of 2-NB alongside the reference output at 240W

From *figure 5.1.5.2*,  $\Delta = 115.6 \mu W$  or  $116 \times 10^{-6} W$

Using the zero-order calorimetric equation, the second task is to find the enthalpy of reaction  $H$  for the calibration reaction, based on the values found for  $k$  and  $\Delta$  above:

$$\text{If} \quad \Phi = k.H.V \quad \text{Eqn 5.1.1.1}$$

$$\text{then} \quad 116 \times 10^{-6} \text{ W} = 1.4 \times 10^{-7} \text{ dm}^{-3}\text{s}^{-1} . H . 0.004 \text{ dm}^3$$

$$\text{hence} \quad H = 202464 \text{ Jmol}^{-1} \quad \text{or} \quad 202.5 \text{ kJmol}^{-1}$$

This value of  $H$  will now be used to obtain values of  $k$  in the subsequent photodegradation experiments carried out in the TAM where no prior knowledge of the rate constant is assumed.

#### **Applying the value of $H$ to find $k$**

The outputs below show subsequent 2-NB photodegradation experiments carried out using the same experimental method described in *section 5.1.4*. The preparation of 2-NB solution was carried out as described in *section 5.1.5.1*

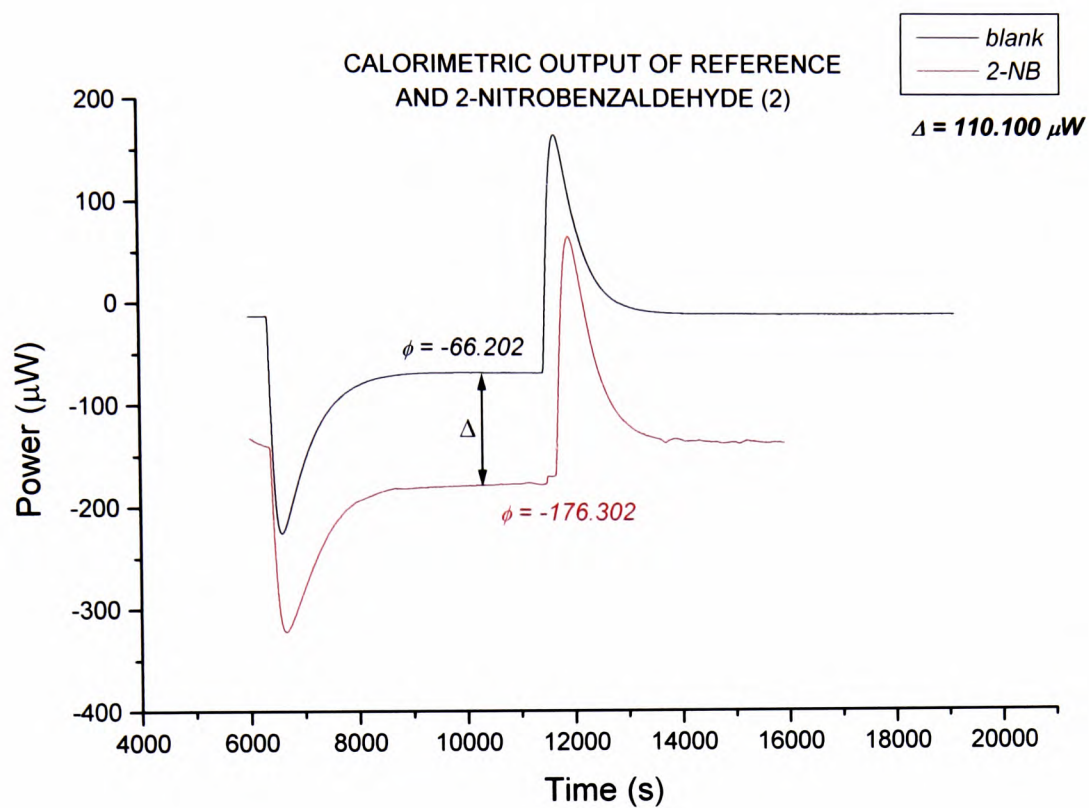


Figure 5.1.5.3 The photodegradation of 2-NB alongside the reference output at 240W (2)

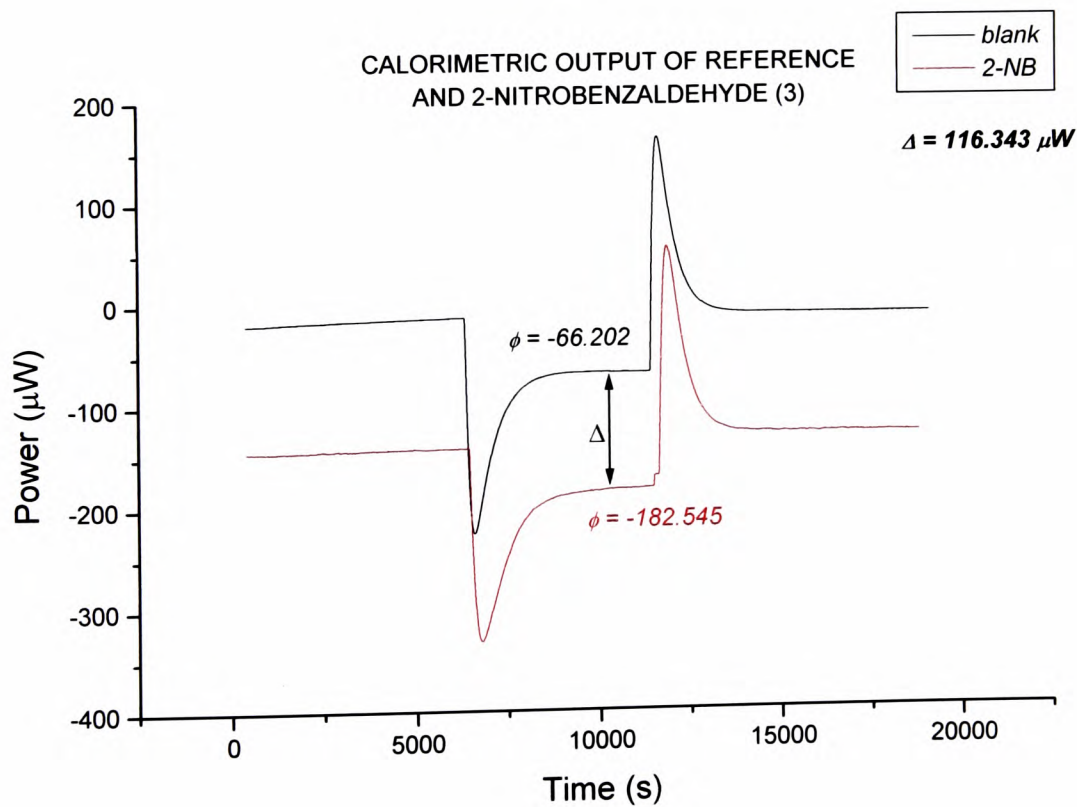


Figure 5.1.5.4 The photodegradation of 2-NB alongside the reference output at 240W (3)

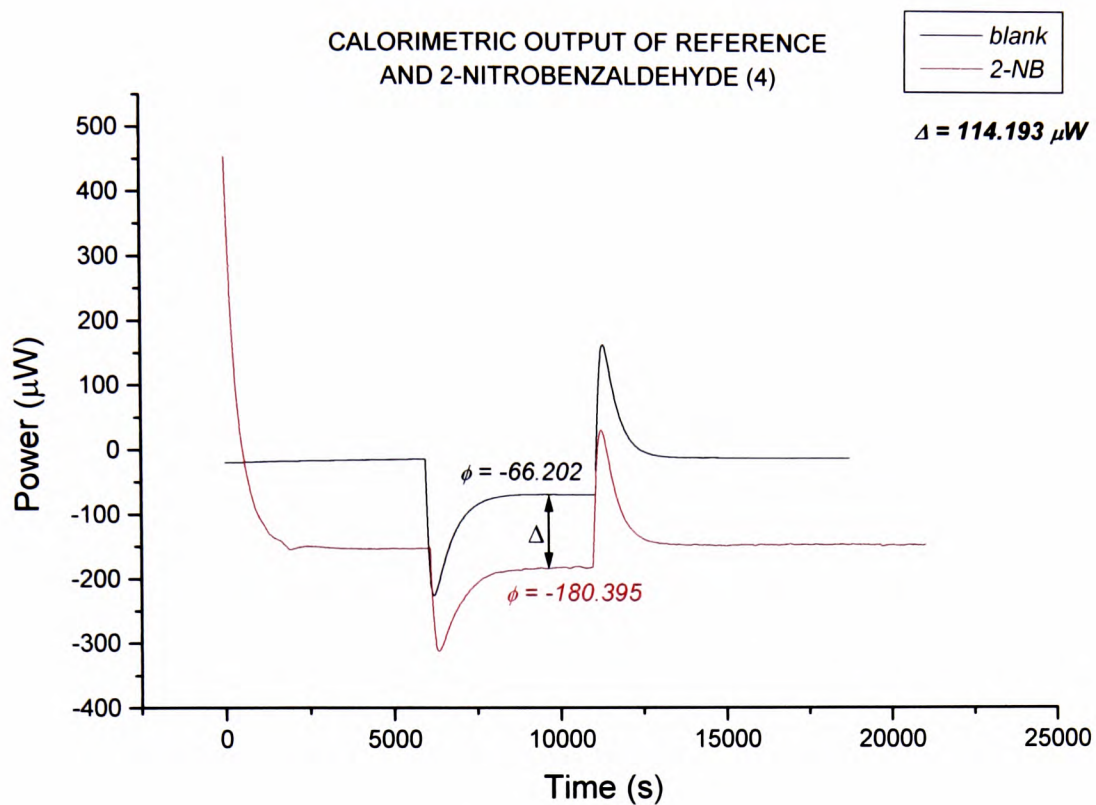


Figure 5.1.5.5 The photodegradation of 2-NB alongside the reference output at 240W (4)

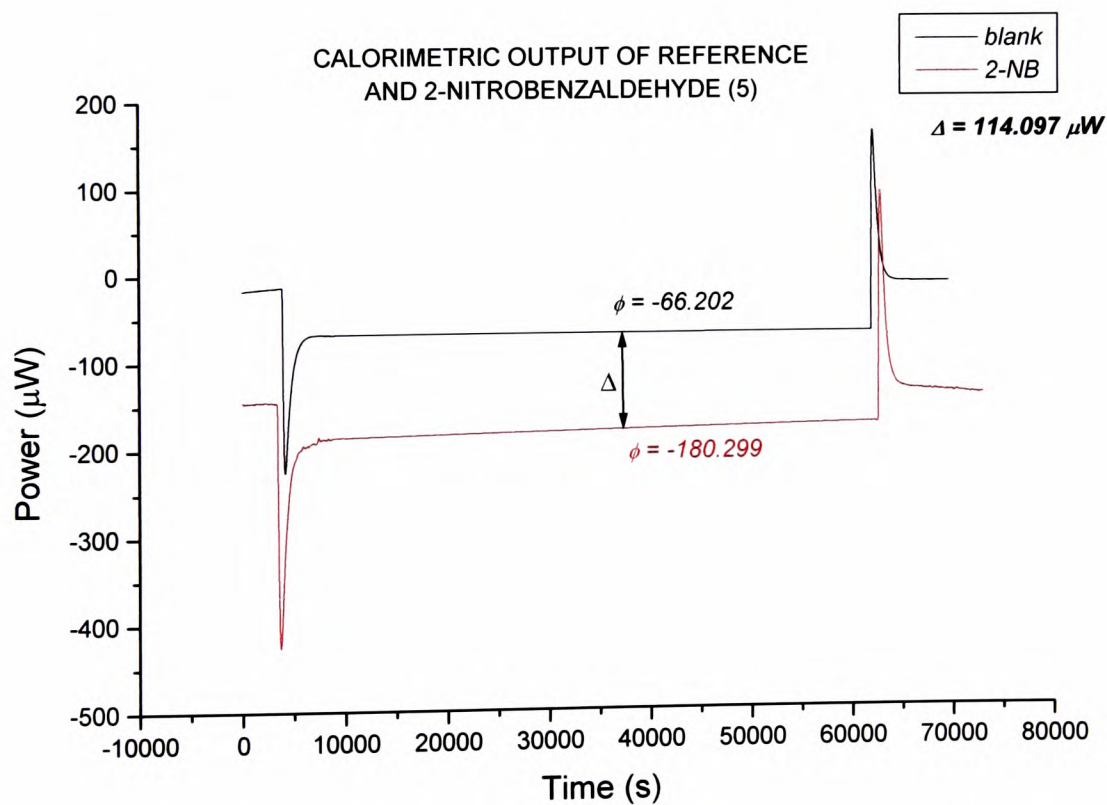


Figure 5.1.5.6 The photodegradation of 2-NB alongside the reference output at 240W (5)

The values required for the calculation of  $k$  are  $\Phi$  ( $\equiv \Delta$ ),  $H$  and  $V$ . These are summarised in *Table 5.2* below:

**Table 5.2** Parameters required for the calculation of  $k$

Experiment Number	$\Phi$ ( $\mu W$ )	$H$ ( $Jmol^{-1}$ )	$V$ ( $dm^3$ )
1	-		-
2	110	202464	0.004
3	116	202464	0.004
4	114	202464	0.004
5	114	202464	0.004
SD	2.6		
Mean	113		
% error	2.3		

Rearranging *Equation 5.1.1.1* gives:

$$k = \Phi / H.V \quad \text{Eqn 5.1.5.2}$$

and applying this equation to the figures in *Table 5.2* gives the following values of  $k$  for each reaction:

**Table 5.3** Values of  $k$  and the standard deviation

Experiment Number	Rate constant, $k$ ( $\text{mol dm}^{-3} \text{s}^{-1}$ )
2	$1.36 \times 10^{-7}$
3	$1.46 \times 10^{-7}$
4	$1.41 \times 10^{-7}$
5	$1.41 \times 10^{-7}$
SD	$4.1 \times 10^{-9}$
Mean	$1.41 \times 10^{-7}$
% error	2.1

Applying these values of the rate constant,  $k$  to the irradiance and photon flux equations outlined in *section 5.1.3* gives the following values:

**Table 5.4** Values of  $I_0$  and  $F_0$ , the mean values, standard deviation and corrected values: 2-NB

	<i>Irradiance, <math>I_0</math></i> ( <i>einstein <math>dm^{-3} s^{-1}</math></i> )	<i>Photon Flux, <math>F_0</math></i> ( <i><math>Wm^{-2}</math></i> )
Value 2	$2.7 \times 10^{-7}$	0.70
Value 3	$2.9 \times 10^{-7}$	0.76
Value 4	$2.8 \times 10^{-7}$	0.73
Value 5	$2.8 \times 10^{-7}$	0.73
Mean	$2.8 \times 10^{-7}$	0.73
SD	$8.2 \times 10^{-9}$	0.02
Mean Value x 1.5	$4.2 \times 10^{-7}$	1.1

These values were calculated via the Mathcad™ worksheets printed below:

**Stage 1** : enter the 4 values for  $k$  established in section 5.1.5.2 . Mathcad will know these as  $k_2$ ,  $k_3$ ,  $k_4$  and  $k_5$

$$k_2 := 1.36 \cdot 10^{-7} \quad k_3 := 1.46 \cdot 10^{-7} \quad k_4 := 1.41 \cdot 10^{-7} \quad k_5 := 1.41 \cdot 10^{-7}$$

**Stage 2** : enter the common values: the quantum yield, known to Mathcad as  $Q$ , the enthalpy, known to Mathcad as  $H$  and the volume, known to Mathcad as  $V$

$$Q := 0.5 \quad V := 0.004$$

**Stage 3** : to calculate the energy of a photon ( $E$ ), Mathcad needs data for Planck's Constant ( $h$ ), the speed of light ( $c$ ) and the average wavelength of the light ( $\lambda$ ). Additionally, Mathcad requires values for Avagadro's number ( $N$ ) and the cross-sectional area of solution under test ( $A$ ) to calculate the photon flux ( $F_0$ )

$$h := 6.63 \cdot 10^{-34} \quad c := 2.99 \cdot 10^8 \quad \lambda := 3.74 \cdot 10^{-7} \quad N := 6.02 \cdot 10^{23} \quad A := 4.91 \cdot 10^{-4}$$

$$E := \frac{(h \cdot c)}{\lambda}$$

**Stage 4 :** Mathcad uses *equation 5.1.1.2* to calculate the irradiance for each experiment

$$I_2 := \frac{k_2}{Q} \quad I_3 := \frac{k_3}{Q} \quad I_4 := \frac{k_4}{Q} \quad I_5 := \frac{k_5}{Q}$$

**Stage 5 :** Mathcad uses *equation 5.1.1.3* to calculate the photon flux for each experiment

$$F_2 := \frac{(I_2 \cdot V \cdot N \cdot E)}{A} \quad F_3 := \frac{(I_3 \cdot V \cdot N \cdot E)}{A} \quad F_4 := \frac{(I_4 \cdot V \cdot N \cdot E)}{A} \quad F_5 := \frac{(I_5 \cdot V \cdot N \cdot E)}{A}$$

**Stage 6 :** The values of the irradiance and photon flux at each experiment are summarised below:

$$I_2 = 2.72 \times 10^{-7} \quad F_2 = 0.707$$

$$I_3 = 2.92 \times 10^{-7} \quad F_3 = 0.759$$

$$I_4 = 2.82 \times 10^{-7} \quad F_4 = 0.733$$

$$I_5 = 2.82 \times 10^{-7} \quad F_5 = 0.733$$

Hence for the 240W light source using the 2-NB actinometer the mean corrected values for the irradiance,  $I_0$  and the photon flux,  $F_0$  are as follows:

$$F_0 = 1.1 \text{ Wm}^{-2}$$

$$I_0 = 4.2 \times 10^{-7} \text{ einstein dm}^{-3} \text{ s}^{-1}$$

The approximate value for the photon flux supplied by LOT Oriel, the suppliers of the photocalorimetric light source is  $1.3 \text{ Wm}^{-2}$  for the xenon arc lamp at 300W (100% power) and agrees with the calculated values as follows;

Calculated value =  $1.1 \text{ Wm}^{-2}$  (80% lamp power, 240W)

LOT Oriel value <sup>85</sup> =  $1.3 \text{ Wm}^{-2}$  (100% lamp power, 300W)

Considering the lamp was not operating at full power when the photodegradation of 2-NB was carried out, the figure of  $1.1 \text{ Wm}^{-2}$  represents a good result obtained from actinometry.

These values of irradiance and photon flux established through the photodegradation of 2-NB must be compared with the alternative methods described later in this chapter i.e. the *potassium ferrioxalate* reaction and spectroradiometry.

Note that studies of 2-NB at 300W (100%) lamp power were not carried out owing to the limited time allocated to the actinometric part of the project.

Having already established actinometric theory for photodegradation reactions (section 5.1.3), it is proposed to perform similar photodegradation experiments with the *potassium ferrioxalate* system and compare the values established for the irradiance and the photon flux from the two different chemical actinometers.

### 5.1.6 Application of theory to *Potassium Ferrioxalate*

The major advantage of using *potassium ferrioxalate* as an actinometer is that the reaction enthalpy is already well-established.<sup>108</sup> This means that unlike the case for *2-NB*, the solution can be tested in the calorimeter and the output inserted into the Mathcad™ sheet directly to obtain values for the irradiance and photon flux. No pre-preparation (i.e. titration to establish a value of *k*) is required.

#### 5.1.6.1 Experimental Method – Preparation of stock *Ferrioxalate* Solution

- Prepare 1.5M *potassium oxalate* in H<sub>2</sub>O by dissolving 46.06g of *potassium oxalate* in 167ml H<sub>2</sub>O
- Prepare 1.5M *ferric chloride* solution by dissolving 13.538g *ferric chloride* in 56ml H<sub>2</sub>O.
- Mix the two solutions with vigorous stirring to precipitate  $K_3[Fe(C_2O_4)_3] \cdot 3H_2O$  (*potassium ferrioxalate*)
- Air-dry the precipitate using a Buchner flask over 5 hours
- Recrystallise three times from warm water before drying by vacuum filtration
- Dissolve 9.21g of solid in 112.5ml H<sub>2</sub>O and 12.5ml H<sub>2</sub>SO<sub>4</sub> (0.1N)
- Resultant solution is 0.15M

Once prepared, the solutions were stored in glass vessels with stirring and kept in a dark room under red light. The solutions were each kept as long as required in order to carry out a whole series of tests in the calorimeter; typically 12 – 15 hours in duration.

### 5.1.6.2 Photodegradation experiments: *Potassium Ferrioxalate*

The TAM experiments for the *potassium ferrioxalate* reaction were run exactly as for the 2-NB experimental method described in section 5.1.4. The only difference is the lamp output which is now at 300W (100% power). As before, a blank run was carried out first, followed by a series of sample runs and the difference in TAM signal recorded ( $\Delta$ ) as the value for  $\Phi$ .

As the *potassium ferrioxalate* reaction has been adopted as a reliable method of actinometry for conventional photochemistry, the prepared solution should be stable and produce a reproducible signal when exposed to UV light under the same conditions. The TAM output should therefore be constant for each experiment.

Figure 5.1.6.1 below is the calorimetric output for a pair of blank ampoules. The outputs from the subsequent series of *potassium ferrioxalate* experiments are shown below. In each case, the value of  $\Phi$  for the *potassium ferrioxalate* photodegradation was read off at the point at which the output had settled down and the expected flat line ensued ( a *minimum* of 2000 seconds after the switching on of the light)

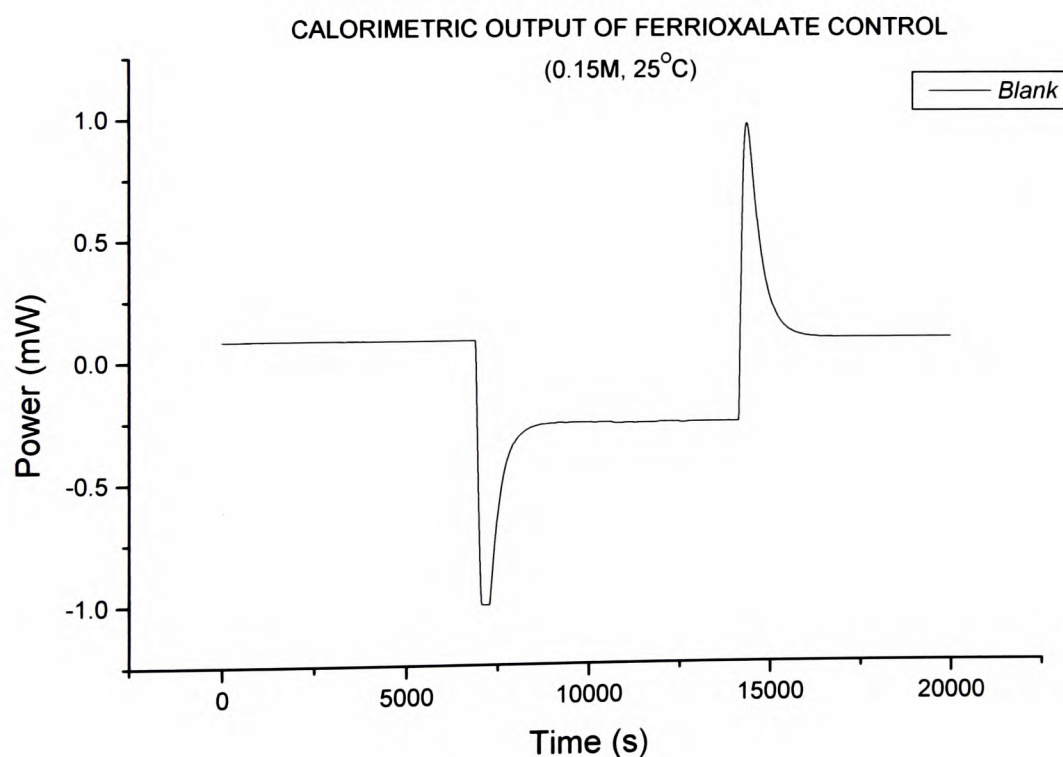
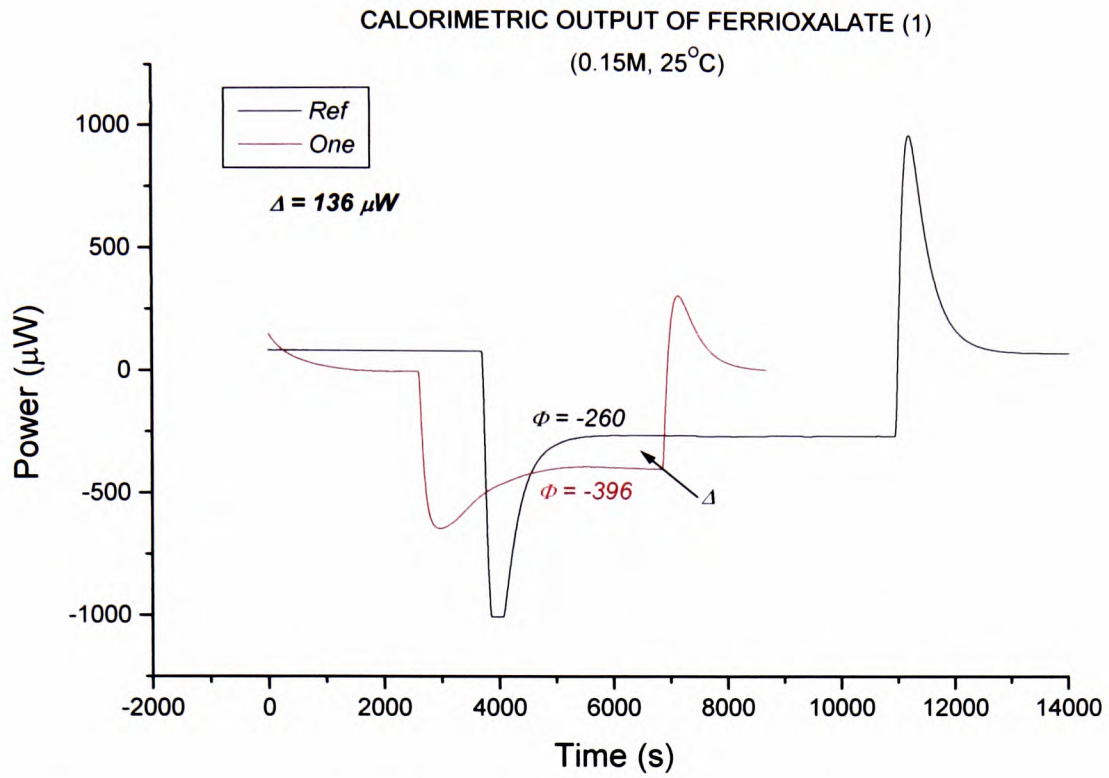
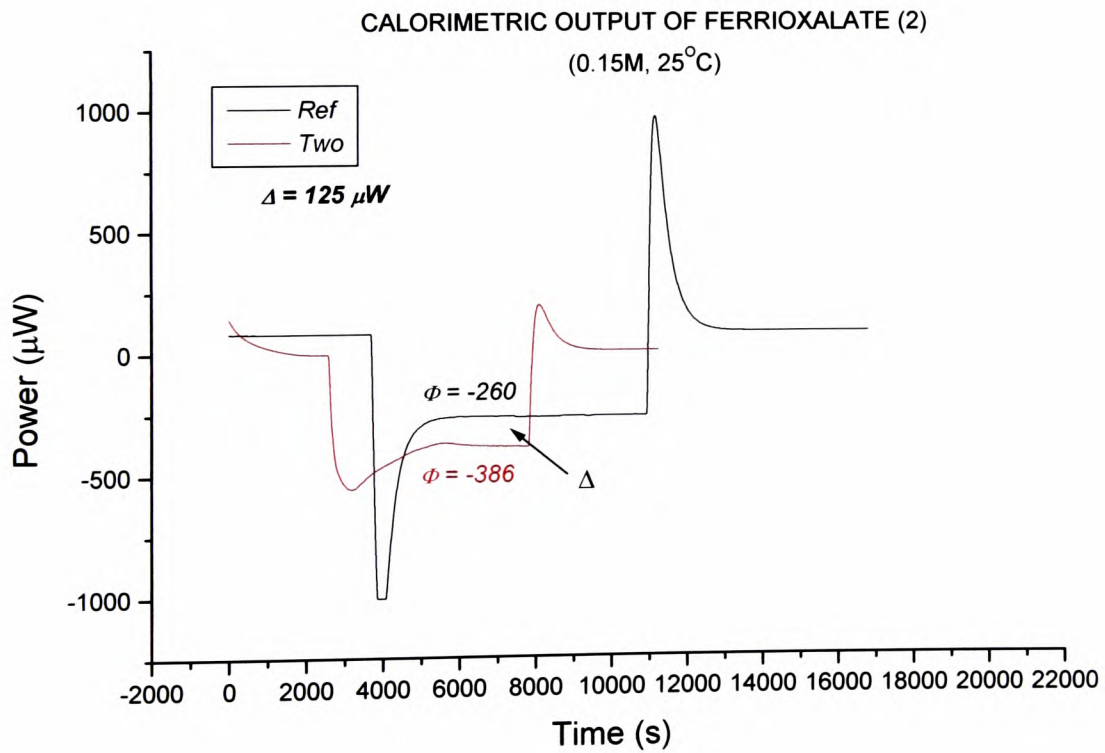


Figure 5.1.6.1 Reference output for the TAM testing of *potassium ferrioxalate* photodegradation



**Figure 5.1.6.2** First output for the TAM testing of potassium ferrioxalate photodegradation



**Figure 5.1.6.3** Second output for the TAM testing of potassium ferrioxalate photodegradation

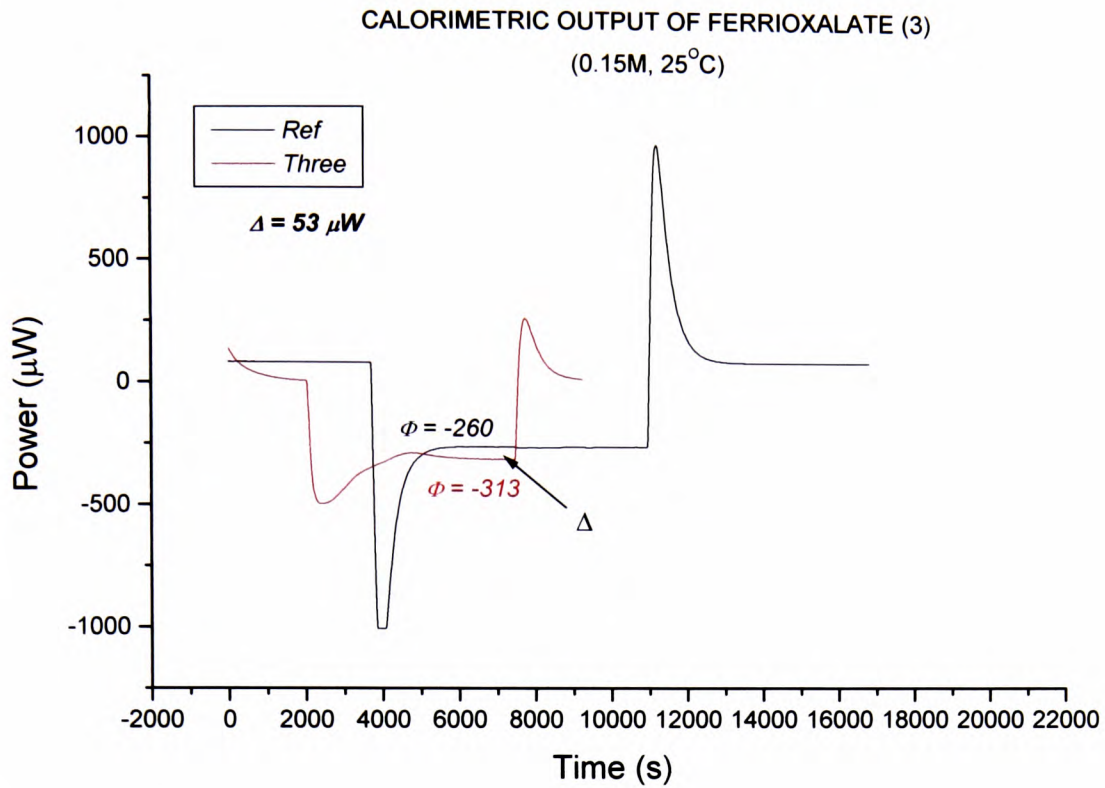


**Figure 5.1.6.4** Third output for the TAM testing of potassium ferrioxalate photodegradation

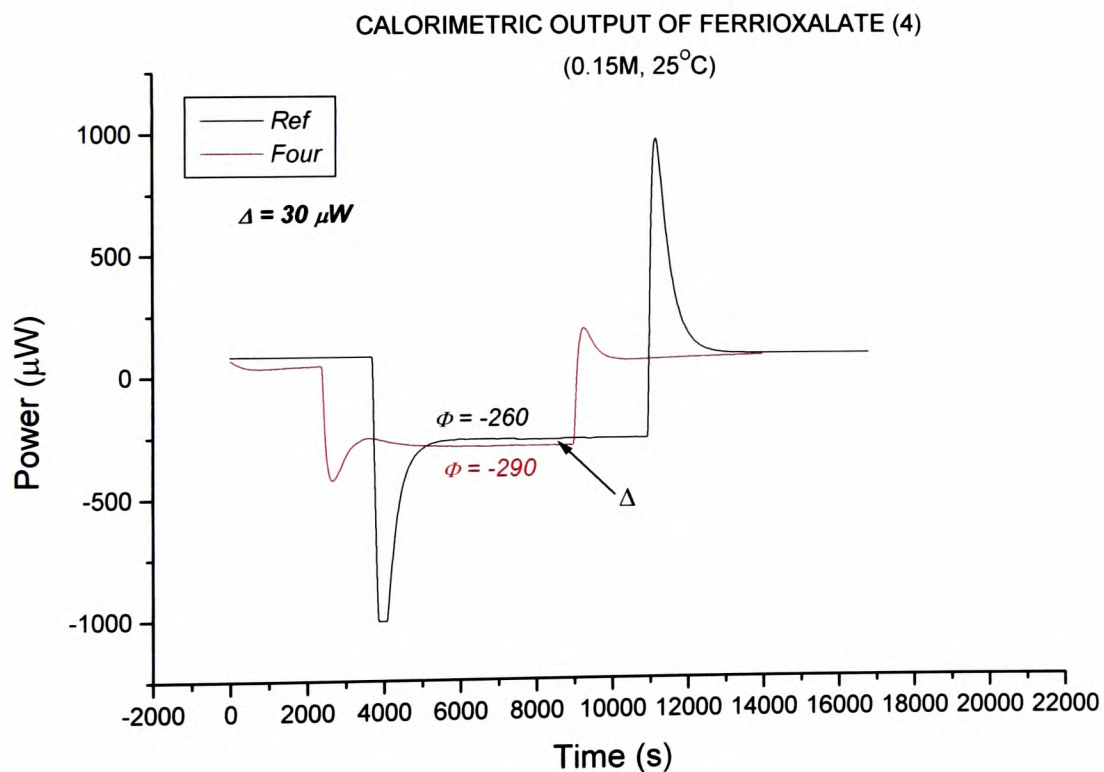


**Figure 5.1.6.5** Fourth output for the TAM testing of potassium ferrioxalate photodegradation

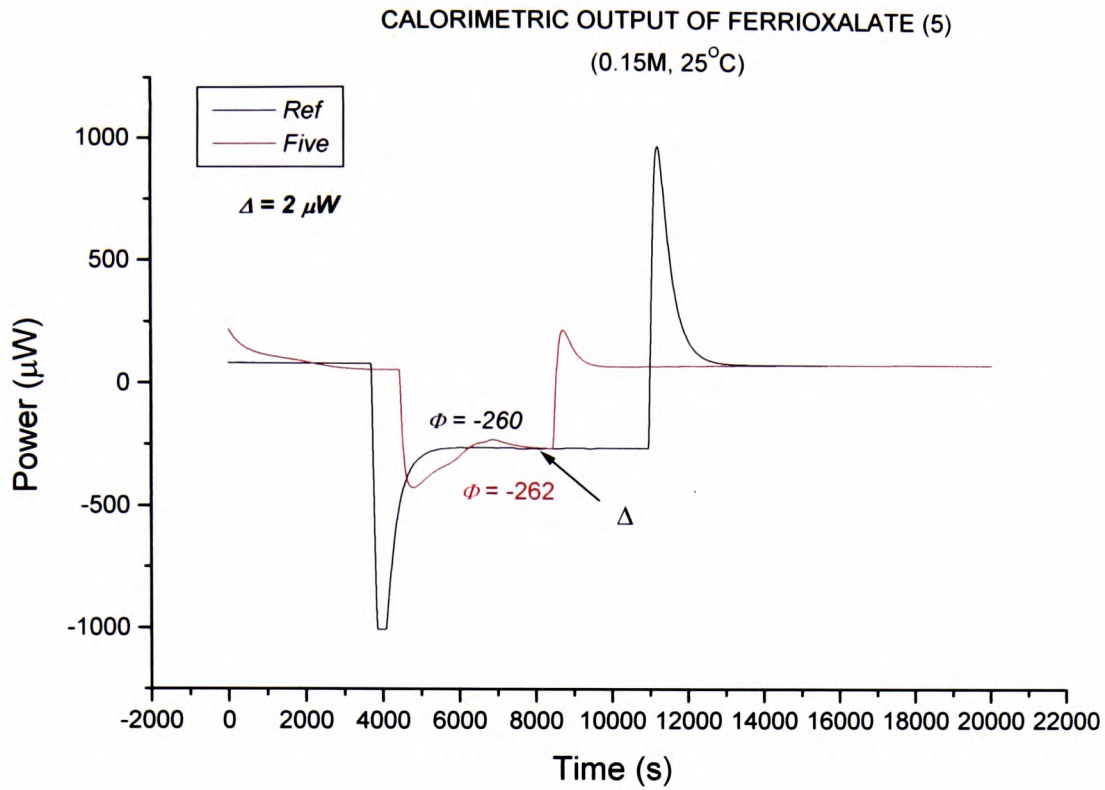


**Figure 5.1.6.6** Fifth output for the TAM testing of potassium ferrioxalate photodegradation

These plots can be combined as shown below:

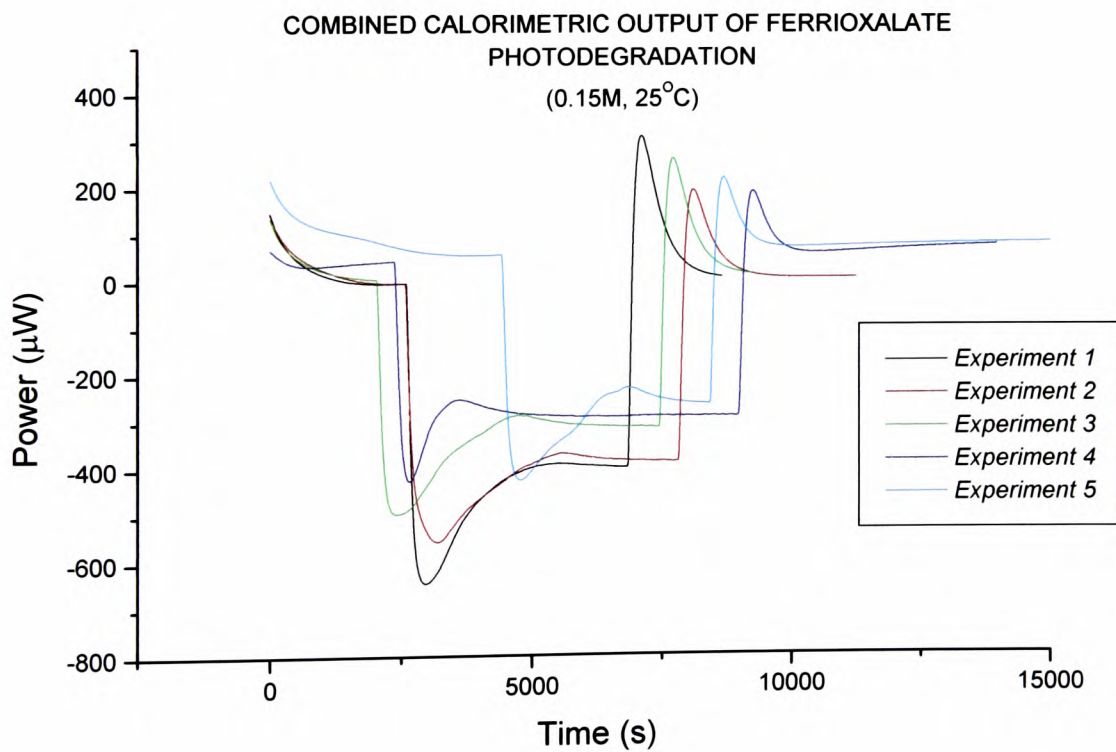


**Figure 5.1.6.7** Combined outputs for the TAM testing of potassium ferrioxalate photodegradation

It is clear from the above figure that the TAM signal is neither consistent nor reproducible. The plots suggest that the photodegradation reaction is diminishing the longer the solution is stored after preparation. The successive differences in the signal between reference and sample runs indicate this as shown in *Table 5.5* and the trend can be shown graphically in *Figure 5.1.6.8* below:

**Table 5.5** *The change in signal difference with age of solution*

Time elapsed (h)	Calorimetric signal ( $\mu W$ )	Change in orig. signal ( $\mu W$ )
0	136	0
3	125	-11
27	53	-83
51	30	-106
56	2	-134

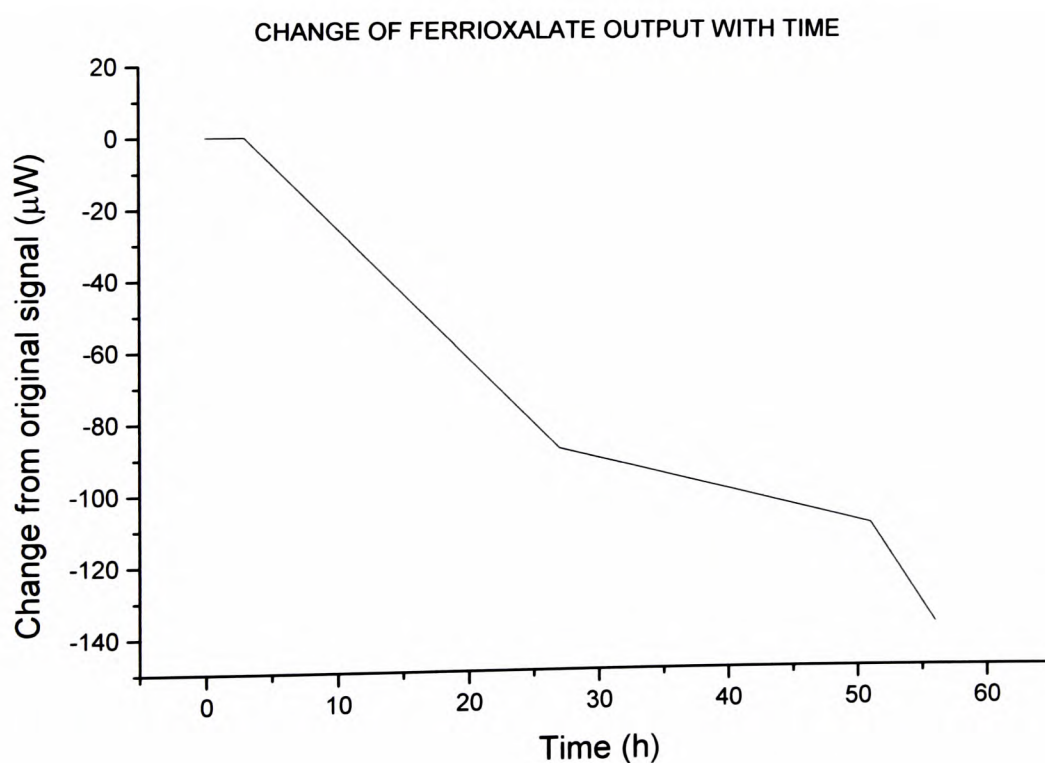


**Figure 5.1.6.8** *The change in calorimetric output with solution lifetime*

Clearly there is a problem with the stability of the *potassium ferrioxalate* solution the longer it is left after preparation. *Potassium ferrioxalate* is of limited use as a chemical actinometer unless this stability issue can be addressed.

### Modified Preparation of Stock *Ferrioxalate* Solution

The problem with first batch of experiments was the failure to prepare the solutions under an inert atmosphere. To solve this problem for a second round of *potassium ferrioxalate* experiments, a Schlenk-type apparatus was purchased. The side-arm allowed the system to be purged by nitrogen during preparation. On closing the tap, the *potassium ferrioxalate* solution could be stored under oxygen-free conditions indefinitely without the need for a continuous supply of nitrogen.

An illustration of the apparatus is shown below:



**Figure 5.1.6.9** The Schlenk flask allows oxygen-free solution preparation

Following preparation of the solution this time in an inert atmosphere, the same testing procedure as previously described was carried out, with the solutions allowed to stand in storage for the same length of time as for the original *potassium ferrioxalate* experiments.

In the absence of settled flat-line zero-order outputs observed previously (in Figures 5.1.6.3 to 5.1.6.6 above), measurements for the values of  $\phi$  in the experiments below were taken 3000 seconds after the light was switched on to ensure the same extent of reaction was taking place for each experiment. The outputs show that the reaction is complex and not made up of simple first or second order processes.

Empirically-based results are displayed in Table 5.6 and the TAM outputs are shown below;

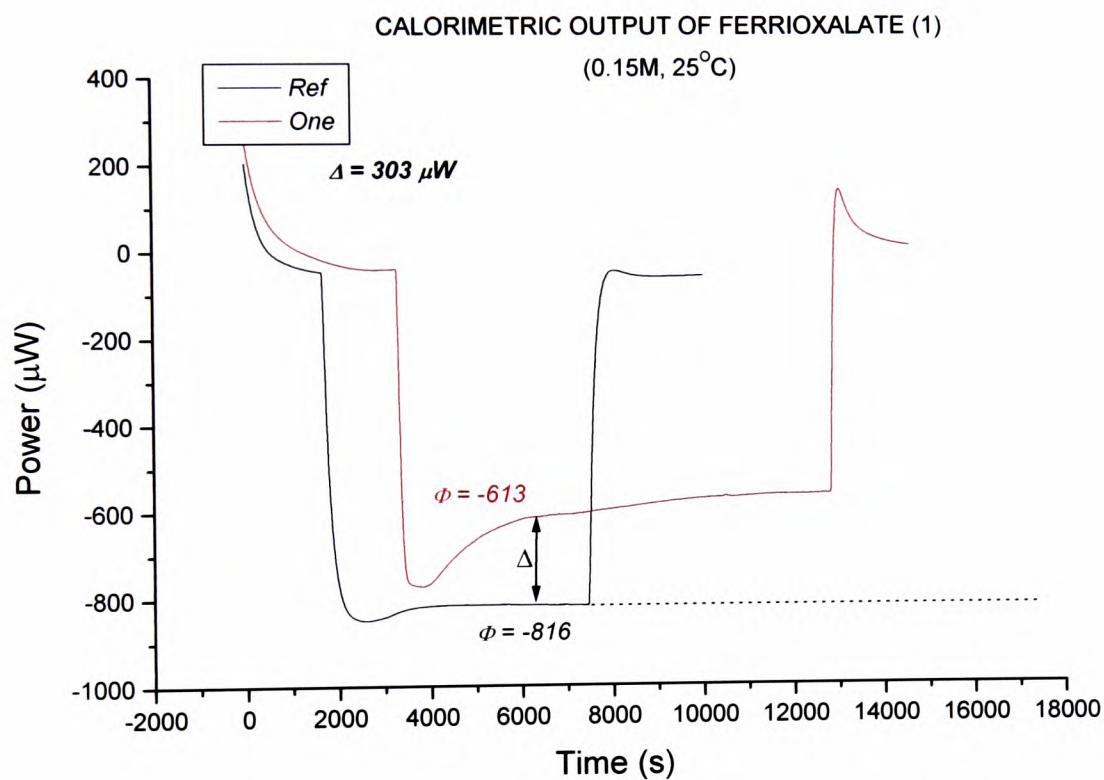
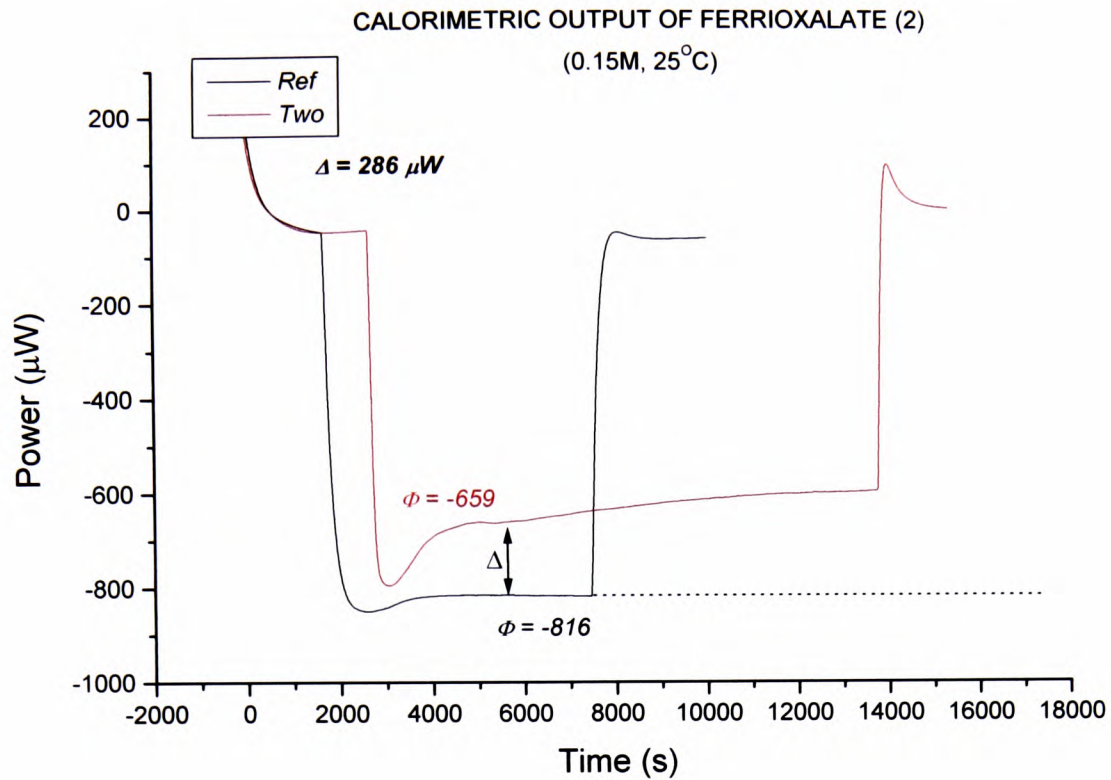
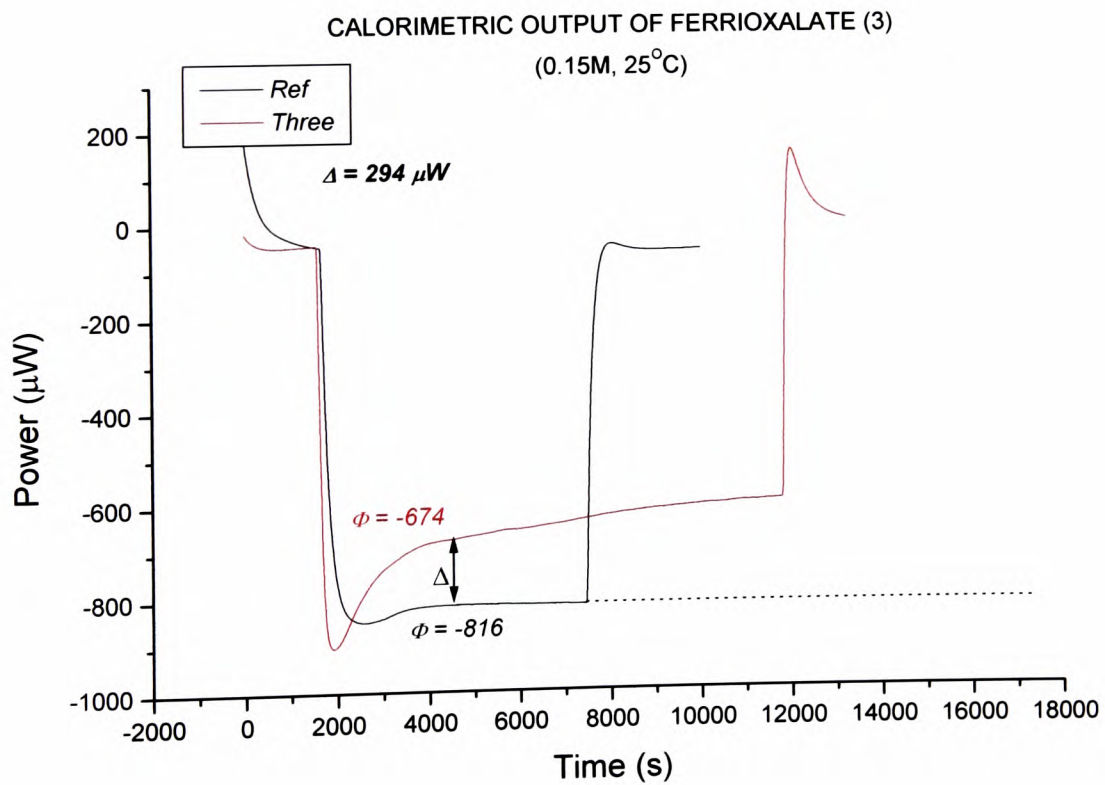


Figure 5.1.6.10 First output for the TAM testing of potassium ferrioxalate photodegradation



**Figure 5.1.6.11** Second output for the TAM testing of potassium ferrioxalate photodegradation



**Figure 5.1.6.12** Third output for the TAM testing of potassium ferrioxalate photodegradation

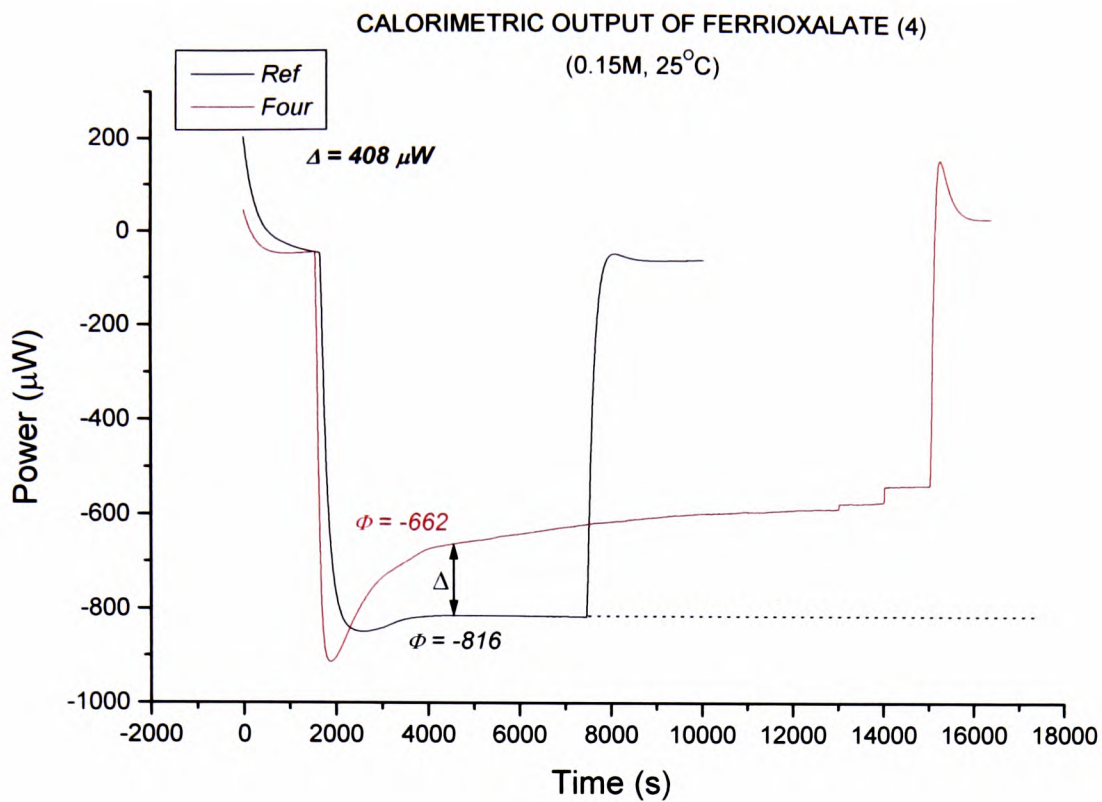


**Figure 5.1.6.13** Fourth output for the TAM testing of potassium ferrioxalate photodegradation

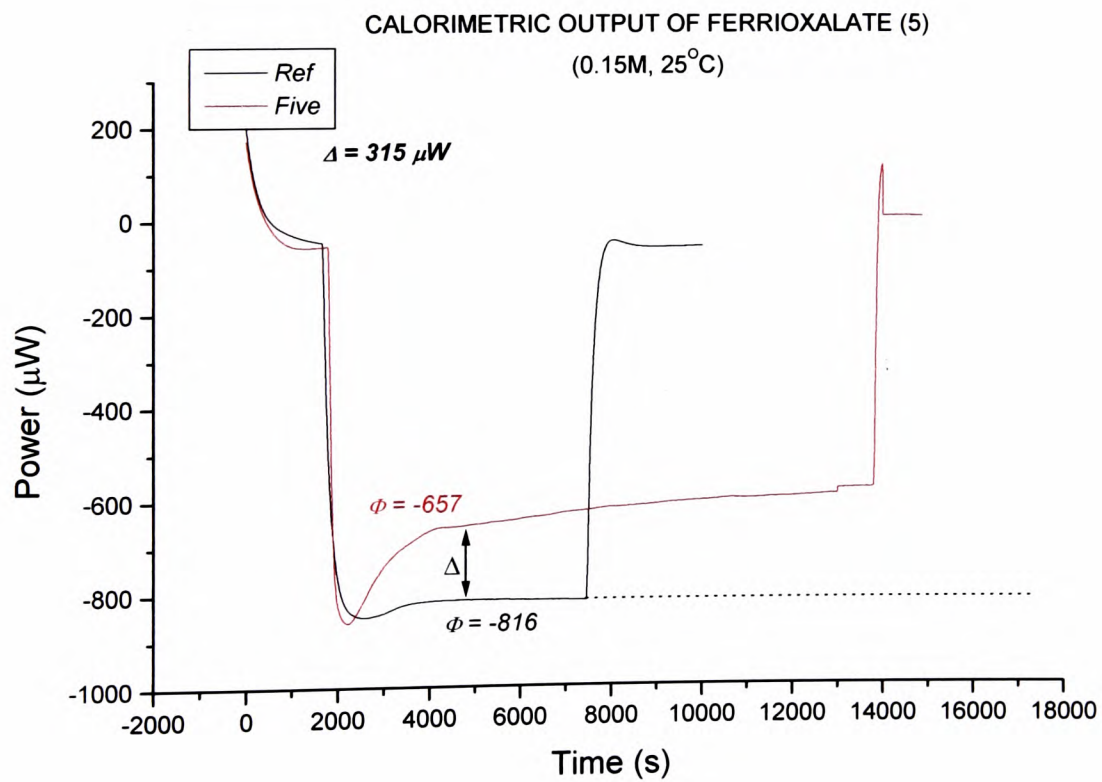


**Figure 5.1.6.14** Fifth output for the TAM testing of potassium ferrioxalate photodegradation

These plots can be combined for comparison as shown below:

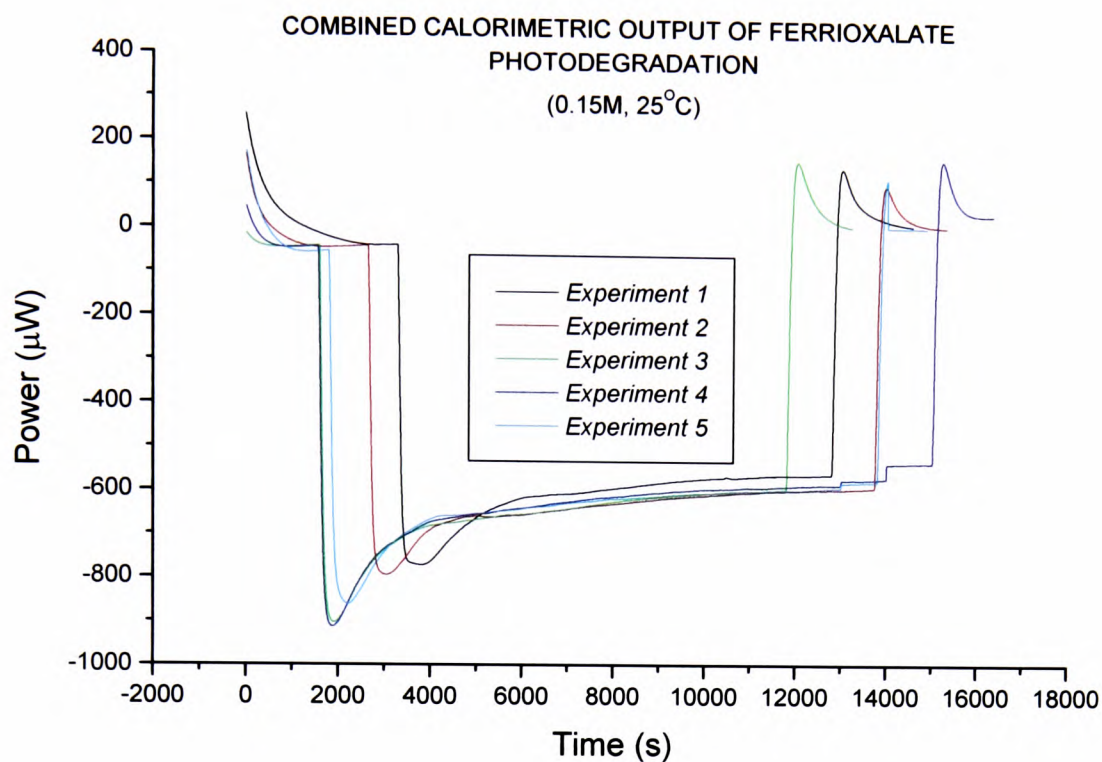


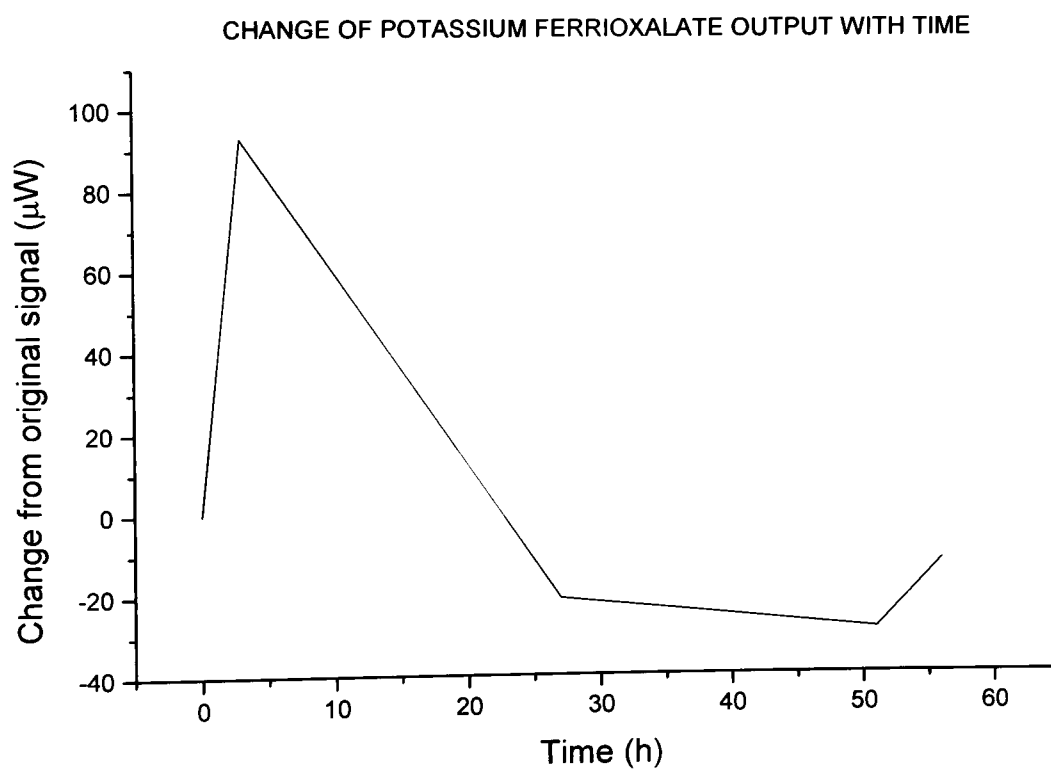
**Figure 5.1.6.15** Combined outputs for the TAM testing of potassium ferrioxalate photodegradation

The comparative plot (*Figure 5.1.6.15*) shows that the TAM signal has improved its repeatability, suggesting that the solution is not undergoing any change upon storage after preparation. The successive differences in the signal between reference and sample runs are shown in *Table 5.6*:

**Table 5.6** The change in signal difference with age of solution

Time elapsed (h)	Calorimetric signal ( $\mu W$ )	Change in orig. signal ( $\mu W$ )
0	315	-
3	408	93
27	294	-21
51	286	-29
56	303	-12

This trend can be shown graphically as before:

**Figure 5.1.6.16** The change in calorimetric output with solution lifetime

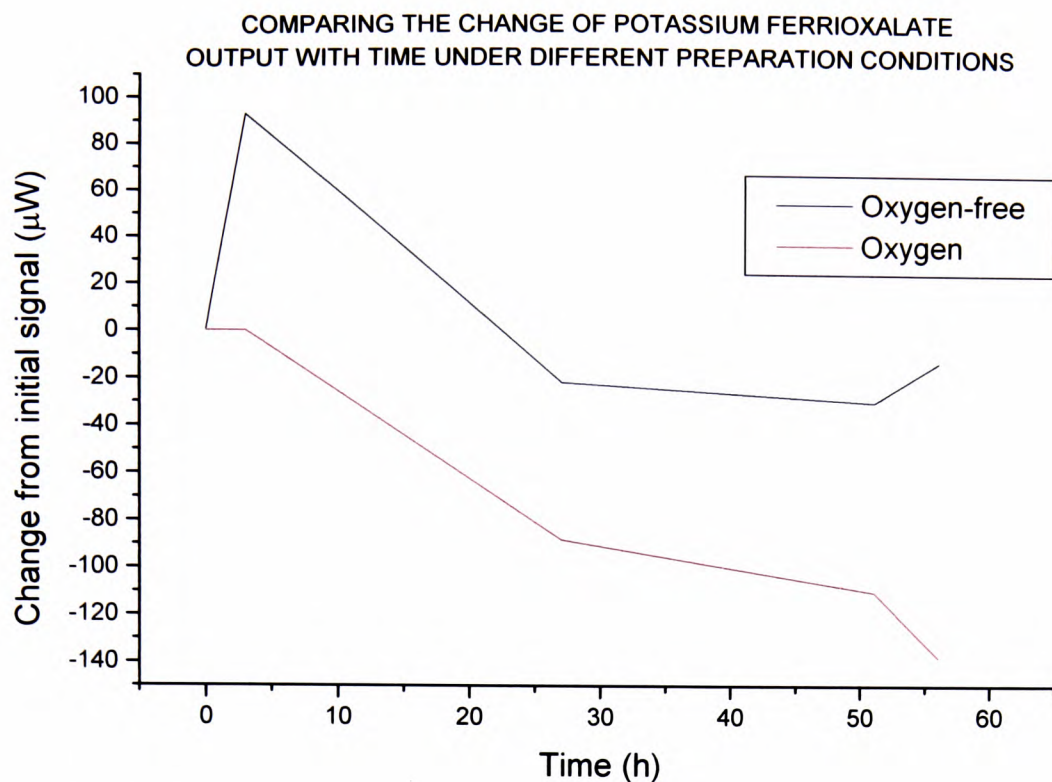


**Figure 5.1.6.17** Comparing the change in calorimetric output with solution lifetime

As can be from the above comparison, the *potassium ferrioxalate* performed much more consistently when prepared and stored in oxygen-free conditions. The repeat *potassium ferrioxalate* experiments show evidence of complexity of reaction and this is discussed below.

It is these more consistent results for the photodegradation of *potassium ferrioxalate* that are used in the following section to calculate the values for the irradiance,  $I_0$  and photon flux,  $F_0$  using the same procedure described in *section 5.1.3*.

### Applying the values of $\Phi$ to find $k$ , the irradiance, $I_0$ and the photon flux, $F_0$

Using exactly the same equations and Mathcad™ worksheets described in section 5.1.3, the irradiance and photo flux were calculated for each photodegradation of potassium ferrioxalate described above.

The values established for  $\Phi$  from the second round of photodegradation experiments are listed below:

**Table 5.7** Values of  $\Phi$  for the photodegradation of potassium ferrioxalate

Experiment Number	$\Phi$ ( $\mu W$ )
1	315
2	408
3	294
4	286
5	303
SD	49.7
Mean	321
% error	15.5

And apply these values to the basic zero-order calorimetric equation:

$$k = \Phi / H.V \quad \text{Eqn 5.1.5.2}$$

where  $H$  is  $-52600 \text{ Jmol}^{-1}$

and  $V = 0.004 \text{ dm}^3$

to give the following values of the rate constant,  $k$ :

**Table 5.8** Values of  $k$  for the photodegradation of ferrioxalate

Experiment Number	Rate constant, $k$ ( $\text{mol dm}^{-3} \text{s}^{-1}$ )
1	$1.44 \times 10^{-6}$
2	$1.36 \times 10^{-6}$
3	$1.40 \times 10^{-6}$
4	$1.94 \times 10^{-6}$
5	$1.50 \times 10^{-6}$
SD	$2.36 \times 10^{-7}$
Mean	$1.53 \times 10^{-6}$
% error	15.5

The final stage of the process is to apply the established values of  $k$  listed above to find the irradiance and photon flux of the light source – in this case the Xe arc lamp.

The stages of the calculation are outlined in *section 5.1.3*. Reference should be made to the Mathcad™ worksheets below which produce values for the irradiance and photon flux for all 5 experiments carried out with the Xe arc lamp at 300W output. These are shown in *Table 5.9* which includes the mean values of  $I_0$  and  $F_0$ , the standard deviations and the corrected value.

As for the 2-NB experiments, the corrected value of the photon flux is evaluated by multiplying by 3/2 since only two of the three fibre optic cables were used in the experiment, hence two-thirds of the light and therefore two-thirds of the real photon flux will have been recorded.

**Table 5.9** Values of  $I_0$  and  $F_0$ , the mean values, standard deviation and corrected values

	<i>Irradiance, <math>I_0</math></i> <i>(einstein <math>dm^{-3} s^{-1}</math>)</i>	<i>Photon Flux, <math>F_0</math></i> <i>(<math>Wm^{-2}</math>)</i>
Value 2	$1.2 \times 10^{-6}$	3.00
Value 3	$1.1 \times 10^{-6}$	2.83
Value 4	$1.1 \times 10^{-6}$	2.91
Value 5	$1.6 \times 10^{-6}$	4.03
Value 6	$1.2 \times 10^{-6}$	3.12
Mean Value	$1.2 \times 10^{-6}$	3.18
SD	$2.1 \times 10^{-7}$	0.49
Mean Value x 1.5	$1.9 \times 10^{-6}$	4.77

## The Irradiance and Photon Flux Calculator

**Stage 1** enter the 5 values for  $k$  established in section 5.1.3 Mathcad will know these as  $k_2, k_3, k_4$  and  $k_5$

$$k_2 := 1.44 \cdot 10^{-6} \quad k_3 := 1.36 \cdot 10^{-6} \quad k_4 := 1.40 \cdot 10^{-6} \quad k_5 := 1.94 \cdot 10^{-6} \quad k_6 := 1.50 \cdot 10^{-6}$$

**Stage 2** enter the common values: the quantum yield, known to Mathcad as  $Q$ , the enthalpy, known to Mathcad as  $H$  and the volume, known to Mathcad as  $V$

$$Q := 1.25 \quad V := 0.004$$

**Stage 3** to calculate the energy of a photon ( $E$ ), Mathcad needs data for Planck's Constant ( $h$ ), the speed of light ( $c$ ) and the average wavelength of the light ( $\lambda$ ). Additionally, Mathcad requires values for Avagadro's number ( $N$ ) and the cross-sectional area of solution under test ( $A$ ) to calculate the photon flux ( $F_\theta$ )

$$h := 6.63 \cdot 10^{-34} \quad c := 2.99 \cdot 10^8 \quad \lambda := 3.74 \cdot 10^{-7} \quad N := 6.02 \cdot 10^{23} \quad A := 4.91 \cdot 10^{-4}$$

$$E := \frac{(h \cdot c)}{\lambda}$$

**Stage 4 :** Mathcad uses *equation 5.1.1.2* to calculate the irradiance for each experiment

$$I_2 := \frac{k_2}{Q} \quad I_3 := \frac{k_3}{Q} \quad I_4 := \frac{k_4}{Q} \quad I_5 := \frac{k_5}{Q} \quad I_6 := \frac{k_6}{Q}$$

**Stage 5 :** Mathcad uses *equation 5.1.1.3* to calculate the photon flux for each experiment

$$F_2 := \frac{(I_2 \cdot V \cdot N \cdot E)}{A} \quad F_3 := \frac{(I_3 \cdot V \cdot N \cdot E)}{A} \quad F_4 := \frac{(I_4 \cdot V \cdot N \cdot E)}{A} \quad F_5 := \frac{(I_5 \cdot V \cdot N \cdot E)}{A} \quad F_6 := \frac{(I_6 \cdot V \cdot N \cdot E)}{A}$$

**Stage 6 :** The values of the irradiance and photon flux at each experiment are summarised below:

$$\begin{array}{ll} I_2 = 1.152 \times 10^{-6} & F_2 = 2.995 \\ I_3 = 1.088 \times 10^{-6} & F_3 = 2.828 \\ I_4 = 1.12 \times 10^{-6} & F_4 = 2.911 \\ I_5 = 1.552 \times 10^{-6} & F_5 = 4.034 \\ I_6 = 1.2 \times 10^{-6} & F_6 = 3.119 \end{array}$$

Hence for the 300W light source using the *potassium ferrioxalate* actinometer the mean corrected values for the irradiance and the photon flux are as follows:

$$F_0 = 4.8 \text{ Wm}^{-2}$$

$$I_0 = 1.9 \times 10^{-6} \text{ mol dm}^{-3} \text{ s}^{-1}$$

As already discussed, the approximate value for the photon flux supplied by LOT Oriel, the suppliers of the photocalorimetric light source is  $1.3 \text{ Wm}^{-2}$  for the xenon arc lamp at 300W (100% power) and compares with the calculated values (also at 100%) as follows;

$$\text{Calculated value} = 4.8 \text{ Wm}^{-2}$$

$$\text{LOT Oriel value}^{85} = 1.3 \text{ Wm}^{-2}$$

Despite the fact that the *potassium ferrioxalate* experiment was carried out at 300W (100% light power), the difference between the light manufacturer's value and the *potassium ferrioxalate* actinometry value is 369%. This would initially suggest there is a problem with the actinometric result. There is no guarantee, however, that the book value quoted above is correct for this particular experimental setup. Care must be taken not to treat the LOT figure as the "correct answer" since the photon flux value can change with differing experimental setups such as the length of the fibre optic cable, the age of the bulb, the "footprint" of the light irradiating the sample and the distance between the "output end" of the fibre optic cable and the sample. These factors can change between different sets of experiments (e.g. between the times at which 2-NB and *potassium ferrioxalate* experiments were carried out), even though the outputs plotted in *Figures 5.1.6.10 to 5.1.6.14* demonstrate a relatively high degree of repeatability (10% error) within a series of experiments.

The photoreduction of *potassium ferrioxalate* seems to be more problematic for use than was the case for 2-NB described above. The need of a Schlenk apparatus to prepare and store the solutions in an inert atmosphere has already been discussed. An additional problem, however, is apparent when looking at the calorimetric outputs for the repeat *potassium ferrioxalate* experiments (plotted in *Figures 5.1.6.10 to 5.1.6.14*).

---

To ensure the extent of reaction was the same for each of the repeat *potassium ferrioxalate* experiments shown in *Figures 5.1.6.10 to 5.1.6.14* (i.e. to ensure consistent results), the reading for the value of  $\phi$  was taken 3000 seconds after the light was first irradiated onto the sample. It is clear from the outputs, however, that the TAM calorimetric signal has not settled down to be flat at that point. This suggests the new *potassium ferrioxalate* solutions are not undergoing just a single zero-order photoreduction reaction but that the photoreaction is complex. This is the first time complexity has been observed for the photodegradation of *potassium ferrioxalate* and can only be observed through photocalorimetry. Note that flat line outputs were obtained for the original *potassium ferrioxalate* experiments shown in *figures 5.1.6.2 to 5.1.6.6* and further investigation into why the outputs are significantly different for the reaction not containing oxygen must be carried out.

There is one final actinometric method to investigate – that of spectroradiometry. This method may have the casting vote as to the correct value for the photon flux of the Xe arc lamp.

## 5.2 Spectroradiometry

Spectroradiometers are commercially-available instruments capable of precise measurement of absolute spectral intensities of light in the UV, visible, NIR and IR regions. With the latest apparatus and software, spectroradiometers can perform a number of additional functions including the real-time recording of irradiance data, calculated in lumens or lux per unit area.

A spectroradiometer generally consists of an entrance slit, collimator, a dispersive element (such as a grating or a prism), focussing optics and a detector.

To complete the process of evaluating the irradiance and photon flux for the Xe arc lamp used as the light source in the photocalorimeter, an *S2000* Spectroradiometer (Ocean Optics Inc, Dunedin, Florida, USA) was used with the photocalorimeter using the third branch of the trifurcated fibre-optic cable described previously in *chapter four*.

The *S2000* spectrometer is shown below: <sup>110</sup>



**Figure 5.2.1** The Ocean Optics™ “S2000” spectroradiometer

---

Using the dedicated software alongside the instrument,<sup>111</sup> the system was first calibrated using a calibration lamp before being connected to the third fibre optic cable of the photocalorimeter, as shown above, to record the photon flux output of the lamp in real time.

The method is straight forward:

- Connect the spectroradiometer to the third branch of the fibre-optic cable
- Set the software to record photon flux in real time and select the required power output of the lamp (240W, 270W, 300W)
- Ignite the lamp and leave it for an hour to “warm up” – ensuring a steady output
- Open the shutter allowing the light into the radiometer and begin data recording
- After the required length of time, end the data recording and turn off the lamp

The data collected was then imported into Origin™ and plots of photon flux vs. time compared for different lamp powers. The combined plots for lamp powers from 240W to 300W are shown below:

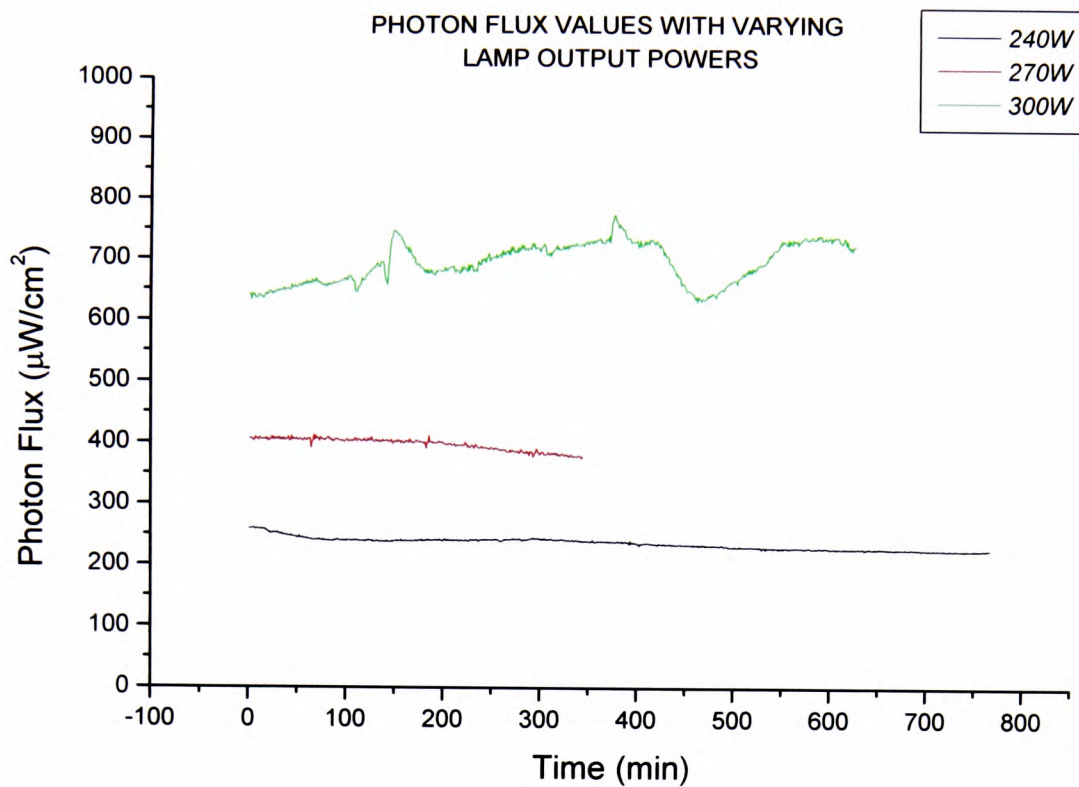


**Figure 5.2.2** Comparing the change in photon flux with lamp output

The values read from the plotted output can be converted from  $\mu\text{W}/\text{cm}^2$  to  $\text{W}/\text{m}^2$  and the mean values tabulated below:

**Table 5.8** Mean values of photon flux for the Xe arc lamp using spectroradiometry

Lamp Output (W)	Photon Flux ( $\text{W}/\text{m}^2$ )
240	2.4
270	4.0
300	7.0

These results are relatively consistent with those achieved through chemical actinometry and will be compared in *section 5.3* below.

### 5.3 Comparison of the Three Actinometric Methods

Having explored three different methods of quantifying the output from a Xe arc lamp, the final task before moving on to the final development stage of the photocalorimeter (*chapter six*) is to compare the values obtained for the photon flux from the three actinometric methods described in this chapter.

The following table lists the method used together with the mean value established for the photon flux,  $F_0$ .

**Table 5.9** Comparing photon flux values for the three actinometric methods

Method	Mean Photon Flux, $F_0$ ( $W/m^2$ )
2-NB (240W)	1.100
Spectroradiometry (240W)	2.365
Potassium ferrioxalate (300W)	4.800
Spectroradiometry (300W)	6.954

The values for the photon flux obtained by the two chemical actinometric methods agree more favourably with the book value than the spectroradiometric method.

The book value supplied by manufacturers LOT Oriel of  $1.3Wm^{-2}$  is probably inaccurate for the experimental setup of the photocalorimeter which has never been carried out before and direct comparison of manufacturer and experimental values of the photon flux should be avoided.

NB The value for the weighted average wavelength used in the calculations in *section 5.1.3* is also supplied by the manufacturers as part of the calculation of the book value for the photon flux. This is also likely to be erroneous and the values calculated

experimentally for the photon flux for both *2-NB* and *potassium ferrioxalate* will contain inherent error.

## Conclusions and Further Work

A suitable reaction for use as an actinometer needs to be robust and repeatable with a simple reaction mechanism and low-sensitivity to non-photochemical processes. It should also be able to be stored for a few days without degrading or changing significantly and should be easily analysed calorimetrically.

Despite the discordance between the calculated photon flux values obtained by chemical actinometry and those published by LOT Oriel, chemical actinometry can be considered more appropriate than spectroradiometry since both chemical methods produced values for the photon flux that compared more favourably with the book value.

Out of the two chemical methods tested, *2-NB* appears to be the more suitable candidate. As well as meeting all the requirements above, the calorimetric output of *2-NB* exhibits zero-order mechanism (i.e. a flat line) which can be easily analysed to obtain values for  $\phi$ , as outlined in *section 5.1.5.2* above.

*Potassium ferrioxalate*, however, is sensitive to oxygen on preparation and storage which has a detrimental effect on the calorimetric output when photoreaction is carried out (see *Figure 5.1.6.8*). Although this problem was solved by preparing and storing the solution in oxygen-free conditions, the repeat experiments on *potassium ferrioxalate* revealed that the photoreduction process is complex and not zero-order. Although it is of note that this is the first time that complexity during the *potassium ferrioxalate* photoreduction has been observed experimentally, analysing the output after 3000 seconds whilst competing reactions are still occurring is not ideal and represents a further major drawback of using *potassium ferrioxalate* in actinometry. The complexity of reaction observed needs to be investigated further as part of future work.

The 50% difference between the chemical actinometric values and the spectroradiometric values is difficult to fully explain. One explanation is that the footprint and geography of the light shone into the spectroradiometer is different to that for the calorimetric experiments leading to different levels of light intensity between experiments. It should also be noted that the calculations made when using

chemical methods includes the LOT Oriel value for the average wavelength energy for the light source which introduces embedded error into the calculated values.

The chosen reference system must produce a value for the required parameter to fit the reaction under study (in this case,  $k$  which leads to  $I_0$  and  $F_0$ ). If the chosen system is then replaced by another, however and a new value of  $k$  is required, the value derived from the reference system must be easily adjusted via a correction factor to suit this new reaction. The robust and repeatable nature of the 2-NB reaction offers this possibility.

NB The choice of 2-NB over *potassium ferrioxalate* is interesting since *potassium ferrioxalate* is the method of chemical actinometry suggested by IUPAC.

Further work must include carrying out 2-NB at 300W (100%) lamp power to be able to compare the value directly with the book value.

The *potassium ferrioxalate* experiments must also be repeated with particular interest in whether future calorimetric outputs exhibit zero order kinetics as was expected originally.

Finally, further studies into the use of spectroradiometry must be carried out since this method enables an absolute measurement of the photon flux in real time.

## *CHAPTER 6*

### *APPLICATIONS*

## 6. Applications

Having established methods of validation and actinometry allowing quantitative measurements of photon flux and irradiance, the final stage of development is to apply the apparatus to the analysis of the photodegradation of a solid.

*Chapter two* described the development of theory dealing with solid state reactions, whilst *chapter three* described the use of the *triacetin* reaction in solution to optimise test conditions for solid state future work.

For photodegradation experiments using solids, therefore, no calorimetric inserts will be used and samples will be placed on the bottom of the ampoule when undergoing irradiation.

One of the objectives of developing the novel photocalorimeter was to be able to study “causative wavelengths” of photodegradation of pharmaceutical solids. As outlined in the introduction, current methods of solid state photostability testing have their limitations. The calorimeter, however, if fitted with a monochromator, facilitates selection of wavelengths to be tested for their effect on photodegradation.

“Causative wavelengths” can be defined as the wavelengths of light at which photochemistry occurs. Specific chemical entities will have specific “causative wavelengths”.

The installation of the monochromator as part of the photocalorimeter is described in this chapter, as is its application in testing novel solid-state systems and pharmaceutical products, of unknown kinetic and thermodynamic properties.

In addition to developing a scanning technique to detect or identify “causative wavelengths”, the theory described in *chapter two*, and actinometric methods, developed in *chapter five*, will allow quantitative analysis of photodegradation reactions that occur as a result of wavelength scanning with the monochromator.

## 6.1 The Monochromator

Purchased as an accessory to the LOT Oriel™ light source and beam focussing system described in *chapter four*, the 0.25 metre monochromator was installed as part of the system in preparation for the testing of solid-state materials.

A monochromator is capable of selecting a single wavelength which can be scanned through a wide range. The LOT Oriel™ monochromator is of the *Czerny-Turner* design, consisting of fixed entrance and exit slits, fixed focussing mirrors and a rotatable diffraction grating. As the grating rotates a different wavelength is focussed onto the exit slit.

The optical configuration of the monochromator is shown below, <sup>85</sup> where either lateral or side-by-side outputs can be selected:

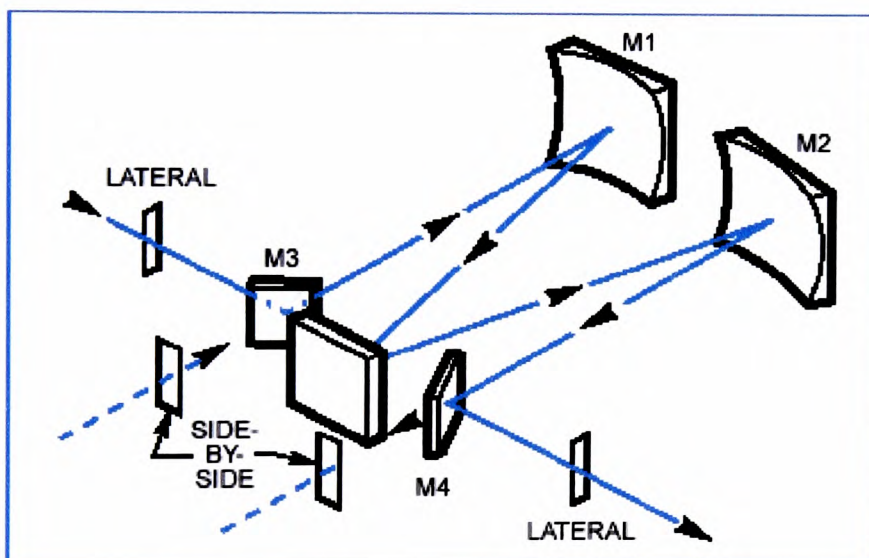


**Figure 6.1.1** The optical configuration of the 0.25 metre monochromator

The monochromator has the following specifications:

- Wavelength range: 180nm to 24  $\mu\text{m}$
- Twin input and output ports (allows lateral or side-by-side inputs and outputs)
- 0.1nm resolution
- Negligible stray light
- Ability to automate the wavelength sweep using a stepper motor
- Wavelength dial accuracy:  $\pm 1\text{nm}$
- Wavelength precision:  $\pm 0.1\text{nm}$

Figure 6.1.2 below shows the monochromator as a stand-alone unit and as part of the photocalorimetric setup in Figure 6.1.3:

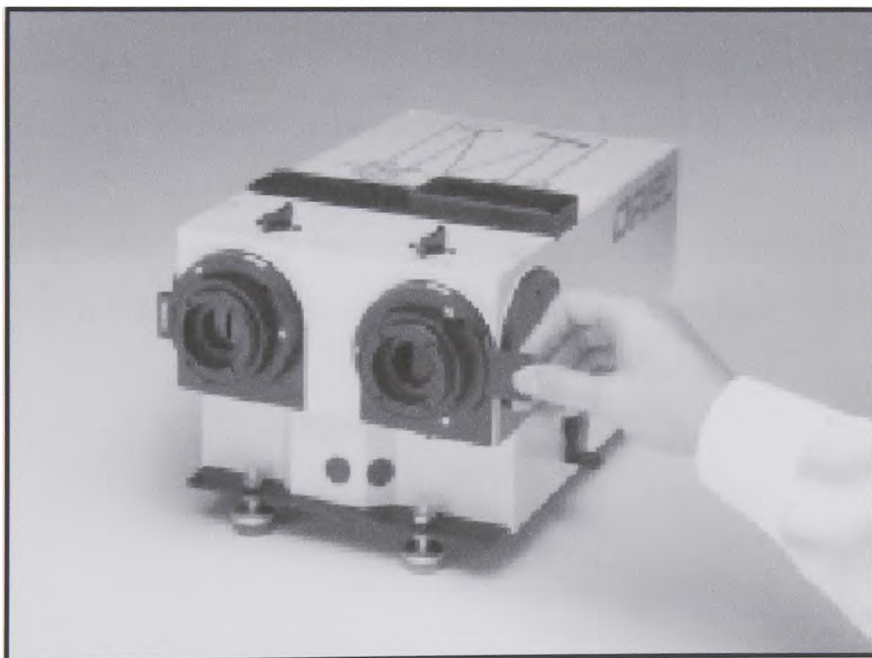


**Figure 6.1.2** The optical configuration of the 0.25 metre monochromator



**Figure 6.1.3** The monochromator incorporated as part of the photocalorimeter

A handle on the side of the monochromator turns the grating and changes the wavelength. A five-digit wavelength counter on the top of the instrument displays the selected wavelength in nanometres when a 1200 *lines / mm* grating is used.

After calibrating the monochromator according to the LOT Oriel™ manual,<sup>112</sup> the system was setup as shown in *Figure 6.1.3* above ready for use.

## 6.2 The effect of Wavelength on Photon Flux

Up until this point in the development of the photocalorimeter, only white light has been shone into the system with the assumption that the irradiance was of the same intensity every time the lamp was lit. The addition of a monochromator, however, allows light of different wavelengths and hence different energies to be shone into the system.

It was shown in *chapter five, section 5.2* that the photon flux (i.e. the amount of energy ( $W$ ) delivered by the light over a set area ( $m^2$ )) changes with lamp power.

*Section 5.1.1.5* in *chapter five* used *Planck's Law* to relate the energy of a photon,  $E$  to the wavelength as follows:

$$E = hv = hc/\lambda \quad \text{Eqn 5.1.1.5}$$

where  $h$  is Planck's constant ( $6.63 \times 10^{-34} \text{ Js photon}^{-1}$ )  
 $c$  is the speed of light ( $2.99 \times 10^8 \text{ ms}^{-1}$ )  
 $\lambda$  is the wavelength over which the actinometer is used ( $m$ )

and the energy of a photon is related to the photon flux,  $F_0$  (in  $Wm^{-2}$ ) by the following:

$$F_0 = I_0 \cdot V \cdot N_A \cdot E_\lambda / A \quad \text{Eqn 5.1.1.3}$$

where  $I_0$  is the irradiance ( $\text{einstein dm}^{-3} \text{ s}^{-1}$ ) (and 1 *einstein*  $\equiv$  1 *mol* of photons)  
 $V$  is the volume of solution ( $\text{dm}^3$ )  
 $N_A$  is Avogadro's number ( $\text{mol}^{-1}$ )  
 $E_\lambda$  is the energy of a photon of wavelength  $\lambda$  (in  $\text{J photon}^{-1}$ )  
 $A$  is the cross-sectional area of exposed actinometric solution ( $m^2$ )

and it can be expected, therefore, that changing the wavelength of light shone into the calorimeter will have an after effect on the value of the photon flux.

The effect of the wavelength of light on the photon flux must be determined before any solid state photodegradation experiments can be carried out. The following section describes the procedures undertaken to carry out this investigation.

### 6.2.1 Experimental

- The apparatus was set up as shown in *figure 6.1.3* above
- The Xe arc lamp was set at maximum output (360W)
- The spectroradiometer was calibrated<sup>111</sup> and set to record photon flux in real-time
- After allowing the lamp to “warm up” for an hour, the shutter was opened and the light allowed to enter the PC-driven spectroradiometer
- The data recording on the spectroradiometer was started
- The wavelength was scanned from 520nm to 300nm by manually changing through 5nm every 5 minutes
- Three runs were carried out to ensure repeatability ( $\pm 5\%$  is acceptable error)

The results were plotted as wavelength vs. photon flux as shown below:

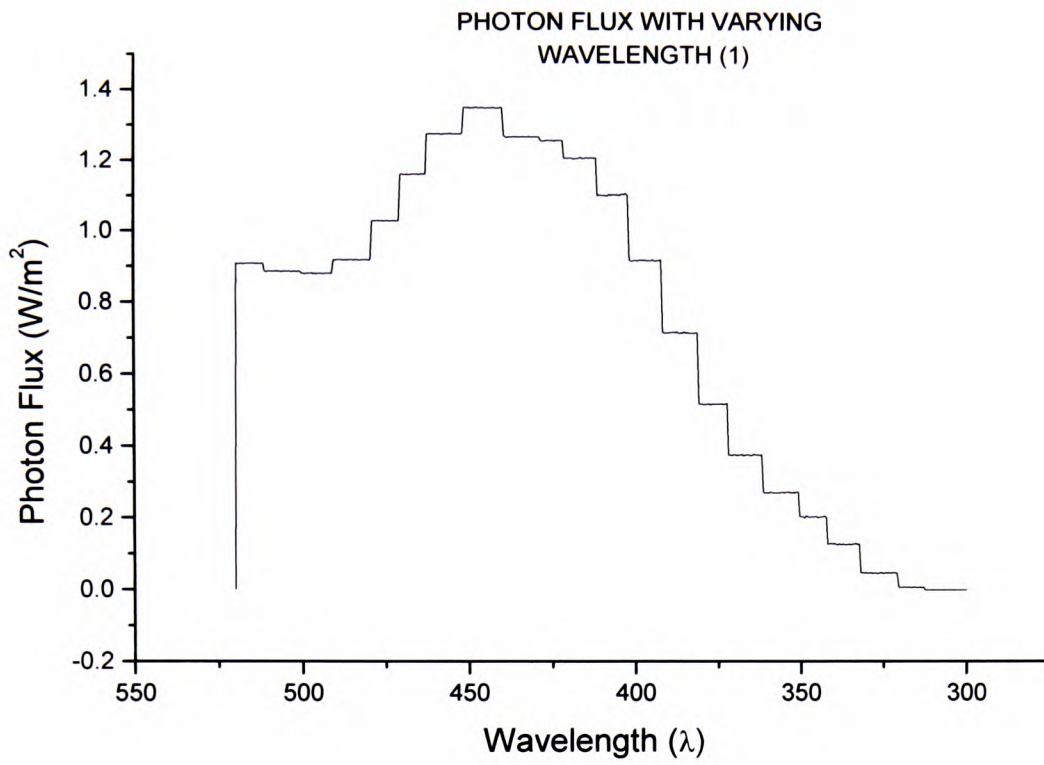


Figure 6.2.1 The variation in photon flux with wavelength at 360W (1)

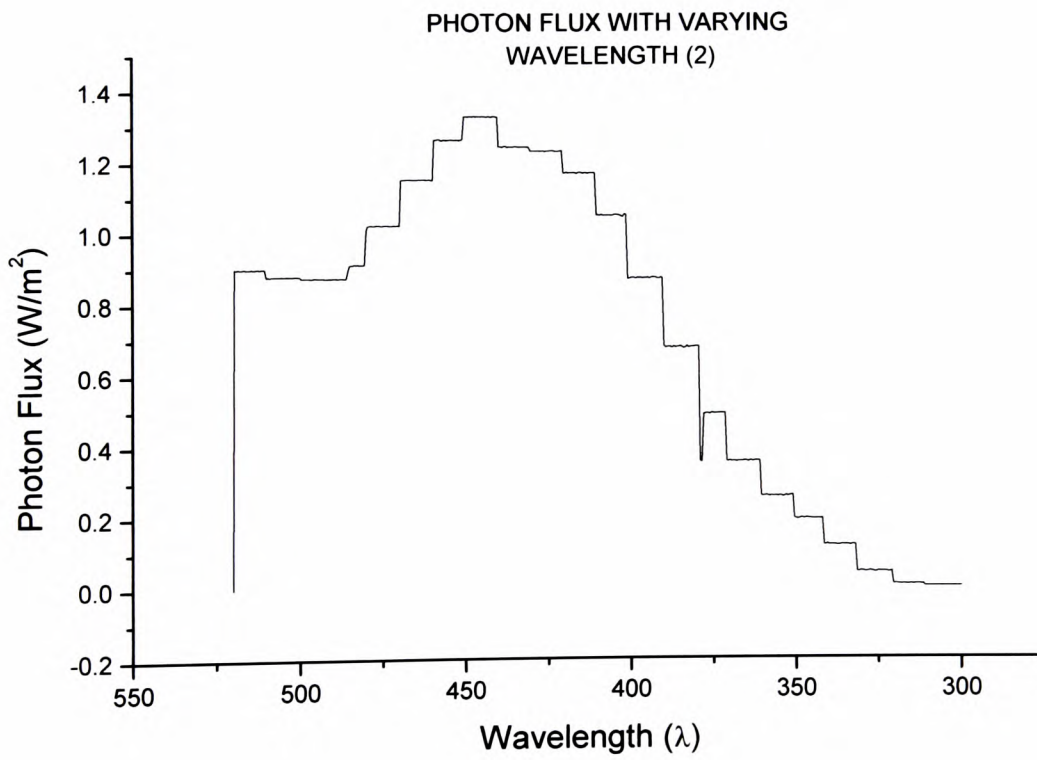
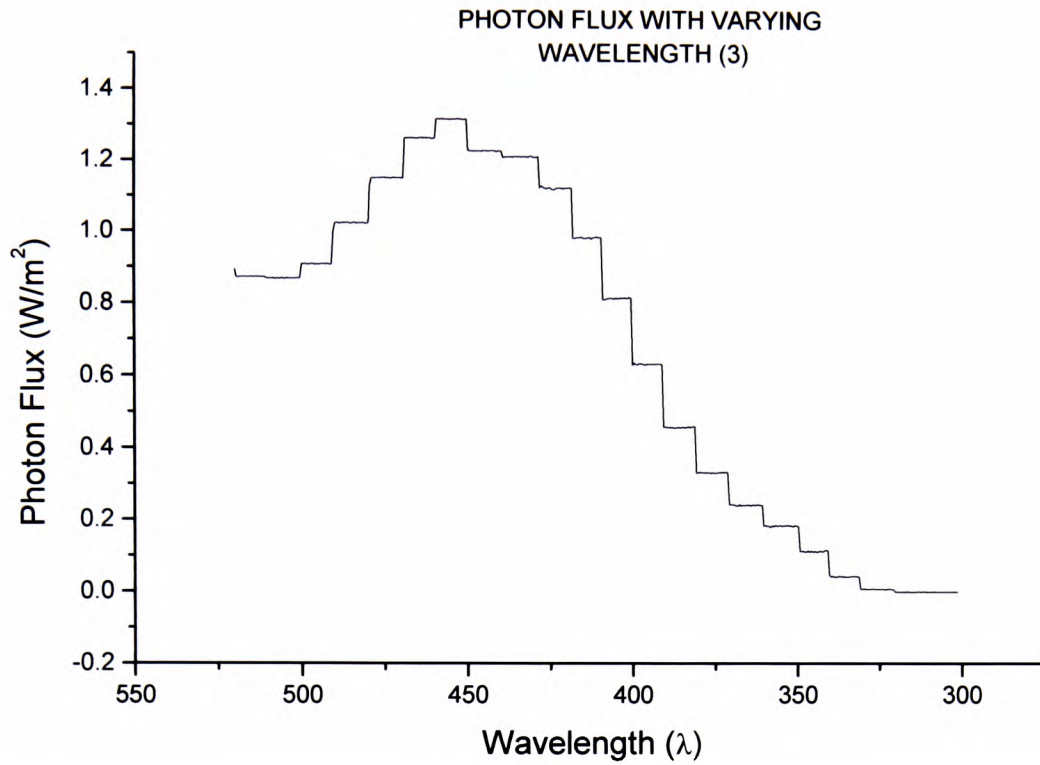
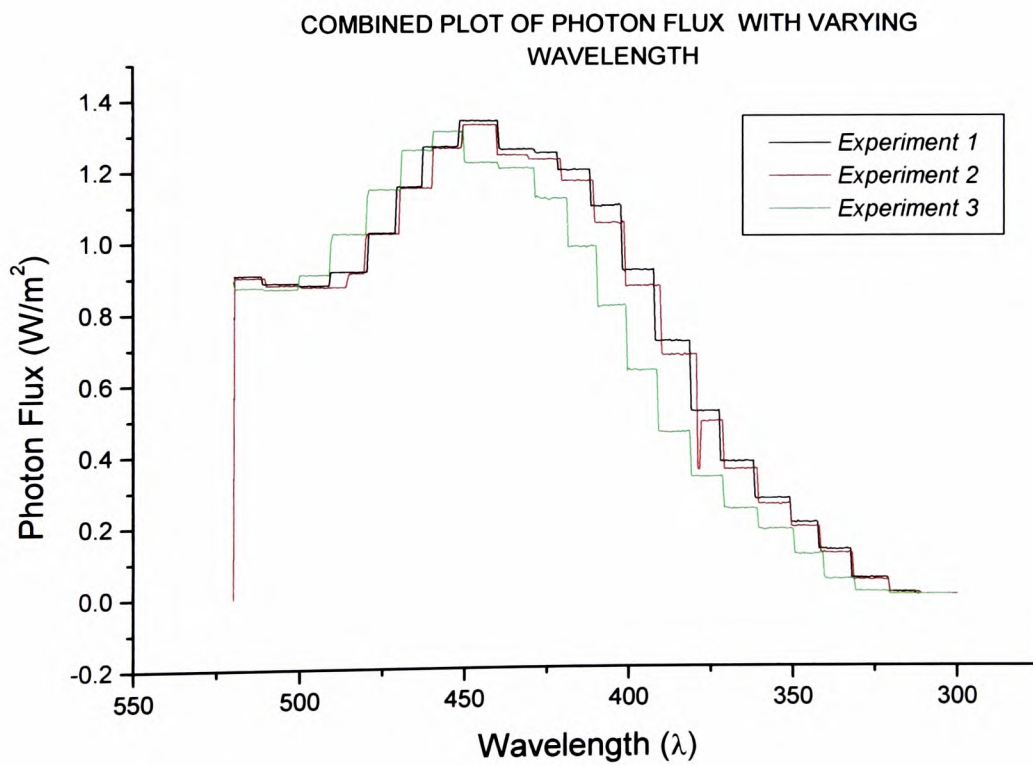


Figure 6.2.2 The variation photon flux with wavelength at 360W (2)



**Figure 6.2.3** The variation in photon flux with wavelength at 360W (3)

and a combined plot of all three outputs is shown below:



**Figure 6.2.4** Combined output of photon flux variation with wavelength at 360W

To allow a numerical comparison of the photon flux values obtained for the three experiments, three specific wavelengths were chosen and the corresponding flux value recorded. The wavelengths chosen were 500nm, 425nm and 350nm, representing the beginning, middle and end of the sweep range.

*Table 6.1* below lists values for the wavelengths, the corresponding values of photon flux and the mean values. *Table 6.2* shows the standard deviations and percentage errors (based on the standard deviation over the mean) for each experiment.

***Table 6.1*** Comparison of wavelengths and corresponding photon flux

Experiment Number	Wavelength (nm)	Photon Flux ( $\mu W/m^2$ )
1	500	879
2	500	879
3	500	908
1	425	1251
2	425	1232
3	425	1119
1	350	2048
2	350	1912
3	350	1836

**Table 6.2** Statistical comparison of wavelengths and corresponding photon flux

Wavelength (nm)	Mean Photon Flux ( $\mu W/m^2$ )	SD	% error (SD / mean)
500	889	17.32	1.95
425	1200	71.36	5.94
350	1935	107.40	5.56

From *Tables 6.1* and *6.2*, the values of the photon flux for the three experiments all fall within  $\pm 6\%$  (at worst) of each other.

*Figure 6.2.4* above demonstrates that the photon flux is consistent over the three runs carried out. It also clearly shows, however, that there is a considerable variation in the value of the photon flux as the wavelength is ramped up from the visible into the UV region.

At  $520nm$ , the photon flux is approximately  $0.9W/m^2$ , rising to a maximum of  $\sim 1.3W/m^2$  at  $450nm$ . The values for the photon flux then fall away to zero at approximately  $300nm$ . This is contrary to predictions made from *Equations 5.1.1.6* and *5.1.1.4* which suggest that the photon flux should increase with energy.

This effect has been observed in industry<sup>113</sup> and also by lamp manufacturers,<sup>85</sup> who both have reported the same trend shown in *Figure 6.2.5* below. A peak at  $\sim 450nm$  is observed, followed by a significant tailing-off of the irradiance of the lamp at wavelengths less than  $400nm$ .

Although the variation in irradiance with wavelength is inherent in an arc lamp, it is, however, much smoother than other potential sources and will continue to be used in subsequent experiments.

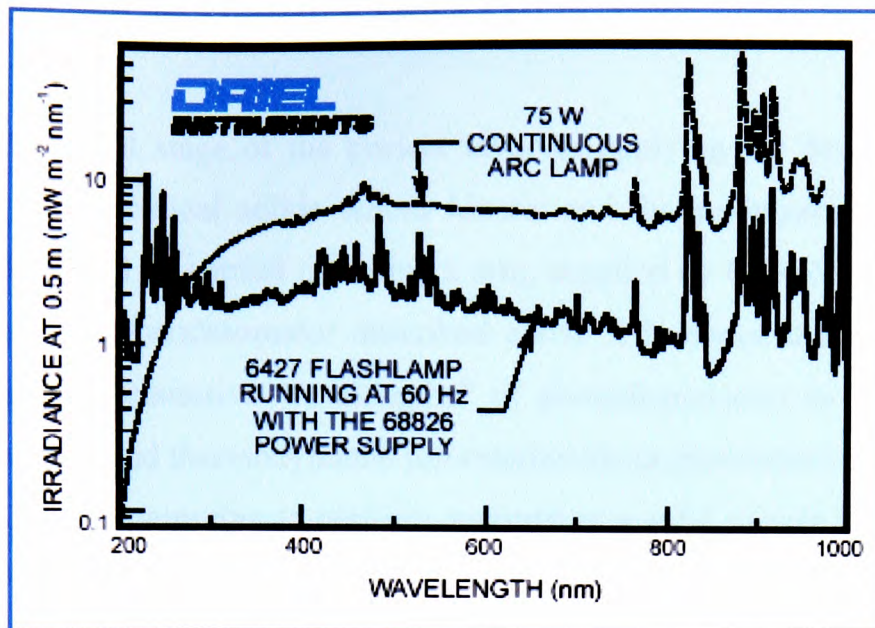


*Figure 6.2.5 Comparison of the irradiances of a Xe arc lamp and a conventional flashlight*

The favourable comparisons made between the xenon arc lamp shown in *Figure 6.2.5* and the spectroradiometric outputs shown in *Figure 6.2.4* demonstrate that the photocalorimeter is working as it should be.

### 6.3 Application of a known solid to the novel photocalorimeter

The final stage of the project involves applying the developed photocalorimeter to pharmaceutical solids whose kinetic and thermodynamic parameters are unknown. This will be carried out using a drug supplied by GlaxoSmithKline. With the addition of the monochromator described above it is hoped that the system will be able to screen “causative wavelengths” of photodegradation in real-time; as well as yield kinetic and thermodynamic information about photoreactions taking place.

Before attempting to perform analysis on a solid sample that is completely unknown, it is necessary to test the system on a solid whose properties and reactions are established in the literature.

#### 6.3.1 Using *Nifedipine* as a model solid-state material

*Nifedipine* (dimethyl 1,4-dihydro-2,6-dimethyl-4-(2-nitrophenyl) pyridine-3,5-dicarboxylate,  $C_{17}H_{18}N_2O_6$ ) is a well-known photolabile substance.

*Nifedipine* has been used therapeutically for years. One example is its use in blood pressure regulation.<sup>114-121</sup> It has also been used extensively as a calcium channel blocker which is useful in hypertension therapy.<sup>122</sup> *Myocardial ischemia* is often prevented by nifedipine<sup>123</sup> which can also prevent *post-partem preeclampsia-eclampsia*.<sup>124</sup> Other uses are in treatment of high altitude *pulmonary oedema*,<sup>125</sup> *atherosclerosis*<sup>126</sup> and cocaine addiction.<sup>127</sup>

*Nifedipine* has also been used as the test drug in the development of new photon sources for irradiation lamps.<sup>128</sup> In addition, possible strategies for the photo-protection of *nifedipine* have been studied intensively.<sup>129-130</sup>

The photoreactivity of *nifedipine* is a result of the co-presence of the hydrogen abstracting nitro group and an easily abstractable benzylic hydrogen. *Nifedipine* decomposes concurrently into four components when exposed to daylight or UV light.<sup>131-134</sup> The three major photodegradation products are shown below. Product I is the thermodynamically stable modification whilst products II and III are metastable modifications.<sup>135, 136</sup> The fourth product is formed in trace amounts and is yet to be

identified. Under sunlight, the nitro group is reduced to nitroso while the ring is oxidised. However, under UV irradiation the nitroso group is reoxidised, reforming the nitro.

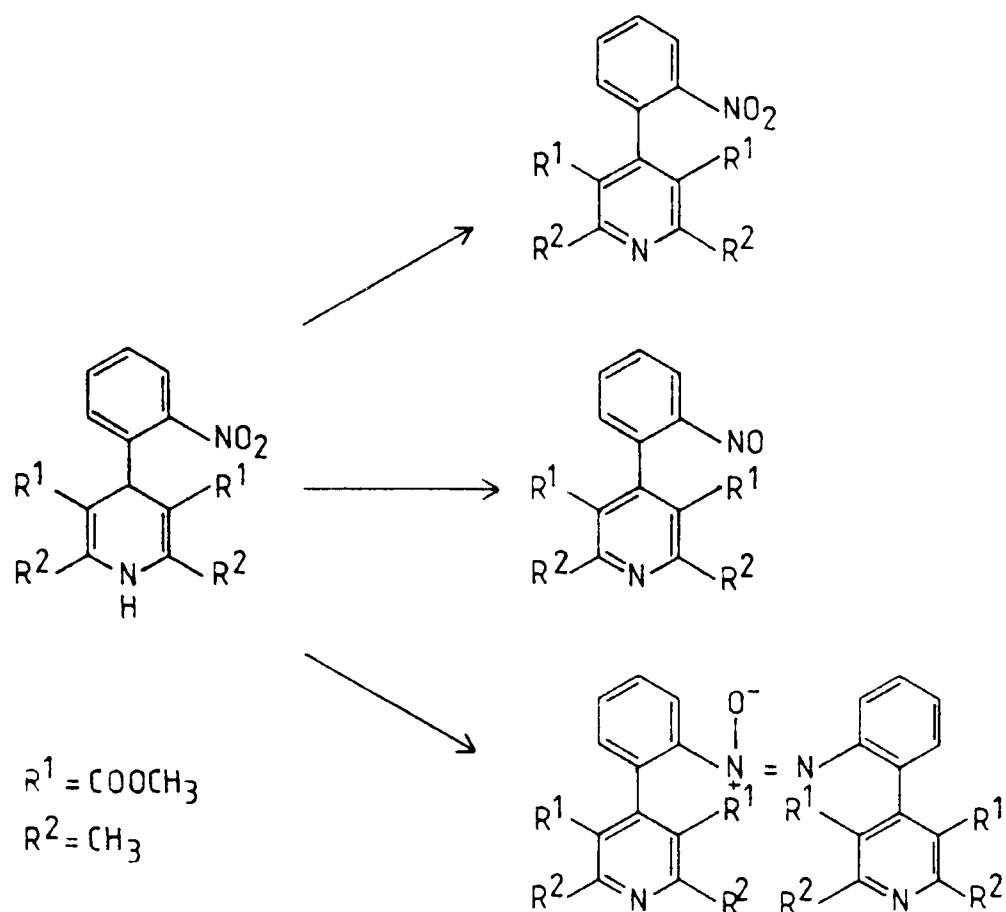


**Figure 6.3.1** The three major photodegradation products of nifedipine

Photodegradation occurs with apparent first order kinetics, with a first order rate constant of  $7.45 \pm 0.32 \times 10^{-5} \text{ s}^{-1}$ .<sup>120</sup> *Nifedipine* also exhibits a marked colour change as a result of photodegradation – turning from vibrant yellow to yellow-brown. It should be stored in the dark at  $<10^\circ\text{C}$ .

*Nifedipine's* photosensitivity at known wavelengths of light is ideal for testing the photocalorimeter. It is proposed to use the material in two specific areas of development

- Irradiate *nifedipine* with white light to test the response of the calorimeter to the photodegradation that ensues
- Irradiate *nifedipine* with various wavelengths of light to screen for “causative wavelengths”

Lehto *et al.*<sup>65</sup> were the first to use *nifedipine* in photosensitivity experiments of this type when they constructed an apparatus to test drug photostability in real time. Their work concluded that *nifedipine* molecules are only sensitive to light in the range 520nm to 280nm, with a threshold value at 510nm and a maximum at 390nm. No quantitative data was ever recorded however. To obtain similar results to those reported by Lehto *et al.* would indicate the photocalorimeter is working properly.

It should be noted, however, that the data recorded by Lehto *et al.* was only qualitative and not quantitative. The ability to obtain quantitative data for the photoreaction of *nifedipine* would mark significant progress in photocalorimetric studies.

### 6.3.1.1 Photodegradation of nifedipine with white light

It is important to determine that the photocalorimeter is functioning correctly in “white light” mode before experiments are carried out at individual wavelengths using the monochromator. This is done by carrying out experiments to establish the rate constant,  $k$  for the degradation of *nifedipine* and comparing the values obtained with the literature value<sup>120</sup> of  $7.45 \pm 0.32 \times 10^{-5} s^{-1}$ .

NB This mean value is obtained by taking the mean of four values of  $k$  quoted for the photodegradation of *nifedipine* in the solid state at different wavelengths of monochromatic light. The value is therefore approximate and this should be borne in mind when making comparisons between literature and experimental values.

Experiments were carried out according to a standard protocol:

- 500mg of *nifedipine* were loaded into the sample ampoule of the TAM
- 500mg of talc were loaded into the reference ampoule as the reference material
- The ampoules were lowered into the calorimeter as described in *chapter four*
- The lamp was switched on, set at 360W, and allowed to warm up for 1 hour After an hour the light source shutter was opened and the light allowed into the calorimeter to irradiate the sample. The data recording on the TAM was started simultaneously
- After ~1 hour, the light was extinguished and the TAM data recording stopped
- The outputs were plotted as shown below:

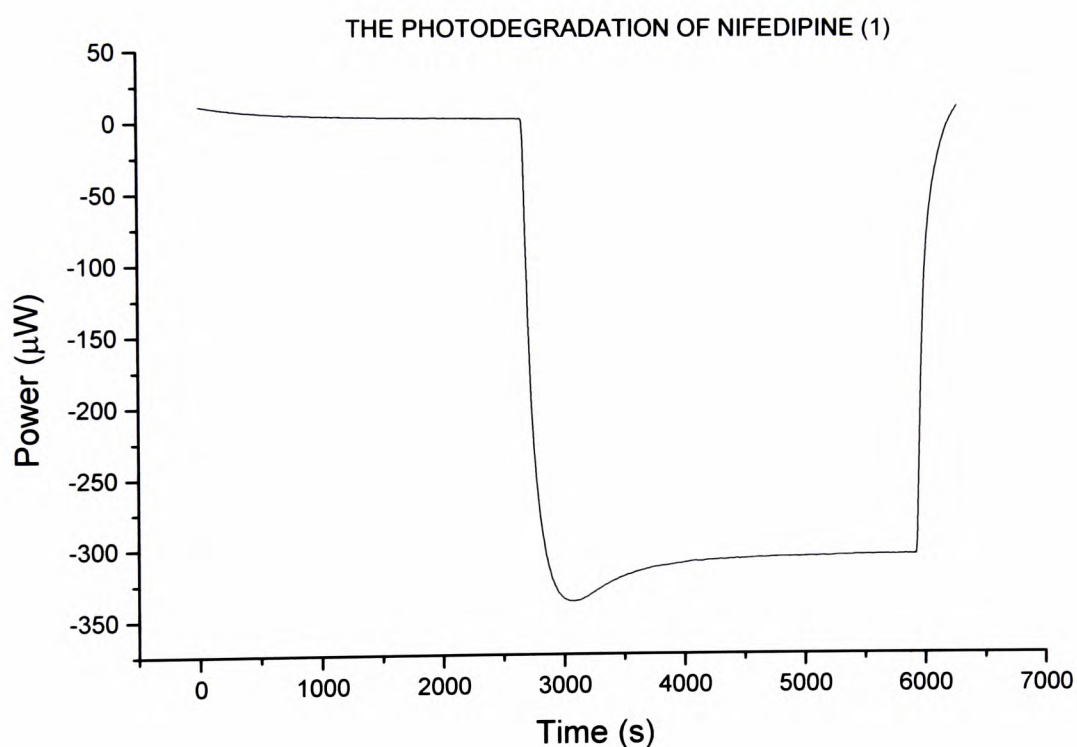


**Figure 6.3.2** Calorimetric output for nifedipine under white light (1)

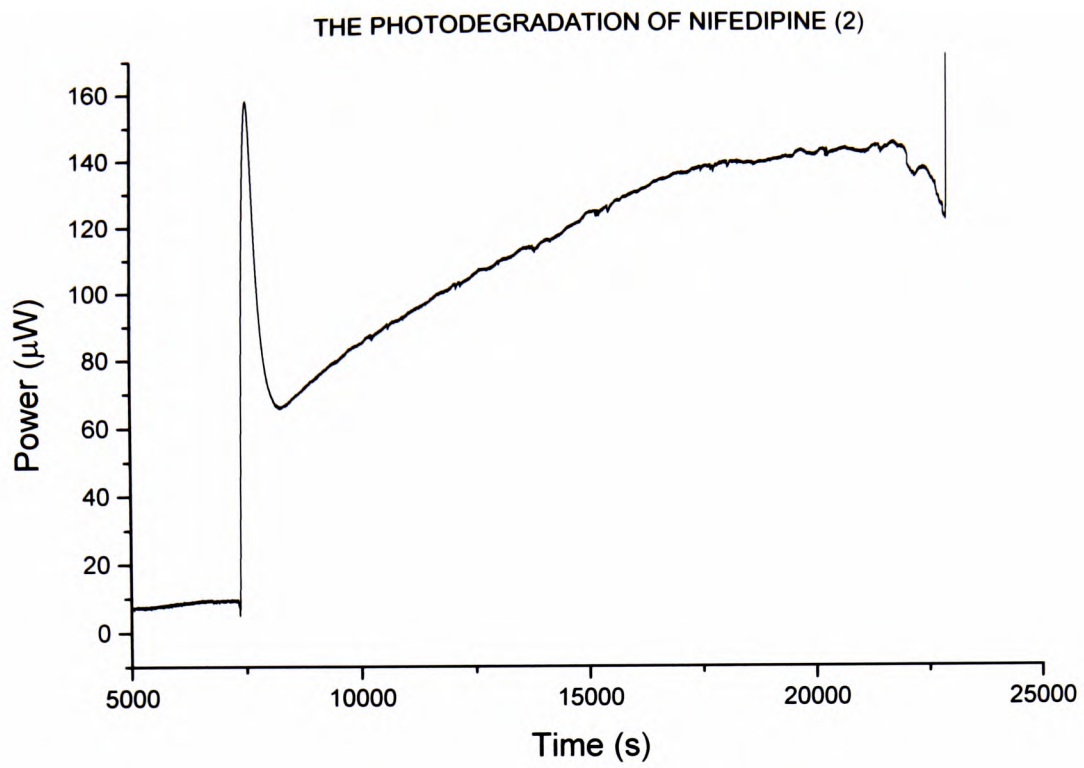


**Figure 6.3.3** Calorimetric output for nifedipine under white light (2)

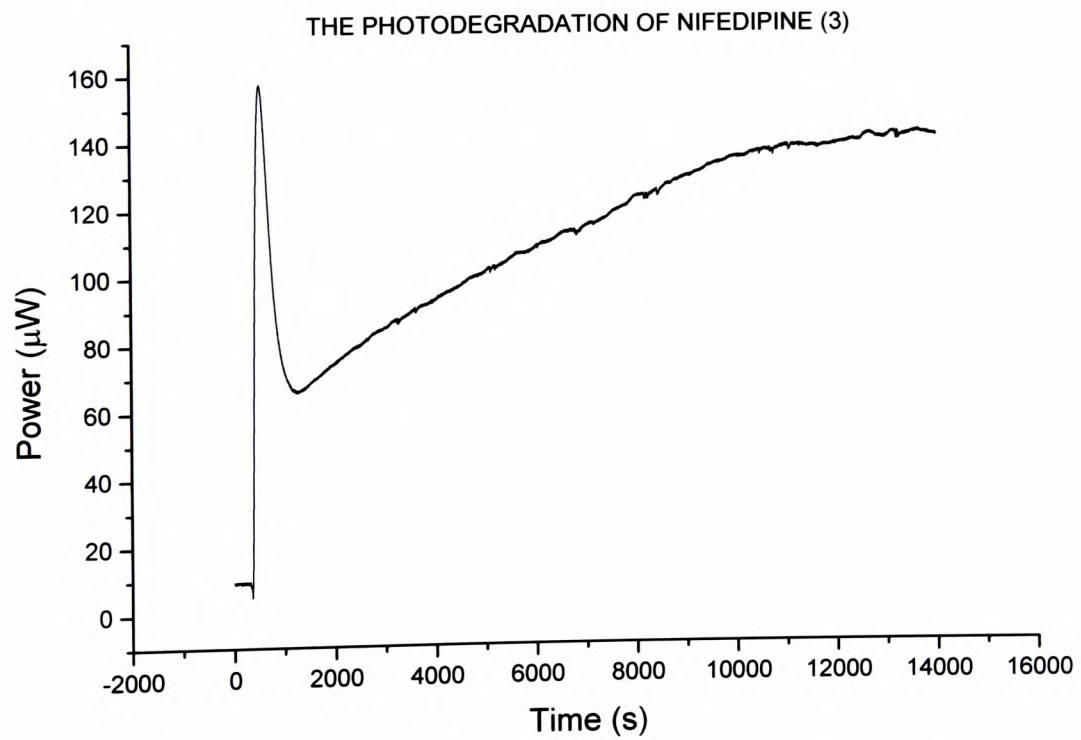


**Figure 6.3.4** Calorimetric output for nifedipine under white light (3)

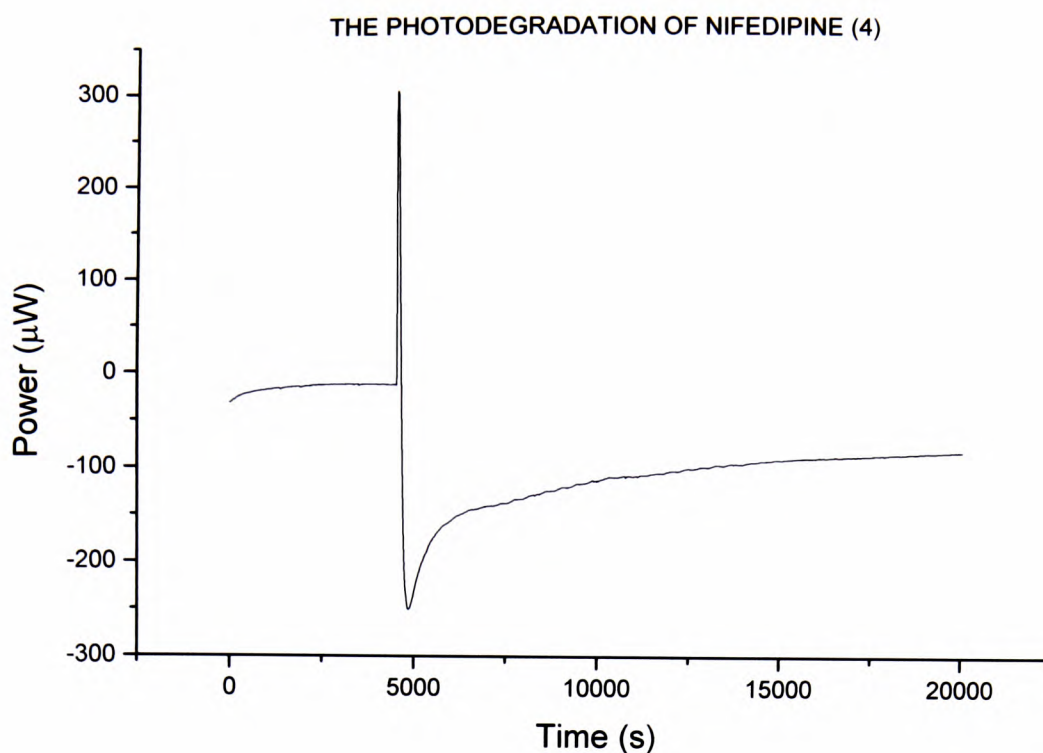


**Figure 6.3.5** Calorimetric output for nifedipine under white light (4)

All the plots above show an apparent first-order reaction period, (not for the whole lifetime of the reaction) which may be the result of the photodegradation of *nifedipine*. The first order process was confirmed by plotting the natural logarithm of power vs. time ( $\Phi$  vs.  $t$ ) to obtain a straight line plot with slope equal to the rate constant,  $k$ . To ensure that the shape of the output observed really is photodegradation, a control experiment was setup involving the shining of light into a pair of empty ampoules under the same conditions as for the experiments above:

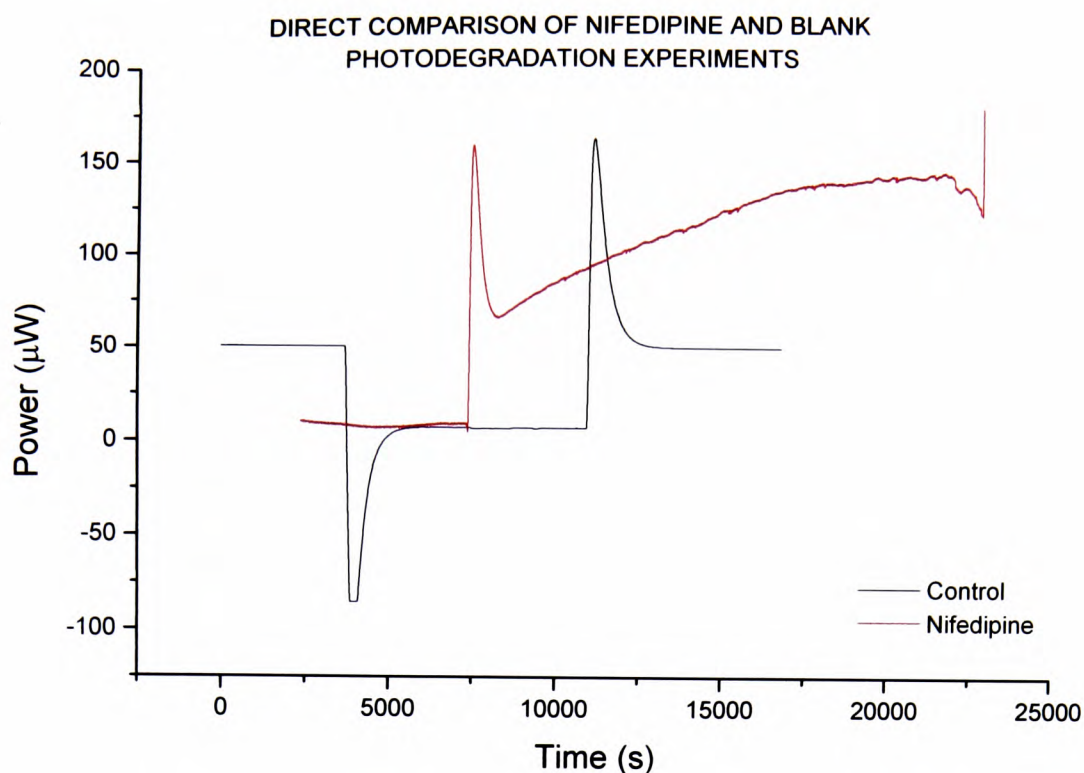


**Figure 6.3.6** Calorimetric output illustrating the clear difference between nifedipine and blank runs

The above output, *Figure 6.3.6*, shows that the shape of the plot is significantly different when no *nifedipine* is present in the system. This would suggest that the shapes of the outputs observed in *Figures 6.3.2* to *6.3.5* are a result of the photodegradation of *nifedipine*.

As suggested above, the next stage is to confirm first order kinetics by plotting the natural logarithm of power against time for each experiment.

*Figures 6.3.8* to *6.3.11* below exhibit plots with multiple first order periods. The subsequent challenge is to analyse the straight line that results from the photodegradation of *nifedipine* and not the response of the calorimeter to light being shone onto the system.

*Chapter four, section 4.3.2* described experiments to establish the recovery time of the system after going into “thermal shock” as a result of shining light into the calorimetric ampoules. The time taken for the calorimeter to have recovered completely from the point at which the light was shone into the TAM was measured as 2000 seconds. This is illustrated in *Figure 6.3.7* below:

## CALORIMETRIC OUTPUT OF REFERENCE MATERIAL

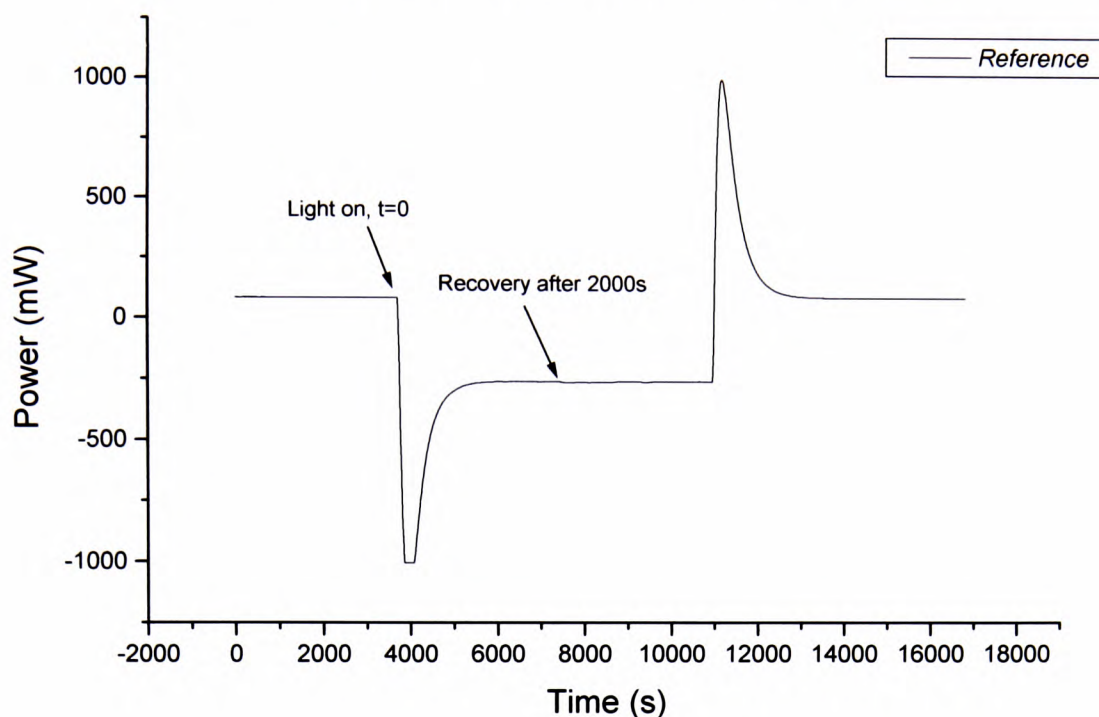


**Figure 6.3.7** Blank calorimetric output illustrating the recovery of the instrument from thermal shock

For the analysis of the first-order *nifedipine* plots, therefore, the slope of the linear  $\ln \Phi$  vs.  $t$  plots lines were analysed after 2000 seconds, when the signal is a result of photodegradation and not the recovery time of the instrument.

The time over which linear behaviour is seen is only for a maximum of 4000 seconds.

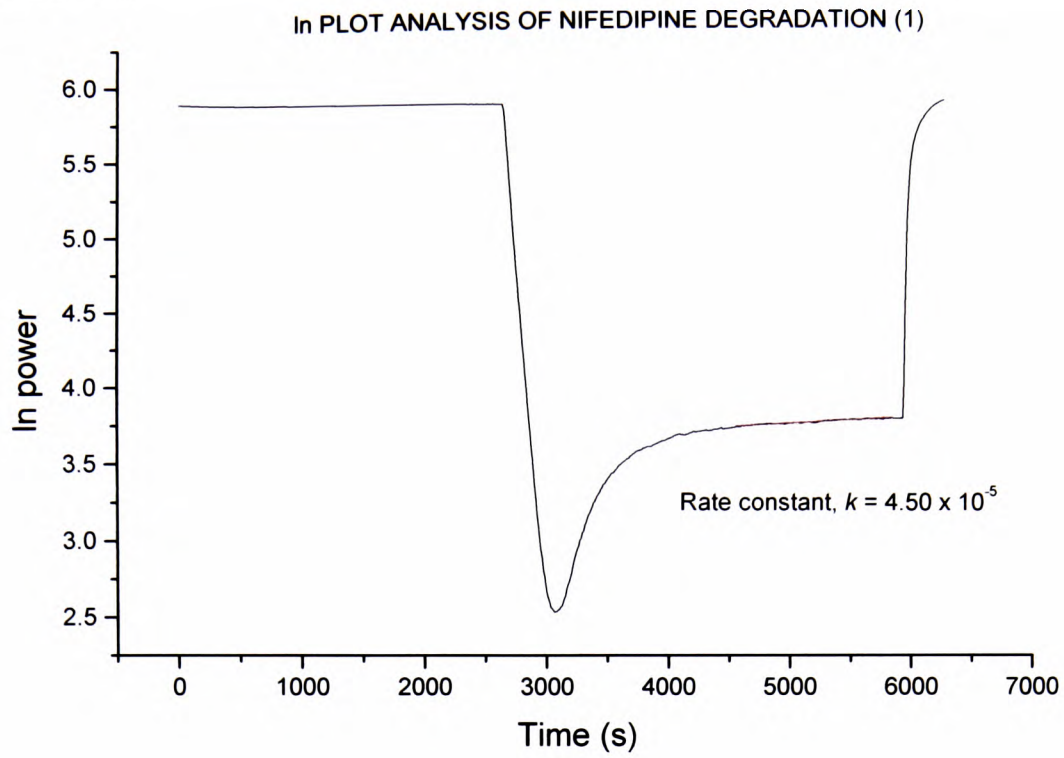


**Figure 6.3.8** ln plot analysis of the 1st order photodegradation of nifedipine (1)

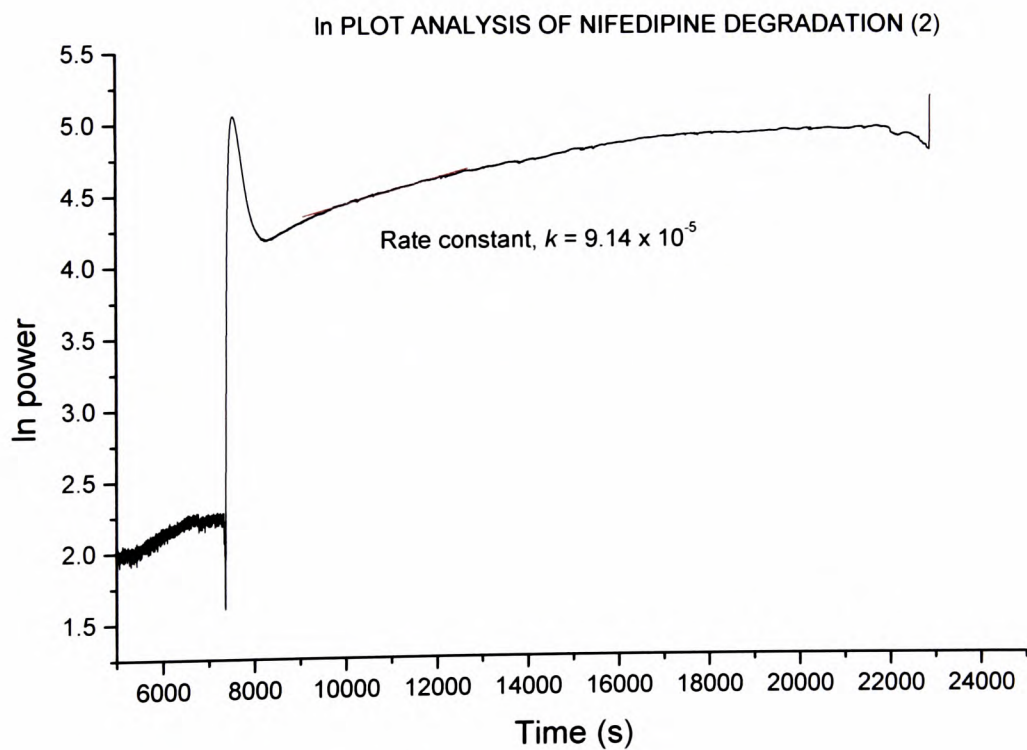


**Figure 6.3.9** ln plot analysis of the 1st order photodegradation of nifedipine (2)

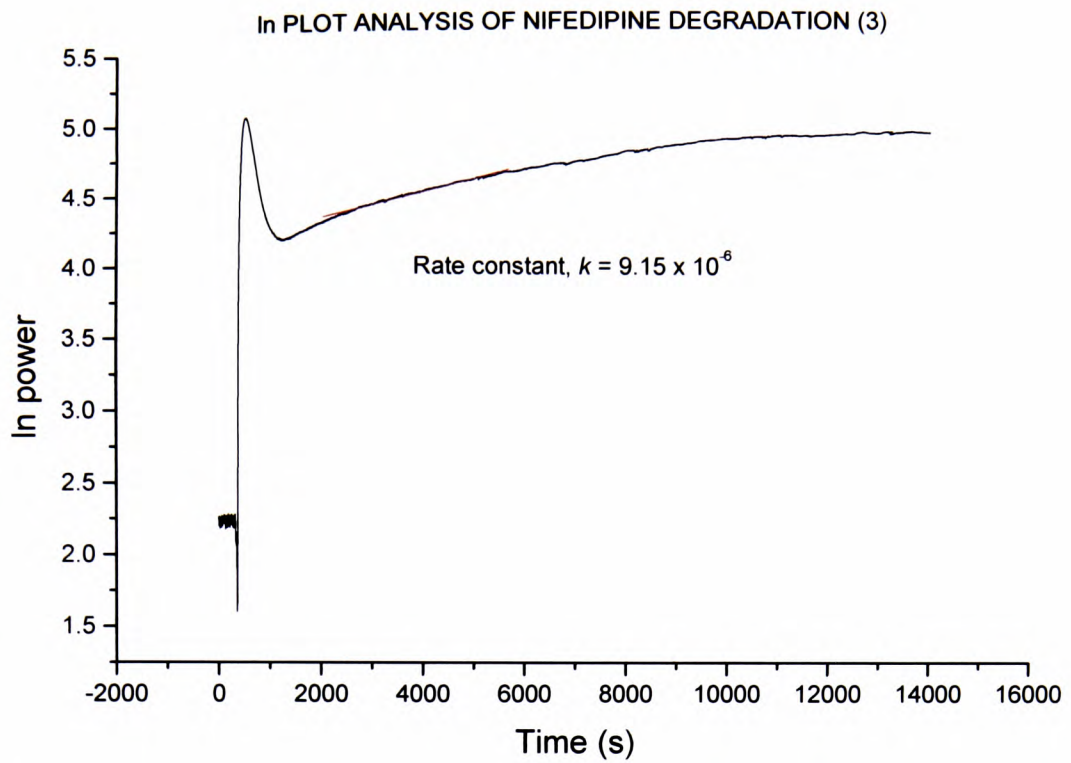


**Figure 6.3.10** *In plot analysis of the 1st order photodegradation of nifedipine (3)*

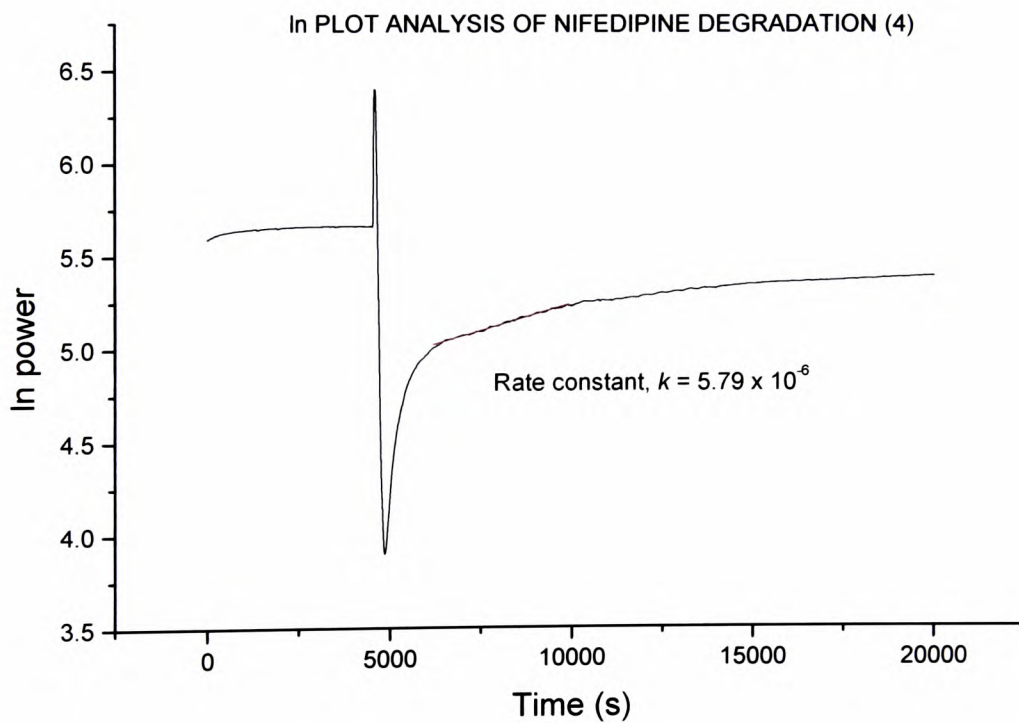


**Figure 6.3.11** *In plot analysis of the 1st order photodegradation of nifedipine (4)*

The rate constants obtained from the slope of each plot are tabulated below:

**Table 6.3** Summary of literature and experimental values for the rate constant,  $k$ 

Experiment Number	Literature Rate constant, $k$ ( $s^{-1}$ )	Experimental Rate constant, $k$ ( $s^{-1}$ )
1	$7.47 \times 10^{-5}$	$5.79 \times 10^{-5}$
2	$7.28 \times 10^{-5}$	$9.15 \times 10^{-5}$
3	$7.19 \times 10^{-5}$	$9.14 \times 10^{-5}$
4	$7.27 \times 10^{-5}$	$4.50 \times 10^{-5}$
Mean	$7.30 \times 10^{-5}$	$7.15 \times 10^{-5}$
SD	$1.19 \times 10^{-6}$	$2.37 \times 10^{-5}$
% err (SD / mean)	1.6	33.2

and the % difference between the mean values for  $k$  obtained experimentally and from the literature can be calculated as follows:

$$[(7.15 \times 10^{-6}) / (7.30 \times 10^{-6})] \times 100 = 2.2\%$$

These figures represent very successful analyses of the photodegradation of *nifedipine* under white light. It should be remembered, however, that these values are for an observation period of a single reaction of no more than 4000 seconds since the photodegradation of *nifedipine* is complex.

## Conclusions

The data show that the photocalorimeter can observe the photodegradation of *nifedipine* and produce data which can be analysed both qualitatively and quantitatively. The mean value for the rate constant of the photodegradation obtained experimentally is within 98% of the mean literature value which shows that the photocalorimeter is capable of accurately analysing solid state pharmaceutical reactions. Further experiments are required in this area, however, before the photocalorimeter can be used to produce reliable and repeatable quantitative data since the four photodegradation experiments carried out above vary with each other by as much as 33%.

Since the analytical plots of natural logarithm vs. time do not produce one continuous straight line, it is clear that during the photodegradation of *nifedipine*, no one single reaction rate constant is involved. More than one reaction is contributing to the photodegradation. i.e. the reaction system is complex.

Equations developed and discussed in this thesis in chapter two are sufficient for processes which do not change over the lifetime of the reaction (note this means even for solid-phase systems). Sequential and parallel reactions therefore present problems. We should anticipate that all degradation reactions are complex. This is clear from the *nifedipine* photodegradation results where only a limited first-order period is observed. In the data analysis, no account was taken of proceeding or succeeding reactions (clearly this situation is unsatisfactory and to attempt all possible patterns, orders etc. for complex reaction sequences is not useful. Therefore more useful methods, as yet not fully evolved, are chemometric based.<sup>137</sup>

Chemometrics is the application of statistical methods to efficient experimental design and to the identification of trends, relationships and patterns in existing datasets. Specifically in the case of calorimetric data, chemometrics is able to deconvolute complex reaction data into integral-order outputs which can then be analysed using conventional methods described in *chapter two*. This work is currently under development.

In the absence of chemometric analysis at this early stage, however, semi-quantitatively the apparatus demonstrated that photodegradation was definitely taking place in all three *nifedipine* experiments.

Overall, two very good results out of three for this experiment suggest that the photocalorimeter is functioning well and that the next stage of the project - the introduction of “causative wavelength” studies could get underway.

Further work in this area would include performing repeat experiments on *nifedipine* to obtain values of  $k$  that are consistently accurate compared with the literature value. Other photolabile materials, such as *ascorbic acid* could also be evaluated as potential test materials for the photocalorimeter.

### 6.3.1.2 Photodegradation of nifedipine with variable wavelength light

Having determined that the photodegradation of *nifedipine* under white light could be successfully observed by the photocalorimeter, the next stage was to see if similar observations could be made under monochromatic light.

As described in *section 6.3.1*, *nifedipine* is known<sup>131-136</sup> to be sensitive to light of certain wavelengths. Some years ago, Lehto *et al.* reported<sup>65</sup> *nifedipine* stability in the wavelength range 510nm to 280nm, with a maximum at 390nm. Consider a *nifedipine* experiment in the TAM where the light shining onto the sample is swept through a range of wavelengths using the monochromator. It is reasonable to expect that as the wavelength of light reaches a point at which *nifedipine* is photosensitive, some degree of photodegradation will occur and a signal will be recorded by the TAM. Passing beyond this particular wavelength will result in diminution of the photodegradation and with it the TAM signal until the next area of sensitivity is reached when a new signal is observed.

Using this technique, it is easy to see how the photocalorimeter has the potential for rapid screening of the causative wavelengths of photosensitive drugs in real time.

Having successfully demonstrated the technique on *nifedipine*, the final stage of development will be to apply the technique to drugs about which little is known of their photosensitivity is known.

### Establishing the change in Photon Flux with Photodegradation signal

It was shown in *chapter four* that the effect of irradiating a sample within the TAM is to displace the calorimetric power output by a number of *micro watts*.

Although a flat and stable baseline is achieved for both “light on” and “light off” sections of the experiment, the micro watt readings at which they occur differ considerably. With the light off, the baseline value is  $\sim 200\mu W$ . With the light on the figure is  $\sim -250\mu W$ ; a displacement of  $\sim 450\mu W$ .

As discussed in *chapter four*, this unexpected displacement of the calorimetric signal upon irradiation is probably a result of an imbalance in the capacity of the two fibre optic cables that supply light to the ampoules. This imbalance will lead one side of the system to receive more energy than the other, hence changing the calorimetric signal. The higher the energy input, the greater the displacement.

An experiment was carried out on *nifedipine* to establish how the photon flux (a measure of the energy of the irradiated light) changes with wavelength and how the corresponding calorimetric output changes accordingly.

The method used is described below. The scan range was  $520nm$  to  $300nm$ , the scan rate  $10nm / hour$  (manual change) and the mass of *nifedipine* used was  $500mg$ . The result is plotted in *figure 6.3.12* and establishes the pattern of change in TAM output with changing photon flux as a result of the change in light wavelength.

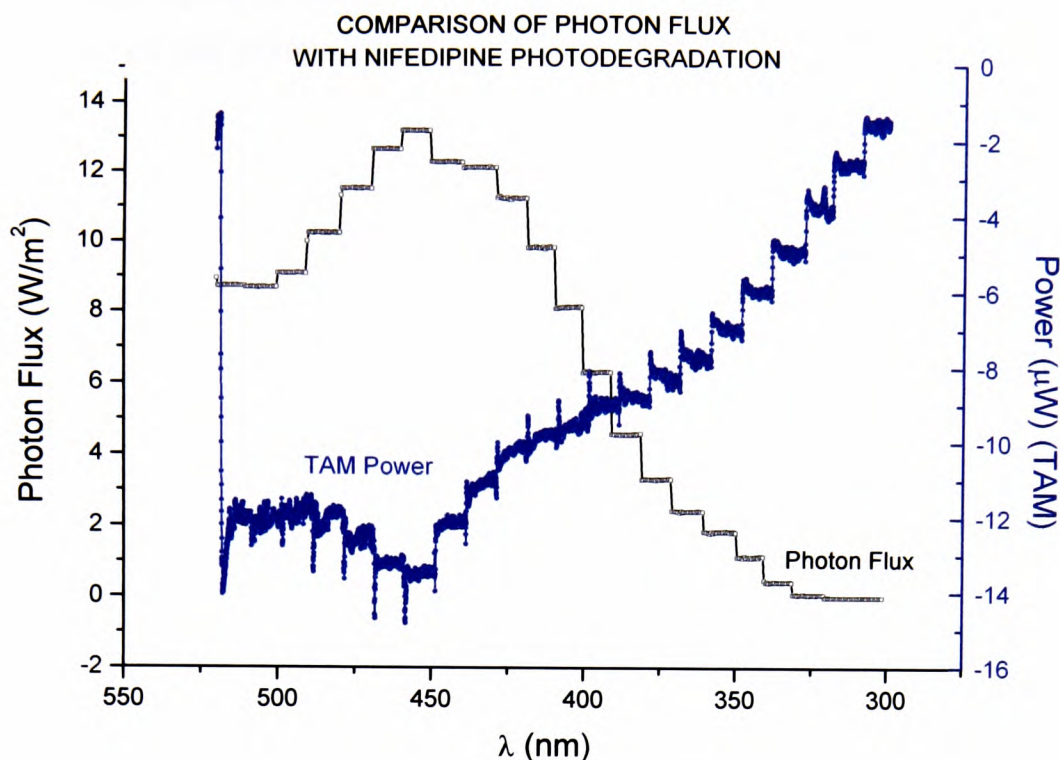


Figure 6.3.12 Comparing photon flux with photodegradation

It is possible, therefore, that the outputs observed in all of the following experiments are the result of the change of photon flux with wavelength and not solely the result of photodegradation.

There are several experiments that can be performed to establish the extent of this link:

1. To perform photodegradation experiments on a photosensitive material with a known activation energy in the red end of the spectrum. Examples would include materials used in photodynamic therapy,<sup>138</sup> where red light is used to cleave the photosensitive molecule and activate the material. The red end of the output of the lamp is reasonably flat and any peaks in this area would be indicative of a real effect.
2. To perform an experiment on a photosensitive material that is yellow in colour. The compound should absorb all other light except that at around 500nm (where

the output spike is worst). *Riboflavin* is a suitable material because it is partly photolabile and yellow.

The best way to clarify the situation, however, is to test a different material with different “causative wavelengths”. This should be carried out early on in any future work in the further development of the photocalorimeter.

### **Photodegradation of *Nifedipine* with variable wavelength light**

#### **Experimental**

Wavelength-scan experiments were carried out according to the following procedure:

- 500mg of *nifedipine* were loaded into the sample ampoule of the TAM
- 500mg of talc were loaded into the reference ampoule
- The ampoules were lowered into the calorimeter according to the method described in *chapter four*
- The lamp was switched on and set at 360W and allowed to warm up for 1 hour prior to sample irradiation
- The monochromator was set at the first wavelength of the sweep
- After an hour the light source shutter was opened and the light allowed to enter the calorimeter through the monochromator
- Data recording on the TAM was started simultaneously
- The wavelength was changed manually according to the scan rate detailed below

### Experiment 1

Wavelength range: 520nm to 300nm

Scan rate: 10nm / hour

Sample mass: 500mg

The first experiment operated through a wavelength range that included those that *nifedipine* is known<sup>131-136</sup> to be sensitive to. The slow rate of scanning of 10nm per hour was chosen to ensure the TAM had time to react to any photodegradation that might occur.

The output is shown below:

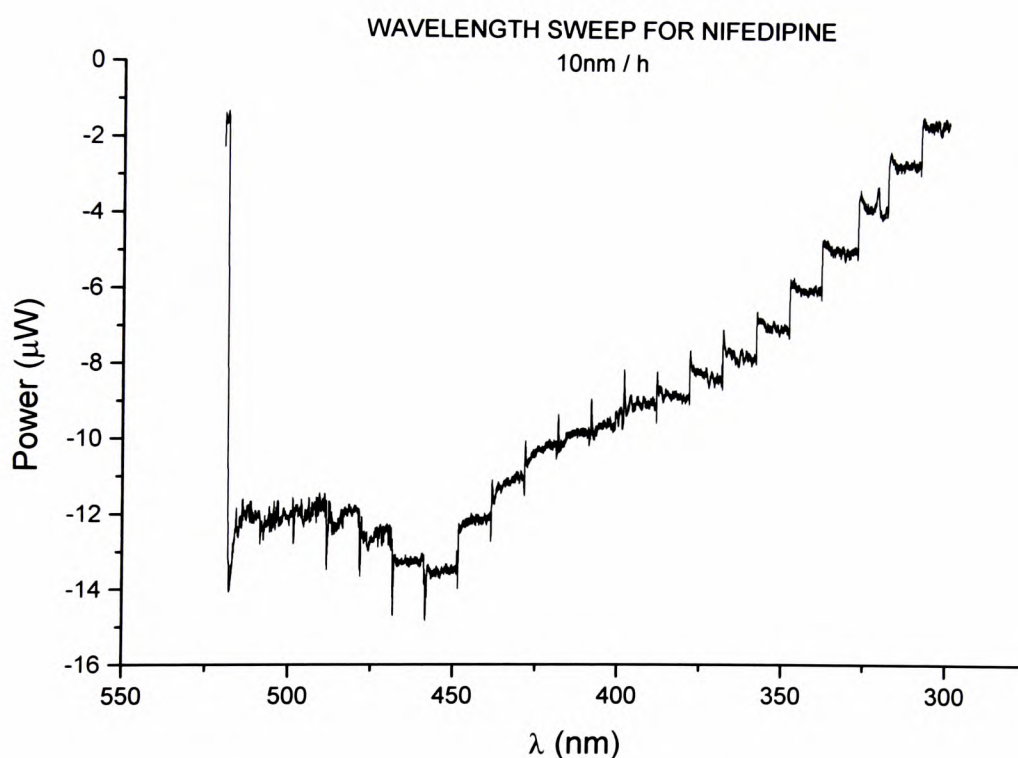


**Figure 6.3.13** The photodegradation of nifedipine with wavelength sweep

The plot shows a significant change in power as the wavelength decreases (energy increases). In particular, there is a minimum at  $\sim 460\text{nm}$ , a shoulder at  $\sim 390\text{nm}$  and smaller shoulders at  $\sim 490\text{nm}$  and  $\sim 520\text{nm}$ . The magnitude of the power output ( $\sim 6\mu\text{W}$ )

is however quite small. For clarity, smoothing was carried out using Origin™ software (300 point FFT filter) and the result shown below:

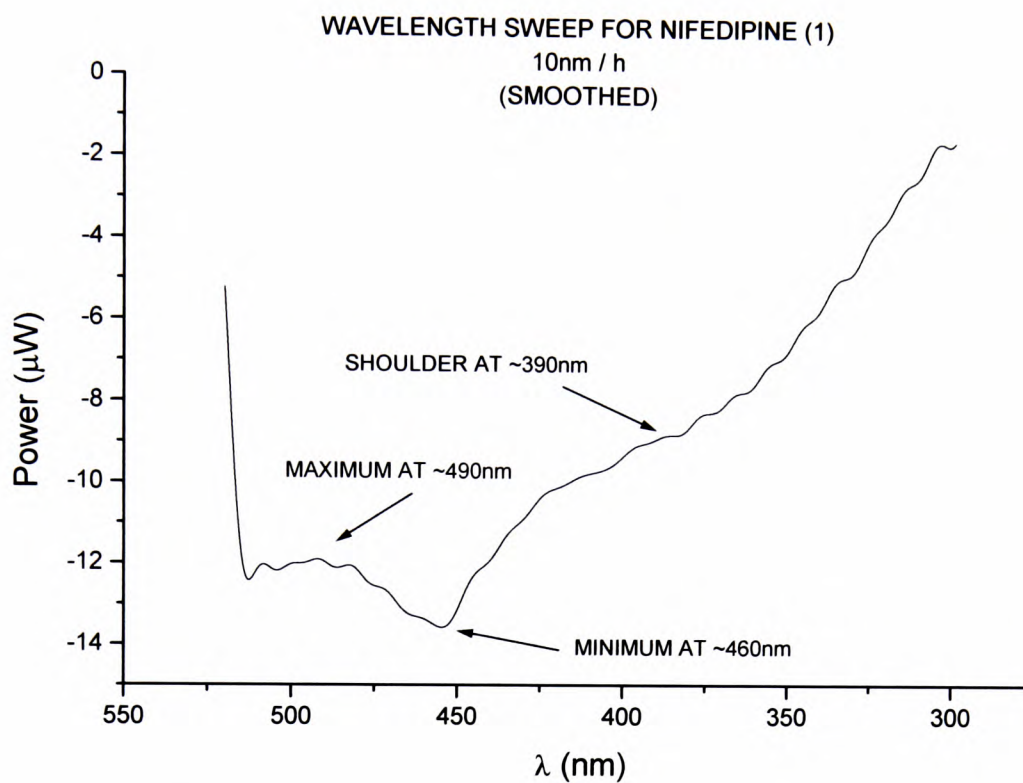


**Figure 6.3.14** The photodegradation of nifedipine with wavelength sweep (smoothed)

If this plot is inverted, re-scaled and plotted alongside the graph published by Lehto *et al.*<sup>65</sup> then direct comparison of outputs for the same experiment can be made:

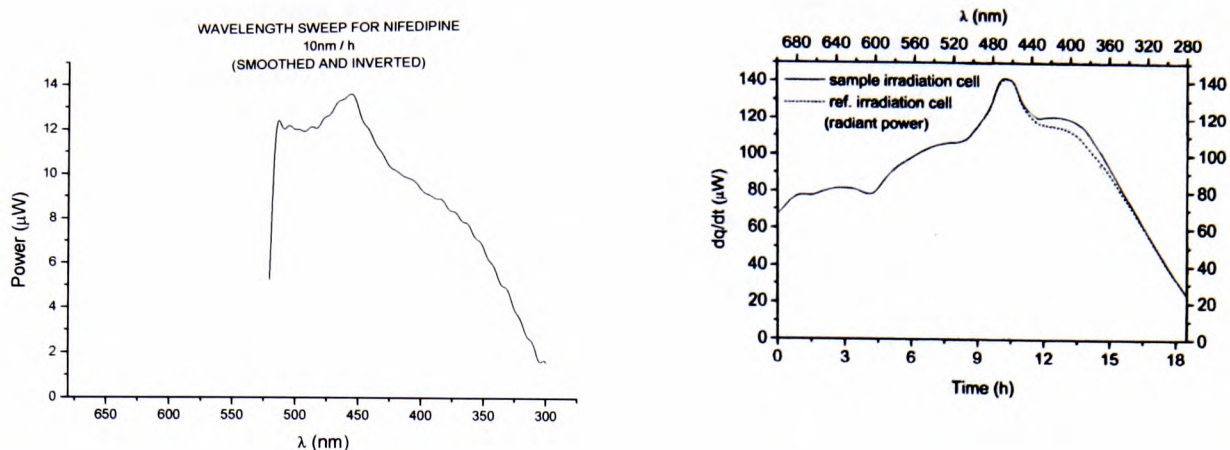


**Figure 6.3.15** Comparison of experimental output (right) with literature (left)

Clearly, on direct comparison, the initial photocalorimeter results are encouraging since they compare favourably with the work of Lehto *et al.*<sup>65</sup> Both plots above have a peak / trough at  $\sim 460\text{nm}$ , and shoulders at  $\sim 390\text{nm}$ ,  $\sim 490\text{nm}$  and  $\sim 520\text{nm}$ .

Issues concerning why there are troughs instead of peaks have been dealt with in the previous chapter but is most likely a result of the imbalance of the capacity of the two fibre optic cables that feed the sample and reference sides of the calorimeter.

Two further experiments (2 and 3) were carried out to verify the results where a new faster scan rate of  $1\text{nm} / \text{minute}$  was adopted to see if the speed of the experiment could be increased.

### **Experiments 2 and 3**

Wavelength range:  $520\text{nm}$  to  $300\text{nm}$

Scan rate:  $60\text{nm} / \text{hour}$

Sample mass:  $500\text{mg}$

The combined outputs were smoothed using the same process as for *experiment 1* and then plotted together.

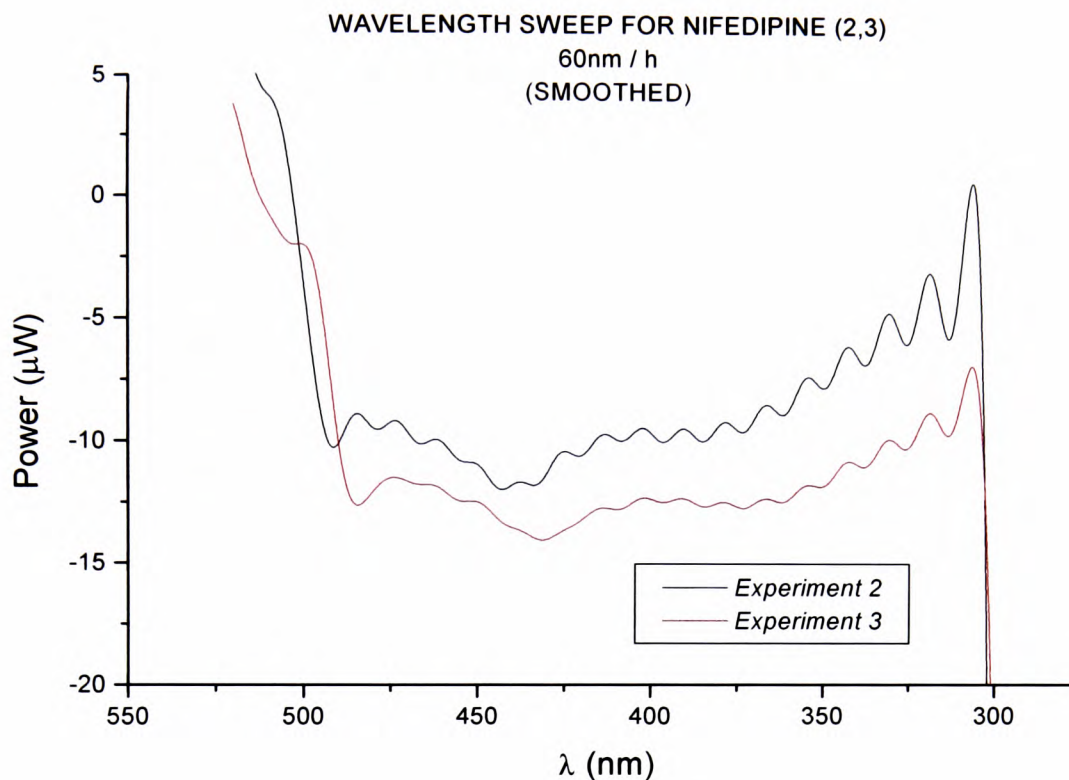


**Figure 6.3.16** The photodegradation of nifedipine with wavelength sweep (smoothed)

The plots show that under the new scanning rate, the peak / trough at  $460\text{nm}$  has moved closer to  $430\text{nm}$  (particularly for *experiment 3*). However, the “causative wavelength” information obtained before can still be gained albeit with a greater error. i.e. significant wavelengths at  $390\text{nm}$ ,  $490\text{nm}$  and  $520\text{nm}$ .

It must be remembered that at this early stage of development, the objective of the causative wavelength studies is to develop a screening process. For this reason, approximations are acceptable at this stage.

---

### ***Experiments 4 and 5***

Wavelength range: 520nm to 300nm

Scan rate: 60nm / hour

Sample mass: 500mg

Humidity: 94%

It is known <sup>139</sup> that adding a degree of elasticity to a solid (i.e. as a consequence of increasing the humidity) can cause it to undergo photodegradation more readily. In an attempt to increase the somewhat modest TAM signals observed for the previous experiments and produce better resolution of the “causative wavelengths” observed in *experiments 1 to 3*, a number of experiments were carried out under increased relative humidity.

A hydrostat is a small glass container of volume approximately 1ml. When a hydrostat is filled with a saturated salt solution and then placed in a sealed environment, the salt solution creates the desired known relative humidity when the system allowed to reach equilibrium.

In the two experiments that follow, a hydrostat containing *potassium nitrate*,  $KNO_3$  was added to both the sample and reference ampoules (giving a relative humidity of 94% at 298K) and the same test and analytical methods employed as before:

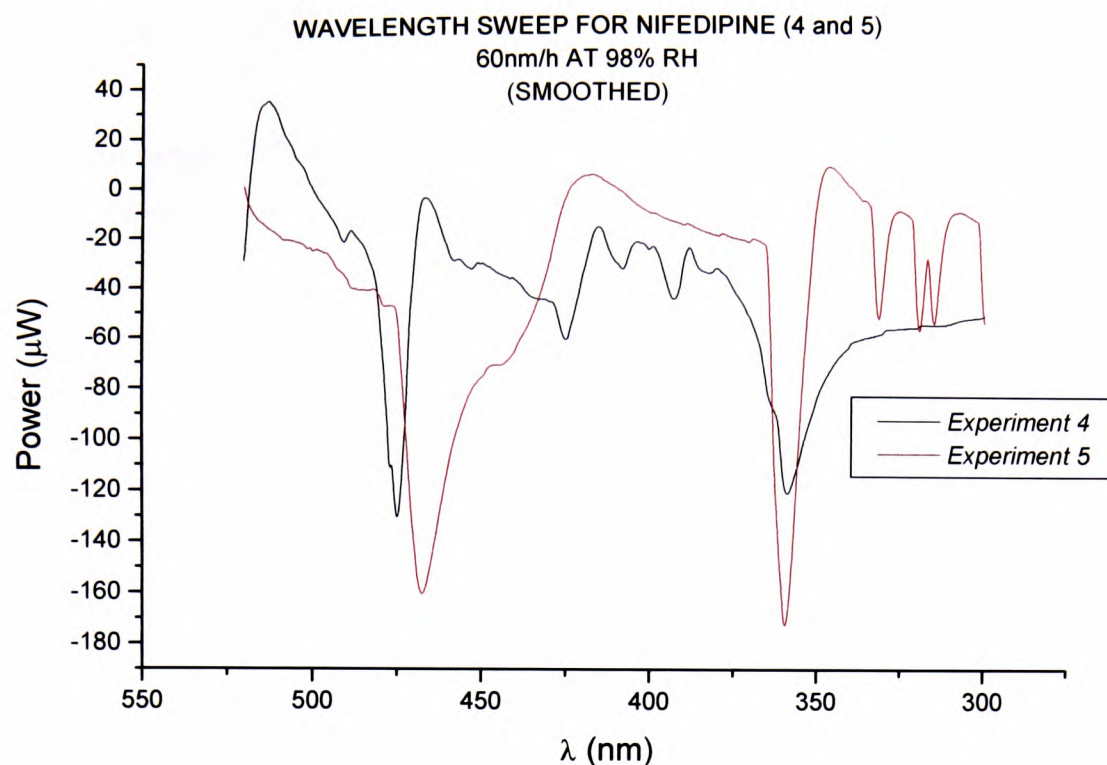


**Figure 6.3.17** The photodegradation of nifedipine with wavelength sweep (smoothed)

These two outputs show that the addition of hydrostats has added considerably to the values of  $\Phi$ , suggesting the addition of moisture may help the photodegradation process for solids. In both cases, major peaks / troughs can be found at the now familiar  $\sim 475\text{nm}$  and  $\sim 355\text{nm}$  at 10 times the power output seen before. Again the wavelengths are approximate. The major drawback of increased values of  $\Phi$ , however, is that there are now additional peaks and troughs that complicate the picture.

Clearly there is room for improvement in terms of obtaining outputs that suggest constant “causative wavelengths”. Generally, however, the addition of hydrostats can be seen as an important step towards using the photocalorimeter to produce clear and unmistakable “causative wavelength” spectra.

### Experiment 6

Wavelength range: 520nm to 300nm

Scan rate: 60nm / hour

Sample mass: 500mg

Humidity: 58%

Following the encouraging results observed for the hydrostat-aided photodegradation in *experiments 4* and *5*, an experiment was carried out with a different level of relative humidity. This was achieved by changing the saturated salt solution to *sodium bromide, NaBr*, providing a relative humidity of 58% at 298K.

All other experimental details were left unchanged.

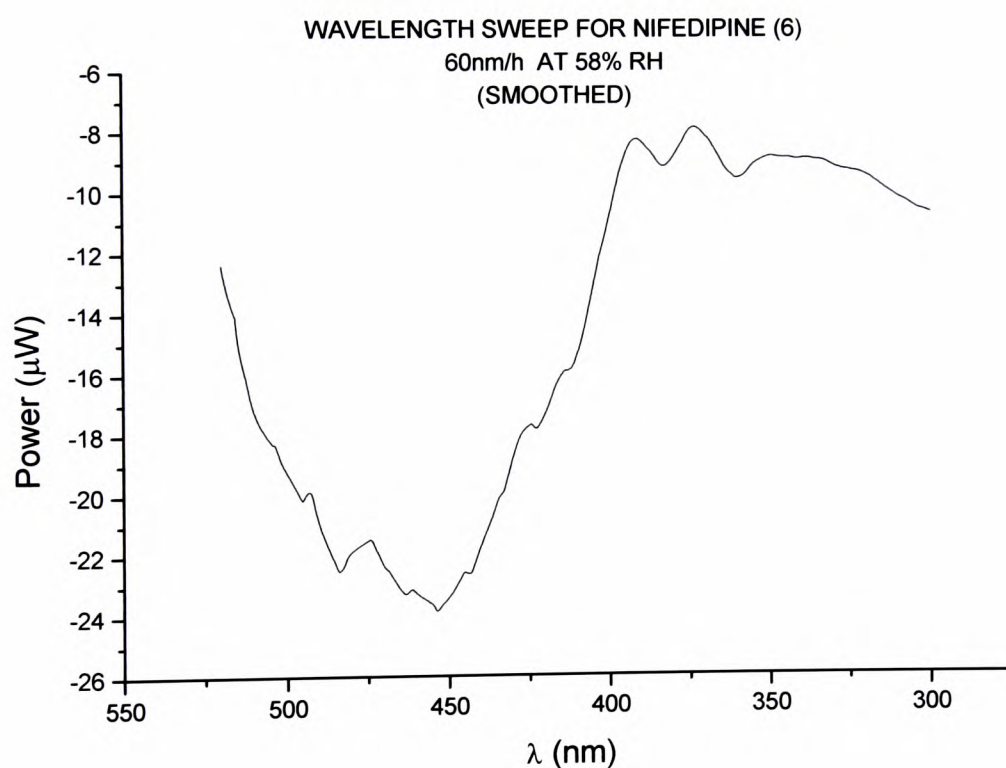


**Figure 6.3.18** The photodegradation of nifedipine with wavelength sweep (smoothed)

Again, the familiar peaks / troughs at  $\sim 355\text{nm}$  and  $\sim 460\text{nm}$  are observed.

It should be noted that the “spectrum” for this experiment is simpler than those produced in *experiments 4* and *5* and that the values of  $\Phi$  have dropped back down to the magnitude observed in the first experiments performed with *nifedipine*. This may be a reflection on the change of saturated solution and hence the change in relative humidity. More work is needed in this area in the future; both in terms of testing the reproducibility of the outcome and making further changes to the relative humidity in which experiments are performed.

### ***Experiments 7,8,9 and 10***

Wavelength range: 520nm to 300nm

Scan rate: 60nm / hour

Considering that the complexity of solid-state systems makes photostability testing more difficult than is the case for solutions (see *chapter one*), it was decided to repeat the wavelength sweep carried out in *experiments 2* and *3* but this time for *nifedipine* in solution. It was hoped that testing solutions would produce a much bigger TAM signal than is the case for solids, producing a better defined output for the photodegradation.

Four experiments for the degradation of *nifedipine* in the solution-phase were carried out and the outputs plotted below:

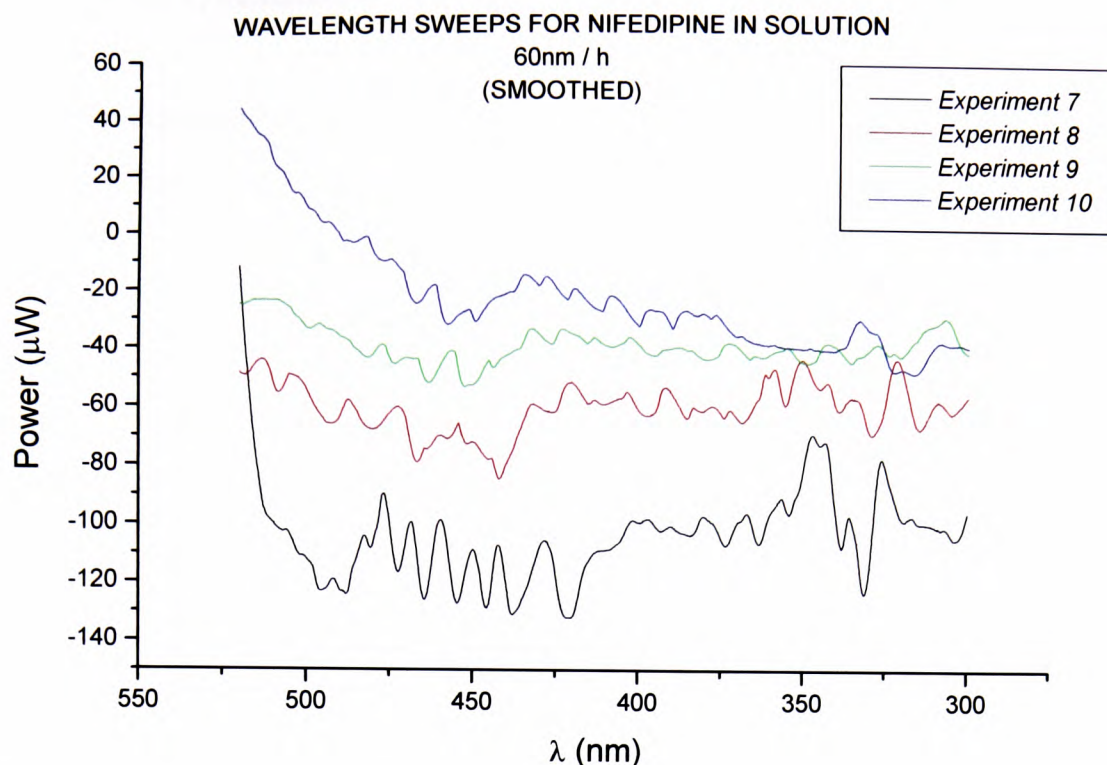


**Figure 6.3.19** Comparison of the photodegradation of nifedipine in solution with changing wavelength

It should be noted that the values of power have increased compared with the previous solid state experiment (*number 6, figure 6.3.18*) using a *NaBr* solution hydrostat.

The output shows possible degradation occurring at the familiar causative wavelength of *nifedipine* at *355nm* (for *experiments 7 and 10*) but in not sufficient clarity or repeatability especially when compared with *experiments 8 and 9*. Overall, the testing of *nifedipine* in solution has not produced the results either desired or expected. Future solution-phase experiments could include increasing the concentration of *nifedipine* or the testing of different fill volumes of *nifedipine* solution (see *chapter three*).

Focus in future work, however, will be on improving the repeatability of causative wavelengths obtained in the studies carried out in the solid state.

### Qualitative vs. Quantitative Analysis

As already discussed at the beginning of this chapter (and also in *chapter five*), the energy of a photon,  $E$  can be found using the following equation:

$$E = hv = hc/\lambda \quad \text{Eqn 5.1.1.5}$$

where  $h$  is Planck's constant ( $6.63 \times 10^{-34} \text{ Js photon}^{-1}$ )

$c$  is the speed of light ( $2.99 \times 10^8 \text{ ms}^{-1}$ )

$\lambda$  is the wavelength ( $m$ )

The irradiance,  $I_0$  can be found from:

$$I_0 = k_0 / \phi \quad \text{Eqn 5.1.1.2}$$

where  $k_0$  is the rate constant

$\phi$  is the quantum yield

and the energy of a photon is related to the photon flux,  $F_0$  by the following:

$$F_0 = I_0 \cdot V \cdot N_A \cdot E_\lambda / A \quad \text{Eqn 5.1.1.3}$$

where  $I_0$  is the irradiance ( $\text{einstein dm}^{-3} \text{ s}^{-1}$ ) and can be written  $k / \phi$

$V$  is the volume of solution ( $\text{dm}^3$ )

$N_A$  is Avogadro's number ( $\text{mol}^{-1}$ )

$E_\lambda$  is the energy of a photon of wavelength  $\lambda$  (in  $\text{J photon}^{-1}$ )

$A$  is the cross-sectional area of exposed actinometric solution ( $\text{m}^2$ )

Equation 5.1.1.3 can therefore be rewritten as:

$$F_o = k_o.V.N_A.h.c / A.\phi.\lambda \quad \text{Eqn 6.3.1.1}$$

The terms  $V$ ,  $N_A$ ,  $h$ ,  $c$ ,  $A$  and  $\phi$  are constant for an individual reaction. If these are grouped together and defined as a constant,  $C$ , then the equation becomes:

$$F_o = (k_o / \lambda) . C \quad \text{Eqn 6.3.1.2}$$

During the wavelength sweep experiments described above,  $\lambda$  changes constantly and (as described in *section 6.2*) so does the photon flux and so the relationship between  $\lambda$ ,  $k$  and  $F_o$  is not simple. To obtain a value for the rate constant,  $k$ , therefore, the procedure must be to choose a wavelength of interest (obtained from the initial sweep experiments carried out above) and carry out photodegradation at that point. The photon flux and wavelength become constant and  $k$  can be obtained from *equation 6.3.1.2*.

Note: A major disadvantage of *equation 5.1.1.3* above is that solution-phase and zero-order conditions must be assumed

## Conclusions

The study of the wavelength-dependent photodegradation of *nifedipine* using the photocalorimeter has been carried out quite successfully.

Most notably, “causative wavelengths” for the photodegradation of *nifedipine* have been identified by application of the photocalorimeter and match those reported by Lehto *et al.*<sup>65</sup> – a good indication that the apparatus is working successfully.

Increasing the relative humidity in which the experiments were carried out seemed to encourage photodegradation to occur and lead to better-defined “causative wavelength” calorimetric outputs. The difference in size of the calorimetric signal obtained through the use of different levels of relative humidity is an area of interest that requires more investigation in the future.

The results of the experiments carried out on *nifedipine* solution show potential and more work needs to be carried out in this area before decisive conclusions can be made.

Overall, the results show that the photocalorimeter can be used qualitatively, providing a method of scanning *nifedipine* for causative wavelengths in the range 550nm to 300nm in a matter of a few hours. This initial use of the apparatus in qualitative mode to identify key photodegradation-causing wavelengths will then allow further analysis to be carried out. Fixing the monochromator at a wavelength of interest and allowing photodegradation to occur will then produce calorimetric outputs that can be analysed quantitatively using the equations described in *chapter two*.

### 6.3.2 Applying the Photocalorimeter to an Unknown Material

Having developed the photocalorimeter and tested it, with reasonable success, on *nifedipine*, the final stage is to apply the instrument to a drug of which little is known thermodynamically or kinetically. This application would represent one of the main uses for the novel photocalorimeter in industry when used to screen materials for “causative wavelengths”.

*SB787976* is a solid-state pharmaceutical material which is known to be photosensitive. It is stored in the dark at under  $10^{\circ}\text{C}$ . Approximately 200mg of sample were supplied by manufacturers GlaxoSmithKline for testing in the photocalorimeter following the method outlined below. Testing of this novel material was carried out according to the method followed for the initial “causative wavelength” experiment.

- 200mg of *SB787976* was loaded into the sample ampoule of the TAM
- 200mg of talc was loaded into the reference ampoule
- The ampoules were lowered into the calorimeter as described in *chapter four*
- The lamp was switched on set at 360W and allowed to warm up for 1 hour prior to sample irradiation
- The monochromator was set at the first wavelength of the sweep
- After an hour the light source shutter was opened and the light allowed to shine through the monochromator and onto the sample
- Data recording on the TAM was started simultaneously
- The wavelength was changed according to the scan rate required

Wavelength range: 600nm to 200nm

Scan rate: 10nm / hour

Sample mass: 200mg

The photocalorimetric output for the photodegradation of *SB787976* is shown below:

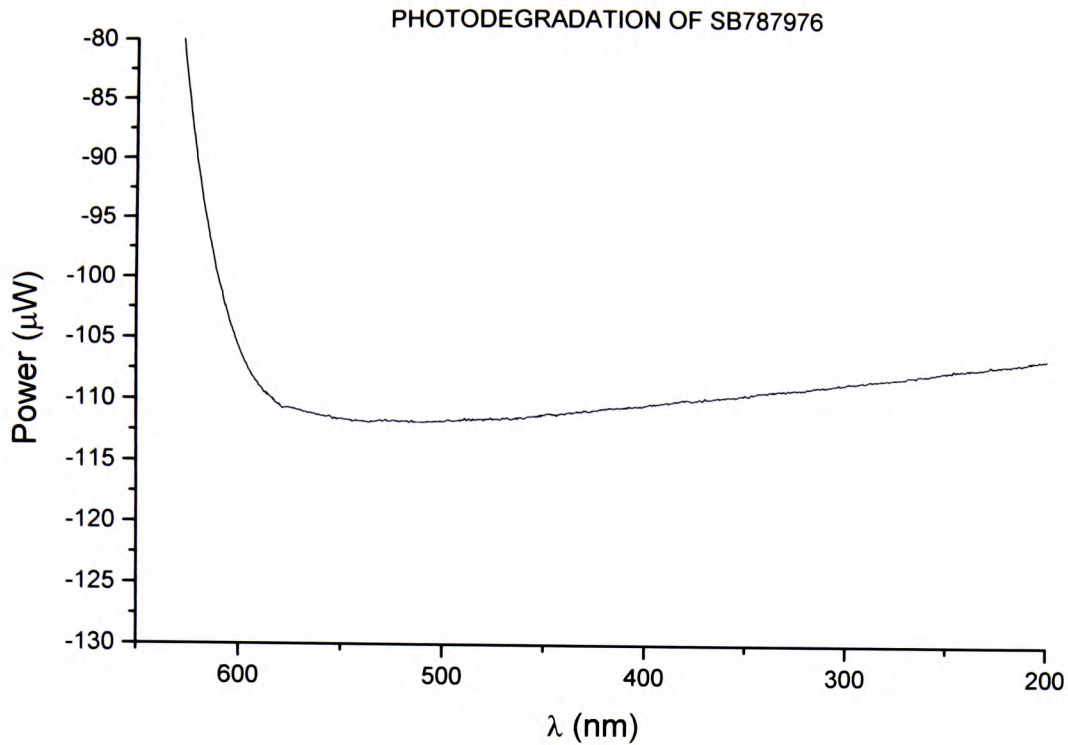


**Figure 6.3.18** The photodegradation of SB787976

Although there are no “spikes” at individual “causative wavelengths” as exhibited by the outputs for *nifedipine*, the output shows that *SB787976* is undergoing some kind of reaction in the photocalorimeter. This can be seen clearly if the output above is compared with a control experiment for photodegradation previously described in this thesis. The figure below shows significant differences between a blank output and the output for *SB787976*.

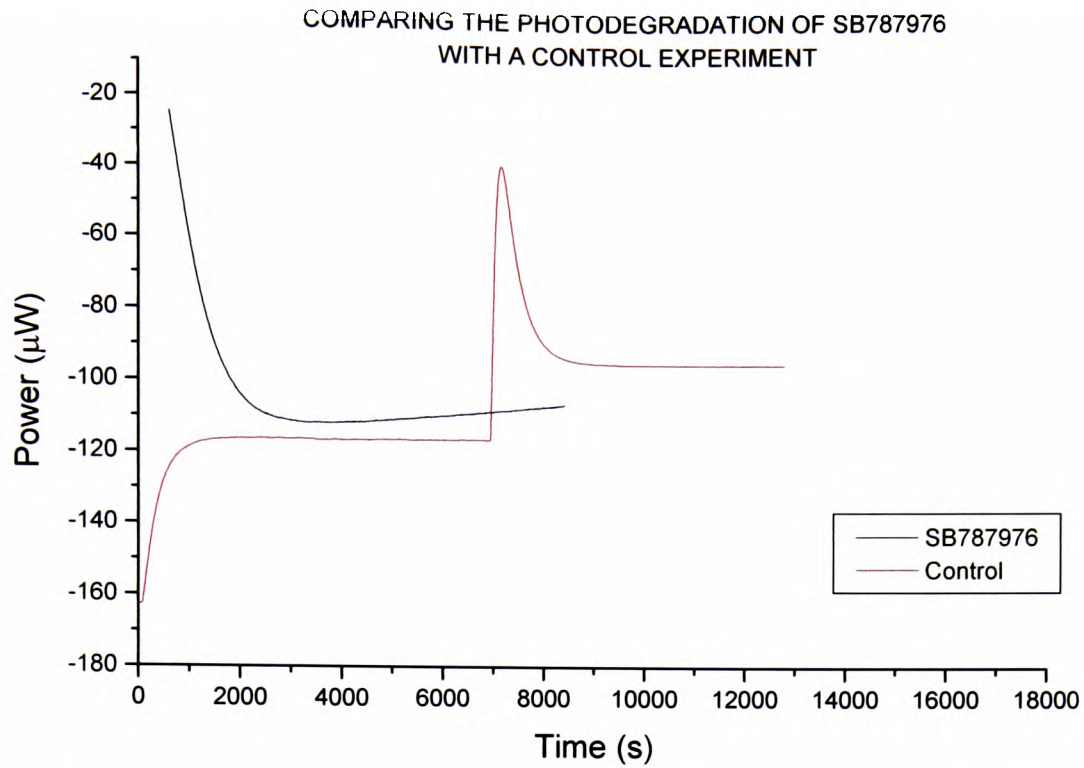


**Figure 6.3.19** The photodegradation of SB787976 compared with a “blank” output

Unfortunately, however, there was insufficient sample and time to be able to repeat the experiment for *SB787976*. The result seen in *Figure 6.3.18* was the one and only chance to test an unknown material for causative wavelength using the photocalorimeter.

Further work in this area is suggested in the conclusions below.

## Conclusions and Further Work

The work above has described the first successful experiment to obtain the rate constant photocalorimetrically for the photodegradation of solid state *nifedipine*. where previous workers Lehto *et al.* only previously obtained qualitative data.

The results obtained by the photocalorimeter compare favourably with rate constant values obtained from more established analytical methods (i.e. obtained from *nifedipine* in solution). The correspondence between the two values of  $k$  is however only true over the first period of reaction after the minimum 2000 seconds has elapsed. After this, the calorimeter illustrates the complexity of *nifedipine* photochemistry, with many individual reactions clearly seen to be contributing to the overall process. This may also be the case for the *potassium ferrioxalate* photoreaction described in *chapter five*. Further investigation of this photoreaction is needed before conclusions can be drawn but it would appear from *potassium ferrioxalate* and *nifedipine* that complexity is more common in photoreactions than first thought.

If this is the case, then new methods for dealing with complexity in reaction systems need to be developed. One such method is the application of chemometrics, which can deconvolute the complexity data of the photoreaction (detected by the photocalorimeter) into individual non-complex outputs. These individual reactions can then be analysed by the methods described in *chapter two*.

For the testing of *SB787976*, having to leave the project with a promising initial result is disappointing but leaves plenty of scope for future work to take the investigation forwards. Repeat experiments employing the same experimental method may produce better results given sufficient time and material. Experiments adding hydrostats to the solid may produce improved results. This provided encouraging results for the photodegradation of *nifedipine* and may be successful for *SB787976*.

Changing the temperature at which the calorimetric experiment is carried out, changing the quantity of material placed in the ampoule or repeating the photodegradation using a new bulb in the light source to ensure high levels of UV irradiation are all experiments that need consideration.

What the initial result does prove, however, is that the relationship between photon flux and wavelength, discussed early in this chapter, does not play a significant part in influencing the results of a wavelength sweep for an unknown solid. This is

demonstrated by the fact that the output observed for *SB787976* does not mirror the shape of the change in photon flux with time observed for *nifedipine*.

## *CHAPTER 7*

### *CONCLUSIONS AND FURTHER WORK*

## 7. Conclusions and Further Work

The aim of the project was to design and build a photocalorimeter able to test the photostability, in real time, of pharmaceuticals in both solid and solution phases. To achieve this goal, the project progressed from the development of theory that could deal with reactions in the solid state (described in *chapter two*) through to the testing of a solid material of unknown photostability using a light of variable monochromatic wavelength (described in *chapter six*).

Overall, the outcome of the project is pleasing in that a photocalorimeter has been successfully developed that produces quantitative as well as qualitative data, although some issues remain to be dealt with by future work.

As a result of the theoretical development described in this thesis, equations now exist that can deal with reactions in both the solid and solution phase. Adapting equations for use in solid state systems has been particularly useful in developing the photocalorimeter for use where solid state photostability analysis is of prime importance. This has meant the introduction of fitting parameters,  $m$  and  $n$  and a reaction co-efficient,  $k$ . The extent of reaction,  $\alpha$ , has merited particular attention since the assumption that a reaction will go to completion given sufficient time cannot be applied for solids where photodegradation may only occur at the surface of the material and then stop.

If the reaction occurring in the solid state is complex (e.g. the photodegradation of *nifedipine* as discussed in *chapter six*), then chemometrics can be applied to deconvolute the reaction into its individual contributing components and the analysis carried out using the equations described in *chapter two*. This development work is currently in progress.

The *imidazole*-catalysed hydrolysis of *triacetin* was selected as a test-reaction for calorimeters since it meets all criteria required of such a standard. As well as being robust, reliable and repeatable, the reaction is relatively easy to set up, it is inexpensive and literature values for the rate constant and enthalpy of reaction are well-established, enabling the reaction to also be applied as a fault-finding and operator-training tool.

Since the *triacetin* reaction is robust, reliable and repeatable, further studies allowed the establishment of optimal test conditions (e.g. sample position studies) in preparation for the constructing of the photocalorimeter. The results showed the best position for a sample to be in when undergoing testing in the calorimeter was the bottom of the ampoule without the presence of any additional calorimetric inserts.

The work on *triacetin* also established that the direct calculation of parameters for the rate constant and reaction enthalpy represents a better method of data analysis than the iterative technique used previously. The direct calculation method should be used in all future work which should involve further testing of different test conditions such as increasing the concentration of *triacetin* in the system, performing the test at different temperatures and further studies using calorimetric inserts and their effect on experimental output.

Part of the reason why *triacetin* makes a good test system is because the reaction involves a kinetic process which is dynamic and visible when viewed as a calorimetric output that progresses with time. In actinometric terms, chemical methods, such as *2-NB* and *potassium ferrioxalate* offer similar kinetic processes that can be followed in the calorimeter, whilst the spectroradiometric method does not and is therefore less attractive as a method considering the photocalorimeter itself follows kinetic processes.

Although both chemical actinometers tested are zero-order and should produce power vs. time plots of horizontal lines when exposed to light, *2-NB* gave the more satisfactory output since the calorimetric output for the *potassium ferrioxalate* photoreduction suggests the reaction is complex and therefore needs further investigation in the future.

*2-NB* is also easier to prepare than *potassium ferrioxalate*, it can be kept for longer in storage and the reaction scheme is relatively simple.

It is for these reasons that *2-NB* is the preferred actinometric option until further work is carried out on *potassium ferrioxalate* and other potential chemical actinometric systems that have yet to be investigated for use with the photocalorimeter.

The application of the developed photocalorimeter to test the photostability of solid materials was successful in that the rate constant for the photodegradation of *nifedipine* was found to be within 6% for the majority of experiments carried out. This

obtained value for  $k$  represents the first time a photocalorimeter has been used to obtain quantitative data and the initial results are pleasing. Further work in this area will include further repeat runs of *nifedipine* degradation under white light and the application of chemometrics to analyse the photocalorimeter-obtained data. Further work of interest will be the effect on the photodegradation and relative humidity on the particle size of the solid under test.

The study of “causative wavelength” testing on *nifedipine* was pleasing in that experimental results suggested concurrence with other workers and that the results were repeatable across a range of experimental conditions. Particularly promising results were achieved upon the addition of extra humidity to the system and optimising test conditions for “causative wavelength” work using *nifedipine* as a model system will be carried out in the future.

The single experiment carried out on the unknown pharmaceutical material *SB787976* gave clear evidence of photolability although much more work is required to be carried out on this material before both qualitative and quantitative analysis can be made.

Before testing any other pharmaceutical materials of unknown photostability (*SB787976* was done whilst the opportunity remained to carry out the experiment), other systems with known photostability properties (similar to *nifedipine*) must be carried out first to fully establish how well the photocalorimeter performs with a series of solid materials.

Future work not yet explored as part of the project needs to concentrate on the development of methods to test the compatibility of photolabile drug and drug products under irradiation conditions. This work will involve testing of familiar products such as *nifedipine* as well as materials that currently haven't been investigated in the photocalorimeter. The sort of question that needs to be addressed is, for example, whether the photostability properties of *nifedipine* are altered when it is exposed to both white and monochromatic light if interacting with another material, such as starch.

## REFERENCES

1. Willson, R. J; Beezer, A.E; Mitchell, J.C; Loh, W, *J. Phys. Chem*, 99, 7108-7113, **1995**
2. Zaman, F; Beezer, A.E; Mitchell, J.C, Clarkson, Q; Elliot, J; Nisbet, M; Davis, A.F, *Int. J. Pharm.*, 225, 135, **2001**
3. Zaman, F; Beezer, A.E; Mitchell, J.C, Clarkson, Q; Elliot, J; Davis, A.F; Willson, R.J, *Int. J. Pharm.*, 277, 133, **2001**
4. Gaisford, S; Hills, A.K; Beezer, A.E; Mitchell, *Thermochim. Acta*, 328, 39-45, **1999**
5. Willson, R. J; Beezer, A.E; Mitchell, J.C, *Thermochim. Acta*, 264, 27-40, **1995**
6. Beezer, A.E; Willson, R. J; Mitchell, J.C; Hills, A.K; Gaisford, S, Wood; Connor, J.A, *Pure and Applied Chem*, 70, 633-638, **1998**
7. Beezer, A.E; Gaisford, S; Hills, A.K; Willson, R.J; Mitchell, *Int. J. Pharm*, 179, 159-165, **1999**
8. Beezer, A.E, *Thermochim. Acta*, 349, 1-7, **2000**
9. Willson, R. J; Beezer, A.E; Mitchell, J.C, *C. Int. J. Pharm*, 132, 45-51, **1996**
10. Ng, W.L; Aust, *J. Chem.*, 28, 1169, **1975**
11. Urbanovici, *J. Therm. Anal. Cal.*, 55, 919, **1995**
12. Beezer, A.E; Hills, A.K; O'Neill, M.A.A; Morris, A.C; Kiersten, K.T.E; Deal, R.M; Waters, L.J; Hadgraft, J; Mitchell, J.C; Connor, J.A; Orchard, J.E; Willson, R.J; Hofelich, T.C; Beaudin, J; Wolf, G; Baitalow, F; Gaisford, S; Lane, R.A; Buckton, G; Phipps, M.A; Winneke, R.A; Schmitt, E.A; Hansen, L.D; O'Sullivan, D; Parmar, M.K, *Thermochim. Acta*, 380,13-17, **2001**
13. Willson, R. J; Beezer, A.E; Hills, A.K; Mitchell, J.C, *Thermochim. Acta*, 325, 125-132, **1999**
14. Chen, A; Wadso, I.J, *Biochem. And Biophys. Meth.*, 6, 297-306, **1982**

15. Beezer, A.E; Morris, A.C; O'Neill, M. A. A; Willson, R.J; Hills, A.K; Mitchell, J.C; Connor, J.A, *J. Phys. Chem*, 105, 1212, **2001**
16. Beezer, A.E, *Thermochim. Acta*, 380, 205-208, **2001**
17. O'Neill, M.A.A; Beezer, A.E; Deal, R.M; Morris A.C; Mitchell, J.C; Orchard, J.E; Connor, J.A; *Thermochim. Acta*, 397,163-169, **2002**
18. Kuhn, H.J; Braslavsky, S. E; Schmidt, R, *Pure and Appl. Chem.*, 61, 2, 187-210, **1989**
19. Parker, C.A, *Proc. R. Soc. London, Ser. A*, 220, 104, **1953**
20. Parker, C.A, *Trans. Faraday Soc.*, 50, 1213, **1954**
21. Pitts, J.N; Vernon, J.M, Wan, J.K.S, *Int. J. Air Poll.*, 9, 595 – 600, **1965**
22. Allen, J.M; Allen, S.K; Baertschi, S.W, *J. Pharm and Biomedical Anal.*, 24, 167-178, **2000**
23. Eliel, E.L.; Prosser, T.; Young, G.W. *J. Chem. Educ.* 34,72, **1957**
24. Constantinescu, A; Han, D; Packer, L; *Biol. Chem.* 268, 10906 – 10915, **1993**
25. Fleming, J. E; Miyashita, K; Quay, S.C; Bensch, K.G; *Biochem. Biophys Res. Commun.* 115, 531-535, **1983**
26. Reijenga, J. C, *J. Rad. Anal. And Nuc. Chem. Articales.* Vol. 163, No 1, 155-167, **1992**
27. Schafer, W; Klunder, J, *J. Chem. Educ.* Vol. 72, No 6, 537-540, **1995**
28. Carts, Y. Y, *Laser Focus World*, Vol. 31, No 1, 24-26, **1995**
29. Buckton, G; Beezer, A. E, *Int. J. Pharm*, 72, 181-191, **1991**
30. Willson, R.J, *PhD Thesis* University of Kent, UK, **1995**
31. Willson, R. J; Beezer, A.E; Mitchell, J.C, *J. Phys. Chem*, **1995**
32. Gaisford, S, *PhD Thesis* University of Kent, UK, **1997**
33. Hills, A.K, *PhD Thesis* University of Kent, UK, **2000**
34. Willson, R. J; Beezer, A.E, *Thermochim. Acta*, 402, 75-80, **2003**

35. O'Neill, M. A. A; Beezer, A.E; Morris, A.C; Urakami, K; A; Willson, R.J; Connor, J.A, *J. Thermal Analysis and Calorimetry*, 73, 709-714, **2003**
36. Suurkuust, J; Wadso, I, *Chemica Scripta*, 20, 155-163, **1982**
37. The isothermal calorimetric manual, Thermometric AB, Jarfalla, Sweden
38. Hansen, L.D; Eatough, D.J; Lewis, E.A, *Can. J. Chem.*, 68, 2111-2114, **1990**
39. Angberg, M; Nystrom, C; Castensson, S, *Int. J. Pharm*, 90, 19-33, **1993**
40. Fontana, L.H; Criddle, R.S; Hansen, L.D; Wilhelmsen, E.J, *Food Science*, 58, 1411-1417, **1993**
41. Selzer, T; Radau, M; Kreuter, J, *Int. J. Pharm*, 171, 227-241, **1998**
42. Atkins, P.W; *Physical Chemistry*, 6th ed, Oxford, pp219-220, **1998**
43. Galwey, H.K; Brown, M.E, *Thermochim. Acta*, 268/270, 1, **1995**
44. Galwey, H.K, *J. Therm. Anal. Cal.*, 863, 60, **2000**
45. Sewry, J.D; Brown, M.E, *Thermochim. Acta*, 390, 217, **2002**
46. Morris, A.C, *MSc Thesis* University of Greenwich , UK, **2000**
47. Cooper, A; Converse, C.A, *Biochemistry*, 15, 14, 2970-2978, **1976**
48. Nicodem, D.E; Aquilera, O.M.V, *J. Photochem.*, 21,189-193, **1983**
49. Fernandez, E; Figurea, J.M; Tobar, A, *J. Photochem.*, 11,69-71, **1979**
50. Murata, K; Yamaguchi, Y; Shizuka, H, *J. Photochem. Photobio. A: Chem*, 60, 207-214, **1991**
51. Adick, H.J; Schmidt, R; Braver, H.D, *J. Photochem. Photobio. A: Chem*, 45, 89-96, **1988**
52. Adick, H.J; Schmidt, R; Braver, H.D, *J. Photochem. Photobio. A: Chem*, 49, 311-316, **1989**
53. Briggner, L; Wadso, I, *J. Biochem. And Biophys. Meth.*, 22, 101-118, **1991**
54. Hills, A.K; Beezer, A.E; Mitchell, J.C; Connor, J.A, *Thermochim. Acta*, 380,19-26, **2001**
55. Teixeira, C; Wadso, I, *J. Chem. Thermodynamics*, 22,703-713, **1990**

56. Tonnesen, H; Karlsen, J, *Pharmeuropa*, 9, 735-736, **1997**
57. Thatcher, S.R; Mansfield, R.K; Miller, R.B; Davis, C.W; Baertschi, S.W, *Pharm. Tech.* **2001**
58. CIE Publication number 69, **1985**
59. Riehl, J; Maupin, C; Layloff, T, *Pharm. Forum*, 21, 1654-1663, **1995**
60. Angelo, B, *Radiometry / Actinometry*, **1999**
61. Drew, H et al., *Pharm. Forum*, 24, 6334-6346, **1998**
62. Tonnesen, H; Karlsen, J, *Pharmeuropa*, 7, 137-141, **1995**
63. Tonnesen, H; Moore, D.E, *Pharm. Technol.*, 17, 2, 1-5, **1993**
64. Berston, J. A; Brown, E, *J. Amer. Chem. Soc.*, 77, 447, **1955**
65. Lehto, V-P; Salonen, J; Laine, E; *Pharm. Research*, 16, 3, **1999**
66. Cooper, A, *Methods in Enzymology*, 8, 79, 667-673, **1982**
67. Hoyle, C.E, *Radiation Curing*, 3, 57-133, **1992**
68. Teixeira, C, *Photochemistry – methods and applications*, 105-136, **1999**
69. Magee, J.L; DeWitt, T.W; Smith, E.C; Daniels, F, *J. Am. Chem. Soc.*, 61, 3529, **1939**
70. Schaarschmidt, B; Lamprecht, I, *Experientia*, 29, 505-506, **1973**
71. McIlvane, P; Langerman, N, *Biophysical Journal*, 17, 17-25, **1977**
72. Adamson, A.W; Vogler, A; Hunkley, H; Wachter, R, *J. Am. Chem. Soc.*, 100, 1298, **1978**
73. Teixeira, C; Wadso, I, *Netsu Sokutei*, 21, 1, 29-39, **1994**
74. Wadso, I, “Experimental Chemical Thermodynamics” 4, 12, 267-301, **1994**
75. Abadie, M.J.M; Appelt, B.K, *Etude de materiaux photosensibles par photocalorimetrie*, 20-24, **1987**
76. Fouassier, J. P; *XVI Congrès de l’Association Française des Techniciens des Peintures, Vernis, Encres d’Imprimerie, Colles de Adhésifs, AFTPV, Double Liason*, 158-167, **1985**

77. Appelt, B.K; Abadie, M.J.M, *Polymer Eng. Sci.*, 25, 931-933, **1984**
78. Appelt, B.K; Abadie, M.J.M, *14th North American Thermal Analysis Society, NATAS*, San Francisco, **1985**
79. Abadie, M.J.M; Appelt, B.K, *22nd International Association for Dental Research, IADR, Paris*, 117, **1985**
80. Abadie, M.J.M; Appelt, B.K, *3e Journées du Collège Française des biomatériaux Dentaires, Paris*, **1986**
81. Abadie, M.J.M; Appelt, B.K, *J. Biomat. Dent.*, 3, 1, 17-27, **1987**
82. Theweleit, E; Kuze, W, *Methods and Applications of Photocalorimetry*, 77, 9, 870-873, **1987**
83. Fischer, E; Soreau, M, *La photocalorimétrie: méthodes et applications, Analusis*, 16, 3, **1988**
84. Manual number 66901, *Oriel Instruments*, **1996**
85. The Book of Photon Tools, *Oriel Instruments*
86. Perfusion Shaft Operating Instructions, *Thermometric Ltd*
87. Spectrometer Operating Software Manual, *Ocean Optics, Inc.* **2000**
88. Urakami, K, Personal Communication, **2003**
89. Calvert, J.G; Pitts, J.N, *Photochemistry*, Wiley, New York, 783-788, **1966**
90. Leifer, A, The kinetics of Environmental Aquatic Photochemistry, *Amer. Chem. Soc., Washington, DC*, 146-149, **1988**
91. International Committee on Harmonization, Guidelines for the Photostability Testing of New Drug Substances and Products, *Federal Register*, 62, 27115-27120, May, **1997**
92. Yoshioka, S; Ishihara, Y; Terazono, T; Tsunakawa, N; Murai, M; Yasuda, T; Kitamura; Kunihero, Y; Sakai, K; Hirose, Y; Tonooka, K; Takayama, K; Imai, F; Godo, M; Matsuo, M; Nakamura, K; Aso, Y; Kojima, S; Takeda, Y; Terao, T, *Drug Der. Industr. Pharm.*, 20, 2049-2062, **1994**
93. Baertschi, S.W, *Drug Stab.*, 1, 193-195, **1997**

94. Bovina, E; DeFillipis, P; Cavrini, V; Ballardini, R, *Drugs: Photochem, Photostabil.*, 305-316, **1998**
95. Ciamician, G; Silber, P, *Ber.* 33, 2911-2913, **1900**
96. Bowen, E.J; Harley, H; Scott, W.D; Watts, H,G, *J. Chem. Soc.*, 1218 – 1221, **1924**
97. Leighton, P.A; Lucy, F.A; *J. Chem. Phys.*, 2, 756-761
98. Pitts, J.N; Wan, J.K.S; Schuck, E.A, *J. Am. Chem. Soc.*, 86, 3606, **1964**
99. Almand, A.J; Webb, W.W, *J. Chem. Soc.*, 1518, **1929**
100. Yamashita, K; Imai, H, *Bull. Chem. Soc., Jpn*, 41, 1339, **1968**
101. Cooper, G.D; DeGraff, B.A, *J. Phys. Chem.*, 75, 2897, **1971**
102. Porter, G.B; Doering, G.W; Karanka, S, *J. Am. Chem. Soc.*, 84, 4027, **1962**
103. Lee, J; Seliger, H.H, *J. Chem. Phys.*, 40, 519, **1964**
104. Baxendale, J; Bridge, N.K, *J. Phys. Chem.*, 59, 783, **1955**
105. Bowman, W.D, Demas, J.N, *J. Phys. Chem.*, 80, 2434, **1976**
106. Avila, M.J; Figuera, J.M; Menendez, V; Perez, J.M, *J. Chem. Soc., Faraday Trans. I*, 72, 422, **1976**
107. Nicodem, D.E; Cabral, M.L.P.F; Ferreira, J.C.N, *Photochem.*, 8, 213, **1977**
108. Hatchard, C.G; Parker, C.A, *Proc. R. Soc. London, Ser. A* 235, 518-536, **1956**
109. Willett, K.L; Hites, R.A, *J. Chem. Education*, 77, 7, **2000**
110. Ocean Optics™ website. <http://www.oceanoptics.com>
111. OOIBase 32™, Spectrometer Operating Manual, **2000**
112. Manual number 77200, *Oriel Instruments*, **1996**
113. Clapham, D, Personal Communication, **2003**
114. Pietta, P; Rava, A; Biondi, A, *J. Chromatogr.*, 210, 516, **1981**
115. Al-turk, W.A; Majeed, I.A; Murray, W.J; Newton, D.W; Othman, S, *Int. J. Pharm.*, 41, 227, **1988**

116. Sadana, G.S; Ghogare, A.B, *Int. J. Pharm.*, 70, 195, **1991**
117. Vargas, F; Rivas, C; Machado, R, *J. Pharm. Sci.*, 81, 399, **1992**
118. Matsuda, Y; Teraoka, R; Sugimoto, I, *Int. J. Pharm.*, 54, 211, **1989**
119. Ogawa, S; Itagaki, Y; Hayase, N; Takemoto, I; Kasahara, N; Akutsu, S; Inagaki, S, *Byoin Yakugaku*, 16, 189, 1990 *through Chem. Abstr.* 114, 12062g, **1991**
120. Marciniac, B; Rychcik, W, *Pharmazie*, 49, 894, **1994**
121. Thoma, K; Kerker, R, *Pharm. Ind.*, 54, 465, **1992**
122. Palna Gamiz, J.L, *Cardiology*, 88 suppl. 1, 39, **1997**
123. Opie, L.H, *Eur. Hearth J.*, 18, A92, **1997**
124. Magann, E.F; Martin, J.N.Jr, *Obstet. Gynecol. Clin. North. Am.*, 22, 337, **1995**
125. Hultgren, H.N, *Ann. Rev. Med.*, 47, 267, **1996**
126. Luscher, T.F; Wenzel, R.R; Moreu, P; Takase, H; *Cardiol. Clin.*, 13, 579, **1995**
127. Calcagnetti, D.J; Keck, B.J; Quatrella, L.A; Schechter, M.D, *LifeSci.*, 56, 475, **1995**
128. Matsuo, M; Machida, Y; Furuichi, A; Nakamura, A; Takeda, Y, *Drug Stability*, 1, 179-187, **1996**
129. Thoma, K; Klimek, R, *Int. J. Pharm.*, 67: 169-175, **1991**
130. Béchar, S; Quraishi, O; Kwong, E, *Int. J. Pharm.*, 87: 133-139, **1992**
131. Thoma, K; Kerker, R, *Pharm. Ind.*, 54, 359-365, **1992**
132. Vippagunta, S.R; Maul, K.A; Tallavajhala, S; Grant, D.J.W, *Int. J. Pharm.*, 236, 111-123, **2002**
133. Majeeb, I; Murray, W; Newton, D; Othman, S; Al-Turk, W, *J. Pharm. Pharmacol*, 39: 1044-1046, **1987**
134. Al-Turk, W; Othman, S; Majeeb, I; Murray, W; Newton, D, *Drug. Dev. Ind. Pharm.*, 15: 223-233, **1989**

135. Burger, A; Koller, K.T, *Sci. Pharm.*, 64, 293-301, **1996**
136. Eckert, T; Müller, J, *Arch. Pharm.*, 310, 116-118, **1977**
137. Tetteh, J, Personal Communication, **2003**
138. Bonnett, R, *Chemical Aspects of Photodynamic Therapy*, **2000**
139. Hogan, S.E; Buckton, G, *Pharm. Res.*, 18, 112-116, **2001**